Integrated Biosensor Platform for Detection of Waterborne Pathogens: Improving Public Health

Rainbow, Joshua

Award date:
2023

Awarding institution:
University of Bath

Integrated Biosensor Platform for Detection of Waterborne Pathogens: Improving Public Health

A thesis submitted for the degree of Doctor of Philosophy

By Joshua Robert Ian Rainbow

Supervisors: Dr Pedro Estrela (Primary),

Dr Niklaas Buurma, Dr Simon Pope, Professor Nigel Silman and Dr Mirella Di Lorenzo

University of Bath

Department of Electronic and Electrical Engineering

October 2022

Abstract

Waterborne diseases are caused by microorganisms known as pathogens e.g., bacteria, viruses, protists etc. that are commonly spread through contaminated fresh water sources. Diseases caused by these pathogens are today one of the leading causes of infection and mortality. In low- and middle-income countries public health is steadily becoming an increasing risk, with increased development directly producing waste pollution carrying pathogens into freshwater sources. Examples of freshwater sources include reservoirs, rivers and wells with waste pollution being due to poor sanitation, agricultural runoff, illegal dumping etc. The result of this pollution is being further exacerbated by poor wastewater infrastructure, reduced public understanding as well as lack of diagnostic and monitoring systems. One strategy of improving public health is to develop small portable devices that are easy-to-use to monitor levels of waterborne pathogens in drinking water to avoid unnecessary disease from contaminated sources. To do this we aimed to develop an integrated biosensing device for the sensitive detection of highly selective DNA sequences related to several waterborne pathogens.

The first study focusses on the development and optimisation of a biosensor assay using electrochemical impedance spectroscopy (EIS). The work looks at the optimisation of surface chemistry taking advantage of the passive adsorption of thiol groups to form a self-assembled monolayer (SAM). This is not only a relatively simple way of forming a sensing layer, but with the use of re-usable gold electrodes and E. coli specific thiolated ssDNA probes it is also cost-effective to optimise. This study also highlights the importance of different cleaning techniques for reusable gold electrodes and how this can impact ideal SAM formation for increasing probe-target interaction. The results of this study will act as a baseline for the ability of thiol self-assembled DNA probes to detect target sequences without any additional signal amplifying steps.

The second study takes the assay from the first study a step further by integrating a post-signal amplification step using a redox-active intercalator. Intercalators are molecules that bind between the base pairs of the DNA duplex structure. In doing so,

they can alter the secondary structure of the duplex and increase the electrostatic field. This particular work exploits a novel redox-active intercalator called cobalt-aqphen, [Co(GA)2(aqphen)]Cl. The cobalt acts as the redox-active ligand of the compound, while the addition of the extended planar aqphen ligand with conjugated anthraquinone which has been shown to increase binding affinity between the base pairs. Intercalation of this molecule enables the potential for amperometric and non-faradaic detection of target DNA sequences at much lower limits of detection (LOD) without the need for an additional redox couple.

The third study develops a highly sensitive and selective assay integrating CRISPR/Cas-based SHERLOCK detection integrated with isothermal amplification, a conductive-polymer surface chemistry, peptide nucleic acid (PNA) probes and amperometric detection of TMB precipitation for signal-off function detection. This assay was used to demonstrate detection of both synthetic E. coli sequences as well as single-molecule SARS-CoV-2 viral RNA from unprocessed patient saliva. This assay can also be easily modified by altering the guide RNA that programmes the CRISPR/Cas enzyme to detect any target pathogen RNA. This provides great potential for multiplexed detection of multiple pathogen markers of clinically and environmentally relevant pathogens from a single point source sample.

In conclusion, this thesis aims to describe methods of increasing the sensitivity and selectivity of target nucleic acid detection using methods of pre-signal amplification such as isothermal amplification integrated with CRISPR/Cas SHERLOCK diagnostics as well as post-signal amplification using redox-active intercalator molecules. It also aims to explore ways of combining these techniques together to create truly integrated, cost-effective ways of detecting multiple waterborne pathogens of interest.

Table of Contents

Acknowledgements

I would first like to express my gratitude to the Natural and Environment Research Council (NERC) and GW4 FRESH CDT group for the opportunity to carry out this PhD. I would like to thank them for the funding and training that they have provided to me during my PhD and the experiences I've enjoyed and friends I've met along the way. I would specifically like to mention my 1st GW4 Fresh NERC colleagues for their shared experiences and the support they have provided during the last 4 years. Also, for the many brunches shared with Clare Brown and Victoria Hussey. I hope there will continue to be many more cherished times to come.

I would like to offer my profound gratitude to my PI Professor Pedro Estrela for asking me to apply for this PhD in the first place. As well as for all the opportunities he has provided me through the last 6 years, I will always highly value his support and advice. I thank my additional supervisors Dr Niklaas Buurma, Dr Simon Pope, Professor Nigel Silman and Professor Mirella di Lorenzo. I am very grateful for the exceptional 2 East Biosensors research group that we have within the Department of Electrical and Electronic Engineering at the University of Bath. I would like to give mention to Dr Uros Zupancic, Dr Shu Jiang, Dr Serife Ustuner, Dr Despina Moschou, Dr Eliska Sedlackova, Grace Maxted and Kasia Bialas for their friendship and support throughout my time at the University of Bath.

I would also like to thank everyone at the Wyss Institute for Biologically Inspired Engineering at Harvard University for my time there during my internship. Particular thanks go to my Professor Donald Ingber (external PI), Dr Pawan Jolly, Dr Adama Sesay, Dr Helena de Puig, Professor Jim Collins, Dr Devora Najjar, Dr Sanjay Sharma, Dr Mohammed Yafia, Dr João Paulo de Campos da Costa, Dr Danielle de Campos da Costa, and Nooralhuda Arkan.

Finally, I would like to express my never-ending gratitude to my parents and family, without which I certainly wouldn't have come as far as I have. You lift me up, keep me grounded and remind me where I came from and how much that means. I rest easy knowing that I can always come home from a hectic and busy life to a place of calm and respite with the support to get back up and continue onwards.

List of Figures

List of Tables

Nomenclature

F	Faraday constant
A	Area
c	Concentration
C	Capacitance
C*	Complex capacitance
d	distance
D	Diffusion constant
D0	Diffusion coefficient
e	Electron charge
E0'	Formal potential
f	Frequency
Hz	Hertz
i	Current
I	Ionic charge
J	Imaginary number equal to the square root of -1
k	Boltzman constant
kd	Dissociation coefficient
n	Number of electrons transferred
NA	Avogradro number
Q	Charge
R	Universal gad constant
Rct	Charge transfer resistance

Rs	Solution resistance
S	Scan rate
T	Temperature
t	Time
V	Electrode potential
V0	Voltage signal amplitude
W	Warburg element
z	Ion valence
Z	Impedance
Γ	Surface coverage
ε0	Permittivity of free space
εr	Permittivity of dielectric constant of the solution
θ	Phase
λD	Debye length
σ	Theoretical charge density
σ	Standard deviation of the control response
ψ	Electrostatic potential
ω	Angular frequency

List of Abbreviations

AC	Alternating current
AQ	Anthraquinone
AuNP	Gold nanoparticle
AuNW	Gold nanowire
BIP	Backward internal primer
BNA	Bridged nucleic acid
BOP	Backward outward primer
BSA	Bovine serum albumin
Cdl	Double layer capacitance
CE	Counter electrode
CFU	Colony forming unit
CNT	Carbon nanotube
CPE	Constant phase element
CRISPR	Clustered Regularly Interspaced Short Palindromic Repeats
CV	Cyclic voltammetry
DC	Direct current
DETECTR	DNA Endonuclease-Targeted CRISPR Trans Reporter
DL	Double layer
DNA	Deoxyribose nucleic acid
dNTP	Deoxynucleoside triphosphate
DPV	Differential pulse voltammetry
EDC	1-Ethyl-3-(3-dimethylaminopropyl)carbodiimide

EDTA	Ethylenediaminetetraacetic acid
EIS	Electrochemical impedance spectroscopy
ELISA	Enzyme-linked immunosorbent assay
ESA	Electrostatic area
FIP	Forward internal primer
FOP	Forward outward primer
GA	Glutaraldehyde
GNA	Glycol nucleic acid
GOx	Graphene oxide
IHP	Inner Helmholtz plane
LAMP	Loop-mediated isothermal amplification
LMICs	Low- and middle-income countries
LNA	Locked nucleic acid
LOC	Lab-on-chip
LOD	Limit of detection
LOQ	Limit of quantitation
MB	Methylene blue
MCH	6-Mercaptol-1-hexanol
MS	Mass spectroscopy
NGO	Non-governmental organisation
NHS	N-Hydroxysuccinimide
NM	Nile blue
OCP	Open circuit potential

OHP Outer Helmholtz plane

PB Phosphate buffer

PBS Phosphate buffered saline

PBST Phosphate buffered saline with Tween

PCB Printed circuit board

PCR Polymerase chain reaction

PDA Polydopamine

PEG Polyethylene glycol

PNA Peptide nucleic acid

PoC Point of care

Ppy Polypyrrole

QCM Quartz crystal microbalance

RE Reference electrode

rGOx Reduced graphene oxide

RNA Ribose nucleic acid

RPA Recombinase polymerase amplification

RT-LAMP Reverse transcription LAMP

RT-PCR Reverse transcription PCR

SAM Self-assembled monolayer

SHERLOCK Specific High Sensitivity Enzymatic Reporter UnLOCKing

SPE Screen printed electrode

SPR Surface plasmon resonance

SWV Square wave voltammetry

TMB 3,3’,5,5’-Tetramethylbenzidine

UTI Urinary tract infection

WE Working electrode

List of Publications

- **Rainbow, J.**, Judd-Cooper, E., Buurma, J, N. and Estrela, P., In Preparation. Characterisation of a Cobalt Complex for Redox-Active Intercalation in an Electrochemical DNA Biosensor.
- Najjar, D*****., **Rainbow, J*.**, Sharma Timilsina, S*****., Jolly, P*****., De Puig, H*****., Yafia, M., Durr, N., Sallum, H., Alter, G., Li, J.Z. and Yu, X.G *et al.*, 2022. A lab-on-a-chip for the concurrent electrochemical detection of SARS-CoV-2 RNA and anti-SARS-CoV-2 antibodies in saliva and plasma. Nature biomedical engineering, 6(8), pp.968-978. ***** = **equal authorship.**
- Zupančič, U., **Rainbow, J.**, Estrela, P. and Moschou, D., 2021. Utilising Commercially Fabricated Printed Circuit Boards as an Electrochemical Biosensing Platform. Micromachines, 12(7), p.793.
- Robinson-McCarthy, L.R ***et al.***, 2021. Anomalous COVID-19 tests hinder researchers. Science, 371(6526), pp.244-245.
- Robinson-McCarthy, L.R ***et al.***, 2021. Laboratory-Generated DNA Can Cause Anomalous Pathogen Diagnostic Test Results. Microbiology Spectrum, 9(2), pp.e00313-21.
- Zupančič, U., **Rainbow, J.**, Flynn, C., Aidoo-Brown, J., Estrela, P. and Moschou, D., 2021. Strategies for Multiplexed Electrochemical Sensor Development. In Modern Techniques in Biosensors (pp. 63-93). Springer, Singapore.
- **Rainbow, J.**, Sedlackova, E., Jiang, S., Maxted, G., Moschou, D., Richtera, L. and Estrela, P., 2020. Integrated electrochemical biosensors for detection of waterborne pathogens in low-resource settings. Biosensors, 10(4), p.36.
- Jolly, P., **Rainbow, J.**, Regoutz, A., Estrela, P. and Moschou, D., 2019. A PNA-based Lab-on-PCB diagnostic platform for rapid and high sensitivity DNA quantification. Biosensors and Bioelectronics, 123, pp.244-250.
- Dutta, G., **Rainbow, J.**, Zupancic, U., Papamatthaiou, S., Estrela, P. and Moschou, D., 2018. Microfluidic devices for label-free DNA detection. Chemosensors, 6(4), p.43.

1. Introduction

Making up less than 1% of the Earth's surface, freshwater is considered one of the most valuable resources available, playing an important role in population health, economics, and geopolitical interests. Considering its importance, it is of great concern to scientists globally that this resource is constantly receiving high levels of pollution. This contamination can originate both directly and indirectly from anthropogenic activities and can include mining/heavy metal, chemical, agricultural, and microbiological sources. The level and type of these pollutants vary significantly based on the local human activity and extent of urban development. However, the effects of such pollution are not always local and often have wide-spreading implications to further communities and wildlife. For example, the recent COP26 2021 global climate summit highlighted the larger role that highly developed nations have played in polluting freshwater resources. On the other hand, low- and middle-income countries (LMICs) have seen comparatively less urban development and are responsible for considerably less pollutive output. However, those same nations are suffering significantly more due to the pollution of highly developed countries.

Microbiological pollution has arguably one of the highest influences on population health and global economics. It is also the form of freshwater pollution with the most diverse number of causes and effects, affecting not only human health but the success of local flora and fauna resulting in further indirect implications. The effects of freshwater pollution by microbiological sources are further exacerbated in LMICs due to poorer understanding and provision of sanitation, under-developed infrastructure, and lack of freshwater monitoring systems. It is therefore a key focus of scientists all over the world to develop and provide such methods of monitoring microbiological pollution of freshwater systems. The provision of such devices would not only help prevent extensive pollution but hopefully prevent high levels of human disease and implications on the surrounding environment.

The work in this thesis aims at developing an integrated electrochemical biosensor for the detection of waterborne pathogenic DNA commonly found in polluting freshwater. Deoxyribose nucleic acid (DNA) acts as a highly specific target analyte for

bacterial and viral detection, with reverse transcription, and can provide further information regarding pollution causes, bacterial mutations, and population epidemiology in fresh and wastewater. To fabricate such a sensor for the detection of DNA in freshwater it is important to develop a device that can detect low concentrations of target analyte in a complex matrix in rapid time. It is also important that if the device is being used by local NGOs and communities that it is easy to use and provides a simple sample-in-answer-out response.

This chapter will provide a general background to the pathogenic pollution of freshwater systems, examples of microbiological pollution and their effects, an overview of water-based diagnostics and monitoring, the development of biosensors and the projects involved in this thesis. Content in this chapter has been published in Rainbow *et al.* (Rainbow *et al.*, 2020).

1.1. Pathogenic pollution of freshwater systems

Waterborne pathogens are a diverse group of mostly single-celled organisms that cause disease and illness within a living host. Pathogens can exist as either bacteria, viruses, protists, or fungi and vary significantly in the mechanism of infection and relationship with the host organism. Pathogens differ greatly in structural form and contain many different functional mechanisms for infection and survival making them adaptive to almost any environment and host defence. In the cases of bacteria, viruses and protists, these organisms are generally transmitted through water e.g., rivers, lakes, reservoirs, and urban discharge. While fungi can also transmit through water, they primarily use fruit-borne spores that can enter the air and be transported by the wind. Waterborne diseases are therefore diseases that are caused by pathogens that encounter a host through direct contamination and the use of polluted water sources. Further contamination from the effects of these diseases can be observed in the wastewaters that flow downstream of human settlements, both urban and rural. Waterborne pathogens such as *E. coli* (specifically serotype EO157:H7), *Salmonella typhi*, *Vibrio cholerae*, *Campylobacter jejuni*, *Giardia intestinalis* etc. (Table 1.1) are commonly found in both fresh and wastewater sources (Ramírez-Castillo *et al.*, 2015).

Table 1.1. Commonly found pathogens found in drinking water systems and their related diseases and patient/water supply significance (Ramírez-Castillo et al., 2015).

Pathogen	**Associated disease**	**Effect on patient**	**Water supply persistence**
Bacteria			
Campylobacter jejuni	Diarrhoea, gastroenteritis	High	Moderate
Escherichia coli, specifically strain EO157:H7	Acute diarrhoea, bloody diarrhoea, and gastroenteritis	High	Moderate
Shigella spp.	Bacillary dysentery, shigellosis	High	Short
Legionella spp.	Acute respiratory illness, pneumonia	High	May proliferate
Pseudomonas aeruginosa	Pulmonary infection, UTI, kidney infection, inflammation, and sepsis	Moderate	May proliferate
Salmonella typhi	Typhoid fevers, salmonellosis	High	Moderate
Vibrio cholerae	Gastroenteritis, cholera	High	Short-Long
Viruses			
Adenovirus	Gastroenteritis	High	Long

Enteroviruses	Gastroenteritis	High	Long
Hepatitis viruses	Hepatitis	High	Long
Rotavirus	Gastroenteritis	High	Long
Norovirus	Gastroenteritis	High	Long
Protozoa			
Acanthamoeba spp.	Amoebic meningoencephalitis, keratitis, encephalitis	High	May proliferate
Cryptosporidium spp.	Diarrhoea, cryptosporidiosis	High	Long
Giardia intestinalis	Diarrhoea	High	Moderate

There exists approximately 1400 species of pathogenic organisms that directly interact with humans as a host-pathogen interaction, though this accounts for only 1% of total microbial organisms that are currently known (Microbiology by numbers, 2011). The number and types of pathogenic species vary greatly across the globe due to local environmental features. However, the increases in pathogenic populations and the associated rates of human disease and mortality can be directly associated with anthropogenic environmental degradation and pollution. This observed pathogenic population increase is not only a risk to human health but is also, as mentioned previously, a significant negative impact on both economics and geopolitical interests.

Waterborne pathogens that enter freshwater infrastructure e.g., reservoirs, water holding facilities, hospitals, housing etc. have the capability to cause disease rapidly throughout entire cities. This does not only occur by drinking water but also through consuming food that has been prepared using contaminated sources and has not been properly treated before consumption. Such an example is seen in the Billings Reservoir in Brazil which supplies fresh water to half of the city of Sao Paulo with a population of roughly 12.3 million. This reservoir experiences a seasonal fluctuation of pathogenic bacteria with dangerously high levels during the hot summer months of persistent pathogens such as *Escherichia coli (E. Coli*). Several studies have been conducted by research groups in Brazil that look at these seasonal trends of pathogenic bacteria to determine the risk and provide evidence to local governing bodies (Orsi *et al.*, 2007; Leme *et al.*, 2018).

Determining the exact source of waterborne pathogens is difficult due to the rapid turnover of surface waters in many aquatic environments (Pandey *et al.*, 2014). Nonetheless, many common sources of waterborne pathogens are now known, with mitigation strategies in place in many countries to reduce the chances of pathogen contamination to freshwater bodies. Well-known sources of new waterborne pathogens can include human and wildlife waste, adaptation/mutation, and intensive agricultural practices. Additionally, with the development of globalization, pathogens may be introduced by human or wildlife host migrations as well as recently thawing ice from previous epochs due to global warming. Incidence rates of

waterborne diseases may also be further exacerbated by extreme weather events such as:

- High rainfall assists in the transport and dissemination of waterborne pathogens across land and from highlands to lowlands.
- High temperatures and drought increase concentrations of pathogens by prolonging survival and enhancing growth rates as well as impeding ease of hygiene.
- Ice melt and sea-level rise releases isolated water sources and enhance the risk of flooding.
- Flooding can cause disruption particularly in urban areas and developing countries with inadequate wastewater transport and treatment infrastructure. Leading to the contamination of freshwater sources from wastewater sources.

Waterborne pathogens are diverse and thus have evolved numerous mechanisms for the infection of hosts to cause disease. These evolved mechanisms are often called 'virulence factors and can include potent toxins, surface proteins for increased cell adhesion, increased methods of motility such as flagellum etc. The number or lethality of these mechanisms underpins the virulence of each pathogen. However, the consensus of how pathogens cause an infection within a host can be generally explained (van Baarlen *et al.*, 2007) (Figure 1.1).

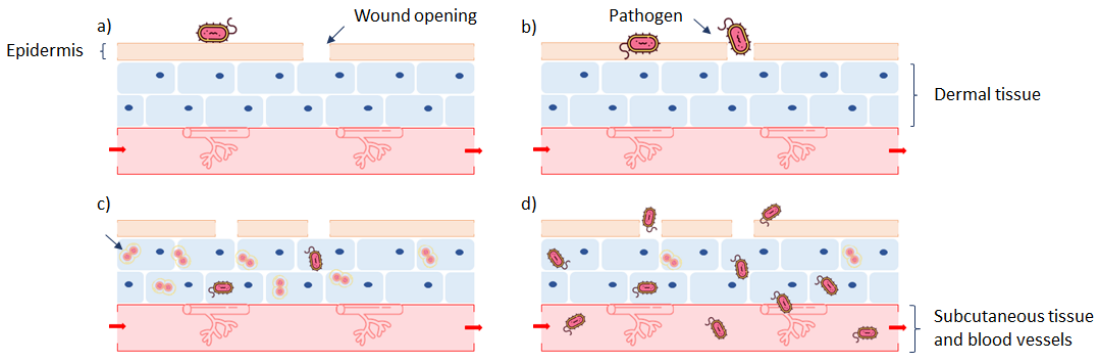

Figure 1.1. A simplified infection process of pathogens. (a) The pathogen attaches to an epidermal surface on the host, this may be exterior skin or interior respiratory/gastrointestinal surfaces. (b) After attachment, the pathogen will enter the host's tissues via. open wounds or through a burrowing process. (c) The pathogen has now colonized the host and will begin division either within tissue cells or within the interstitial fluid. (d) In the next stage, daughter pathogens are dispersed either within the host's circulatory system in a process known as metastasis or externally to enter the environment and infect a new host (adapted from van Baarlen et al., 2007).

1.2. Modern and historical impacts of waterborne diseases

The modern-day water crisis sees 785 million people worldwide without access to clean and safe water, 144 million of which are solely dependent on surface water sources. It is estimated that a minimum of 2 billion people drink water that is contaminated with faecal matter. This water is directly leading to the transmission of common waterborne pathogens (Table 1.2) and is estimated to cause around 485,000 deaths linked to communicable diarrheal death annually (World Health Organization, 2019). It is estimated that approximately 29% of all child deaths per year (~2 million children) are due to diarrhoea and pneumonia (World Health Organization, 2013). Therefore, it can be argued that water, particularly freshwater, is one of the most valuable natural resources in need of protection and sustainability efforts. Approximately 1.42 billion people worldwide are currently living with high or extremely high waterborne pathogen vulnerability (Selim, 2021). According to the World Health Organization (WHO), almost 4 million deaths globally in 2019 were associated with communicable diseases including lower respiratory infections and diarrheal diseases. Lower respiratory infections, often caused by waterborne

pathogens found in drinking water, were the highest source of communicable disease and the fourth highest cause of mortality. While both lower respiratory infections and diarrheal diseases have seen a large decline since 2000-2019, the largest declines are likely associated with middle-higher income countries. Whereas in low-income countries, people are still most likely to die due to a communicable rather than non-communicable disease (World Health Organization, 2020).

Incidences of waterborne disease-related mortality are concentrated in the most remote locations of the world, specifically in parts of Africa, Asia, and South America. Suggested reasons for the concentrated effect of disease prevalence in these areas are thought to be related to high levels of poverty. Inhibiting the development of adequate wastewater treatment, freshwater transport infrastructure and affordable water monitoring systems. This further intensifies the lack of sanitation, reduced by a public misunderstanding of the relationship between hygiene, sanitation, and water pollution. Finally, a lack of education causes a reduction in public engagement and pressure on authorities to obtain the evidence required by government bodies and policymakers. This evidence could then be used to push regulation and effective legislation for hygiene, further research, and infrastructure development. In low-income countries, 22% of the health care sector lacks access to freshwater sources, 21% have no provision of adequate sanitation, and 22% have a low standard of wastewater management infrastructure (World Health Organization, 2019). Increasing public engagement in education of hygiene and sanitation as well as providing adequate infrastructure for the provision of fresh water and treatment of wastewater is key to reducing these levels of mortality in low-middle income countries (LMICs).

Pathogens are one of the leading causes of global mortality, with pathogen-based causes present in the top leading causes of death in both high-income and low- and middle-income countries (see Table 1.2). In high-income countries, lower respiratory infections were the fourth leading cause of mortality rate with 0.34 million death per year. However, in low- and middle-income countries the third and fourth leading causes of mortality were caused by infectious diseases in the forms of lower respiratory infections and HIV/AIDS (Michaud, 2009). It is worth mentioning that the

number of deaths caused by lower respiratory infections in high-income countries (0.34 million) was significantly lower than LMICs (3.41 million). This is likely due to the lower quality of waste infrastructure, hygiene, and diagnostic and monitoring capabilities in LMICs.

Table 1.2. The five leading causes of mortality by country-based broad income group (adapted from Michaud, 2009).

Rank	**High-income countries**	**Deaths (in millions)**	**Low- and middle-income countries**	**Deaths (in millions)**
1	Ischemic heart disease	1.36	Ischemic heart disease	5.70
2	Cerebrovascular disease	0.78	Cerebrovascular disease	4.61
3	Trachea, bronchus, and lung cancer	0.46	Lower respiratory infections	*3.41*
4	Lower respiratory infection	*0.34*	HIV/AIDS	*2.55*
5	Chronic obstructive pulmonary disease	0.30	Perinatal conditions	2.49

Outbreaks of pathogen-caused infections are not a novel cause of mortality in global populations, with well-documented pandemics dating back as far as the Antonine plague originating in ancient Mesopotamia in 161-180 AD (Huremović, 2019). Some of the most notable global pandemics include the Plague of Justinian (541-542 AD, 25 million deaths), the Black Death (1346-1353, 75-200 million deaths), the Spanish influenza pandemic (1918, 20-50 million deaths), and the HIV/AIDS pandemic (1976-present, 36 million deaths) (Bloom, Black and Rappuoli, 2017). Since the outbreak of the SARS-CoV-2 pandemic in Wuhan, China in 2019, the total recorded deaths have reached more than 5.8 million (Johnston *et al.*, 2022). Considering the modern standards of hygiene and medicine the extraordinarily high number of deaths from

modern outbreaks can be attributed to several factors, namely globalisation leading to faster spread of pathogens, urbanisation and densely populated areas with outdated infrastructure and sanitation, climate change due to migration of disease-borne insects and floods carrying waterborne pathogens, as well as the increased transfer of zoonotic diseases due to increased overlap between human and animal habitat encroachment. Although most pandemics have been caused by viral species, bacterial pathogens have led to a significant number of outbreaks, each time causing thousands of deaths. Examples of significant bacterial outbreaks including the 1854 London Broad Street cholera outbreak leading to 14,137 deaths (Paneth *et al.*, 1998), an *E. coli* (O104:H4) outbreak in Germany in 2011 with 3,950 cases and 53 deaths (European Food Safety Authority, 2011; King *et al.*, 2012), and recently the Yemen cholera outbreak in 2016 to present, which has caused more than 2.5 million cases and 4,000 deaths (Federspiel and Ali, 2018).

1.3. Potential biomarkers for waterborne pathogen

Waterborne pathogens contain several potential targets for detection by diagnostic and monitoring techniques. These targets are useful in detection of species-specific waterborne pathogens and are commonly referred to as biomarkers. Biomarkers are biological molecules that occur in organisms that enable the detection and quantitation of specific pathogens, pathological states in patients, and physiological processes in environments. Such biomarkers for waterborne pathogens include nucleic acids, proteins, and whole cells. This thesis will focus on the detection of waterborne pathogenic bacterial and viral species. With that in mind, pathogenic infections are much more cost-effective to prevent and mitigate than they are to treat in a subsequently infected patient (Hughes, 2008). Thus, the importance of providing a means of real-time diagnostics or monitoring for pathogens in water-based sources is significant to limit the cost and burden on health services and governments.

1.3.1. Deoxyribose nucleic acid (DNA)

Deoxyribose nucleic acid (DNA) is a common biomarker that has been used extensively with a variety of techniques to determine, with high specificity, pathogen

presence and quantity in freshwater and wastewater quality testing (Shanks *et al.*, 2007). In this thesis, the focus of detection will be on DNA commonly found in single-cell organisms such as bacteria and viruses, including genomic DNA and plasmid DNA. A common genomic DNA type used for detection of pathogenic bacteria such as *Escherichia coli* is 16S ribosomal DNA (rDNA). This DNA type is found in all genera of bacteria and is responsible for the translation of messenger RNA (mRNA) into proteins. Due to this vital functionality, the 16S rDNA genes are highly conserved within bacterial genomes and are well understood by researchers (Janda and Abbott, 2007). Information regarding 16S rDNA for various genera of bacteria is also widely available from online databases. However, genus-level identification is usually not specific enough for diagnostic purposes when related to monitoring and treatment of water contamination. For bacterial detection more specific than the genus level, it is required to target genes of low commonality and thus high specificity to the individual species of bacteria e.g., *E. Coli*, *Salmonella tyhpi* (*S. typhi*), and *Pseudomonas aeruginosa* (*P. aeruginosa*).

Such a group of highly specific genes are known as 'virulence genes' coding for molecules that enable the high survivability of the pathogen that interacts with its environment, whether that be a hosts' cell or temporary surface substrate (see Figure 1.2). Unlike the 16S rDNA genes which are found within heavily conserved genomic bacterial DNA, virulence genes are in plasmids which are small double-stranded loops of DNA located free within the cytoplasm of bacterial and viral cells (Johnson and Nolan, 2009). Examples of virulence genes include cytotoxins on the surface of cell membranes or capsids, surface proteins which aid in adhesion, endo- and enterotoxins for incapacitation of host immune cells. For example, the O157:H7 strain of *E. Coli* bacteria have a highly specific cell surface protein gene called Z3276 that codes for a surface-based tip adhesion protein (Wurpel *et al.*, 2013).

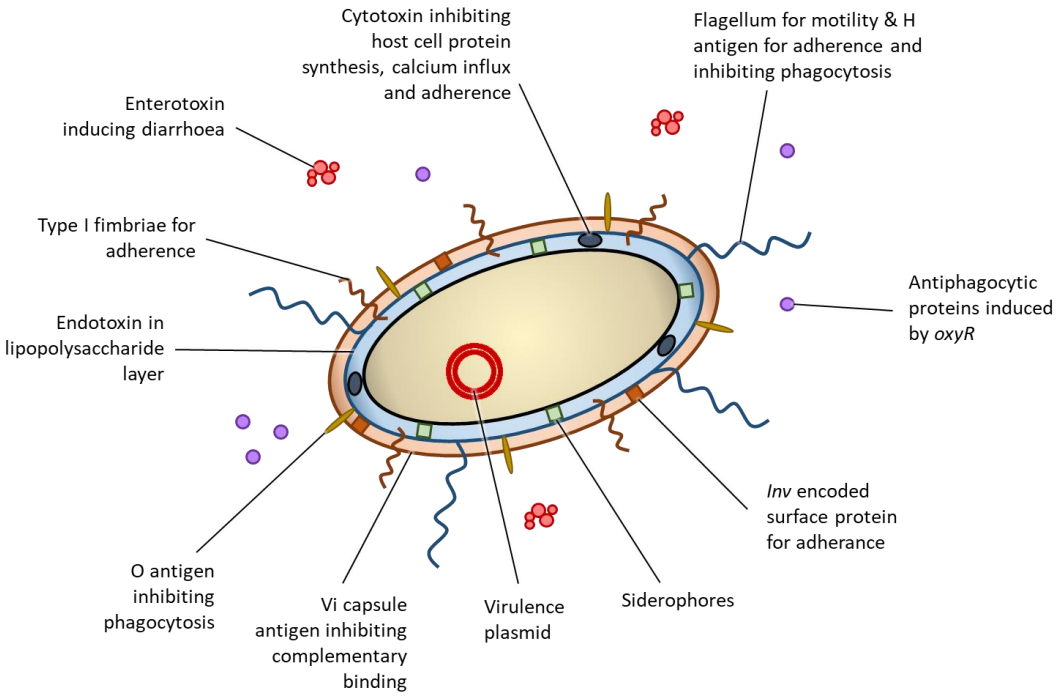

Figure 1.2. Common virulence factors used by pathogenic bacteria and viruses to cause infection (adapted from Zachary, 2017).

Another DNA biomarker that can be used to detect the presence, but not concentration, of pathogens within water samples is environmental DNA (eDNA) also known as free extracellular DNA. This is DNA that is free flowing in water due to the breakage of the bacterial/viral cell membrane/capsid, causing release of all pathogen contents e.g., DNA, RNA, proteins, and lipids into the environment. However, eDNA is not commonly used in the detection of pathogens within water samples because it is not specifically indicative of viable pathogen populations (Azeredo *et al.*, 2017).

1.3.2. Other biomarkers for waterborne pathogen detection

Aside from DNA, there are several other molecules that can be employed as biomarkers for detection of waterborne pathogens. One example includes ribonucleic acid (RNA), an analogue of DNA that replaces the nucleotide base thymine with uracil for the translation of DNA into proteins. Types of RNA may include messenger RNA (mRNA), transfer RNA (tRNA), micro-RNA (miRNA) or ribosomal RNA (rRNA). RNA is primarily responsible for the process of translating DNA to protein, however, also enable production of other molecules and enables

control over the expression levels of those proteins. Common RNA associated with pathogenic bacterial detection is the genus level 16S ribosomal RNA responsible for the translation of DNA, making many rRNAs also associated to virulence factor genes (Janda and Abbott, 2007). However, due to the nature of bacterial RNA, it is difficult to utilise in field-based monitoring circumstances. This is due to the 5' end of the bacterial RNA being associated with rapid degradation by commonly present nuclease enzymes (Gill *et al.*, 2018). Thus, there is currently a shortage in the literature regarding the detection of waterborne pathogenic bacteria using solely RNA samples for rapid, *in*-situ or on-site monitoring devices.

Other molecules that are commonly described being used in the literature for pathogenic bacterial detection include proteins, lipids as well as whole cell detection. Both extracellular and intracellular proteins can be monitored using binding affinity studies implementing antibodies, aptamers, or peptides as capture probes. However, as with RNA, there is a shortage of studies looking at the detection of bacterial presence targeting only protein. However, viral diagnostic devices focussing on the detection of surface proteins have been developed. Studies focusing on the detection of waterborne pathogenic bacteria commonly use capture probes taking advantage of proteins and aptamers to bind to cell-surface proteins for whole-cell detection (Kumar *et al.*, 2018). Additionally, several traditional techniques target direct detection of the cell including cell culturing quantifying colony-forming units (CFU) and optical techniques e.g., flow cytometry or rapid amplification by polymerase chain reaction (PCR) (Rajapaksha *et al.*, 2019). Various novel diagnostic techniques being developed for the detection of waterborne pathogens are now focussing on either direct or affinity binding-based detection of nucleic acids, extracellular proteins, or whole cells (Kumar *et al.*, 2018a; Yu *et al.*, 2018).

1.4. Water-based diagnostics and monitoring

Global freshwater shortage and pollution of water resources by pathogenic sources are steadily increasing issues. Thus, it is of great importance to improve our methods for water quality monitoring to mitigate the increase of the global disease burden. When water sources such as lakes, rivers, and reservoirs become unsafe for

consumption due to pathogen pollution, the responses of authorities in high-income countries and LMICs are widely dissimilar. In many high-income countries, it is the responsibility of water service providers and the government to ensure that water quality is consistently above a safe threshold. These companies are held to that standard by their customers and the regulatory inspectorates and governments (Ellis *et al.*, 2018). It is usually the responsibility of water service providers to detect point source water contamination and to implement mitigation strategies. Within LMICs it is often the case that water service providers are not held to the same level of regulation due to less strict levels of legislation regarding hygiene and sanitation. Within low-income countries, in which communities may be relying solely on surface water sources, there are little to no water providers or companies and there is no significant government legislation.

The standards of freshwater availability and wastewater removal must be of a high level in every community. Freshwater is important for potable water, cooking, cleaning, and removal of waste to name a few important daily uses. Without freshwater, the effort required for these daily tasks will significantly reduce the quality of life, just as they do in certain low-income countries and especially in rural communities. When sources such as wells are then contaminated through waterborne pathogens quality of life drops significantly. Monitoring and treatment techniques must exist to deal with point and source contaminations. Wastewater is any water that results as a product of these activities as well as industrial and agricultural activity. In higher-income countries, this water is typically flowed through enclosed systems to wastewater treatment facilities and treated using techniques such as filtration, aeration, biological degradation, ultraviolet treatment etc. After this, water then flows back into the natural water systems such as lakes and rivers. Studies have found that, with the rapidly increased population in urban and rural settlements (Ashipala and Armitage, 2011; Chirisa *et al.*, 2017), people in low- and middle-income countries (LMICs) are often living with poorly developed infrastructures, such as low sewage coverage (Palanca-Tan, 2017) and low wastewater treatment capacity (Karpouzoglou and Zimmer, 2016). These issues result in excreta and greywater being directly disposed of into drainage or flood

canals and, eventually, being discharged into rivers and lakes with no treatment at all or only partial treatment using primary measures. Subsequently, untreated wastewater is reused for irrigation (Raschid-Sally, 2010), which has a negative impact on not only the consumers of the agricultural products but also the local farming communities (World Health Organization, 2006). In some cases, under-maintained freshwater supply pipes with leakages may also be at risk of being contaminated by the neighbouring drainage. Untreated wastewater imposes serious problems for the environment and climate, as well as public health. Due to the absence of adequate treatment, organic chemicals, heavy metals, and microorganisms (Ejeian *et al.*, 2018) that began in domestic households or industry are released into the ecosystem as pollutants, further providing waterborne pathogens with a thriving environment.

Current approaches to water quality monitoring hold several disadvantages that make them unsuitable for monitoring *in-situ* over long time periods and in low-resource settings. Traditional methodologies include techniques such as microbiological culturing and colony counting, mass spectroscopy (MS), polymerase chain reaction (PCR), pyrosequencing, microarrays, pathogen extraction, and lysis etc. Matrix-assisted laser desorption/ionisation mass spectroscopy (MALDI-MS) is a popular laboratory technique used for the analysis of water to differentiate between present bacterial species and subspecies directly in water samples. PCR is the most used gold standard technique for the specific amplification of DNA (and RNA with reverse transcriptase) as well as quantitative PCR (qPCR) for direct detection and quantification of the products of amplification. This technique yields high sensitivity but can be open to false-positives in contaminated samples as well as contaminants that can inhibit reaction, causing false-negatives. Microbiological cultivation and microscopy techniques are one of the oldest methods of identifying pathogens involves the culturing of target pathogens within/upon nutrient mediums for phenotypic classification and quantification. Pyrosequencing was one of the first sequencing methods developed in place of the Sanger method. It involves the detection of pathogen species through a series of enzymatic reactions in which the addition of individual deoxynucleotide triphosphates (dNTPs) into the synthesised

sequence, due to production of visible radiation, is recorded for detection and quantitation.

These diagnostic and monitoring approaches are limited by their requirement of expertise, high costs (both monetary and time), and lack of quantitative data etc. Due to variations in these limitations, the available techniques also differ between high-income countries and LMICs. Microbiological culturing techniques have been used as the gold standard for determining water source contamination, with more techniques becoming available in developed areas and high-income countries as technologies have improved. However, bacterial culturing and microbiological techniques remain the standard. Even so, these existing standard methods of pathogen detection are difficult to perform in LMICs due to limited resources, sterile lab access and skilled individuals to perform them. Additionally, microbiological culturing techniques are laborious and take a long time, usually ~16 h for colony growth, before any result can be obtained and so cannot be used for in-situ monitoring or real-time data (Bridgeman *et al.*, 2015; Ward, 2021). It is in these countries specifically that fast and reliable results are required owing to the higher risk of mortality from contaminated sources by waterborne pathogens (Troeger *et al.*, 2017; Ward *et al.*, 2020).

For the detection and monitoring of waterborne pathogens in LMICs to be improved, new efficient methods of detection are required to be developed. There exist established criteria that need to be considered for the development of diagnostic tools for monitoring in LMICs. In 2003, the World Health Organization published the ASSURED criteria for the development of diagnostic tools that can be used at the point-of-care (PoC) in LMICs (Mabey *et al.*, 2004). The ASSURED criteria include affordability, sensitivity, specificity, user-friendliness, rapid analysis, reduction of excessive equipment and portability (deliverable to those in LMICs). In 2019, this was then reassessed to include two more criteria: real-time connectivity and ease of sample collection to create the REASSURED criteria (Table 1.3) (Land *et al.*, 2019).

Table 1.3. Criteria for a REASSURED diagnostic test developed for PoC detection in the developing world (Land et al.*, 2019).*

Criteria		**Description**
R	Real-time connectivity	The capability of the device to be connected to a reader or mobile phone for test result reading and transmission to end-user
E	Ease of sample collection	Development of devices should be mindful of non-invasiveness and limited effect on the environment
A	Affordability	Devices are affordable to both end-users and environment or healthcare systems
S	Sensitivity	Mitigates false negatives
S	Selectivity	Mitigates false positives
U	User-friendliness	Use of the device is simple and requires minimal training
R	Rapid and robust	Sample-in-answer-out time should be between 15 mins to 2 hours to support rapid decision making
E	Equipment-free or simple to use	Preferably does not require the use of specialist or mains-powered equipment
	Environmentally friendly	Waste products from tests should be sustainably made and easily disposable
D	Deliverable to end-user	Easily distributed to end-users that need them

Current techniques of water quality diagnostics and monitoring present several weaknesses. Among these techniques, a degree of expertise or expert training is required to carry out either the testing itself or interpret the data produced. This expertise usually comes in the form of a highly qualified technician operating the technology and analysing the data, involving time and associated labour costs. Cost is another common feature of current techniques used for the detection of waterborne pathogens, not only in the form of money spent for resources and expensive technology but also the amount of waste produced e.g., glassware, pipette tips, microscope slides, centrifuge tubes etc. This is further exacerbated by the large volumes of liquid in the form of samples and reagents to carry out traditional laboratory techniques.

For most current methodologies, tests can take up to one hour per sample and may take one to two days for total sample-in-result-out. In rapid real-life scenarios of pathogen disease outbreaks and environmental monitoring, this can lead to results becoming redundant before they are even available. Another important feature for the future of diagnostics not seen in most of the present techniques is portability. Many of the techniques used today require large or heavy equipment that cannot, or has not, currently been miniaturized for mobility purposes. This limits the usage of many of these techniques in laboratories and hospitals, often far from the areas or communities that most need them. Finally, the user-friendly output of the technology is rarely considered by developers with the public and untrained professionals in mind. This means that remote communities would have no way of using the technology that is usually situated so far from them even if they had it at their disposal. The development of future diagnostic technologies must focus on at least six important features. These are ease-of-use, simple data output, low-cost/waste, rapid detection time, portability of the device and small sample requirements/reagent use. Research and development over the last couple of decades in diagnostics have provided a possible solution for devices that can meet these criteria in the form of biosensors.

1.5. Biosensors

Biosensors are diagnostic devices capable of detecting biological molecules by measuring a signal from biological recognition events. Biosensors are these days ubiquitous within modern-day life and can be increasingly seen on the market e.g., glucose, lactate, and recently COVID-19 sensors. Some are even as readily available as in supermarkets such as the pregnancy test, exploiting paper-based lateral flow devices and ELISA assays with integrated electrical signal outputs for quantification. These devices can be used for many different purposes, some examples include food safety, drug detection, environmental monitoring, disease diagnostics, counterterrorism as well as detection of waterborne pathogens.

The general workflow of any simple biosensing device begins with the target analyte binding to the probe (bioreceptor) on the surface of a transducer. These bioreceptors can include nucleic acids such as DNA, RNA, synthetic analogues such as peptide nucleic acid (PNA) or locked nucleic acids (LNA) as well as proteins, nanoparticles, and even entire cells. The transducer will then convert the physical signal e.g., heat, mass, light etc. into an electrical signal which can be analysed, amplified, and displayed to a user interface (see Figure 1.3). There are four main categories of biosensor currently including optical, acoustic, electrochemical, and thermal (Bhalla *et al.*, 2016). This report will focus on the development of electrochemical biosensors.

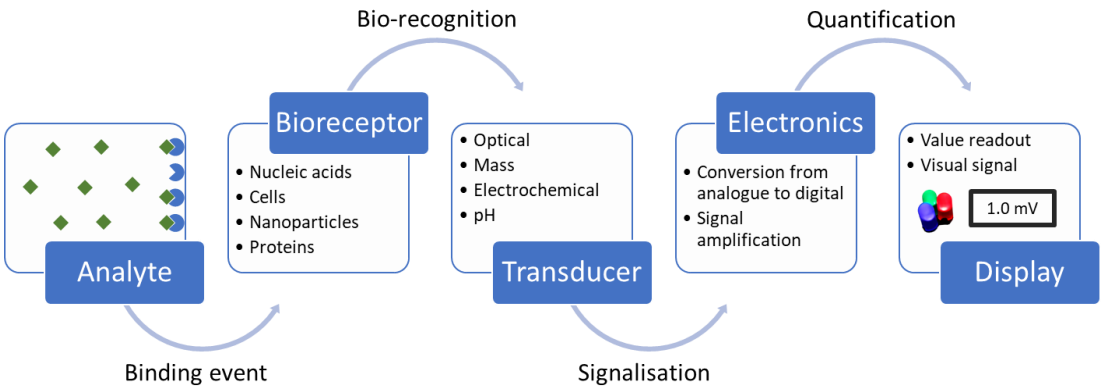

Figure 1.3. General workflow of a simplified biosensing device (adapted from Bhalla et al., 2016).

Electrochemical biosensors are devices that take advantage of the inherent charges of bioreceptors functionalized to the surface of a transducer and the molecules that bind to them. The sensing platform can then be immersed into a solution containing charged ions such as charged redox couples e.g., $[Fe(CN)_6]^{3-/4-}$ and $[Ru(NH_3)_6]^{2+/3+}$ (Schrattenecker *et al.*, 2019; Lee, Kim and Chung, 2021). This allows the study of electrical characteristics of various biological probe compounds on the surface as well as their interactions with other molecules. Electrochemical experiments for the development of biosensors typically use a 3-electrode cell configuration (see Figure 1.4) including a working electrode (WE), a reference electrode (RE) and a counter electrode (CE). This setup allows for the measurement of current travelling between the WE and CE, as well as the potential difference between the RE and the WE for analysis using both amperometric and potentiometric techniques.

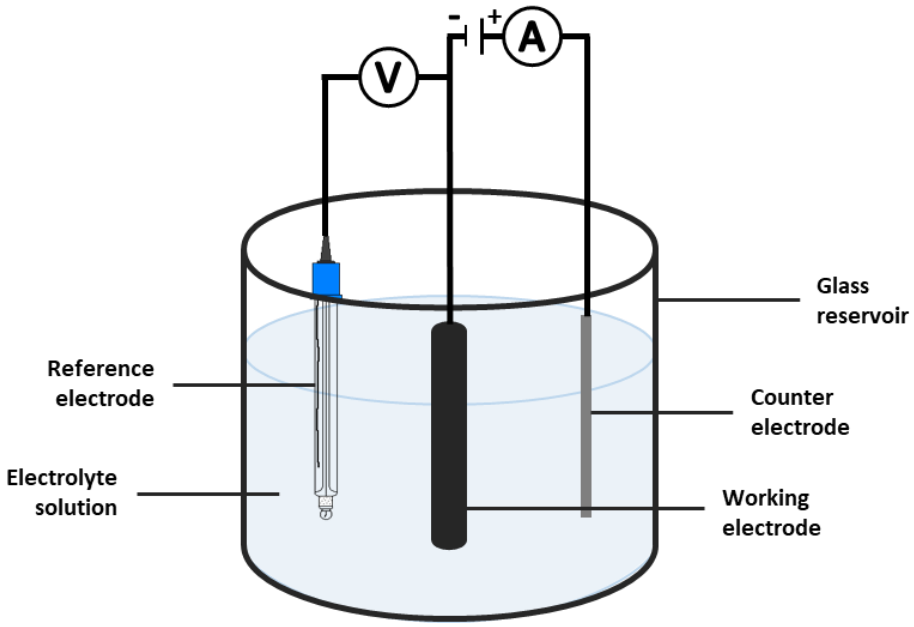

Figure 1.4. Typical 3-electrode cell setup with a working electrode usually made of Au, graphene and carbon, a reference electrode which may be Ag/AgCl, Hg/HgSO4 or SCE and a thin-wire Pt counter electrode.

Electrochemical biosensors have several advantages compared with their counterparts. Advantages of electrochemical biosensing systems include low limits of detection (LOD), a wide linear response ranges with many target molecules, superior self-assembled monolayer (SAM) stability and high reproducibility

(Faridbod, Gupta and Zamani, 2011). There are two key types of electrochemical biosensors seen in the literature regarding binding affinity studies, these are amperometric and potentiometric. Amperometric techniques involve the measurement of current relating to the oxidation and reduction potential of molecular species such as redox-capable ions in a solution (Elgrishi *et al.*, 2018a). While potentiometric techniques analyse the potential variation between the RE and WE to ascertain the behaviour of ions in solution when affected by biological molecules on the surface of the transducer (Pisoschi, 2016).

1.6. Electrochemical genosensors

Biosensing devices employing nucleic acids as probes for the detection of other nucleic acids, also known as electrochemical genosensors, take advantage of the biological phenomena first described by James Watson and Francis Crick (Watson and Crick, 1953). Genosensors employ immobilised probe oligonucleotides, which are small length sequences usually around 12-50 base pairs long, on the surface of a transducer with a particular property e.g., magnetic, optical, piezoelectric etc. (Jung *et al.*, 2016). The immobilization of that probe will provide a baseline signal depending on the transducer and analyte solution used. Upon successful hybridization of the DNA probe to the target DNA sequence, there will be a change in the signal that will be transduced into a measurable signal (see Figure 1.5) (Jolly et al., 2019).

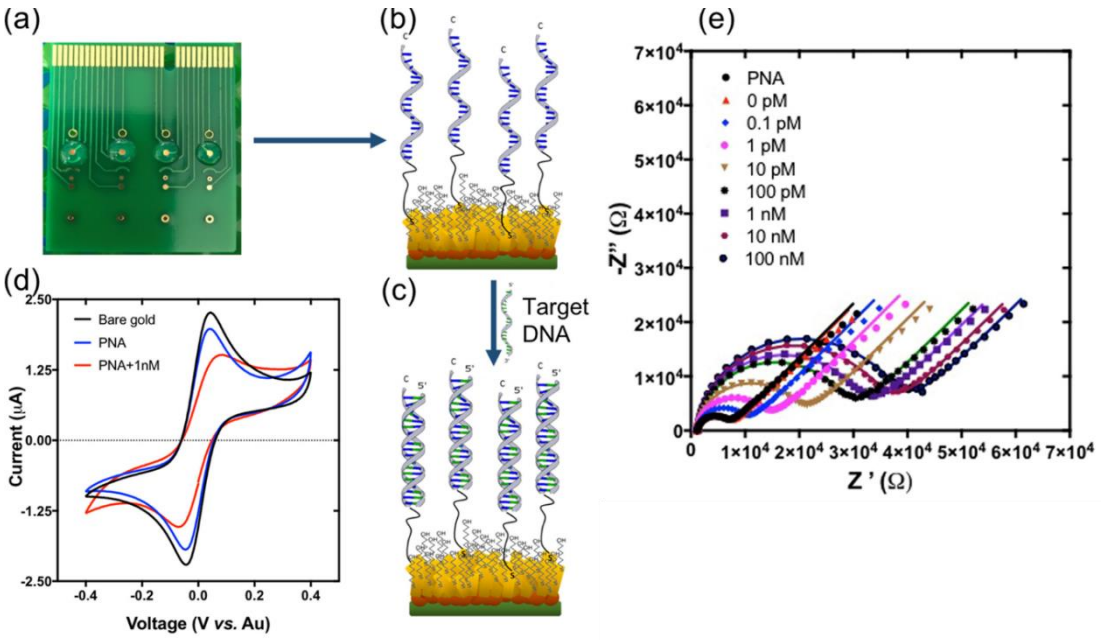

Figure 1.5. Example of an impedance-based genosensor implementing peptide nucleic acid probes functionalized to the gold electrode on a printed circuit board. Upon target hybridization with a surface-bound probe, both amperometric and potentiometric signal changes can be observed using cyclic voltammetry and electrochemical impedance spectroscopy (Jolly et al., 2019).

This can be done using a few different transducers, for example, quartz crystals can be utilized for their piezoelectrical properties, while gold disk electrodes can be used for their characteristic plasmon resonance and electrical transduction properties etc. Specifically, in electrochemical biosensors, it is also possible to take advantage of the inherent charge of nucleic acids. For example, a single monolayer of immobilized DNA oligonucleotides will give a measurable negative charge and upon hybridization with target DNA that negative charge will significantly increase with increasing target concentrations (Wu *et al.*, 2019). This is typically exploited in electrochemical biosensing methods to measure the resistance or capacitance of DNA monolayers or to analyse charge properties.

1.7. Synthetic nucleic acids as electrochemical probes

Within the last few decades, research has allowed for the development of synthetic analogues of DNA that can be used in the affinity-based detection of target nucleic acids such as DNA and RNA. Such examples of synthetic analogues of DNA include

peptide nucleic acid (PNA), locked nucleic acid (LNA) sometimes referred to as bridged nucleic acid (BNA), and glycol nucleic acid (GNA) (Jones, 1979; Taskova, Mantsiou and Astakhova, 2017). Each of these analogues have been developed for specific characteristics that make them preferable for certain biochemistry and biotechnology techniques. For example, locked nucleic acids (LNAs) contain various methylene bridge structural changes which lock the nucleic acids into a rigid bicyclic secondary structure that can enhance assay performance in certain instances (Latorra, Arar and Hurley, 2003; Ustuner, Lindsay and Estrela, 2021). Whereas glycol nucleic acids (GNAs) exhibit difference to DNA/RNA nucleic acids whereby their usual phosphate deoxyribose/ribose backbones are replaced by repeating glycol units linked by phosphodiester bonds. By doing so, Ueda *et al*. where able to develop a nucleic acid analogue that displayed more stable base pairing with higher thermostability (Ueda, Kawabata and Takemoto, 1971; Zhang, Peritz and Meggers, 2005).

One synthetic analogue of particular interest is peptide nucleic acids (PNAs), first termed as 'polyamide nucleic acids' (Nielsen *et al.*, 1991). As with GNA, PNA replaces the phosphate-sugar backbone, in this case by repeating units of N-(2-aminoethyl) glycine linked by methyl carbonyl (see Figure 1.6). By doing so, a molecule with a neutrally charged backbone is developed with higher binding affinity to complementary DNA/RNA sequences that form highly stable duplexes with high thermal resistance. Due to the neutral charge of PNA sequences, no electrostatic repulsion or steric hindrance is observed during hybridisation which is of particular interest for electrochemical genosensors (Pellestor and Paulasova, 2004; Jolly et al., 2019). Additionally, because of the peptide backbone of PNA, sequences are less sensitive to enzymatic degradation and even resistant to collateral cleavage during reactions involving CRISPR/Cas enzymes (Najjar, Rainbow, Sharma Timilsina, *et al.*, 2022a).

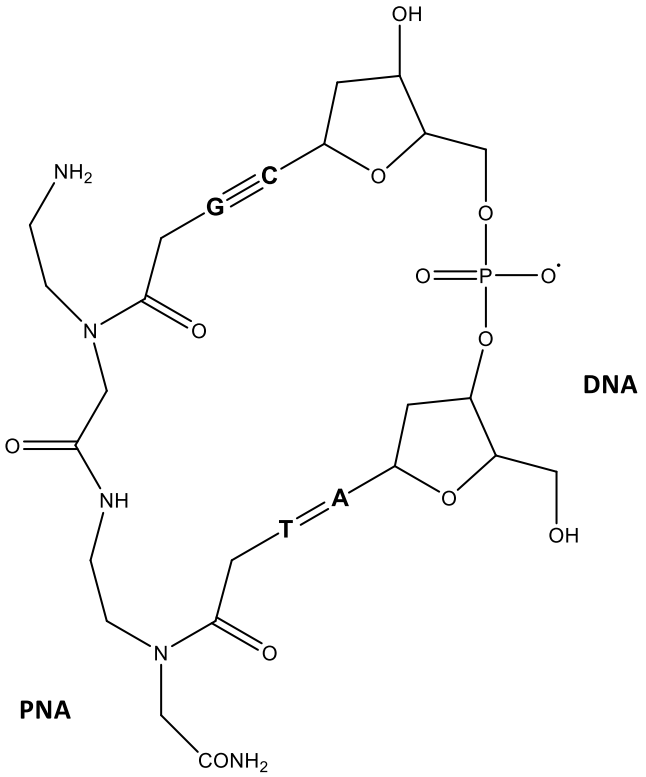

Figure 1.6. Chemical structures of peptide nucleic acid (PNA) and deoxyribose nucleic acid (DNA) in hybridised confirmation. With PNA molecules the C-terminus (characterised by the $CONH_2$ group) binds to the 5' end of DNA, while the N-terminus (characterised by the NH_2 group) binds to the 3' end.

1.8. Project overview

This thesis is an outcome of the project entitled "Integrated Biosensing Platform for Waterborne Pathogen Detection: Improving Public Health" funded by the Natural Environment Research Council GW4 Freshwater CDT focusing on solving issues associated with freshwater environmental pollution. The primary focus of this project is the development of a biosensor capable of implementing nucleic acid molecules for sensitive and selective detection of waterborne pathogens through the detection of their specific genetic code. Key fields of research explored in this project include surface chemistry, nanotechnology, material characterisation, electrochemical detection, electrochemical signal amplification, and microfluidics. The main aim of the thesis is to develop an integrated DNA-based biosensor for sensitive and selective detection of a waterborne pathogen. The objectives can be broadly separated into four different areas of biosensor development: optimisation

of nucleic acid-based surface chemistry on gold, signal amplification using chemical intercalator molecules, pathogen detection using CRISPR-related diagnostic techniques and integration with off-the-shelf components and microfluidics.

The key points to be highlighted in this thesis are:

1. Characterisation of DNA-based probe molecules by thiol surface chemistry to gold electrode surfaces for detection of *E. Coli* DNA.
2. Amplification of impedimetric and amperometric signal through intercalation of a novel redox-active chemical sensitiser molecule.
3. Development of electrochemical CRISPR-based detection platforms for highly sensitive and specific detection of SARS-CoV-2 viral RNA.
4. Integration of off-the-shelf components using microfluidics with a biosensor device.

1.8.1. Outline of thesis

When fabricating biosensor devices for the detection of pathogens in fresh- and wastewater, it is important to understand the complexity of developing devices for point-of-care purposes. Chapter 1 of this thesis has introduced water as a resource and its importance, pathogen pollution of freshwater systems, water-based diagnostics and monitoring, the biomarkers that are available to enable the detection of waterborne pathogens and an introduction to electrochemical genosensors. The project aims and objectives have also been outlined. In chapter 2, the theory of the various methods and techniques used in this thesis will be described in detail. The chapter will outline the electrode platform used within this thesis. It will also look at surface pre-treatment techniques for improving surface chemistry immobilisation on reusable gold electrode surfaces. Electrochemical detection methods will be described with detail towards electrochemical impedance spectroscopy (EIS) and amperometric techniques used in this thesis. Background theory on nucleic acid intercalation, DNA amplification techniques and CRISPR-Cas technology will also be discussed.

Chapter 3 presents the optimisation of surface chemistry for the development of a DNA-based biosensor to detect *E. coli* target DNA material. A thiol-functionalized DNA probe was utilised alongside 6-mercapto-1-hexanol (MCH) to develop a stable and highly reproducible self-assembled monolayer on gold disk electrodes. This chapter specifically looks at the importance of charge probe molecule interspersion to allow for sensitive detection while mitigating electrochemical phenomena such as steric hindrance by over-crowding. Chapter 4 presents a case study of nucleic acid intercalation implementing a novel compound called cobalt-aqphen, $[Co(GA)_2(aqphen)]Cl$, which is investigated for its soluble and redox-active properties to amplify signal detection in DNA-based biosensor devices. Various methods of testing the solubility of the intercalator are described as well as electrochemical characterisation of the different methods of intercalating the compound between the dsDNA.

Chapter 5 presents a study related to the development of a biosensing device implementing the CRISPR-Cas diagnostic technology SHERLOCK to detect SARS-CoV-2 viral RNA and *E. Coli* genomic DNA. This chapter describes the application of Cas12a in the collateral cleavage of DNA reporters in solution with a pre-amplification step by loop-mediated isothermal amplification (LAMP). This study further employs an antifouling highly conductive graphene-based surface coating, and peptide nucleic acid (PNA) probes for an integrated approach to amperometric labelled biosensing. Due to the outbreak of the COVID-19 pandemic during this work, the research focus was redirected to the detection of SARS-CoV-2 viral RNA instead of *E. Coli* genomic DNA. Finally, chapter 6 will conclude the overall thesis and discuss future directions that could be further explored based on the findings in this thesis.

Figure 1.7 displays the various areas of research involved within this thesis and the experimental research involved. As can be seen, the research involved in this thesis is inherently interdisciplinary and involved knowledge and understanding of multiple fields from biochemistry and microbiology to electrochemistry and microfabrication. The work in this thesis addresses several aspects of the overall system that we aimed

to develop which with further work will lead to the development of a full point-of-care (PoC) of on-site diagnostic device in further work.

Figure 1.7. Research themes and disciplines included in this thesis throughout the various experimental projects, the chapters involved in each research area are displayed.

References

Ashipala, N. and Armitage, N.P. (2011) 'Impediments to the adoption of alternative sewerage in South African urban informal settlements', *Water Science and Technology*, 64(9), pp. 1781–1789. Available at: https://doi.org/10.2166/wst.2011.746.

Azeredo, J. *et al.* (2017) 'Critical review on biofilm methods', *Taylor & Francis*, 43(3), pp. 313–351. Available at: https://doi.org/10.1080/1040841X.2016.1208146.

van Baarlen, P. *et al.* (2007) 'Molecular mechanisms of pathogenicity: how do pathogenic microorganisms develop cross-kingdom host jumps?', *FEMS Microbiology Reviews*, 31(3), pp. 239–277. Available at: https://doi.org/10.1111/j.1574-6976.2007.00065.x.

Bhalla, N. *et al.* (2016) 'Introduction to biosensors', *Essays in Biochemistry*. Edited by P. Estrela, 60(1), pp. 1–8. Available at: https://doi.org/10.1042/EBC20150001.

Bloom, D.E., Black, S. and Rappuoli, R. (2017) 'Emerging infectious diseases: A proactive approach', *Proceedings of the National Academy of Sciences of the United States of America*, 114(16), pp. 4055–4059. Available at: https://doi.org/10.1073/PNAS.1701410114/ASSET/9605D5BA-3DAC-4F84-B8F0-40284C4D0E5F/ASSETS/GRAPHIC/PNAS.1701410114FIG03.JPEG.

Bridgeman, J. *et al.* (2015) 'Portable LED fluorescence instrumentation for the rapid assessment of potable water quality', *Science of The Total Environment*, 524–525, pp. 338–346. Available at: https://doi.org/https://doi.org/10.1016/j.scitotenv.2015.04.050.

Chirisa, I. *et al.* (2017) 'Decentralized domestic wastewater systems in developing countries: the case study of Harare (Zimbabwe)', *Applied Water Science*, 7(3), pp. 1069–1078. Available at: https://doi.org/10.1007/s13201-016-0377-4.

Ejeian, F. *et al.* (2018) 'Biosensors for wastewater monitoring: A review', *Biosensors and Bioelectronics*, 118, pp. 66–79. Available at: https://doi.org/https://doi.org/10.1016/j.bios.2018.07.019.

Elgrishi, N. *et al.* (2018) 'A Practical Beginner's Guide to Cyclic Voltammetry', *Journal of Chemical Education*, 95(2), pp. 197–206. Available at: https://doi.org/10.1021/acs.jchemed.7b00361.

Ellis, K. *et al.* (2018) 'Understanding the costs of investigating coliform and E. coli detections during routine drinking water quality monitoring', *Urban Water Journal*, 15(2), pp. 101–108. Available at: https://doi.org/10.1080/1573062X.2017.1398762.

European Food Safety Authority (2011) 'Shiga toxin-producing E. coli (STEC) O104:H4 2011 outbreaks in Europe: Taking Stock', *EFSA Journal*, 9(10). Available at: https://doi.org/10.2903/J.EFSA.2011.2390.

Faridbod, F., Gupta, V.K. and Zamani, H.A. (2011) 'Electrochemical Sensors and Biosensors', *International Journal of Electrochemistry*, 2011, p. 352546. Available at: https://doi.org/10.4061/2011/352546.

Federspiel, F. and Ali, M. (2018) 'The cholera outbreak in Yemen: Lessons learned and way forward', *BMC Public Health*, 18(1), pp. 1–8. Available at: https://doi.org/10.1186/S12889-018-6227-6/TABLES/1.

Gill, E.E. *et al.* (2018) 'High-throughput detection of RNA processing in bacteria', *BMC Genomics*, 19(1). Available at: https://doi.org/10.1186/S12864-018-4538-8.

Hughes, R. (2008) 'Patient safety and quality: An evidence-based handbook for nurses'. Available at: https://books.google.co.uk/books?hl=en&lr=&id=QFg_YnoXR6IC&oi=fnd&pg=PA1&dq=Collins,+A.S.,+2008.+Preventing+health+care%E2%80%93associated+infections.+In+Patient+safety+and+quality:+an+evidence-based+handbook+for+nurses.+Agency+for+Healthcare+Research+and+Quality+(US).&ots=F5Nbs5IxlJ&sig=OHfWjXaWjuRrF6gx8XACsDcd5O4 (Accessed: 26 September 2022).

Huremović, D. (2019) 'Brief History of Pandemics (Pandemics Throughout History)', *Psychiatry of Pandemics*, p. 7. Available at: https://doi.org/10.1007/978-3-030-15346-5_2.

Janda, J.M. and Abbott, S.L. (2007) '16S rRNA gene sequencing for bacterial identification in the diagnostic laboratory: Pluses, perils, and pitfalls', *Journal of Clinical Microbiology*, 45(9), pp. 2761–2764. Available at: https://doi.org/10.1128/JCM.01228-07.

Johnson, T.J. and Nolan, L.K. (2009) ' Pathogenomics of the Virulence Plasmids of Escherichia coli ', *Microbiology and Molecular Biology Reviews*, 73(4), pp. 750–774. Available at: https://doi.org/10.1128/MMBR.00015-09.

Johnston, M. *et al.* (2022) 'Multiplexed biosensor for point-of-care COVID-19 monitoring: CRISPR-powered unamplified RNA diagnostics and protein-based therapeutic drug management', *medRxiv*, p. 2022.03.30.22271928. Available at: https://doi.org/10.1101/2022.03.30.22271928.

Jolly, Pawan *et al.* (2019) 'A PNA-based Lab-on-PCB diagnostic platform for rapid and high sensitivity DNA quantification', *Biosensors and Bioelectronics*, 123, pp. 244–250. Available at: https://doi.org/10.1016/J.BIOS.2018.09.006.

Jones, A.S. (1979) 'Synthetic analogues of nucleic acids — a review', *International Journal of Biological Macromolecules*, 1(5), pp. 194–207. Available at: https://doi.org/10.1016/0141-8130(79)90013-8.

Jung, I.Y. *et al.* (2016) 'Oligonucleotide-based biosensors for in vitro diagnostics and environmental hazard detection', *Analytical and bioanalytical chemistry.* Heidelberg :, pp. 2383–2406. Available at: https://doi.org/10.1007/s00216-015-9212-2.

Karpouzoglou, T. and Zimmer, A. (2016) 'Ways of knowing the wastewaterscape: Urban political ecology and the politics of wastewater in Delhi, India', *Habitat International*, 54, pp. 150–160. Available at: https://doi.org/https://doi.org/10.1016/j.habitatint.2015.12.024.

King, L.A. *et al.* (2012) 'Outbreak of Shiga Toxin–Producing Escherichia coli O104:H4 Associated With Organic Fenugreek Sprouts, France, June 2011', *Clinical Infectious Diseases*, 54(11), pp. 1588–1594. Available at: https://doi.org/10.1093/CID/CIS255.

Kumar, N. *et al.* (2018) 'Emerging biosensor platforms for the assessment of water-borne pathogens', *Analyst*, 143(2), pp. 359–373. Available at: https://doi.org/10.1039/C7AN00983F.

Land, K.J. *et al.* (2019) 'REASSURED diagnostics to inform disease control strategies, strengthen health systems and improve patient outcomes', *Nature microbiology*. 2018/12/13, 4(1), pp. 46–54. Available at: https://doi.org/10.1038/s41564-018-0295-3.

Latorra, D., Arar, K. and Hurley, J.M. (2003) 'Design considerations and effects of LNA in PCR primers', *Molecular and Cellular Probes*, 17(5), pp. 253–259. Available at: https://doi.org/10.1016/S0890-8508(03)00062-8.

Lee, S., Kim, W.J. and Chung, M. (2021) 'Enhanced electrochemical biosensing on gold electrodes with a ferri/ferrocyanide redox couple', *Analyst*, 146(17), pp. 5236–5244. Available at: https://doi.org/10.1039/D1AN00952D.

Leme, E. *et al.* (2018) 'Billings reservoir water used for human consumption presents microbiological contaminants and induces both behavior impairments and astrogliosis in zebrafish', *Ecotoxicology and Environmental Safety*, 161, pp. 364–373. Available at: https://doi.org/https://doi.org/10.1016/j.ecoenv.2018.06.009.

Mabey, D. *et al.* (2004) 'Diagnostics for the developing world', *Nature Reviews Microbiology*, 2(3), pp. 231–240. Available at: https://doi.org/10.1038/nrmicro841.

Michaud, C.M. (2009) 'Global Burden of Infectious Diseases', *Encyclopedia of Microbiology*, p. 444. Available at: https://doi.org/10.1016/B978-012373944-5.00185-1.

'Microbiology by numbers' (2011) *Nature Reviews Microbiology*, 9(9), p. 628. Available at: https://doi.org/10.1038/nrmicro2644.

Najjar, D. *et al.* (2022) 'A lab-on-a-chip for the concurrent electrochemical detection of SARS-CoV-2 RNA and anti-SARS-CoV-2 antibodies in saliva and plasma', *Nature Biomedical Engineering 2022*, pp. 1–11. Available at: https://doi.org/10.1038/s41551-022-00919-w.

Nielsen, P.E. *et al.* (1991) 'Sequence-Selective Recognition of DNA by Strand Displacement with a Thymine-Substituted Polyamide', *Science*, 254(5037), pp. 1497–1500. Available at: https://doi.org/10.1126/SCIENCE.1962210.

Orsi, R.H. *et al.* (2007) 'Genetic variability and pathogenicity potential of Escherichia coli isolated from recreational water reservoirs', *Research in Microbiology*, 158(5), pp. 420–427. Available at: https://doi.org/https://doi.org/10.1016/j.resmic.2007.02.009.

Palanca-Tan, R. (2017) 'Health and water quality benefits of alternative sewerage systems in Metro Manila, Philippines', *Environment and Urbanization*, 29(2), pp. 567–580. Available at: https://doi.org/10.1177/0956247817718402.

Pandey, P.K. *et al.* (2014) 'Contamination of water resources by pathogenic bacteria', *AMB Express*, 4(1), p. 51. Available at: https://doi.org/10.1186/s13568-014-0051-x.

Paneth, N. *et al.* (1998) 'A rivalry of foulness: official and unofficial investigations of the London cholera epidemic of 1854.', *American Journal of Public Health*, 88(10), p. 1545. Available at: https://doi.org/10.2105/AJPH.88.10.1545.

Pellestor, F. and Paulasova, P. (2004) 'The peptide nucleic acids (PNAs), powerful tools for molecular genetics and cytogenetics', *European Journal of Human Genetics 2004 12:9*, 12(9), pp. 694–700. Available at: https://doi.org/10.1038/sj.ejhg.5201226.

Pisoschi, A.M. (2016) 'Potentiometric Biosensors: Concept and Analytical Applications-An Editorial', *Biochemistry & Analytical Biochemistry*, 5(3). Available at: https://doi.org/10.4172/2161-1009.1000e164.

Rainbow, J. *et al.* (2020) 'Integrated Electrochemical Biosensors for Detection of Waterborne Pathogens in Low-Resource Settings', *Biosensors.* Basel, Switzerland :, p. 36. Available at: https://doi.org/10.3390/bios10040036.

Rajapaksha, P. *et al.* (2019) 'A review of methods for the detection of pathogenic microorganisms', *Analyst*, 144(2), pp. 396–411. Available at: https://doi.org/10.1039/C8AN01488D.

Ramírez-Castillo, F.Y. *et al.* (2015) 'Waterborne Pathogens: Detection Methods and Challenges', *Pathogens* . Available at: https://doi.org/10.3390/pathogens4020307.

Raschid-Sally, L. (2010) 'The role and place of global surveys for assessing wastewater irrigation', *Irrigation and Drainage Systems*, 24(1), pp. 5–21. Available at: https://doi.org/10.1007/s10795-009-9092-8.

Schrattenecker, J.D. *et al.* (2019) 'Hexaammineruthenium (II)/(III) as alternative redox-probe to Hexacyanoferrat (II)/(III) for stable impedimetric biosensing with gold electrodes', *Biosensors and Bioelectronics*, 127, pp. 25–30. Available at: https://doi.org/https://doi.org/10.1016/j.bios.2018.12.007.

Selim, L. (2021) *4 things you need to know about water and famine*, *Unicef*. Available at: https://www.unicef.org/stories/4-things-you-need-know-about-water-and-famine (Accessed: 24 January 2022).

Shanks, O.C. *et al.* (2007) 'Identification of bacterial DNA markers for the detection of human fecal pollution in water', *Applied and Environmental Microbiology*, 73(8), pp. 2416–2422. Available at: https://doi.org/10.1128/AEM.02474-06.

Taskova, M., Mantsiou, A. and Astakhova, K. (2017) 'Synthetic Nucleic Acid Analogues in Gene Therapy: An Update for Peptide–Oligonucleotide Conjugates', *ChemBioChem*, 18(17), pp. 1671–1682. Available at: https://doi.org/10.1002/CBIC.201700229.

Troeger, C. *et al.* (2017) 'Estimates of global, regional, and national morbidity, mortality, and aetiologies of diarrhoeal diseases: a systematic analysis for the Global Burden of Disease Study 2015', *The Lancet Infectious Diseases*, 17(9), pp. 909–948. Available at: https://doi.org/https://doi.org/10.1016/S1473-3099(17)30276-1.

Ueda, N., Kawabata, T. and Takemoto, K. (1971) 'Synthesis of N-(2,3-dihydroxypropyl) derivatives of nucleic bases', *Journal of Heterocyclic Chemistry*, 8(5), pp. 827–829. Available at: https://doi.org/10.1002/JHET.5570080527.

Ustuner, S., Lindsay, M.A. and Estrela, P. (2021) 'Pre-concentration of microRNAs by LNA-modified magnetic beads for enhancement of electrochemical detection',

Scientific Reports 2021 11:1, 11(1), pp. 1–10. Available at: https://doi.org/10.1038/s41598-021-99145-8.

Ward, J.S. (2021) 'Investigating novel approaches for detecting microbial contamination in drinking water in Africa'. University of Surrey.

Ward, J.S.T. *et al.* (2020) 'Large-scale survey of seasonal drinking water quality in Malawi using in situ tryptophan-like fluorescence and conventional water quality indicators', *Science of The Total Environment*, 744, p. 140674. Available at: https://doi.org/https://doi.org/10.1016/j.scitotenv.2020.140674.

Watson, J.D. and Crick, F.H.C. (1953) 'Molecular Structure of Nucleic Acids: A Structure for Deoxyribose Nucleic Acid', *Nature*, 171(4356), pp. 737–738. Available at: https://doi.org/10.1038/171737a0.

World Health Organization (2006) 'Excreta and greywater in agriculture', in *Guidelines for the Safe Use of Wastewater, Excreta, Greywater.* Volume IV. World Health Organization, p. 204.

World Health Organization (2013) *Ending preventable deaths from pneumonia and diarrhoea by 2025*. Available at: https://www.who.int/news/item/10-04-2013-ending-preventable-deaths-from-pneumonia-and-diarrhoea-by-2025 (Accessed: 24 January 2022).

World Health Organization (2019) *Drinking-water*. Available at: https://www.who.int/news-room/fact-sheets/detail/drinking-water (Accessed: 24 January 2022).

World Health Organization (2020) *The top 10 causes of death*. Available at: https://www.who.int/news-room/fact-sheets/detail/the-top-10-causes-of-death (Accessed: 24 January 2022).

Wu, Q. *et al.* (2019) 'Review of Electrochemical DNA Biosensors for Detecting Food Borne Pathogens', *Sensors* . Available at: https://doi.org/10.3390/s19224916.

Wurpel, D.J. *et al.* (2013) 'Chaperone-Usher Fimbriae of Escherichia coli', *PLoS ONE*, 8(1). Available at: https://doi.org/10.1371/JOURNAL.PONE.0052835.

Yu, X. *et al.* (2018) 'Whole-bacterium SELEX of DNA aptamers for rapid detection of E.coli O157:H7 using a QCM sensor', *Journal of Biotechnology*, 266, pp. 39–49. Available at: https://doi.org/10.1016/J.JBIOTEC.2017.12.011.

Zachary, J.F. (2017) 'Mechanisms of Microbial Infections', *Pathologic Basis of Veterinary Disease*, p. 132. Available at: https://doi.org/10.1016/B978-0-323-35775-3.00004-7.

Zhang, L., Peritz, A. and Meggers, E. (2005) 'A simple glycol nucleic acid', *Journal of the American Chemical Society*, 127(12), pp. 4174–4175. Available at: https://doi.org/10.1021/JA042564Z/SUPPL_FILE/JA042564ZSI20050216_104828.PDF.

2. Methods and Materials

This chapter will cover the theory behind the methods and techniques used within this thesis, specifically it will detail various electrochemical techniques including amperometric, potentiometric and impedimetric used in this thesis for optimisation, characterisation, and diagnostic purposes. Transducer platforms will also be explored such as standard working electrodes, printed circuit boards and evaporated gold electrodes and the various pros and cons of each of these options. Electrode pre-treatment techniques will be discussed relating to different transducer types and surface chemistry requirements. Different techniques of surface modification of probe molecules will be discussed, including thiol and amine-based chemistries as well as conductive polymers. Finally, nucleic acid intercalation and amplification methods will be outlined, specifically applications for DNA intercalation in post-signal amplification and the use of nucleic acid amplification techniques for sample pre-concentration in point-of-care and on-site devices.

2.1. Electrochemical Techniques

To fully exploit the kind of data that results from electrochemical biosensor measurements, it is important to understand the electrochemical environment around the electrode/electrolyte interface. This section will explore the electrochemical environment and how it plays an important role in the measurement of surface modifications and analyte interactions. Various transducer platforms that are commonly used within electrochemical biosensing will also be briefly discussed, as well as the surface pre-treatments used to prepare an electrode for surface modification. Finally, the techniques that have been used for characterisation and measurement of analytes will be described.

2.1.1. The electrochemical environment

Electrochemical methods can be described as those that measure the relationship between electrodes and electrolytes and the respective electrical and chemical properties and effects. Electrochemical processes of interest are therefore predominantly controlled by the electrode surface and bulk electrolyte interface

(Bard and Faulkner, 2001). In terms of applications for biosensors, having the process of interest occurring in proximity of the electrode/electrolyte interface is beneficial. This is due to higher sensitivity, higher control over surface modification of probe molecules and smaller reagent requirements. Within an electrochemical cell, the main point of interest for electrochemists is the surface of the working electrode (WE). By manipulating the potential applied at the WE surface, it is possible for electrochemists to influence the movement of electrons between the electrode surface and bulk electrolyte. For example, by interfacing gold as an electrode surface and the redox marker $[Fe(CN)_6]^{3-/4-}$ in the bulk electrolyte it is possible to influence the movement of electrons between the interface. When a more negative potential is applied at the surface of the gold, electrons achieve a higher energy level and are then capable of leaving the gold electrode surface to the $[Fe(CN)_6]^{3-/4-}$ electrolyte (reduction). Thus, when a more positive potential is applied the opposite occurs from the bulk electrolyte to the electrode surface (oxidation). Meaning that upon application of a more negative potential, $[Fe(CN)_6]^{3-}$ becomes $[Fe(CN)_6]^{4-}$ and the opposite occurs when applying a more positive potential. This movement of electrons between the electrode surface and the bulk electrolyte is known as Faradaic current. Any Faradaic current will adhere to Faraday's law given by the following equation:

$$i = nF$$

Where, the current (*i)* is directly proportional to the number of electrons (*n*) and the Faraday Constant (F) (Bard and Faulkner, 2001). Another form of current is also commonly seen in electrochemistry, known as non-Faradaic current. This form of current does not exhibit any back-and-forth electron flow and so leads to accumulation of charge at the electrode surface, causing a phenomenon known as electrode polarization. In electrochemistry, polarization refers to a diminishing potential difference between the electrode surface and the bulk electrolyte during the flow of electrons.

Within an electrolyte solution, an applied potential at the electrode surface causes rearrangement of the mobile charged ions within the electrolyte in proximity of the electrode surface. This occurs to counter the electrode surface potential, forming

what is known as the electrical double layer (DL) (Bard and Faulkner, 2001). The electrical double layer was first illustrated by the Helmholtz model which described the interface between a metal surface and electrolyte solution, however, this only accurately describes situations that involve high ionic concentrations. At the beginning of the last century, the interface between metal and electrolyte solution as it related to the electrical DL was re-imagined by the Gouy-Chapman theory which explained the behaviour at low ion concentrations (Schmickler, 2014). The electrical DL was best modelled and described by Otto Stern in 1924, combining the two previous models (see Figure 2.1).

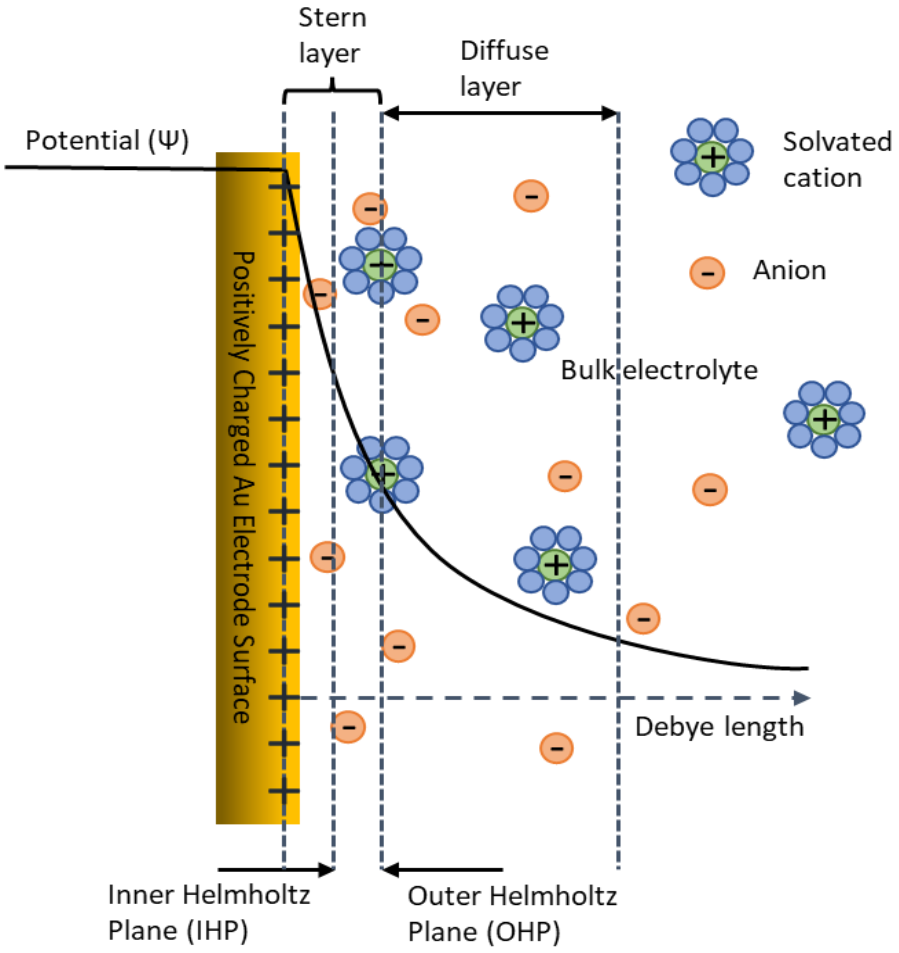

Figure 2.1. Schematic of the electrical double layer according to the Gouy-Chapman-Stern model (adapted from Bard and Faulkner, 2001).

In Stern's model of the electrical DL, the electrode is immersed in a charged electrolyte solution to produce an electric field and displays a row of specifically adsorbed ions. The region between the electrode surface and the centre of these

specifically adsorbed ions is known as the Inner Helmholtz Plane (IHP). Outside of the IHP, ions diffuse to the electrode surface to electrostatic interaction, however they do not adsorb to the surface as they are still solvated and so are termed non-specifically adsorbed. This region of non-specifically adsorbed molecules is known as the Outer Helmholtz Plane (OHP), and alongside the IHP are together known as the Stern layer. Any molecules outside of the Stern layer are unable to overcome the overall charges and instead form an ion cloud known simply as the diffuse layer. It is also worth mentioning that there is an observable effect on the electrical potential as distance increased from the electrode surface to the bulk electrolyte. Between the electrode surface and the IHP, potential is shown to decrease almost linearly. However, upon reaching the diffuse layer the observable decrease in potential occurs exponentially. Additionally, due to the two Helmholtz planes forming a double layer it is possible to observe capacitance, often termed 'double layer capacitance' (C_{dl}). The C_{dl} consists of two capacitances, the first being that of the Stern layer or the 'Stern capacitance' and the second consisting of the diffuse layer capacitance.

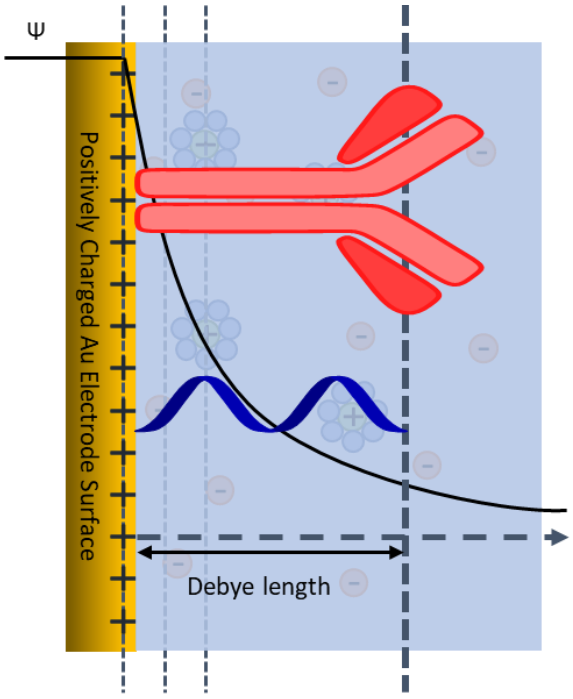

Figure 2.2. Difference in surface functionalised probe molecules with respect to the electrical double layer and Debye length.

Another important component of the Gouy-Chapman-Stern model is the region between the OHP and the maximum point at which ions are no longer affected by electrostatic attraction to the electrode surface called the Debye length (λ_D). The Debye length is directly proportional to the thickness of the diffuse layer and in potentiometric and impedance-based devices play a major role in sensitivity and limit of detection (LOD) (Bard and Faulkner, 2001). The Debye length has also been defined as the characteristic distance exhibiting decay in system potential from the electrode surface through electrolyte solutions (Kesler, Murmann and Soh, 2020). In normal physiologically relevant electrolyte concentrations (150 mM) the Debye length is approximately 0.7 nm, significantly smaller than several molecules including nucleotides (1.0 nm), DNA helices (10 nm) and certain protein molecules including antigens and antibodies (≈10 nm) (Chen *et al.*, 2019) (see Figure 2.2). Additionally, many biomolecules have an inherent charge, such as DNA having a negative charge due to its phosphate containing backbone. In 2007, it was demonstrated that surface bound molecules such as DNA or proteins will become surrounded by ions of the opposite charge once placed within an electrolyte due to electrostatic interactions (Stern *et al.*, 2007). This is termed the Debye screening effect, leading to the exponential decrease in electrostatic potential from charges on the biomolecule further from the electrode surface (Bhattacharyya and Shalev, 2020). Debye length can be expressed by the following equation:

$$\lambda_D = \sqrt{\frac{\varepsilon_0 \varepsilon_r kT}{2N_A q^2 I}}$$

Where, ε_0 is the permittivity of free space, ε_r is the permittivity of dielectric constant of the solution, k is Boltzmann constant, T is temperature, N_A is Avogadro's constant, q is the electron charge, and I is ionic strength of the electrolyte. Ionic strength of the electrolyte can then be further expressed by:

$$I = \frac{1}{2}\sum_j c_j z_j^2$$

Where, c_j is the concentration of ion j and z_j is the concentration of the j^{th} ionic species. Meaning that the Debye length is inversely proportional to the square root

of the ionic strength of the electrolyte solution. It is important when designing a biosensor that the ionic strength of the electrolyte solution does not unnecessarily reduce sensitivity and is advantageous to work with surface modifications within the Debye length.

2.1.2. Electrode surface pre-treatments

The primary electrode surface used in this thesis consisted of polycrystalline gold electrodes for biomolecule functionalisation using thiol modifiers for surface attachment. To achieve successful surface functionalisation of thiolated biomolecular probes a clean and smooth surface is required (Fischer *et al.*, 2009). To achieve this with electrodes that are re-used with previously bound thiols, several cleaning techniques are required to effectively regenerate the surface. These techniques include pre-treatment, mechanical, chemical, and electrochemical polishing as well as post-treatments to prevent surface oxide monolayers formed by the highly oxidative cleaning methods (Tkac and Davis, 2008).

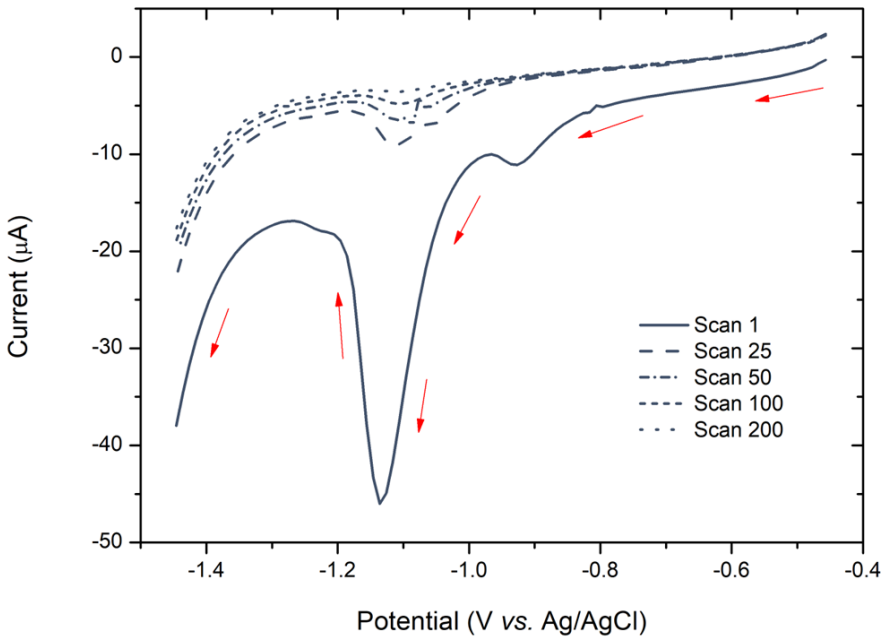

Figure 2.3. A cyclic voltammogram showing reductive desorption of C_6SH/MCH co-SAM in 100 mM NaOH aqueous solution. Potential range was from -1.45 to -0.45 V with a scan rate of 1.0 V/s.

As previously mentioned, the polycrystalline gold electrode surfaces used in this thesis are reused and routinely functionalised with thiol-based self-assembled monolayers (SAMs). The first step of gold electrode cleaning requires removal of previously bound alkanethiols. A pre-treatment technique called reductive thiol desorption is used for this, whereby an electrode is immersed in NaOH solution, and a potential range applied between -1.45 V and -0.45 V to electrochemically reduce the thiols from the surface (see Figure 2.3). This reductive cycling technique removes all trace of previously bound short chain thiol linkers and thiolated biomolecules (see Figure 2.4).

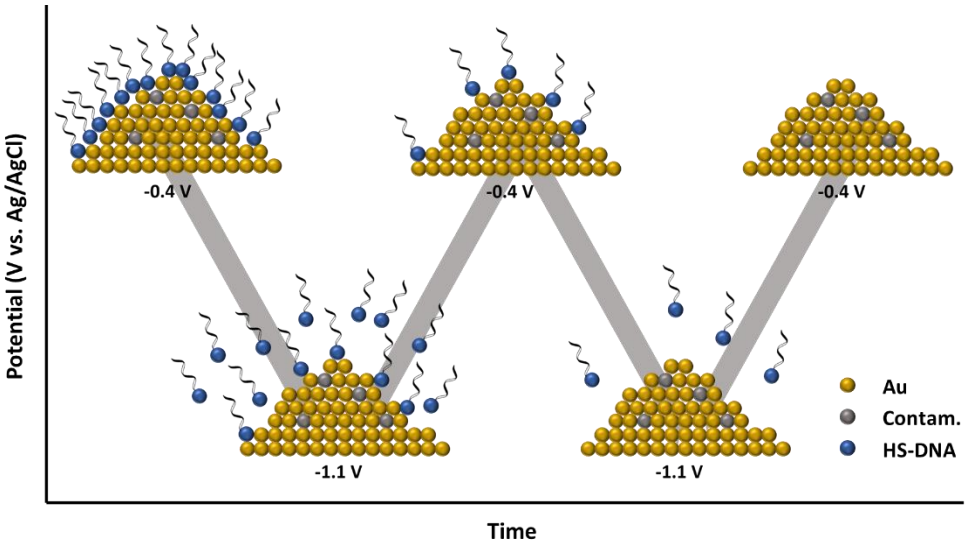

Figure 2.4. Schematic showing the thiol stripping process on the surface of gold electrodes in NaOH aqueous solution. Process is shown at the atomic level with spheres representing Au, organic and inorganic contaminants and thiolated DNA molecules.

Once all previously bound thiols are removed, electrodes are mechanically polished using a slurry containing 0.05 µm alumina particles in a figure of eight pattern to achieve a heterogenous polish. This was followed by a chemical pre-treatment consisting of dipping the gold surface into piranha solution, also known as Caro's acid, containing concentrated sulphuric acid (H_2SO_4) and hydrogen peroxide solution (H_2O_2). This is done to chemically dissolve any organic residues or contaminants from the electrode surface and can be represented by the following formula:

$$H_2SO_4 + H_2O_2 \rightarrow H_3O^+ + HSO_4^- + O^\bullet$$

Electrochemical polishing (E_p) is the oxidation and reduction of the electrode surface to clean difficult-to-remove contaminants and to return the electrode surface to a smoother geometry. This is done by immersing the electrode into diluted sulphuric acid aqueous solution and cycling the potential to oxidise and reduce the gold (see Figure 2.5). In polycrystalline gold electrodes, three characteristic peaks can be observed from a cyclic voltammogram after electrochemical polishing. These peaks represent separate domains of the gold surface and can be found at 1.1 V Au (100), 1.2 V Au (110) and 1.3 V Au (111) on a cleaned electrode.

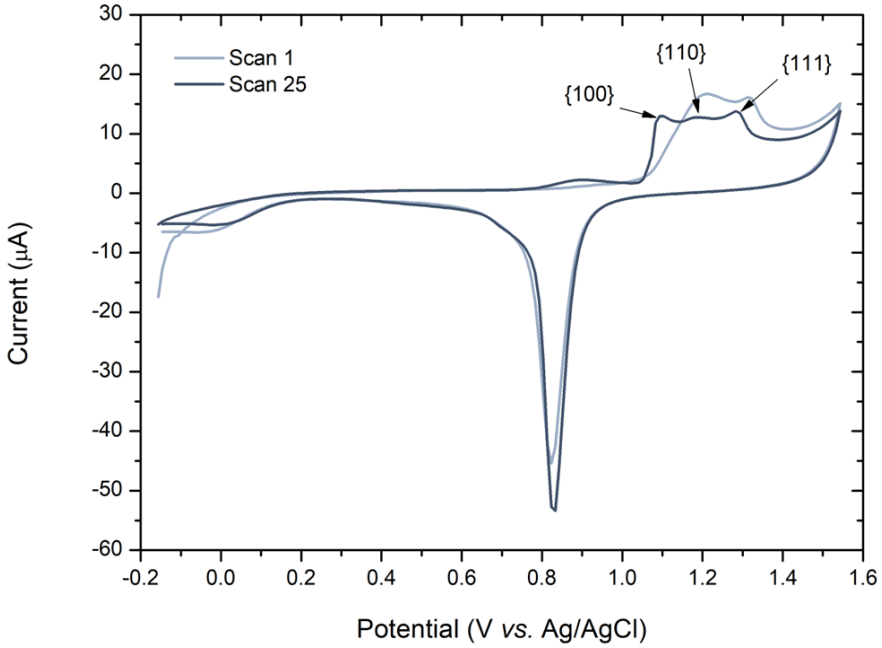

Figure 2.5. Cyclic voltammogram of electrochemical polishing (E_p) of polycrystalline gold electrodes at the start (1st scan) and end (25th scan) in 100 mM H_2SO_4 aqueous solution run from -0.156 to 1.544 V at a scan rate of 100 mV/s. Three crystallinities of gold are shown between 1.0-1.4 V.

Upon oxidation and reduction of the gold electrode surface, gold atoms are continuously disassociated and reassociated on to the surface (Cherevko et al., 2013; Zupančič et al., 2021). Gold oxidation occurs between 1.0 and 1.4 V on the forward scan while reduction of the gold oxide occurs between 1.0 and 0.6 V on the reverse scan, with the region between 0.6 and -0.15 V being largely capacitive

charging. As gold atoms are disassociated upon application of more positive potentials, surface bound organic contaminants are removed into the bulk electrolyte (Tkac and Davis, 2008). As the potential sweep reached potentials below 1.0 V gold atoms in proximity to the electrode surface are reassociated with a smoother surface structure (see Figure 2.6). It should be noted that due to the highly oxidative nature of the previous techniques, not all oxides on the electrode surface can be removed during the reverse scan and thus requires further gold oxide reduction.

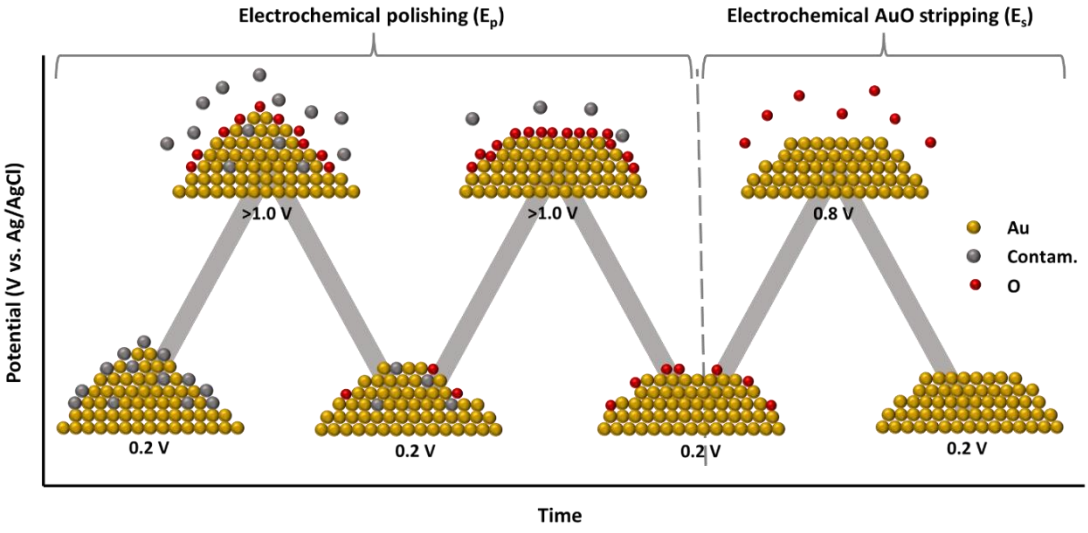

Figure 2.6. Schematic showing the change in microscopic gold geometry during voltametric cycling in 100 mM H_2SO_4 aqueous solution. (Left) The atomic level removal of contaminants and restructuring of the gold electrode surface by electrochemical polishing (E_p), (right) and the subsequent Au/α gold oxide stripping (E_s) at a lower more concise potential range (adapted from Silva Olaya, Zandersons and Wittstock, 2020).

Two techniques are implemented to remove the subsequent gold oxide layer that forms on the electrode surface due to the previous electrode treatments. Electrochemical gold oxide stripping (E_s) involves the potential cycling of electrodes at a potential range between 0.8 V and 0.2 V in sulphuric acid, cathodic of the 1.0-1.4 V range of gold oxide formation (see Figure 2.7a). By doing so, the gold oxide layer is reduced from the surface to leave a pristine and smooth surface (see Figure 2.6). Figure 2.7b shows the subtracted (1st subtracted from 10th) reduction scan of E_s treatment, with a cathodic peak at 0.7 V vs. Ag/AgCl which is consistent with

previous literature of electrode gold oxide reduction (L. H. Guo *et al.*, 1994; Ron, Matlis and Rubinstein, 1998; Tkac and Davis, 2008). To ensure gold oxide removal, a final chemical treatment of immersing the electrodes in pure ethanol is utilised to ensure chemical reduction any gold oxide before immediate modification of a new alkanethiol SAM.

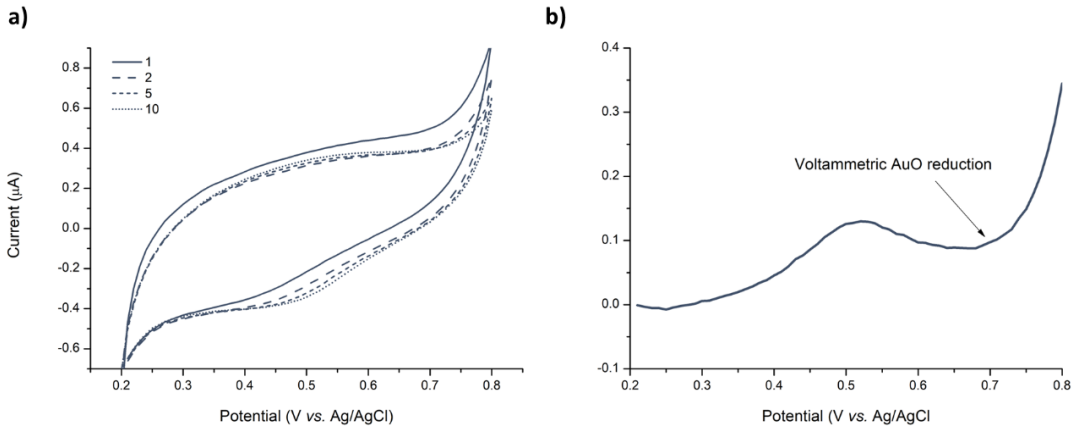

Figure 2.7. Electrochemical stripping of Au/α gold oxide. a) shows a cyclic voltammogram of electrochemical stripping in 100 mM H2SO4 aqueous solution with 10 cycles performed between 0.794 and 0.224 V at a scan rate of 100 mV/s. b) shows the subtracted cyclic voltammogram reduction scan, with the 1st scan subtracted from 10th scan.

2.1.3. Electrochemical impedance spectroscopy

Electrochemical impedance spectroscopy (EIS) is a useful label-free technique within electrochemical sensing for the characterisation of properties in the electrochemical cell associated with interfacial reactions (Magar, Hassan and Mulchandani, 2021). Such interface reactions may include bio-recognition events of molecules at the surface of the electrode e.g., nucleic acid hybridisation, antibody-antigen recognition among other ligands. It is also a useful technique for assessing SAM efficacy i.e., stability and binding affinity between probe and target molecules. By doing so it is possible to characterise the efficacy of SAM preparation as well as analyse the concentration of target molecules (Scholz, 2010; Bahadır and Sezgintürk, 2016). Electrochemical impedance spectroscopy can be both potentiostatic and galvanostatic, meaning you can either apply a potential and measure the output of current (potentiostatic), or you can apply current and measure the output potential

(galvanostatic). This thesis will focus on the use of potentiostatic EIS and its use for determining both Faradaic and non-Faradaic current characteristics within electrochemical systems.

Potentiostatic EIS works by applying a sinusoidal potential and measuring the resulting sinusoidal current output of the system. The sinusoidal potential is applied with a potential amplitude (usually 5-10 mV) to stimulate the system over an equally spaced frequency range (e.g., 0.1 to 100,000 Hz) on a decreasing logarithmic scale. The output current signal is then measured by change in peak current amplitude and shift in phase angle (φ) (see Figure 2.8). Although EIS investigates an entire spectrum of frequency responses, for development in a commercial biosensor, it is entirely possible to measure just at a single frequency. The measurement of the sinusoidal current is a measurement of electrons flowing between the electrodes through the bulk electrolyte solution and any functionalised molecule on the electrode surface.

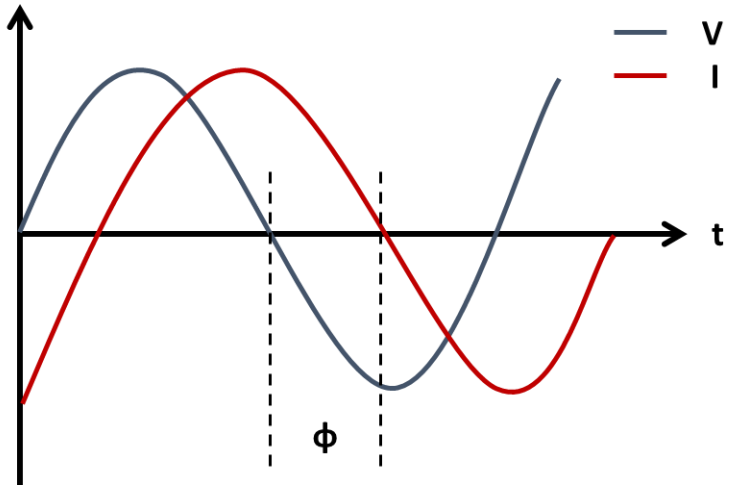

Figure 2.8. Sinusoidal signal of the applied potential and observed current output.

The input signal, or sinusoidal potential signal, can be expressed as a function of time ($V(t)$) as below:

$$V(t) = V_0 \sin(\omega t)$$

Where, V_0 is the voltage signal amplitude and ω is the angular frequency which can be further expressed as ($\omega = 2\pi f$) and f is the frequency in Hertz (Hz). The obtained

output signal can therefore also be expressed as a function of time (*I(t)*) for the same frequency (*f*):

$$I(t) = I_0 \sin(\omega t + \varphi)$$

Where, I_0 is the current signal amplitude, φ is the phase angle observed as a response to the impedance of the electrochemical system. We can then adopt Ohms law to convert the observed signal into impedance (*Z*):

$$Z = \frac{V(t)}{I(t)} = \frac{V_0 \sin(\omega t)}{I_0 \sin(\omega t + \varphi)} = Z_0 \frac{\sin(\omega t)}{\sin(\omega t + \varphi)}$$

Using Euler's method, it is then possible to represent complex impedance expressed as:

$$\exp(j\varphi) = \cos(\varphi) + jsin(\varphi)$$

Where, *j* is an imaginary number equal to the square root of minus one, $(-1)^{1/2}$. The applied sinusoidal potential and current output can then be further expressed as a function of time as below:

$$V(t) = V_0 \exp(j\omega t)$$

$$I(t) = I_0 \exp(j\omega t + j\varphi)$$

The impedance can then be expressed as a complex number to consider both components of complex impedance:

$$Z = \frac{Vt}{It} = Z_0 \exp(j\varphi) = Z_0(cos\varphi + jsin\varphi) = Z' + jZ''$$

Impedance can therefore be broken down into the real part of the impedance (*Z'*) and the imaginary part of the impedance (*Z"*). The real part of the impedance is associated with the resistance to the flow of electrons within the circuit, while the imaginary part is related to the electron storage capacity by the circuit. Put simply, the real part is mainly affected by the resistive components, and the imaginary part by the capacitive component of the biosensor circuit. The impedance of the electrochemical circuit is then interpreted and simulated using equivalent electrical circuit specific to biosensor interface setups (see Figure 2.9).

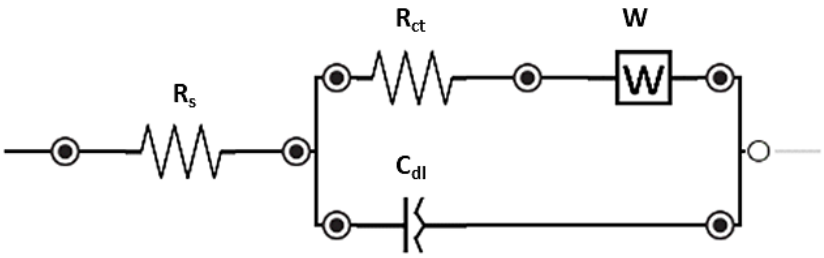

Figure 2.9. Randles equivalent circuit for electrochemical impedance spectroscopy where R_s is the solution resistance, R_{ct} is charge transfer resistance (impedance), C_{dl} is the double layer capacitance and W is the Warburg element.

Randles equivalent circuit is the most used circuit within EIS measurements, implementing components for the solution resistance between the RE and WE (R_s), charge transfer resistance (R_{ct}), the capacitive ability of the double layer (C_{dl}) and a Warburg element to model diffusion of the ions from the bulk solution to the electrode surface. A common change made for a modified version of the Randles equivalent circuit is the replacement of the C_{dl} component with a constant phase element (CPE) to model non-ideal capacitance of double layers involving biological molecules. The impedance of CPE can be given by the equation below:

$$Z_{CPE} = Y_0(j\omega)^{-\alpha}$$

Whereby, ω is the frequency, Y_0 is the magnitude of the admittance, α is an exponent with a value between 0 and 1 (for a pure capacitor, $\alpha = 1$). From Z_{CPE} we can then get an estimation of the capacitance (C_{dl}) by following the below equation:

$$C_{dl} = \frac{(Y_0 R_{ct})^{1/\alpha}}{R_{ct}}$$

The EIS technique is usually based upon faradaic current processes, which is a measurement of the oxidation and reduction of equal concentrations of redox coupled molecules (e.g. $[Fe(CN)_6]^{3-}$ and $[Fe(CN)_6]^{4-}$, at the surface of the electrode interface. During a Faradaic process the charged ions are transferred between the electrode and electrolyte interface due to an electrochemical reaction involving the application of the sinusoidal potential superimposed over the formal potential of the redox couple i.e., for $[Fe(CN)_6]^{3-/4-}$ with an RE such as Ag/AgCl the formal potential would be 0.2 V. Faradaic current is primarily influenced by a diffusion-based process,

with the Warburg element representing the diffusion of charged ions between the solution and electrode interface. At the low frequency range, the Warburg element (W) becomes the prevalent component in modelling the 45° phase angle. To represent a Faradaic EIS response, the Nyquist plot is used to allow for comparison of the charge transfer resistance values along the Z' axis (see Figure 2.10).

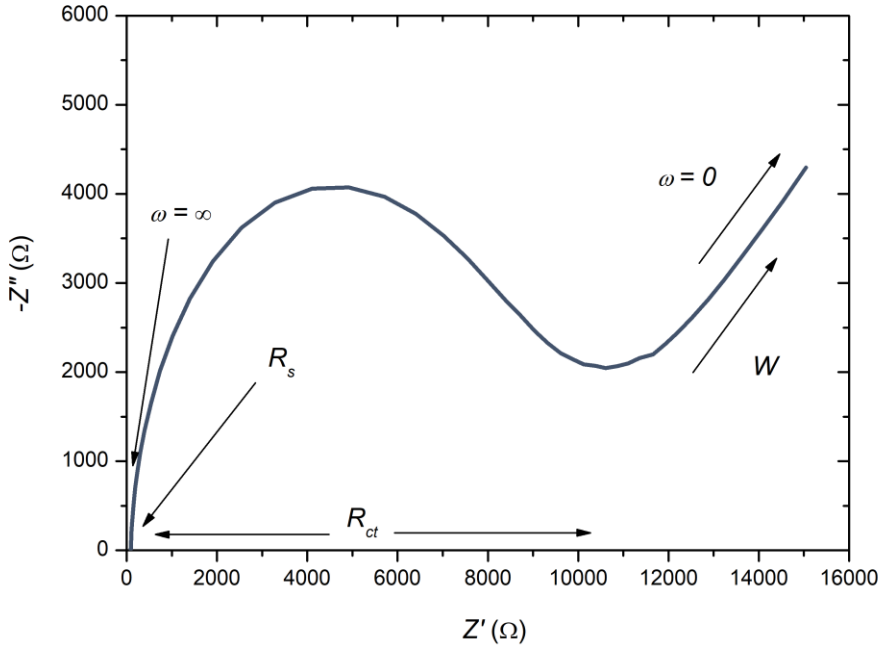

Figure 2.10. Typical Nyquist plot from a faradaic electrochemical impedance spectroscopy measurement. R_{ct} indicates the charge transfer resistance of redox molecules in the bulk electrolyte to the surface.

The Nyquist plot gives the imaginary impedance (*-Z''*) on the y-axis and the real part of the impedance (*Z'*) on the x-axis. The main data of interest from the Nyquist plot is the measurement of charge transfer resistance (R_{ct}).

2.1.3.1. Non-Faradaic EIS

While a Faradaic EIS experiment is performed with the use of redox active coupled molecules to obtain the resistance of charge transfer between the bulk electrolyte and the electrode surface, a non-Faradaic EIS experiment is performed without. For non-Faradaic EIS, particular importance is placed with the analysis of the double layer capacitance (C_{dl}) instead of the charge transfer resistance (R_{ct}) or Warburg element

(W) (Tsouti *et al.*, 2011). Thus, the equivalent circuit is simplified to primarily the solution resistance (R_s) in series with the double-layer capacitance (C_{dl}) (Couniot *et al.*, 2016) (see Figure 2.11).

Figure 2.11. Equivalent circuit for non-faradaic electrochemical impedance spectroscopy measurements.

The capacitance can then be calculated from the Z'' and Z' values and displayed using a Cole-Cole plot with C' on the x-axis and C'' on the y-axis (see Figure 2.12).

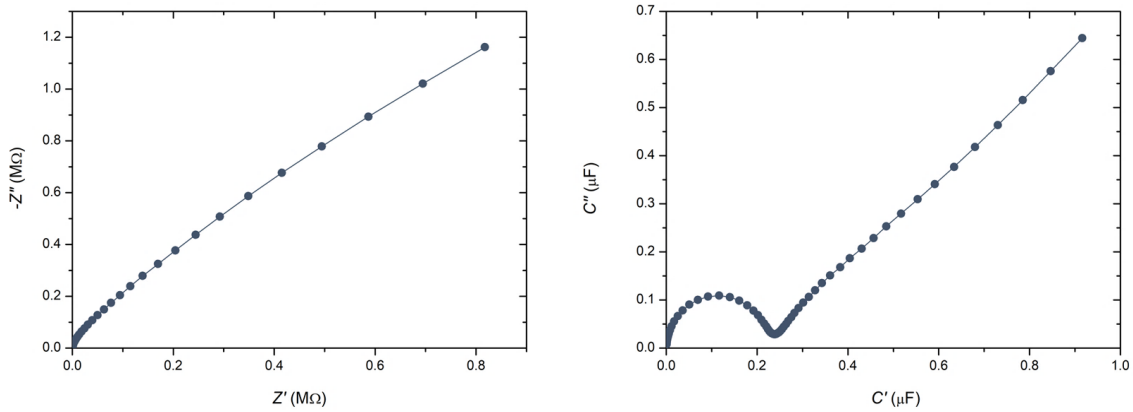

Figure 2.12. Graphical outputs for non-faradaic electrochemical impedance spectroscopy measurements in 100 mM PB. Impedance data can be presented in a Nyquist plot (left), while capacitance data is typically presented using a Cole-Cole plot (right).

A capacitive biosensor requires a compact insulating layer between electrode-electrolyte interface that can prevent current leakage which would decrease device sensitivity. SAMs such as those made up of alkanethiols and PEGs that are defect-free are good insulating layers and have been implemented in multiple sensing devices (Berggren, Bjarnason and Johansson, 2001; Tsouti *et al.*, 2011; Jolly, Batistuti, *et al.*, 2016). The signal changes observed in capacitive devices can be contributed to several sources including electrostatic interactions, interaction of target molecules with probe molecules, addition of metal molecules, displacement of molecules, and dielectric properties of surface bound molecules among others. Using this method,

chapter 4 describes the development of a DNA biosensor that implements the use of a cobalt-based intercalating compound that has been shown to alter the capacitance of the electrode-electrolyte interface.

2.1.4. Amperometric techniques

Amperometry is made up of electrochemical techniques associated with the measurement of current outputs as a result of applied fixed potentials to a working electrode controlled by the potentiostat (Hryniewicz *et al.*, 2021). The applied potentials drive electron transfer reactions and the observed currents are a result of the reduction and oxidation (redox) of analytes or redox-active mediating molecules e.g. $[Fe(CN)_6]^{3-/4-}$ (Roussel *et al.*, 2008). Within amperometry, when a current is measured as a function of the applied potential it is commonly referred to as voltammetry; such measurement techniques include cyclic voltammetry (CV) and differential pulse voltammetry (DPV) (Grieshaber *et al.*, 2008). The objective of fixed potential-based amperometric techniques is the observation of the relationship between a current response related to various concentrations of a target analyte and the applied potential to the WE. This is achieved through measurement of electron transfer during the redox process of the analyte of mediator molecule and can be written as the below equation:

$$Ox + e^{-} \leftrightarrow Red$$

Where, *Ox* and *Red* are the oxidized and reduces forms of the redox active analyte or mediator molecule. Within systems that are controlled by the laws of thermodynamics, the potential applied to the WE can be utilised to control the concentration of the oxidized form of the compound (C_O) and the reduced form (C_R) at the electrode surface using the Nernst equation:

$$E = E^{0} + \left(\frac{2.3RT}{nF}\right)\log\frac{C_O}{C_R}$$

Where, E^0 is the standard potential being the measure of the potential for equilibrium between the electrode and electrolyte, *R* is the universal gas constant, *T* is Kelvin temperature, *n* is the number of electrons transferred in the reaction and *F* is the Faraday constant. The attributed current change due to oxidation state of the

electroactive analyte of mediator molecule is known as the faradaic current and is a direct measurement of the rate of a redox reaction (Lojou and Bianco, 2006). For example, with the $[Fe(CN)_6]^{3-/4-}$ redox couple during oxidation, $[Fe(CN)_6]^{3-}$ diffuses towards the electrode surface where is exchanges an electron, resulting in the electrochemically reduced form, $[Fe(CN)_6]^{4-}$, diffusing from the electrode surface back to the bulk electrolyte. This thesis will focus specifically on the use of cyclic voltammetry (CV) and differential pulse voltammetry (DPV). Chapter 4 utilises CV and DPV to characterise the electrochemical redox capability of a cobalt-based intercalating molecule. While chapter 5 will employ CV in the development of a CRISPR-based electrochemical sensor for the measurement of surface-reduced 3,3',5,5'-Tetramethylbenzidine (TMB).

2.1.4.1. Cyclic voltammetry

Cyclic voltammetry is a commonly used amperometric technique for the study of redox capabilities of charged molecules, as well as the charge-transfer reactions that occur due to electrochemical and biological recognition reactions on the electrode surface (Elgrishi *et al.*, 2018b). It is therefore possible to electrochemically assess the redox kinetics and stability of electrochemically generated compound states using CV. Useful information such as reaction characteristics to assess the complexity of certain redox mechanisms can also be determined (Elgrishi *et al.*, 2018b; Guziejewski *et al.*, 2022). Redox-active species are molecules in solution that are capable of both gaining electrons, reduction (*Red*), and losing electrons, oxidation (*Ox*), within a reversible reaction such as the redox couple ferri-/ferrocyanide, $[Fe(CN)_6]^{3-/4-}$. Cyclic voltammetry works by applying a fixed potential range e.g., -0.5 V and +0.5 V and sweeping between the maximum and minimum ranges at a given scan rate (see Figure 2.13). The current, which relates to the *Red* and *Ox* potentials of the charged redox molecule can then give information of variations in molecular behaviour related to that which is immobilised on the surface of the working electrode (WE) and any target molecules that bind.

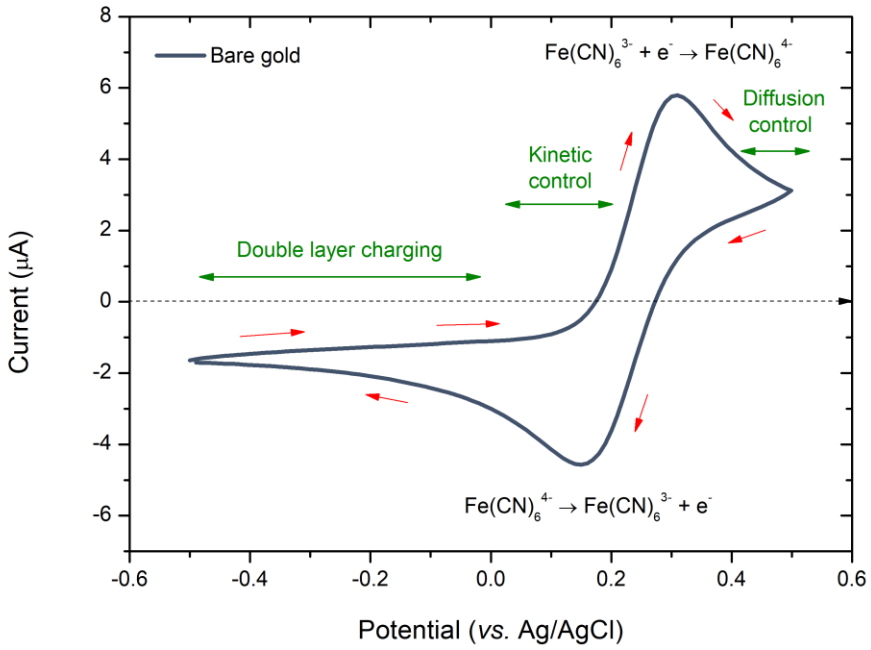

Figure 2.13. Cyclic voltammogram of a reversible redox reaction of $[Fe(CN)_6]^{3-/4-}$ with a bare gold WE surface.

Cyclic voltammetry can also be utilised to obtain the formal potential (E^0) of a redox molecule to be further used in impedance measurement techniques. Formal potential of a given experiment can be calculated using the Nernst equation as below:

$$E = E^0 + \frac{RT}{nF} ln \frac{Ox}{Red} = E^0 + 2.3 \frac{RT}{nF} log_{10} \frac{Ox}{Red}$$

2.1.4.2. Differential pulse voltammetry

Differential pulse voltammetry (DPV) is an amperometric electrochemical technique utilising potential scan made using potential pulses with constant amplitude superimposed over a direct current (DC) potential (see Figure 2.14). The interval time between each pulse can be calculated by E_{step}/scan rate. The current is obtained by sampling twice at each step potential, once before application of the pulse potential (i_1) and once at the end of the pulse (i_2). The current difference (Δ_i) between these two points is then plotted versus the potential as shown below.

$$\Delta_i = i_2 - i_1$$

DPV has a peak-shaped curve and therefore allows us to obtain peak current height and area which can be determined to be proportional to the concentration of ligand binding or concentration in solution (Palmsens, 2022). The peak potential is calculated as below:

$$E_{peak} = E_{1/2} - \frac{E_{pulse}}{2}$$

DPV was developed for the purpose of measuring with increased sensitivity by reducing the capacitive current. Since the wave height of the normal pulse voltammetry wave height is never smaller than the corresponding DPV peak height, the increase in sensitivity is due to the reduced background current rather than the faradaic response (Bard, Faulkner and White, 2022). A notable step with differential pulse voltammetry is the pre-treatment step which applies a reduction potential to the diffusion layer to ensure the surface-bound molecules can be fully interrogated by the pulse.

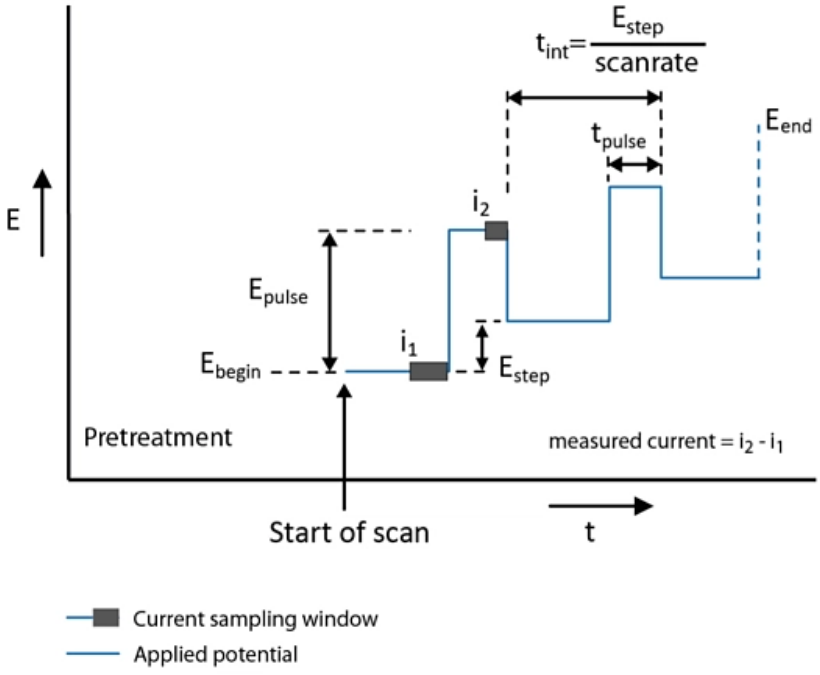

Figure 2.14. Potential waveform for standard DPV measurements. The potential waveform is composed of small pulses (of constant amplitude) that are superimposed upon a staircase wave form (taken from Palmsens, 2022).

2.2. Surface functionalisation techniques

There are several techniques commonly used for the immobilisation of biomolecules onto electrode surfaces (see Table 2.1), it is important to consider certain variables when choosing the method of functionalisation. The surface that the probe is going to be immobilised on is a major factor. Many researchers developing biosensors favour the use of noble metals e.g., gold, silver, and platinum due to their specific physicochemical properties and resistance to corrosion (Doria *et al.*, 2012; Dimcheva, 2020). Electroactive polymers are also commonly used to quickly produce a smooth and heterogeneous surface for immobilisation of biomolecules e.g., polypyrrole (PPy) and polydopamine (PDA) (Jolly, Miodek, *et al.*, 2016; Kim *et al.*, 2018). Glassy carbon and graphene electrodes may also be utilised for their robust signal transduction, additionally 3D architectures can be built using chemical linkers e.g., MCH or PEG with high surface area molecules such as gold nanoparticles (AuNPs), carbon nanotubes (CNTs), and graphene oxide (GOx) etc. (Li, Schluesener and Xu, 2010; Sireesha *et al.*, 2018; Zupančič, Jolly, *et al.*, 2021a).

Another important consideration is that of the probe and target molecules being used for the devices assay. Biosensors utilise biological molecules as probes for the detection of other biological molecules such as proteins, nucleic acids, antibodies, and cells. Each of these molecules contain characteristics e.g., molecule size, inherent charge, and structural stability such as secondary/tertiary structures that make them suitable for different immobilisation techniques. It is also important to consider the type of functionalisation technique that will be used for attachment of the probe to the transducer surface. Many surface chemistries exist including direct adsorption, covalent linkers, affinity chemistries and entrapment.

It is also important to consider the end-product design and what the device will be used for and where it will be deployed. Depending upon the target demographic of the device being developed i.e., hospitals, environmental monitoring services, food safety etc. the biosensor device will have different requirements. For example, hospital testing requires a high level of certainty to inform diagnosis and treatment options and so high specificity above all else is essential. Diagnosis of diseases and

other illnesses also requires a low limit of detection (LOD) for biomarkers present in low concentrations. This can be achieved using signal enhancing molecules such as intercalators or through pre-treatment of the sample via. sample amplification e.g., PCR, LAMP. Conversely, environmental monitoring such as for water quality requires an additional focus. In comparison to blood, water is a matrix of much higher complexity due to constant exposure from the open environment and a plethora of unknown contaminants both anthropogenic and natural (Khatri and Tyagi, 2015). Thus, devices used in these settings require focus on anti-fouling capability to prevent rapid degradation as well as opportunity for multiplexing to analyse a larger number of contaminants conveniently.

There are many different surface functionalisation techniques being used for the attachment of nucleic acid probes to electrode surfaces. This thesis will primarily focus on the immobilisation of probe molecules using covalent attachment techniques such as alkanethiol self-assembled monolayers (SAM) as well as conductive polymer chemistry.

Table 2.1. Common methods of immobilising biological probe molecules onto an electrode surface.

Functionalisation technique	**Functional groups**	**Interaction**	**Pros**	**Cons**	**References**
Adsorption	Various	Electrostatic Hydrophobic	Rapid, simple, and cost-effective	Random orientation, unstable monolayers	(Du *et al.*, 2011; Madaboosi *et al.*, 2015)
Covalent e.g., self-assembled monolayer (SAM)	-NH2 -SH -COOH etc.	Amine coupling Thiol coupling Coupling via glycan	High stable monolayers, well-ordered monolayers, high-sensitivity, and controlled orientation	Required pre-modification of probe molecules, slow formation, irreversible and expensive reagents	(Jolly et al., 2019; Najjar et al., 2022)
Affinity	Fc domain	Highly specific avidin-biotin Intermediate protein (A/G) coupling	Highly controlled orientation, highly specific functionalisation	Expensive reagents, specifically linker molecules	(Zhang *et al.*, 2013; Najjar, Rainbow, Sharma Timilsina, *et al.*, 2022a)
Entrapment	Pre-formed membranes Silica nanobubbles Electro-active polymers e.g., pyrrole, dopamine	Entrapment Encapsulation Electro-polymerisation	Results in high concentration of probes, excellent resistance to biofouling and nuclease activity, simple polymer-growth control	Random orientation, probe leeching and reduced target binding efficiency	(Jolly, Miodek, *et al.*, 2016; Miodek *et al.*, 2016)

2.2.1. Thiol self-assembled monolayers

A commonly used type of surface functionalisation for the attachment of probes, specifically to gold electrodes, are thiol self-assembled monolayers (SAMs). Thiol groups and gold have a particularly strong affinity to one another allowing for simple, passive covalent binding of probes to gold surfaces (see Figure 2.15) (Love *et al.*, 2005). By using short chain alkanethiol linkers alongside thiolated nucleic acid probes, it is possible to form SAMs of tightly packed molecules with a high degree of probe-to-linker ratio control. These characteristics have made SAMs implementing thiols on gold one of the most highly cited techniques for surface electrode modification (Hong, Park and Yu, 1999).

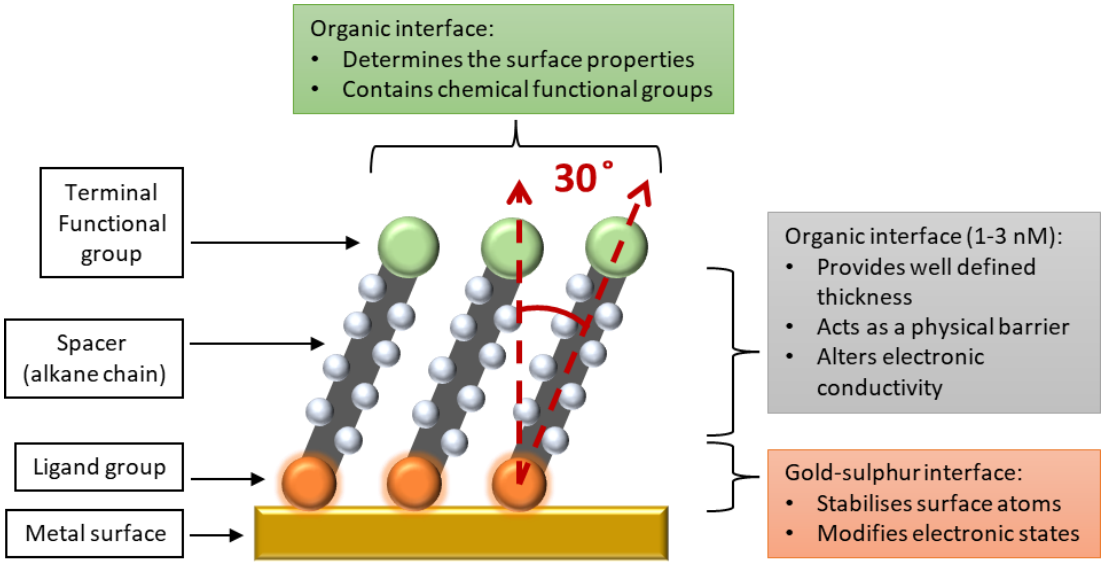

Figure 2.15. Self-assembled monolayer formation of nucleic acids on gold using thiol surface chemistry. The 30° angle is typical of a well-formed monolayer with all probes ideally parallel (adapted from Love et al., 2005).

In close vicinity to gold, the sulphur contained within the thiol group will undergo the following chemical reaction:

$$RSH + Au \leftrightarrow RS - Au + H^+ + e^-$$

Common theory suggests that upon binding of the thiol group to planar gold surfaces, hydrogen is disassociated through the formation of a chemisorbed bond (Pacchioni, 2019). However, recent work by Inkpen et al. suggests that the sulphur-gold interaction may occur through a physiosorbed interaction rather than chemisorbed (Inkpen *et al.*, 2019). Inkpen et al. suggested that instead of the thiol group losing a

hydrogen atom as previously thought, the hydrogen may not be removed and instead a physical adsorption of the molecule occurs through weaker van der Waals forces (see Figure 2.16). If this interaction occurs it is thought to be due to the type of gold that the thiol group is interacting with, as the current work has only tested Au (111) and results showed that chemisorption did still occur in cases whereby a large excess of molecules are surrounding high-energy, uncoordinated gold atoms which are not common on the Au (111) surface. Using planar gold surfaces containing different crystallinities of gold, it is unclear whether the chemisorbed or physiosorbed bonding is prevalent.

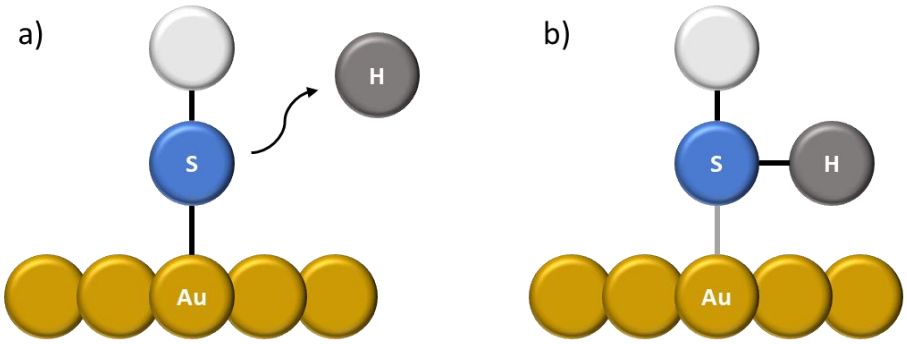

Figure 2.16. Suggested binding interactions of -SH groups to planar gold surfaces with gold (yellow), sulphur (blue), hydrogen (grey), and carbon (white). (a) shows chemisorption of the -RSH group to planar gold whereby the hydrogen atom is lost upon covalent bonding, whereas (b) shows physisorption in which the hydrogen atom is retained, and a bond is formed through Van der Waal forces (adapted from Pacchioni, 2019).

In the case of thiol SAMs, a dual chemisorption and physisorption process is observed on gold surfaces. The bonding of sulphur to gold occurs spontaneously, with 80-90% coverage achieved in only a few minutes. However, for a complete and well organised SAM to be formed a minimum 12-18 hours is required (Schreiber, 2000; Love *et al.*, 2005). A well-formed SAM is largely dependent on surface roughness and the presence of any surface contaminants, such as organic debris or inorganic particulate such as underlying copper in printed circuit board (PCB) electrodes, as well as alkanethiol chain length (L.-H. Guo *et al.*, 1994; Fischer *et al.*, 2009). The 'well-organised' SAM formation undergoes two main phases that include both chemisorption and physisorption. In the early stages of spontaneous adsorption of the alkanethiol group that occurs in the first few minutes, sulphur binds to gold

through the process of physisorption, lying flat in what is known as the 'lying down' phase (Camillone *et al.*, 1996; Celik *et al.*, 2021). During the second phase, the 'standing up' phase, chemisorption results in the formation of Van der Waals that develop into a semi-crystalline structure that causes the alkanethiols to tilt in a lateral direction until a 30° angle is achieved in relation to the planar gold surface (see Figure 2.15) (Love *et al.*, 2005). The effectiveness of this process is heavily reliant upon the well-formed nature of alkanethiols as well as the surface roughness of the gold being functionalised.

A plethora of alkanethiols with different functional terminal groups exist that allow for different surface attachment chemistries to be performed with different molecules. This allows researchers to develop novel and specific assay designs through modification of groups such as carboxylic acid (-COOH) which can be bound to amine-terminated oligonucleotides, peptides, antibodies, chemical groups e.g., ferrocene, and metals such as nanoparticles e.g., gold nanoparticles (AuNPs) (Jolly *et al.*, 2017; Staderini *et al.*, 2018; Díaz-Fernández *et al.*, 2021). This is done by using ethyl (dimethylaminopropyl) carbodiimide (EDC) and N-hydroxysuccimide (NHS) to activate the carboxyl group (Jolly *et al.*, 2015). This technique will be further explained in the next section as well as in chapter 5 for attachment of amine-terminated peptide nucleic acid (PNA) to a conductive graphene oxide (GOx) polymer. For the sake of this thesis, thiolated oligonucleotides were synthesised externally and ordered from Integrated DNA Technologies (IDT, BE).

Due to the variation of alkanethiols that are commercially available and the ability to directly functionalise biomolecules, the development of binary SAMs has become a prominent area of research. By immobilising multiple alkanethiols it is possible to create well-ordered SAMs of alkanethiols constituting both short chain spacers and thiol-functionalised probe molecules at various molar ratios. A study by Keighley et al. explored probe densities with a binary SAM consisting of spacer 6-mercapto-1-hexanol and a thiol-modified oligonucleotide to determine optimal probe density to maximise target DNA binding (Keighley *et al.*, 2008a). Other research has explored the use of ternary SAMs for rough gold surfaces utilising the traditional thiolated oligonucleotides and MCH spacer alongside dithiol moieties e.g., hexanedithiol (HDT) (Campuzano *et al.*, 2011). Miodek et al. demonstrated how the addition of dithiols

allows for the reduced interference of non-specific molecules on rough gold screen printed electrodes (SPEs) (see Figure 2.17). This increased antifouling capacity of the SAM due to their horizontal 'bridge-like' architecture providing greater resistance to non-target molecules (Miodek *et al.*, 2015). This type of surface chemistry may help facilitate sensor devices for long-term monitoring in continuous clinical (blood) and environmental (water) conditions, that would previously have been difficult due to biofouling (Kuralay *et al.*, 2011; Vezza *et al.*, 2021).

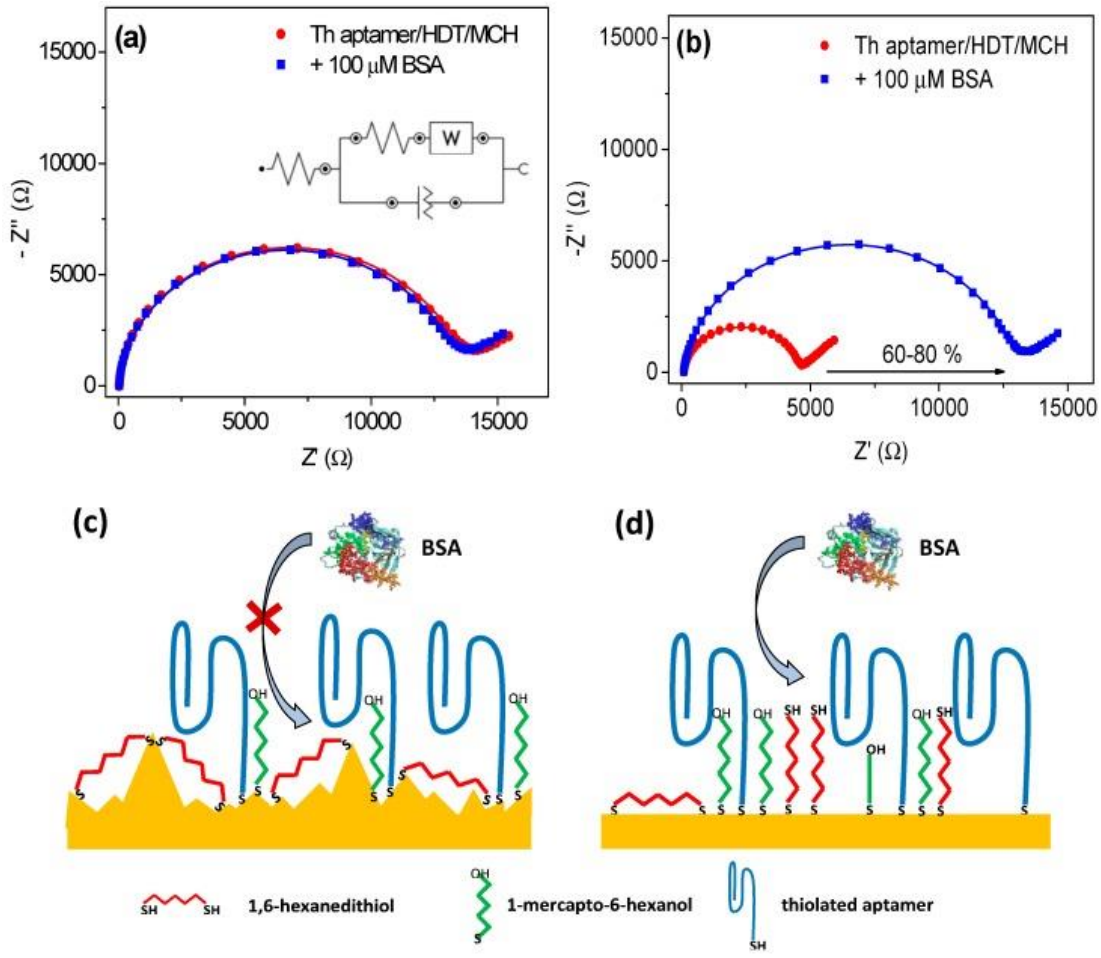

Figure 2.17. Nyquist plots showing electrochemical impedance spectroscopy responses before (red) and after (blue) incubation of 100 µM bovine serum albumin (BSA) for 30 min on biosensor based on (a) screen-printed electrodes (b) macroelectrodes modified with thrombin aptamer/ternary self-assembled monolayer 0.05/300 µM and saturated with 1 mM MCH. Points show experimental results and solid plots show fitting. Scheme of the surface architecture for (c) screen-printed electrodes and (d) macroelectrodes (Miodek et al.*, 2015).*

2.2.2. Conductive antifouling nanocomposite coating

Electrochemical affinity-based sensors are one of the more attractive options for diagnostic and monitoring devices due to their lower limits of detection (LOD), inexpensive fabrication, disposability, ease of integration and miniaturization as well as low power requirements (Sabaté del Río *et al.*, 2019; Zupančič, Jolly, *et al.*, 2021a). However, in point of care (PoC) and on-site or monitoring they suffer from a reduction in sensitivity due to surface biofouling. Biofouling is the deposition and accumulating growth of cells, proteins, and biomolecules as well as organisms such as algae, fungi, bacteria that aggregate on surfaces to form a biofilm. Regarding *in situ* monitoring devices, biofilms cause electrode passivation reducing detection through prevention of target molecules binding to sensor/capture surfaces (Kelly, Codispoti and Harford, 2008; Sabaté del Río *et al.*, 2019) as well as reduced electrode transduction which further decreases device sensitivity over time as more molecules adsorb to the surface (Timilsina *et al.*, 2022).

As previously mentioned, a common technique being explored for reducing potential non-specific binding or fouling on sensor surfaces is the use of antifouling coatings (Lichtenberg, Ling and Kim, 2019). Antifouling coatings including ternary SAMs involving dithiols, as well as bovine serum albumin (BSA) and polyethylene glycol (PEG)-based SAMs provide antifouling properties but impede conductivity due to hindrance of electron transfer (Campuzano *et al.*, 2019). The further one increases the building of the antifouling layer the higher the electron transfer hindrance becomes. One promising approach to resolve the reduced conductivity is to introduce conductive nanomaterials into the antifouling coating to maintain and even enhance electron transfer. Conductive nanomaterials that have been explored for this approach include gold nanoparticles (AuNPs), gold nanowires (AuNWs), carbon nanotubes (CNTs) as well as graphene oxide (GOx). A promising method developed by researchers at the Wyss Institute at Harvard University incorporates highly conductive amine-terminated reduce graphene oxide (rGOx), BSA and glutaraldehyde (GA) to form a high conductive antifouling nanocomposite that can be easily modified with amine-terminated probe molecules (see Figure 2.18) (Sabaté del Río *et al.*, 2019; Timilsina *et al.*, 2021; Zupančič, Jolly, *et al.*, 2021a).

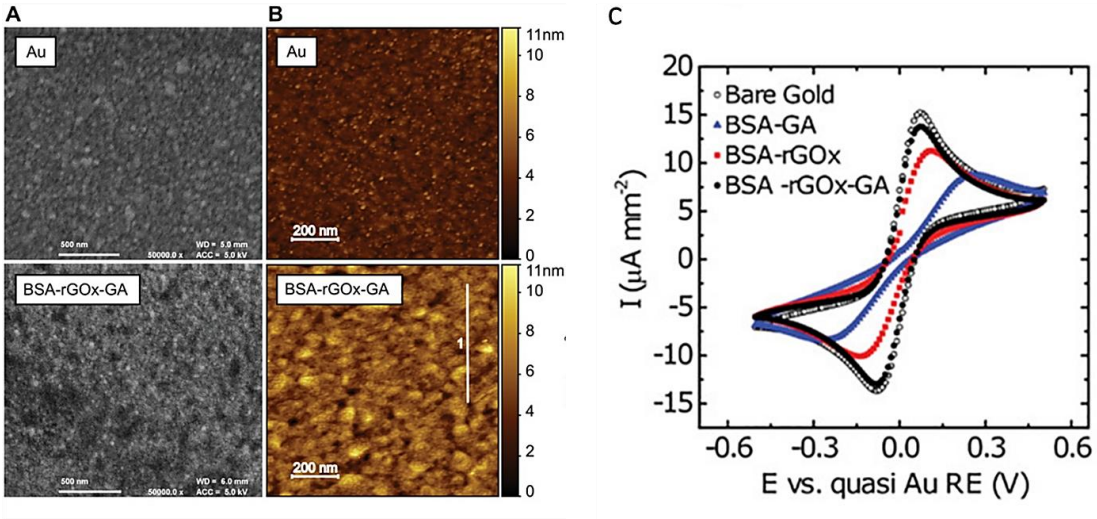

Figure 2.18. Characterization of the BSA/rGOx/GA nanocomposite coating. A) FE-SEM image of bare gold (Au) and nanocomposite coated gold surface. B) AFM topography representation of bare gold (Au) and nanocomposite coated gold surface. C) CV representing oxidation and reduction of 5 mm ferri-/ferrocyanide solution using gold electrodes with various coating stages; BSA crosslinked with GA (BSA-GA), BSA incorporated with rGOx nanoflakes (BSA-rGOx) and GA crosslinked BSA incorporated with rGOx nanoflakes (BSA-rGOx-GA) (taken from Zupančič et al., 2021).

The nanocomposite is formed using GA to bond the rGOx and BSA molecules through non-specific crosslinking of lysine residues. The nanocomposite then binds to the surface of gold electrodes through chemisorption of sulphur groups contained within the BSA as well as amine groups of rGOx and adsorption. The coated electrodes can then be functionalised with probes containing primary amine groups through covalent bonding. Probes that have been explored for use with this coating include antibodies, antigens, and peptide nucleic acids (PNAs). To attach the probes, the surface carboxyl groups are first activated by 1-ethyl-3-(-dimethylamino) propyl carbodiimide (EDC)/N-hydroxysuccinimide (NHS) coupling to produce an NHS ester. Initially, EDC activates carboxyl groups to produce an O-acylisourea intermediate that reacts with primary amines to form an amide bond and isourea waste product. However, O-acylisourea is unstable in aqueous solution and prone to hydrolysis to regenerate back into a carboxyl group if not bound to a primary amine. To prevent hydrolysis, EDC couples NHS to the carboxyl group to form an NHS ester which is significantly more stable in aqueous solution and conjugates efficiently with any

primary amines later introduced within a physiologically relevant pH range (see Figure 2.19).

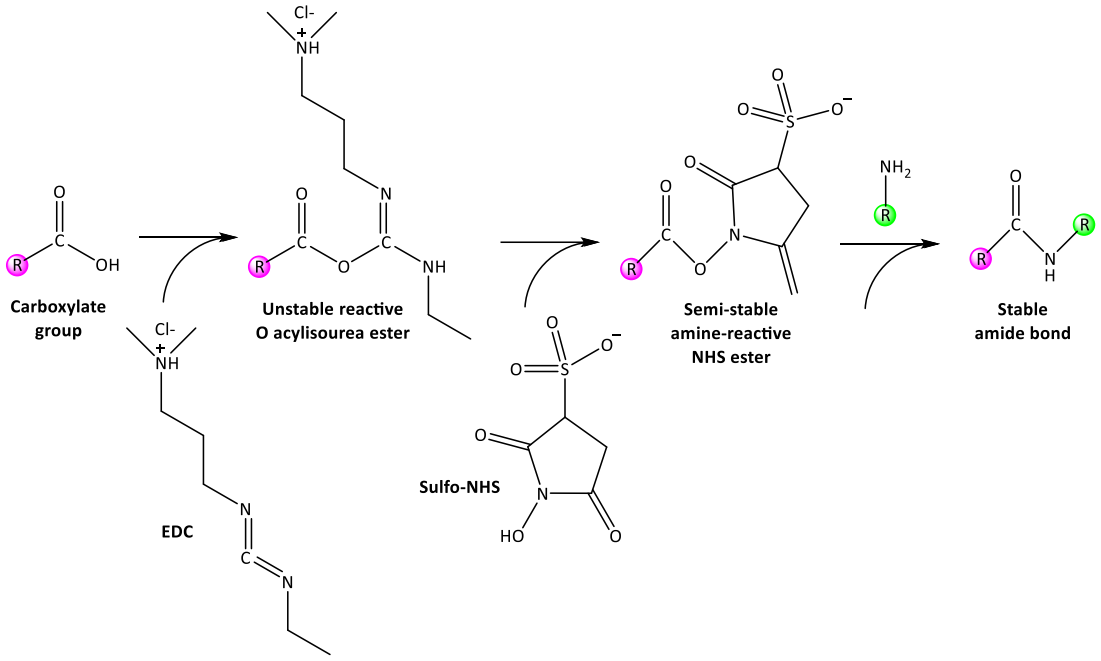

Figure 2.19. EDC/NHS chemistry coupling process. EDC reacts with a carboxyl group forming an amine-reactive O-acylisourea intermediate. The addition of sulfo-NHS stabilises the amine-reactive intermediate by converting it to an amine-reactive sulfo-NHS ester, which efficiently forms amide bons with primary amines (adapted from Bart et al., 2009).

2.3. Nucleic acid intercalators

Biosensors that employ DNA-based probes for the detection of target DNA have typically low sensitivity due to the relative charge of DNA being so low in physiologically relevant buffers alongside their small size. The use of nucleic acid intercalating molecules as signal sensitisers offers the opportunity for post-signal amplification in electrochemistry setups. Nucleic acid intercalators are a family of chemical compounds that exhibit characteristics of disrupting nucleic acid structures. Chemical intercalation by these compounds involves the insertion of the molecule between the planar nitrogenous base pairs. These compounds are usually polycyclic, aromatic planar ligands of similar size to the space between complementary base pairs. Some commonly used DNA intercalating molecules include Ethidium Bromide, Acridine Orange, Proflavine, Adriamycin, Daunomycin and Doxorubicin. Several intercalating molecules are used as chemotherapeutic drugs that bind to mutated

and cancer-causing DNA in cells to prevent further replication. Intercalators can disrupt the structural integrity of DNA in a couple of ways. Helix winding is a common side-effect due to the electrostatic repulsion between adjacent phosphate groups of nucleotides. Helix unwinding is another perturbation caused by the base-stacking interaction of intercalators which involves disruption of hydrogen bonds between nucleotides. For example, studies have shown the disruption of base-stacking by different intercalating molecules including that of Ethidium Bromide causing a 26° shift, and Proflavine which can cause a 17° shift in the DNA helix structure. DNA intercalation results in further structural changes including decreased molecule density and viscosity which can lead to increased contour length of the dsDNA strand. DNA intercalation always leads to functional disruption including DNA replication and translation into proteins, which is considered the main aim of these compounds as drugs. A common intercalating chemotherapeutic drug, Doxorubicin, is important in the treatment of some cancers, primarily Hodgkin lymphoma (see Figure 2.20).

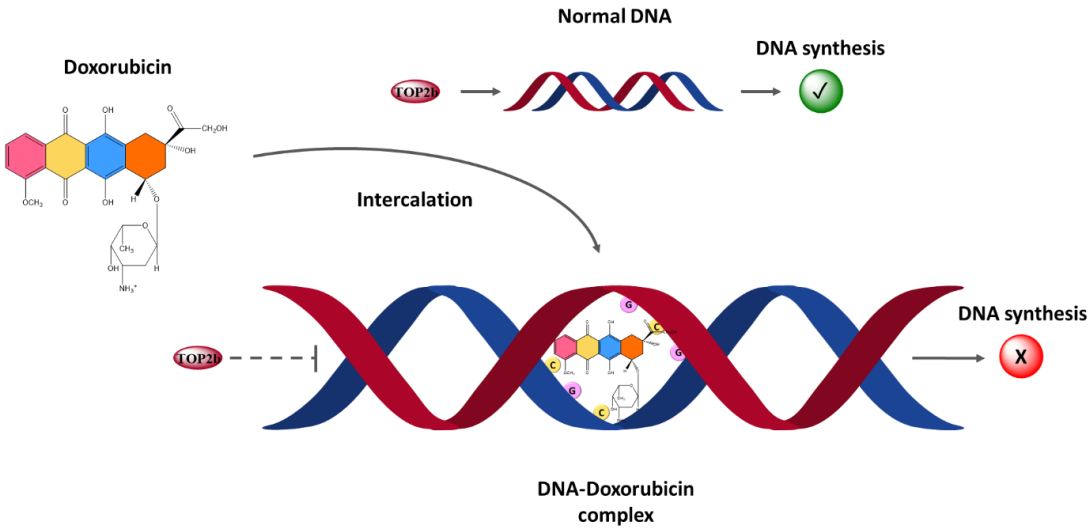

Figure 2.20. Doxorubicin intercalation of DNA. In normal DNA structures TOP2b eases the DNA helix to facilitate DNA replication and amplification. When DNA and Doxorubicin form a complex, structural changes to the helix prevent TOP2b activity. TOP2b = Topoisomerase 2b, G = guanine, and C = cytosine (Mobaraki et al.*, 2017).*

2.3.1. Redox-active metallo-intercalators

Two sub-categories of intercalating compounds that have seen a lot of interest in recent years are redox-active intercalators and metallo-intercalators. Redox-active

intercalators are compounds that stack between duplexed DNA through π-stacking with electroactive properties that can be assessed by way of their oxidative and reductive current response to application of various potentials. Some commonly used redox-active intercalators include Methylene Blue (MB), Nile blue (NB) and Anthraquinone (AQ) (Pheeney and Barton, 2013). The redox properties of these molecules can be conveniently evaluated using amperometric or voltametric techniques such as CV, DPV and square wave voltammetry (SWV) to assess binding to surface-bound DNA molecules (Deféver *et al.*, 2011).

On the other hand, metallo-intercalators are a sub-category of intercalative compounds that are planar, polycyclic, aromatic compounds that are cationic and contain metal ligands. Unlike other intercalators, during the process of π-stacking the hydrogen bonds are not broken and the binding of the intercalator between the nitrogenous base-pairs is further stabilized by van der Waals and electrostatic interactions (Erkkila, Odom and Barton, 1999). Common metallo-intercalators that have been explored in the literature contain metal complexes using Cu, Co and Ru coordinated with planar ligands such as phenanthroline (Erkkila, Odom and Barton, 1999; Qing, Gao and Jiao, 2008; H. bin Lin *et al.*, 2011; Regan *et al.*, 2014a). These compounds cause structural changes in the dsDNA helix and affect the electrical field double layer that can be measured using several techniques including amperometric as well as impedance-based techniques and open circuit potential (OCP).

One interesting area of potential for researchers in electrochemical diagnostics and biosensor devices is the development of redox-active metallo-intercalators that could form stable complexes with their dsDNA targets for electrochemical signal enhancement. These complexes would allow for the further signal enhancement of DNA-DNA interactions by both adding a strong redox-based signal as well as providing structural changes that alter electrical field properties. Chapter 4 of this thesis will focus on the development of such a novel intercalator based on cobalt for redox-active metallo-intercalation of an *E. coli* genosensor device for post-hybridisation signal enhancement.

2.4. Isothermal amplification techniques

Biosensors that employ DNA-based probes for the detection of target DNA have typically low sensitivity as mentioned previously. Additionally, target nucleic acids within environmental samples are usually very low in concentration. Therefore, several techniques have been explored for the pre-amplification of target molecules in the literature (Leonardo, Toldrà and Campàs, 2021). One such method of pre-amplifying target DNA molecules, as well as other nucleic acids, includes isothermal amplification. Isothermal amplification is the rapid amplification of nucleic acid sequences with the specific benefit of doing so at a constant temperature by taking advantage of nucleic acid polymerase enzymes. Due to the need for only a single temperature and additional dosing of nucleic acid polymerases, isothermal amplification is much more technically simple than traditional polymerase chain reaction (PCR) method making it more easily integrated into portable devices that implement microfluidics and simple resistive heaters. This section will cover the isothermal amplification technique used in this thesis, namely, loop-mediated isothermal amplification which will be demonstrated in chapter 5 of this thesis.

2.4.1. Loop-mediated isothermal amplification (LAMP)

Loop-mediated isothermal amplification (LAMP) is quickly becoming a popular alternative to the gold standard common PCR method used in genetics and diagnostics (Soroka, Wasowicz and Rymaszewska, 2021). Isothermal, meaning a thermodynamic process in which the temperature of a system remains constant, can be expressed as the below:

$$\Delta T = 0$$

Therefore, isothermal amplification is any technique amplifying genetic material at a constant temperature. This is a major advantage over traditional thermocycling techniques such as PCR which require cycling between multiple temperatures of 95, 72 and 56 °C, to ensure optimal enzymatic reaction rates. Due to the high variability of reaction temperatures, techniques that employ thermocycling are more prone to interference by inhibiting molecules, while the steady state temperature of 60-65 °C mitigates this potential for interference (Schrader *et al.*, 2012). LAMP is also more

rapid than PCR due to its simpler one-pot protocol and continuously amplifying sequences, not being limited by step-based thermocycling. A DNA polymerase enzyme is also implemented in LAMP that has been designed for very high strand displacement activity called Bst DNA polymerase I derived from *Bacillus stearothermophilus* (Ignatov *et al.*, 2014). The above advantages of the LAMP assay make it particularly well suited to integration with an on-chip device, requiring minimal additional components including a reaction chamber, reagent mixing channel e.g., serpentine fluidics, and a simple constant-voltage resistive heater element to maintain temperature during amplification.

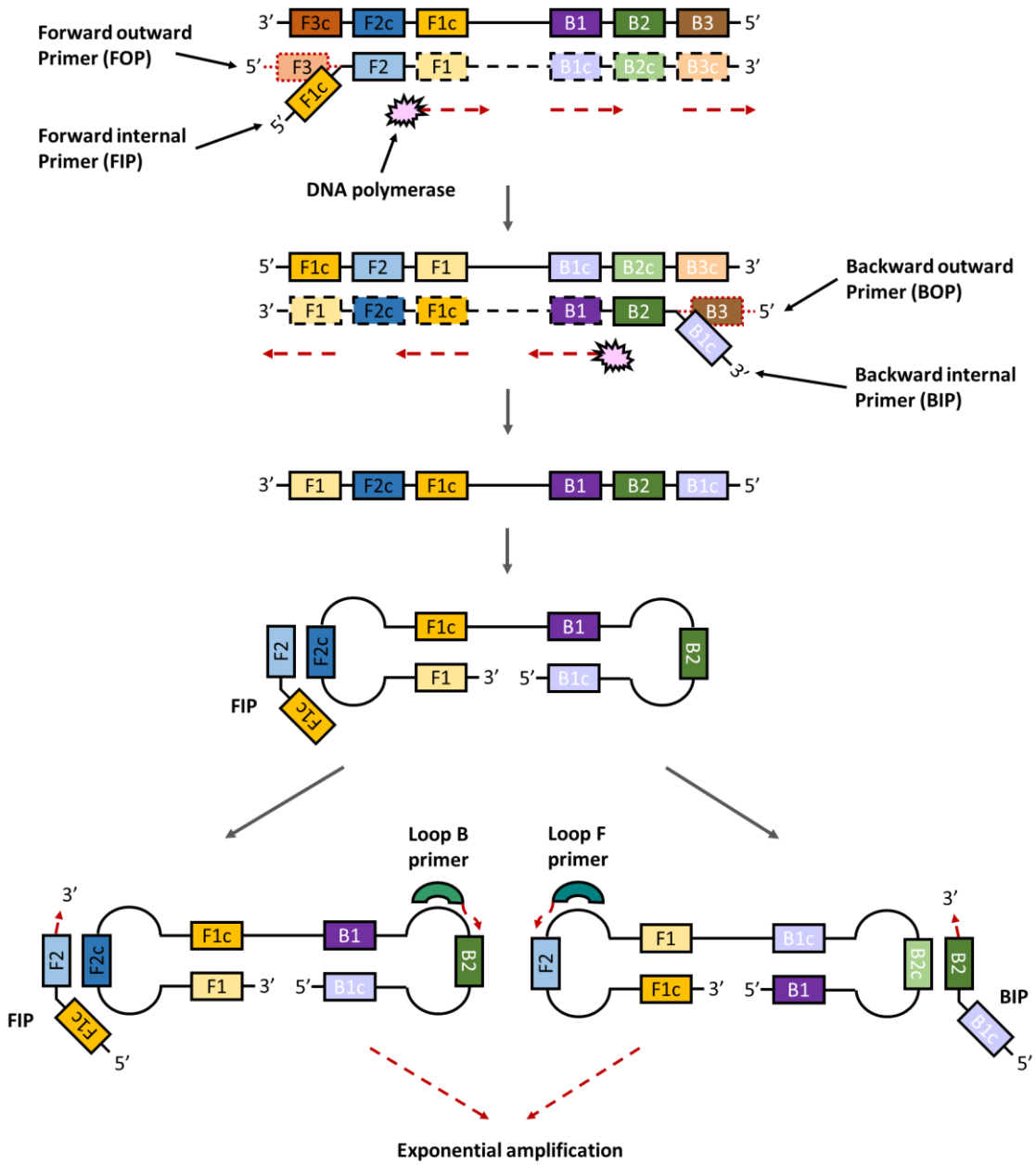

Figure 2.21. Schematic displaying the biochemical mechanisms of the loop-mediated isothermal amplification (LAMP) technique. B = backward, F = forward, and C = complementary strands.

While the protocol for carrying out LAMP is relatively simple and straightforward, the biochemical process is slightly more complicated (see Figure 2.21). LAMP begins with the 5' to 3' strand being displaced by DNA polymerase and attachment of the forward inner primer (FIP) to the 3' end of the target sequence at the F2c region. This leads to complementary strand synthesis of a 5' to 3' sequence that replaces the F3 region with and F1c overhang which is important later in the process. The newly synthesised

strand with the F1c overhang is then displaced by the forward outer primer (FOP) to produce ssDNA. The backward inner primer (BIP) then binds to the B2c region of the synthesised strand and forms a complementary 5' to 3' strand containing a B1c overhang region instead of the B3 region. The backward outer primer (BOP) then displaces the newly synthesised strand containing the F1, F2c, F1c, B1, B2 and B1c regions to produce a self-hybridising ssDNA. The ssDNA can then form a dumbbell structure whereby the F1, F1c, B1 and B1c regions self-hybridise. Further amplification occurs from the F2c region by FIP to produce two seed products. These seed products can then be exponentially amplified using FIP and BIP from the F2c and B2c regions, with amplification being further enhanced by forward and backward loop primers. The amplification products can then be detected for presence of the target sequence by fluorescence, biosensing and CRISPR-diagnostics techniques e.g., Specific High-sensitivity Enzymatic Reporter un-LOCKing (SHERLOCK) and DNA Endonuclease-Targeted CRISPR Trans Reporter (DETECTR) (Gootenberg *et al.*, 2017; Broughton *et al.*, 2020).

2.5. CRISPR-based diagnostics

CRISPR (Clustered Regularly Interspersed Short Palindromic Repeats) is the adaptive immune system found naturally occurring within bacterial genomes. It is simply put, a history of the viral DNA that has been collected by previous infections by invasive viral pathogens. This viral DNA is stored as part of bacteria's immune system as a series of interspersed short sequences between areas of non-coding DNA that were first discovered by Yoshizumi Ishino *et al*. and later fully described by Francisco Mojica *et al*. (Ishino *et al.*, 1987; Mojica, Juez and Rodriguez-Valera, 1993). When a viral pathogen attempts to invade and take over the molecular machinery of its host bacterium, one of two things occur. First, the bacterium can deploy enzymes called nucleases, specifically in bacterium called Cas enzymes, to cleave the target viral RNA. If the bacterium is successful in destroying the invading viruses target RNA, then the bacterium will transpose that viral RNA and insert it into its own genome as another part of its CRISPR infection history. However, if the bacterium has been previously affected by this virus it will have stored a copy of the viral DNA which can be transposed and translated to create targeting Cas enzymes containing guide RNA

which are complementary to the viral RNA to rapidly prevent infection through its characteristic ability of target cleavage.

In 2012, Jennifer Doudna and Emmanuelle Charpentier published a paper describing for the first time the invention of the CRISPR-Cas system for genome editing (Jinek *et al.*, 2012). In this study, the researchers describe the functionality of the CRISPR-Cas system in its ability to target and cleave target nucleic acids. They also explain its potential to be exploited as a gene disrupting tool as well as using designed RNA sequences to target specific areas of a genome to edit it (see Figure 2.22).

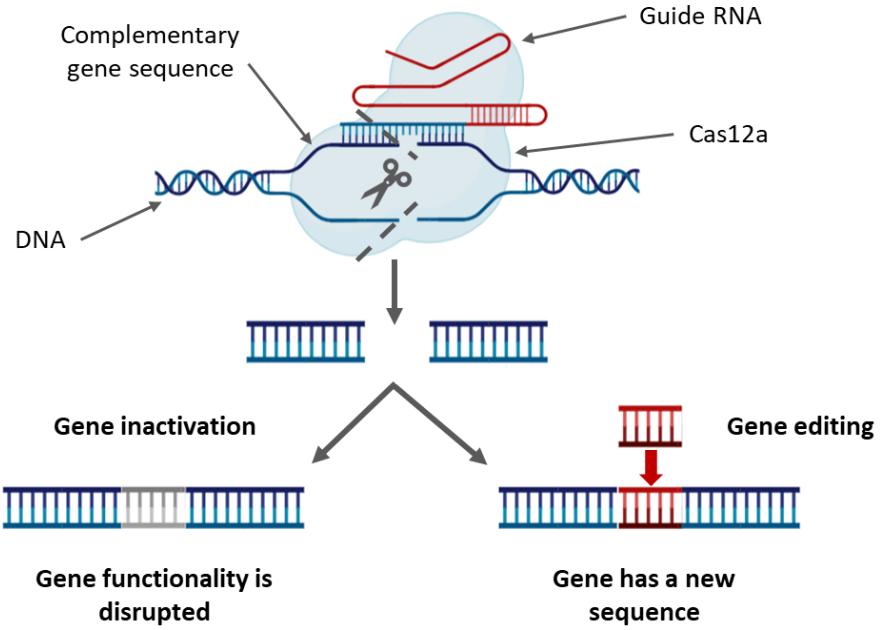

Figure 2.22. Schematic representation of CRISPR-Cas12a based genome editing resulting in either gene deactivation or gene sequence replacement through specific Cas9 nuclease cleavage.

Since the inception of this technique, several CRISPR-Cas related enzymes have been discovered with two classes and 6 subtypes. The primary difference between these varying CRISPR-Cas systems are the specific components and mechanisms they use for the bacterial immune systems associated functionality.

2.5.1. Using the CRISPR-Cas12a system for detection with SHERLOCK

In this thesis, we have taken advantage of the CRISPR-Cas12a system for the specific cleavage of target DNA sequences and its highly characteristic collateral cleavage ability. Using these biomolecular tools, we have implemented a technique developed by Zhang *et al*. through a collaboration between the McGovern Institute, the Broad Institute and Harvard University (Gootenberg *et al.*, 2017). SHERLOCK stands for Specific High-Sensitivity Enzymatic Reporter UnLOCKing and combines the collateral cleavage ability of Cas13a for RNA detection with isothermal amplification for high sensitivity. Once the Cas13a becomes activated through cleavage of the target RNA sequence it continues to collaterally cleave nearby sequences. This collateral cleavage can then be exploited to cleave RNA reporters that have fluorescent labels to provide an optical response in correlation with target concentration (see Figure 2.23).

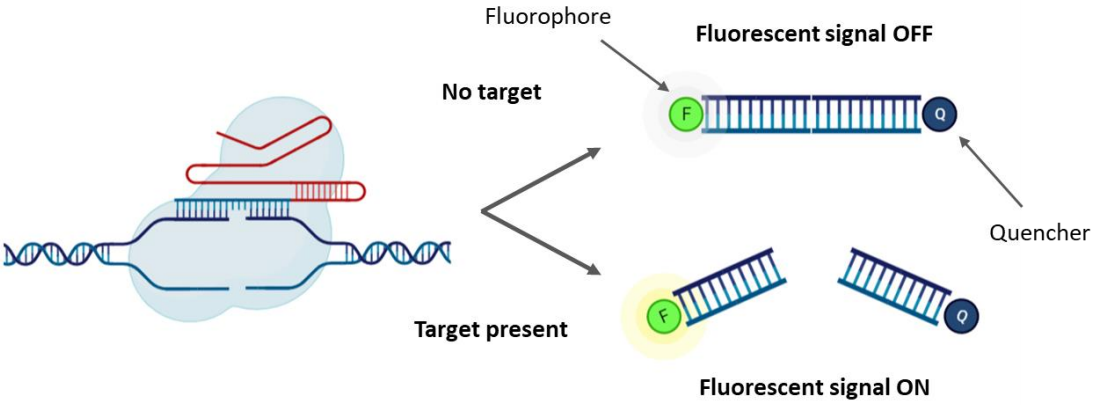

Figure 2.23. Schematic representation of the SHERLOCK CRISPR-Cas diagnostic technique used with a fluorescent reporter probe for qPCR analysis. In the presence of viral target RNA Cas13a cleaves the target and then collaterally cleaves the reporter probe, causing the quencher to be removed and the fluorophore to emit a light signal. When the target is not present in the sample, the reporter probe remains intact, and no light signal is emitted.

In this thesis, SHERLOCK has been implemented with Cas12a enzyme which cleaves target DNA. SARS-CoV-2 viral RNA was amplified using RT-LAMP followed by target cleavage using gRNA activated Cas12a. Collateral cleavage of the Cas12a enzyme was

then exploited for the cleavage of a reporter probe designed with a biotin group for downstream use in a highly sensitive electrochemical assay which will be discussed further in Chapter 5.

2.6. Other characterisation techniques

When developing an electrochemical biosensor, techniques other than electrochemical measurements may be used in the characterisation of probe functionalisation and target binding events. These may include optical techniques such as surface plasmon resonance (SPR), mass-based techniques including quartz crystal microbalance (QCM) as well as contact angle to measure surface wettability may also be used (Fang *et al.*, 2011; Bhalla *et al.*, 2016). In this thesis, contact angle measurements were used as a validatory tool to assess thiol self-assembled monolayer formation of gold electrode surfaces.

2.6.1. Contact angle

In this thesis, contact angle was used to study surface characteristics by measuring the wetting properties of gold electrodes. It can also provide information on the efficiency of probe DNA immobilisation onto gold surfaces (Fang *et al.*, 2011). When the surface of a solid interfaces with that of a liquid, many unique phenomena can be observed. Each surface has a specific level of a quality known as surface tension, with the level of surface tension leading to either hydrophobicity or hydrophilicity when interfaced with a liquid containing water. If the solid surface has a high surface tension it will provide a higher degree of water adhesion and is classified as hydrophilic. Conversely, if the material has a characteristically low surface tension the surface will repel water and is known as hydrophobic.

Typically, a contact angle study is a quick and simple way of characterising a functionalised electrode interface as it requires commonly sourced instrumentation such as a digital camera, optical focus lens and a diffused light source. An example of a typical setup can be seen below (see Figure 2.24). It is then possible to find the contact angle between the surface/solution interface to determine the success of SAM formation on the electrode surface.

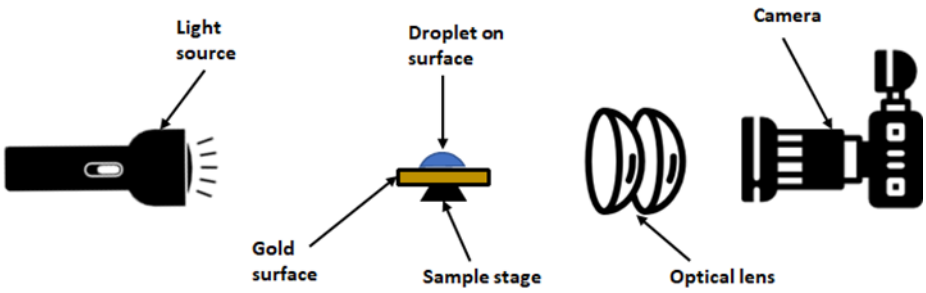

Figure 2.24. Typical setup for instrumentation to carry out in-house contact angle experiment.

References

Bahadır, E.B. and Sezgintürk, M.K. (2016) 'A review on impedimetric biosensors', Artificial Cells, Nanomedicine, and Biotechnology, 44(1), pp. 248–262. Available at: https://doi.org/10.3109/21691401.2014.942456.

Bard, A., Faulkner, L. and White, H. (2022) Electrochemical Methods: Fundamentals and Applications - Allen J. Bard, Larry R. Faulkner, Henry S. White - Google Books. Available at: https://books.google.co.uk/books?hl=en&lr=&id=4ShuEAAAQBAJ&oi=fnd&pg=PT44&dq=bard+and+faulkner+DPV+1980&ots=SIFxEYOxyA&sig=aifryfUexjPQTMUkj0_aiIVFYhA#v=onepage&q=DPV&f=false (Accessed: 22 July 2022).

Bard, A.J. and Faulkner, L.R. (2001) 'Basic Potential Step Methods', Electrochemical Methods: Fundamentals and Applications, pp. 156–225. Available at: https://books.google.com.mx/books?id=kv56QgAACAAJ (Accessed: 2 August 2022).

Bart, J. et al. (2009) 'Room-temperature intermediate layer bonding for microfluidic devices', Lab on a Chip, 9(24), pp. 3481–3488. Available at: https://doi.org/10.1039/B914270C.

Berggren, C., Bjarnason, B. and Johansson, G. (2001) 'Capacitive Biosensors'. Available at: https://doi.org/10.1002/1521-4109.

Bhalla, N. et al. (2016) 'Introduction to biosensors', Essays in Biochemistry. Edited by P. Estrela, 60(1), pp. 1–8. Available at: https://doi.org/10.1042/EBC20150001.

Bhattacharyya, I.M. and Shalev, G. (2020) 'Electrostatically Governed Debye Screening Length at the Solution-Solid Interface for Biosensing Applications', ACS Sensors, 5(1), pp. 154–161. Available at: https://doi.org/10.1021/ACSSENSORS.9B01939/SUPPL_FILE/SE9B01939_SI_001.PDF.

Broughton, J.P. et al. (2020) 'CRISPR–Cas12-based detection of SARS-CoV-2', Nature Biotechnology 2020 38:7, 38(7), pp. 870–874. Available at: https://doi.org/10.1038/s41587-020-0513-4.

Camillone, N. et al. (1996) ‘Chain Length Dependence of the Striped Phases of Alkanethiol Monolayers Self-Assembled on Au(111): An Atomic Beam Diffraction Study’, Langmuir, 12(11), pp. 2737–2746. Available at: https://doi.org/10.1021/la951097j.

Campuzano, S. et al. (2011) ‘Ternary monolayers as DNA recognition interfaces for direct and sensitive electrochemical detection in untreated clinical samples’, Biosensors and Bioelectronics, 26(8), pp. 3577–3583. Available at: https://doi.org/https://doi.org/10.1016/j.bios.2011.02.004.

Campuzano, S. et al. (2019) ‘Antifouling (Bio)materials for Electrochemical (Bio)sensing’, International Journal of Molecular Sciences, 20(2). Available at: https://doi.org/10.3390/IJMS20020423.

Celik, U. et al. (2021) ‘Molecular Level Structural Characterization of Self-Assembled Monolayers of Functionalized Bidentate Aromatic Thiols’, The Journal of Physical Chemistry C, 125(43), pp. 24162–24169. Available at: https://doi.org/10.1021/acs.jpcc.1c07171.

Chen, H. et al. (2019) ‘A new biosensor detection system to overcome the Debye screening effect: dialysis-silicon nanowire field effect transistor’, International Journal of Nanomedicine, 14, p. 2985. Available at: https://doi.org/10.2147/IJN.S198734.

Cherevko, S. et al. (2013) ‘Gold dissolution: towards understanding of noble metal corrosion’, RSC Advances, 3(37), pp. 16516–16527. Available at: https://doi.org/10.1039/C3RA42684J.

Couniot, N. et al. (2016) ‘Capacitive Biosensing of Bacterial Cells: Sensitivity Optimization’, IEEE Sensors Journal, 16(3), pp. 586–595. Available at: https://doi.org/10.1109/JSEN.2015.2485120.

Deféver, T. et al. (2011) ‘Real-time electrochemical PCR with a DNA intercalating redox probe’, Analytical Chemistry, 83(5), pp. 1815–1821. Available at: https://doi.org/10.1021/AC1033374/SUPPL_FILE/AC1033374_SI_001.PDF.

Díaz-Fernández, A. et al. (2021) 'Impedimetric aptamer-based glycan PSA score for discrimination of prostate cancer from other prostate diseases', Biosensors and Bioelectronics, 175, p. 112872. Available at: https://doi.org/10.1016/J.BIOS.2020.112872.

Dimcheva, N. (2020) 'Nanostructures of noble metals as functional materials in biosensors', Current Opinion in Electrochemistry, 19, pp. 35–41. Available at: https://doi.org/https://doi.org/10.1016/j.coelec.2019.09.008.

Doria, G. et al. (2012) 'Noble Metal Nanoparticles for Biosensing Applications', Sensors 2012, Vol. 12, Pages 1657-1687, 12(2), pp. 1657–1687. Available at: https://doi.org/10.3390/S120201657.

Du, D. et al. (2011) 'Multiplexed electrochemical immunoassay of phosphorylated proteins based on enzyme-functionalized gold nanorod labels and electric field-driven acceleration', Analytical Chemistry, 83(17), pp. 6580–6585. Available at: https://doi.org/10.1021/AC2009977/SUPPL_FILE/AC2009977_SI_001.PDF.

Elgrishi, N. et al. (2018) 'A Practical Beginner's Guide to Cyclic Voltammetry', Journal of Chemical Education, 95(2), pp. 197–206. Available at: https://doi.org/10.1021/acs.jchemed.7b00361.

Erkkila, K.E., Odom, D.T. and Barton, J.K. (1999) 'Recognition and reaction of metallointercalators with DNA', Chemical Reviews, 99(9), pp. 2777–2795. Available at: https://doi.org/10.1021/CR9804341/ASSET/IMAGES/LARGE/CR9804341F00022.JPEG.

Fang, T.H. et al. (2011) 'Surface and mechanical characteristics of alkanethiol self-assembled monolayers', Journal of Advanced Microscopy Research, 6(1), pp. 24–28. Available at: https://doi.org/10.1166/JAMR.2011.1054.

Fischer, L.M. et al. (2009) 'Gold cleaning methods for electrochemical detection applications', Microelectronic Engineering, 86(4), pp. 1282–1285. Available at: https://doi.org/https://doi.org/10.1016/j.mee.2008.11.045.

Gootenberg, J.S. et al. (2017) ‘Nucleic acid detection with CRISPR-Cas13a/C2c2’, Science, 356(6336), pp. 438–442. Available at: https://doi.org/10.1126/SCIENCE.AAM9321/SUPPL_FILE/PAPV2.PDF.

Grieshaber, D. et al. (2008) ‘Electrochemical Biosensors - Sensor Principles and Architectures’, Sensors (Basel, Switzerland), 8(3), p. 1400. Available at: https://doi.org/10.3390/S80314000.

Guo, L.H. et al. (1994) ‘Effect of Gold Topography and Surface Pretreatment on the Self-Assembly of Alkanethiol Monolayers’, Langmuir, 10(12), pp. 4588–4593. Available at: https://doi.org/10.1021/LA00024A033/ASSET/LA00024A033.FP.PNG_V03.

Guziejewski, D. et al. (2022) ‘Reversible and Quasireversible Electron Transfer under Conditions of Differential Square-Wave Voltammetry’, The Journal of Physical Chemistry C, 126(12), pp. 5584–5591. Available at: https://doi.org/10.1021/acs.jpcc.2c01188.

Hong, H.-G., Park, W. and Yu, E. (1999) ‘Voltammetric determination of electron transfer kinetic parameters in hydroquinone-terminated self-assembled monolayers on gold’, Journal of Electroanalytical Chemistry, 476(2), pp. 177–181. Available at: https://doi.org/https://doi.org/10.1016/S0022-0728(99)00380-0.

Hryniewicz, B.M. et al. (2021) ‘Nanostructured Platforms Based on Conducting Polymers for Sensing’, Reference Module in Biomedical Sciences [Preprint]. Available at: https://doi.org/10.1016/B978-0-12-822548-6.00024-8.

Ignatov, K.B. et al. (2014) ‘A strong strand displacement activity of thermostable DNA polymerase markedly improves the results of DNA amplification’, BioTechniques, 57(2), pp. 81–87. Available at: https://doi.org/10.2144/000114198/ASSET/IMAGES/LARGE/TABLE1.JPEG.

Inkpen, M.S. et al. (2019) ‘Non-chemisorbed gold–sulfur binding prevails in self-assembled monolayers’, Nature Chemistry, 11(4), pp. 351–358. Available at: https://doi.org/10.1038/s41557-019-0216-y.

Ishino, Y. et al. (1987) 'Nucleotide sequence of the iap gene, responsible for alkaline phosphatase isozyme conversion in Escherichia coli, and identification of the gene product.', Journal of Bacteriology, 169(12), p. 5429. Available at: https://doi.org/10.1128/JB.169.12.5429-5433.1987.

Jinek, M. et al. (2012) 'A programmable dual-RNA-guided DNA endonuclease in adaptive bacterial immunity', Science, 337(6096), pp. 816–821. Available at: https://doi.org/10.1126/SCIENCE.1225829/SUPPL_FILE/JINEK.SM.PDF.

Jolly, P. et al. (2015) 'Label-free impedimetric aptasensor with antifouling surface chemistry: A prostate specific antigen case study', Sensors and Actuators B: Chemical, 209, pp. 306–312. Available at: https://doi.org/https://doi.org/10.1016/j.snb.2014.11.083.

Jolly, P., Miodek, A., et al. (2016) 'Electro-Engineered Polymeric Films for the Development of Sensitive Aptasensors for Prostate Cancer Marker Detection', ACS Sensors, 1(11), pp. 1308–1314. Available at: https://doi.org/10.1021/acssensors.6b00443.

Jolly, P., Batistuti, M.R., et al. (2016) 'Highly sensitive dual mode electrochemical platform for microRNA detection', Scientific Reports 2016 6:1, 6(1), pp. 1–10. Available at: https://doi.org/10.1038/srep36719.

Jolly, P. et al. (2017) 'Self-assembled gold nanoparticles for impedimetric and amperometric detection of a prostate cancer biomarker', Sensors and Actuators B: Chemical, 251, pp. 637–643. Available at: https://doi.org/10.1016/J.SNB.2017.05.040.

Jolly, P. et al. (2019) 'A PNA-based Lab-on-PCB diagnostic platform for rapid and high sensitivity DNA quantification', Biosensors and Bioelectronics, 123, pp. 244–250. Available at: https://doi.org/10.1016/J.BIOS.2018.09.006.

Keighley, S.D. et al. (2008) 'Optimization of DNA immobilization on gold electrodes for label-free detection by electrochemical impedance spectroscopy', Biosensors and Bioelectronics, 23(8), pp. 1291–1297. Available at: https://doi.org/https://doi.org/10.1016/j.bios.2007.11.012.

Kelly, V., Codispoti, L. and Harford, J. (2008) 'Autonomous device with biofouling control and method for monitoring aquatic environment'. United States.

Kesler, V., Murmann, B. and Soh, H.T. (2020) 'Going beyond the Debye Length: Overcoming Charge Screening Limitations in Next-Generation Bioelectronic Sensors', ACS Nano, 14(12), pp. 16194–16201. Available at: https://doi.org/10.1021/ACSNANO.0C08622/ASSET/IMAGES/LARGE/NN0C08622_0004.JPEG.

Khatri, N. and Tyagi, S. (2015) 'Influences of natural and anthropogenic factors on surface and groundwater quality in rural and urban areas', Frontiers in Life Science, 8(1), pp. 23–39. Available at: https://doi.org/10.1080/21553769.2014.933716.

Kim, S. et al. (2018) 'Electrically Conductive Polydopamine–Polypyrrole as High Performance Biomaterials for Cell Stimulation in Vitro and Electrical Signal Recording in Vivo', ACS Applied Materials & Interfaces, 10(39), pp. 33032–33042. Available at: https://doi.org/10.1021/acsami.8b11546.

Kuralay, F. et al. (2011) 'Highly sensitive disposable nucleic acid biosensors for direct bioelectronic detection in raw biological samples', Talanta, 85(3), pp. 1330–1337. Available at: https://doi.org/https://doi.org/10.1016/j.talanta.2011.06.012.

Leonardo, S., Toldrà, A. and Campàs, M. (2021) 'Biosensors Based on Isothermal DNA Amplification for Bacterial Detection in Food Safety and Environmental Monitoring', Sensors (Basel, Switzerland), 21(2), pp. 1–24. Available at: https://doi.org/10.3390/S21020602.

Li, Y., Schluesener, H.J. and Xu, S. (2010) 'Gold nanoparticle-based biosensors', Gold Bulletin, 43(1), pp. 29–41. Available at: https://doi.org/10.1007/BF03214964.

Lichtenberg, J.Y., Ling, Y. and Kim, S. (2019) 'Non-Specific Adsorption Reduction Methods in Biosensing', Sensors 2019, Vol. 19, Page 2488, 19(11), p. 2488. Available at: https://doi.org/10.3390/S19112488.

Lin, H. bin et al. (2011) 'Crystal structure and DNA binding studies of a cobalt(II) complex containing mixed-ligands of 1, 10-phenathroline and glycollic acid', Chinese

Chemical Letters, 22(8), pp. 969–972. Available at: https://doi.org/10.1016/J.CCLET.2011.03.003.

Lojou, É. and Bianco, P. (2006) 'Application of the electrochemical concepts and techniques to amperometric biosensor devices', Journal of Electroceramics 2006 16:1, 16(1), pp. 79–91. Available at: https://doi.org/10.1007/S10832-006-2365-9.

Love, J.C. et al. (2005) 'Self-Assembled Monolayers of Thiolates on Metals as a Form of Nanotechnology', Chemical Reviews, 105(4), pp. 1103–1170. Available at: https://doi.org/10.1021/cr0300789.

Madaboosi, N. et al. (2015) 'A microfluidic immunoassay platform for the detection of free prostate specific antigen: a systematic and quantitative approach', Analyst, 140(13), pp. 4423–4433. Available at: https://doi.org/10.1039/C5AN00364D.

Magar, H.S., Hassan, R.Y.A. and Mulchandani, A. (2021) 'Electrochemical Impedance Spectroscopy (EIS): Principles, Construction, and Biosensing Applications', Sensors (Basel, Switzerland), 21(19). Available at: https://doi.org/10.3390/S21196578.

Miodek, A. et al. (2015) 'Optimisation and Characterisation of Anti-Fouling Ternary SAM Layers for Impedance-Based Aptasensors.', Sensors (Basel, Switzerland), 15(10), pp. 25015–25032. Available at: https://doi.org/10.3390/s151025015.

Miodek, A. et al. (2016) 'Electrochemical functionalization of polypyrrole through amine oxidation of poly(amidoamine) dendrimers: Application to DNA biosensor', Talanta, 154, pp. 446–454. Available at: https://doi.org/https://doi.org/10.1016/j.talanta.2016.03.076.

Mobaraki, M. et al. (2017) 'Molecular Mechanisms of Cardiotoxicity: A Review on Major Side-effect of Doxorubicin', Indian Journal of Pharmaceutical Sciences, 79(3), pp. 335–344. Available at: https://doi.org/10.4172/PHARMACEUTICAL-SCIENCES.1000235.

Mojica, F.J.M., Juez, G. and Rodriguez-Valera, F. (1993) 'Transcription at different salinities of Haloferax mediterranei sequences adjacent to partially modified PstI sites.', Molecular Microbiology, 9(3), pp. 613–621. Available at: https://doi.org/10.1111/J.1365-2958.1993.TB01721.X.

Najjar, D. et al. (2022) ‘A lab-on-a-chip for the concurrent electrochemical detection of SARS-CoV-2 RNA and anti-SARS-CoV-2 antibodies in saliva and plasma’, Nature Biomedical Engineering 2022, pp. 1–11. Available at: https://doi.org/10.1038/s41551-022-00919-w.

Pacchioni, G. (2019) ‘A not-so-strong bond’, Nature Reviews Materials, 4(4), p. 226. Available at: https://doi.org/10.1038/s41578-019-0094-3.

Palmsens (2022) Differential Pulse Voltammetry (DPV). Available at: https://www.palmsens.com/knowledgebase-article/differential-pulse-voltammetry-dpv/ (Accessed: 22 July 2022).

Pheeney, C.G. and Barton, J.K. (2013) ‘Intraduplex DNA-mediated electrochemistry of covalently tethered redox-active reporters’, Journal of the American Chemical Society, 135(40), pp. 14944–14947. Available at: https://doi.org/10.1021/JA408135G/SUPPL_FILE/JA408135G_SI_001.PDF.

Qing, X.W., Gao, F. and Jiao, K. (2008) ‘Voltammetric Studies on the Recognition of a Copper Complex to Single- and Double-Stranded DNA and Its Application in Gene Biosensor’, Electroanalysis, 20(19), pp. 2096–2101. Available at: https://doi.org/10.1002/ELAN.200804291.

Regan, E.M. et al. (2014) ‘A novel cobalt complex for enhancing amperometric and impedimetric DNA detection’, Electrochimica Acta, 128, pp. 10–15. Available at: https://doi.org/https://doi.org/10.1016/j.electacta.2013.10.028.

Ron, H., Matlis, S. and Rubinstein, I. (1998) ‘Self-assembled monolayers on oxidized metals. 2. Gold surface oxidative pretreatment, monolayer properties, and depression formation’, Langmuir, 14(5), pp. 1116–1121. Available at: https://doi.org/10.1021/LA970785V.

Roussel, T.J. et al. (2008) ‘Amperometric Techniques’, Encyclopedia of Microfluidics and Nanofluidics, pp. 39–47. Available at: https://doi.org/10.1007/978-0-387-48998-8_26.

Sabaté del Río, J. et al. (2019) ‘An antifouling coating that enables affinity-based electrochemical biosensing in complex biological fluids’, Nature Nanotechnology, 14(12), pp. 1143–1149. Available at: https://doi.org/10.1038/s41565-019-0566-z.

Schmickler, W. (2014) ‘Electrochemical Theory: Double Layer’, Reference Module in Chemistry, Molecular Sciences and Chemical Engineering [Preprint]. Available at: https://doi.org/10.1016/B978-0-12-409547-2.11149-7.

Scholz, F. (2010) ‘Electroanalytical methods: Guide to experiments and applications’, Electroanalytical Methods: Guide to Experiments and Applications, pp. 1–359. Available at: https://doi.org/10.1007/978-3-642-02915-8/COVER.

Schrader, C. et al. (2012) ‘PCR inhibitors – occurrence, properties and removal’, Journal of Applied Microbiology, 113(5), pp. 1014–1026. Available at: https://doi.org/10.1111/J.1365-2672.2012.05384.X.

Schreiber, F. (2000) ‘Structure and growth of self-assembling monolayers’, Progress in Surface Science, 65(5), pp. 151–257. Available at: https://doi.org/https://doi.org/10.1016/S0079-6816(00)00024-1.

Silva Olaya, A.R., Zandersons, B. and Wittstock, G. (2020) ‘Restructuring of Nanoporous Gold Surfaces During Electrochemical Cycling in Acidic and Alkaline Media’, ChemElectroChem, 7(17), pp. 3670–3678. Available at: https://doi.org/10.1002/CELC.202000923.

Sireesha, M. et al. (2018) ‘A review on carbon nanotubes in biosensor devices and their applications in medicine’, Nanocomposites, 4(2), pp. 36–57. Available at: https://doi.org/10.1080/20550324.2018.1478765.

Soroka, M., Wasowicz, B. and Rymaszewska, A. (2021) ‘Loop-Mediated Isothermal Amplification (LAMP): The Better Sibling of PCR?’, Cells 2021, Vol. 10, Page 1931, 10(8), p. 1931. Available at: https://doi.org/10.3390/CELLS10081931.

Staderini, M. et al. (2018) ‘A tripod anchor offers improved robustness of peptide-based electrochemical biosensors’, Sensors and Actuators B: Chemical, 274, pp. 662–667. Available at: https://doi.org/10.1016/J.SNB.2018.07.100.

Stern, E. et al. (2007) 'Importance of the debye screening length on nanowire field effect transistor sensors', Nano Letters, 7(11), pp. 3405–3409. Available at: https://doi.org/10.1021/NL071792Z/SUPPL_FILE/NL071792ZSI20070910_015801.PDF.

Timilsina, S.S. et al. (2021) 'Enabling Multiplexed Electrochemical Detection of Biomarkers with High Sensitivity in Complex Biological Samples', Accounts of Chemical Research, 54(18), pp. 3529–3539. Available at: https://doi.org/10.1021/acs.accounts.1c00382.

Timilsina, S.S. et al. (2022) 'Ultrarapid Method for Coating Electrochemical Sensors with Antifouling Conductive Nanomaterials Enables Highly Sensitive Multiplexed Detection in Whole Blood', Advanced Healthcare Materials, 11(8), p. 2102244. Available at: https://doi.org/https://doi.org/10.1002/adhm.202102244.

Tkac, J. and Davis, J.J. (2008) 'An optimised electrode pre-treatment for SAM formation on polycrystalline gold', Journal of Electroanalytical Chemistry, 621(1), pp. 117–120. Available at: https://doi.org/https://doi.org/10.1016/j.jelechem.2008.04.010.

Tsouti, V. et al. (2011) 'Capacitive microsystems for biological sensing', Biosensors and Bioelectronics, 27(1), pp. 1–11. Available at: https://doi.org/10.1016/J.BIOS.2011.05.047.

Vezza, V.J. et al. (2021) 'An electrochemical SARS-CoV-2 biosensor inspired by glucose test strip manufacturing processes', Chemical Communications, 57(30), pp. 3704–3707. Available at: https://doi.org/10.1039/D1CC00936B.

Zhang, K. et al. (2013) 'A new strategy based on aptasensor to time-resolved fluorescence assay for adenosine deaminase activity', Biosensors & bioelectronics, 41(1), pp. 123–128. Available at: https://doi.org/10.1016/J.BIOS.2012.07.064.

3. Development of an impedance-based genosensor for the detection of waterborne pathogens

This chapter will outline the assay development of a thiol-based genosensor for detection of *E. coli* bacterial DNA. The study will focus on the use of electrochemical impedance spectroscopy measurements for optimisation of thiol-based surface chemistry and detection of DNA hybridisation. This study will highlight the importance of surface pre-treatment of re-usable gold electrode surfaces. The effects of probe surface density and co-immobilisation ratios between thiolated ssDNA and MCH will be assessed as well as other variables that may affect the efficiency of DNA surface hybridisation and improve signal outputs.

3.1. Background

The detection of nucleic acids is an important tool for the diagnosis of disease, prognosis of disorders as well as applications in food safety (Regan *et al.*, 2014; Bhalla *et al.*, 2016) and monitoring of waterborne pathogens within the urban-affected environment (Rainbow *et al.*, 2020; Singh *et al.*, 2020). Simple and rapid detection of nucleic acid biomarkers by handheld biosensor devices is currently an attractive area of research that holds many advantages over traditional techniques. At present, techniques such as polymerase chain reaction (PCR), fluorescence, mass spectroscopy, microbial culturing and micro-arrays are traditionally used for detection of nucleic acids for a multitude of applications (Lazcka, Campo and Muñoz, 2007). Unfortunately, these techniques suffer multiple drawbacks that make them impractical for real-time, point-of-care (PoC) or *in-situ* monitoring purposes (Rainbow *et al.*, 2020a). These limitations may include long sample to answer times, expensive machinery, high reagent use, expert handling, and complex data output (Land *et al.*, 2019). Thus, the development of handheld lab-on-chip (LOC) electrochemical biosensors for the detection of nucleic acids have been seen as an attractive alternative to solve these issues. Recent developments in biosensor devices have demonstrated advantages such as rapid sample-in-answer-out times, inexpensive off-the-shelf components, low reagent, and sample requirements due to microfluidic integration, simple user interfaces with intuitive data outputs as well as

higher sensitivity suggesting potential for use in PoC and *in-situ* circumstances e.g., doctors' clinics and reservoirs (Gupta *et al.*, 2016; Moschou and Tserepi, 2017).

Electrochemical biosensors that detect the presence of nucleic acids, commonly known as electrochemical genosensors, are devices that convert molecular nucleic acid hybridisation events through a transducer into an electrical signal output (Yang, McGovern and Thompson, 1997; Bonanni and del Valle, 2010). These devices work by functionalising a surface with a molecular probe e.g., DNA, proteins or cells and measuring the current, potential or impedance between the electrolyte solution and the functionalised surface. Upon binding of a target nucleic acid, the observable signal will increase or decrease based on the charge of the molecule or any confirmational change of the probe molecule. Signal changes can be measured by both amperometric techniques such as cyclic voltammetry (CV), square wave voltammetry (SWV) or differential pulse voltammetry (DPV) as well as potentiometric or impedimetric techniques such as electrochemical impedance spectroscopy (EIS). This chapter will focus on the use of Faradaic EIS for the characterisation of a DNA hybridisation assay on gold planar electrodes, using *E. coli* synthesis oligonucleotides as a case study. The development of a thiol-based surface chemistry will be explored as well as the effects of gold surface preparation techniques and the variables that may affect optimal self-assembled monolayer (SAM) formation and target binding efficiency.

3.2. Methods and Materials

3.2.1. Instruments and reagents

Synthetic DNA oligonucleotides, both thiol-modified and unmodified, were purchased HPLC-purified from Sigma-Aldrich (UK). 6-Mercapto-1-Hexanol (97%), potassium phosphate monobasic solution (1 M), potassium phosphate dibasic solution (1 M), potassium sulphate, potassium hexacyanoferrate (III), potassium hexacyanoferrate (II) trihydrate, magnesium chloride, ethylenediaminetetraacetic acid (EDTA, 0.5 M), sulfuric acid (95-98%), hydrogen peroxide solution (30%) and nuclease-free water were all purchased from Sigma-Aldrich (UK). Ethanol (99.8%) was purchased from Fisher Scientific. Polishing pads and alumina slurry (0.05 and 1

µm) were purchased from Electron Microscopy Sciences (USA). All aqueous solutions were prepared using 18.2 MΩ cm ultra-pure water (Millipore, USA) unless otherwise stated. All electrochemical data values were analysed using the PSTrace 5.9 software and graphed using OriginPro 8.5. Contact angle data was analysed using ImageJ open-source image analysis software.

3.2.2. Electrochemical measurements

Electrochemical impedance spectroscopy (EIS) was used for all experiments and performed on a PalmSens4 potentiostat (PalmSens BV, The Netherlands). A three-electrode setup was used with gold disk working electrodes (CH Instruments, USA), a platinum wire counter electrode (ALS Instruments, Japan) and an Ag/AgCl (KCl saturated) reference electrode (BASi, USA) placed into a salt bridge containing 50 mM PB + 100 mM K_2SO_4, pH 7.0. For Faradaic measurements the electrochemical impedance spectrum was measured in a solution of 2 mM $K_4[Fe(CN)_6]$ + 2 mM $K_3[Fe(CN)_6]$ in 50 mM PB + 100 mM K_2SO_4, pH 7.0. The impedance spectrum was measured over the frequency range 100 kHz to 100 mHz, with a 10 mV a.c. voltage superimposed on a d.c. bias of 0.2 V, which corresponds to the formal potential of the redox couple vs. an Ag/AgCl reference electrode.

3.2.3. Electrode cleaning and pre-treatment

Polycrystalline gold disk working electrodes with a radius of 1.0 mm were prepared for surface-functionalisation using two methods of electrode cleaning and pre-treatment. The first cleaning protocol, protocol A, includes traditional techniques for cleaning of reusable gold surfaces recommended by electrode suppliers. The second cleaning protocol, protocol B, is specifically optimised for removal of previously bound molecules as well as removal of a surface AuO layer formed by the harsh oxidative cleaning techniques.

Protocol A involved steps of cleaning gold polycrystalline working electrodes (WEs) including mechanical polishing, chemical stripping, and electrochemical polishing. Briefly, electrodes were sonicated in ultrapure water for 3 minutes before mechanical polishing of each electrode with a 1 µm alumina slurry for 3 minutes per electrode. Electrodes were then sonicated in ultrapure water to remove any alumina

residues and further polished again using a 0.05 µm alumina slurry for a further 3 minutes per electrode. The electrodes were then sonicated in ultrapure water for 3 minutes before chemically stripping in hot piranha solution containing hydrogen peroxide solution and concentrated sulfuric acid at a respective ratio of 1:3 for 15 minutes. This was followed by another 3 minutes of sonication in ultrapure water before each electrode was electrochemically polished. Electrochemical polishing was performed by cycling working electrodes between -0.2 V and 1.5 V vs. Ag/AgCl at a scan rate of 0.2 V/s and step potential of 0.01 V for 50 cycles in 0.5 M H_2SO_4 aqueous solution. Finally, electrodes were rinsed with ultrapure water, dried under nitrogen, and stored in a sealed 0.5 mL Eppendorf tube before functionalisation.

For protocol B, polycrystalline gold disk working electrodes with a radius of 1.0 mm were cleaned using a previously optimised protocol (Tkac and Davis, 2008). Briefly, working electrodes were stripped of any previously functionalised thiols by pre-treatment of cyclic voltammetry (CV) between -1.5 V and -0.5 V vs. Ag/AgCl at a scan rate of 1.0 V/s and a step potential of 0.01 V for 200 cycles in 0.1 M NaOH. This was followed by mechanical polishing of each WE with a 0.05 µm alumina slurry on a polishing pad for 3 minutes per electrode. Electrodes were then rinsed with ultrapure water and ultrasonically cleaned in ultrapure water for 2 minutes to remove any alumina residue. Electrodes were then chemically stripped by dipping in hot piranha solution containing hydrogen peroxide solution and concentrated sulfuric acid at a respective ratio of 1:3 for 15 minutes. The electrodes were then rinsed and ultrasonicated in ultrapure water for a further 1 minute. Electrochemical polishing was performed by cycling working electrodes between -0.2 V and 1.5 V vs. Ag/AgCl at a scan rate of 0.1 V/s and step potential of 0.01 V for 25 cycles in 0.1 M H_2SO_4 aqueous solution. Gold oxides were then immediately electrochemically stripped by running 10 cycles from 0.2 V to 0.8 V vs. Ag/AgCl at the same scan rate and step potential in 0.1 M H_2SO_4. Electrodes were placed in absolute ethanol for 20 minutes to chemically reduce any remaining gold oxides formed during the cleaning process. Finally, electrodes were rinsed with ultrapure water, dried under nitrogen, and stored in sealed 0.5 mL Eppendorf tubes before functionalisation.

3.2.4. Preparation of thiolated DNA self-assembled monolayer

After cleaning, each working electrode was dried under a stream of nitrogen and exposed to 150 µL of a mixed self-assembled monolayer (SAM) containing thiolated DNA and MCH in a humidity chamber for at least 16 hours. Probe ssDNA was modified with a HS-$(CH)_6$ group on the 5' end and had a 22-base sequence of 5'- TTT TTG GTC CGC TTG CTC TCG C -3' from the genome of *E. Coli*, serotype O157:H7. Five thymine bases were added at the 5' end to increase the distance of the probe DNA from the electrode surface. The immobilisation buffer contained 0.8 M phosphate buffer (PB) + 1.0 M NaCl + 5 mM $MgCl_2$ + 1 mM ethylene diamine tetraacetic acid (EDTA), pH 7.0. After initial SAM immobilisation, electrodes were rinsed with a wash buffer containing 50 mM PB + 100 mM K_2SO_4 + 10 mM EDTA, pH 7.0, to remove any residual Mg^{2+} ions. To ensure complete coverage of the gold electrode surface and reduce the chance of pinholes, electrodes were backfilled with a solution of 1 mM MCH in ultrapure water for 1 hour. Finally, electrodes were rinsed with ultrapure water and placed in 50 mM PB + 100 mM K_2SO_4, pH 7.0, for 1 hour to ensure stability of the SAM.

3.2.5. DNA target hybridisation

Synthetic complementary ssDNA was incubated on the surface of the optimised biosensor surface with a 17-base sequence of 5'- GCG AGA GCA AGC GGA CC -3'. Target DNA was prepared as aliquots from lyophilised state in nuclease-free water (Sigma-Aldrich, UK) at a stock concentration (100 µM) and serial diluted to working concentrations in 50 mM PB + 100 mM K_2SO_4, pH 7.0. Once the self-assembled monolayer was stable, electrodes were incubated with 100 µL of target ssDNA (100 pM–1 µM) for 45 or 60 minutes at ambient room temperature (RT). Electrodes were then rinsed with 50 mM PB + 100 mM K_2SO_4, pH 7.0.

3.3. Results and Discussion

An analysis of the different cleaning procedures is presented using voltametric reductive desorption of surface-bound alkanethiols to determine effectiveness of surface coverage. DNA self-assembled monolayer formation controlled by using MCH spacer and target binding conditions were then optimised for efficient target DNA

hybridisation and measured using Faradaic EIS. Target hybridisation was further assessed by the dose response of target DNA concentrations from 100 pM to 1 µM to determine limit of detection (LOD) as well as the binding efficiency (K_D). Finally, a small validation study was carried out using contact angle to determine the difference between liquid-solid interface upon formation of the thiolated DNA/MCH SAM on a gold surface.

3.3.1. Optimised cleaning of polycrystalline gold electrode for efficient alkanethiol surface functionalisation

It has been previously determined that the cause of Au gold oxide formation on gold electrode surfaces is the oxidation of the surface by anodic potentials higher than 1.095 V during electrochemical polishing in H_2SO_4 (Tkac and Davis, 2008). Therefore, to validate the formation of Au gold oxide after electrochemical polishing (E_p), cyclic voltammetry was employed to both determine presence and remove any surface-bound gold oxide alongside chemical reduction in ethanol. Figure 3.1 shows the result of electrochemical Au gold oxide stripping within protocol B of electrode cleaning. From the reductive scans, scan 1 was subtracted from scan 10 and resulting graph shows a peak at 0.7 V, versus Ag/AgCl, indicative of the presence of Au gold oxide formed after electrochemical polishing as was shown previously (Tkac and Davis, 2008). This verified the formation of Au gold oxide formation on gold electrodes, further justifying changes to the gold electrode cleaning by addition of electrochemical stripping (E_s) and chemical reduction in ethanol.

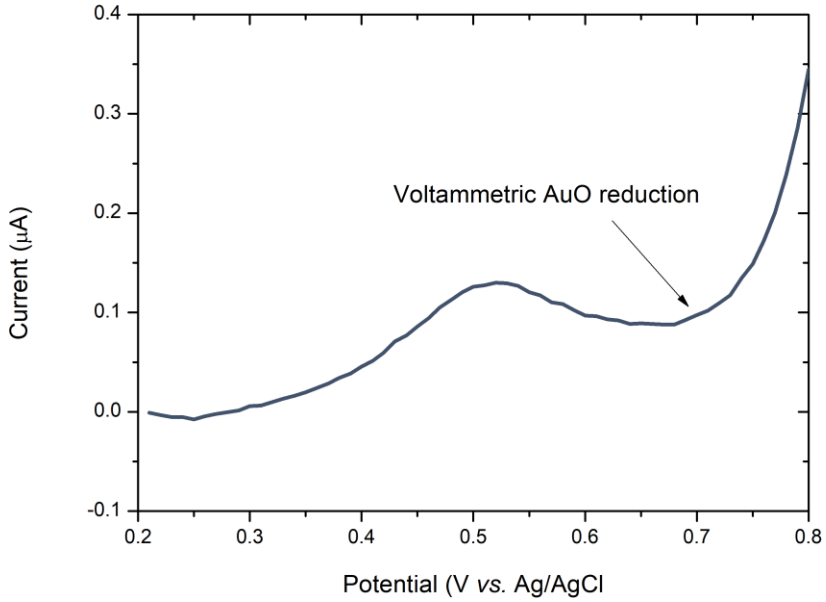

Figure 3.1. Electrochemical stripping of Au oxide in 100 mM H2SO4 aqueous solution. Graphic shows the subtracted CV scans (1st scan subtracted from 10th scan) with clear peak attributed to Au gold oxide presence. CV scan ranged from 0.2 V to 0.8 V vs. Ag/AgCl reference at a scan rate of 1.0 V/s and a step potential of 0.01 V.

To compare and evaluate the surface coverage of alkanethiols on gold surfaces cleaned by both protocol A and B, reductive desorption was carried out in 100 mM NaOH. First, electroactive surface area (ESA) of the gold electrodes was obtained from the cleaning done before incubation with each SAM. Integration of the gold reduction peak from the last E_p scan was used to obtain a charge value for the real ESA of the gold (between 29.8 and 44.2 μC) and compared with the theoretical charge density of polycrystalline gold (390 μC cm^{-2}) as a calibrating factor reported previously (Trasatti and Petrii, 1991; Sekretaryova *et al.*, 2019). The ESA (A) can be expressed as:

$$A = \frac{Q}{\sigma}$$

Where, Q is equal to the charge of the Au gold oxide reduction peak during electrochemical polishing and σ is the theoretical charge density of polycrystalline gold (390 μC cm^{-2}). The resulting average ESA values were determined to be 9.51 and 9.73 mm^2 (n=6) for protocol A and protocol B, respectively. These results suggest that

the electrochemically active area of the electrodes cleaned by protocol B, with thiol stripping and electrochemical gold oxide reduction, is higher due to the reduction of the gold oxide layer which acts as an insulating layer. In Figure 3.2, CV was used to electrochemically strip the SAMs formed after each cleaning protocol with measurements taken for bare gold (solid red line), SAM formed after protocol A (dashed blue line), and SAM formed after protocol B (solid blue line). The reaction occurring at the gold surface during thiol desorption can be expressed as below (Sumi and Uosaki, 2004; Tricase *et al.*, 2022):

$$RS - Au + e^{-} \rightarrow RS + Au$$

Surface coverage was then estimated using a previously described technique (Suroviec, 2012; Tricase *et al.*, 2022), with the following equation:

$$\Gamma = \frac{Q}{nFA}$$

Where, Γ is the surface coverage, Q is the charge transferred during the reduction of thiols equal to the area of the reduction peak during CV between -1.0 and -1.2 V, n is the number of electrons exchanged (n=1 in this case), F is the Faraday Constant, and A is the previously calculated ESA of the electrode during E_p. Surface coverage for the SAM formed after cleaning with protocol A was 1.53 x 10^{-6} mol cm^{-2} while the SAM formed after cleaning with protocol B gave a surface coverage of 3.02 x 10^{-6} mol cm^{-2}. By multiplying these values with Avogadro's Number, the average number of surface bound molecules were estimated as 9.24 x 10^{17} and 1.82 x 10^{18} molecules cm^{-2} for protocol A and protocol B, respectively (n=3). The 96.56% increase in estimated molecule surface coverage is attributed to the removal of the surface Au gold oxide layer after oxidative electrochemical polishing which has been shown to reduce efficient formation of the thiol-gold bond ((Sumi and Uosaki, 2004; Tkac and Davis, 2008).

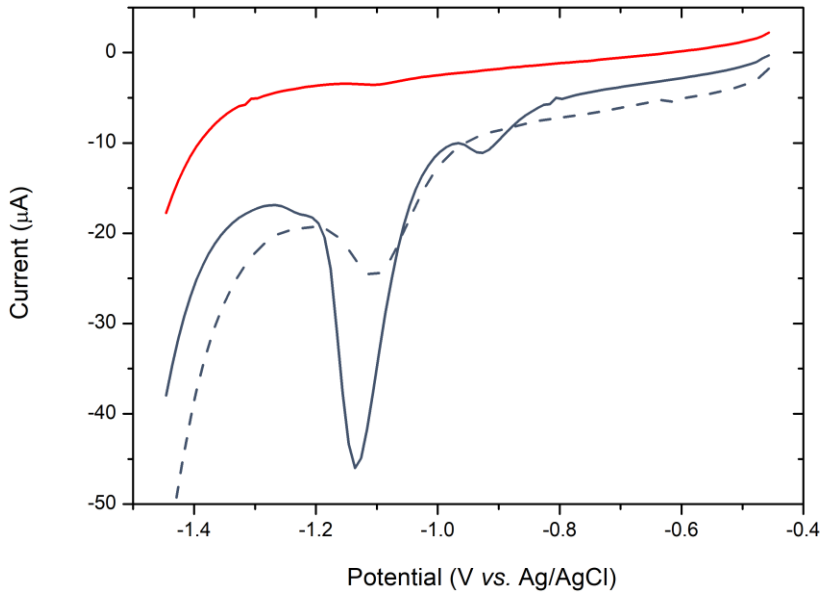

Figure 3.2. Reductive cyclic voltammetry (CV) scans for bare gold (red – solid line), SAM formed on gold cleaned by protocol A (blue – dashed line) and SAM formed on gold cleaned by protocol B (blue – solid line) in 100 mM NaOH. CV scan ranged from -0.5 V to -1.5 V vs. Ag/AgCl reference at a scan rate of 1.0 V/s and a step potential of 0.01 V.

3.3.2. Optimisation of DNA/MCH surface coverage and target binding conditions

Self-assembled monolayer (SAM) formation was measured and characterised using EIS in 50 mM PB + 100 mM K_2SO_4 (pH 7.0) containing 2 mM $[Fe(CN)_6]^{3-/4-}$ redox couple. As shown in Figure 3.3d, a cleaned bare gold surface (see Figure 3.3a) gave a low charge transfer resistance (R_{ct}) of 225 Ω. Upon incubation overnight at 4 °c with a ssDNA/MCH SAM (see Figure 3.3b) an increase in R_{ct} to 8319 Ω was observed which can be ascribed to the ssDNA and MCH acting as a physical resistive barrier to negatively charged redox ions. Figure 3.3c shows binding of the target ssDNA strand, causing a further increase to 9916 Ω, a percentage increase in R_{ct} ($\Delta R_{ct}/R_{ct.0}$) of 19.2% due to hybridisation of the complementary DNA. Due to the successful hybridisation of a high concentration of target DNA to the surface-bound ssDNA, based on the increase in negative charge from the molecular binding event, the assay was optimised further.

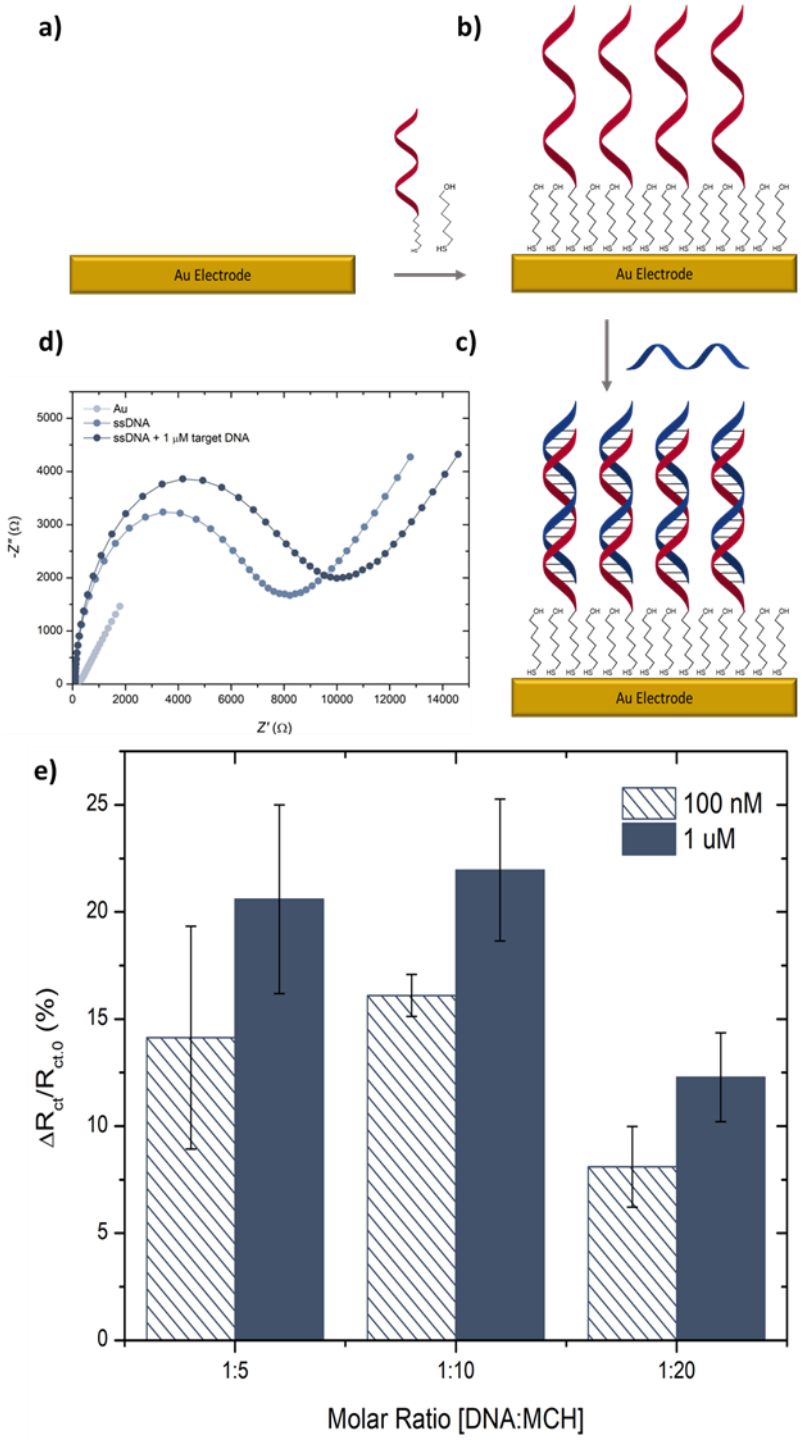

Figure 3.3. E. coli genosensor SAM optimisation scheme and results: a) bare gold electrode, b) co-immobilisation of thiolated probe ssDNA and 6-Mercapto-1-Hexanol (MCH) on gold, c) binding of complementary target DNA sequence, d) and respective changes observed in charge transfer resistance (R_{ct}) by faradaic EIS in 2 mM $[Fe(CN)_6]^{3-/4-}$. e) Observed change in charge transfer resistance ($\Delta R_{ct}/R_{ct.0}$) upon binding of 100 nM and 1 µM complementary target ssDNA for different molar ratios of surface functionalised DNA/MCH. Error bars represent standard deviation determined from three repeats (n ≥ 3).

While obtaining the highest surface coverage of immobilised molecules is important for maximizing potential molecular binding events, the surface density of negatively charged probe molecules requires further optimisation. Probe surface density, especially with charged molecules, carries a vital importance in the effectiveness of any biosensor (Keighley *et al.*, 2008b; Jolly *et al.*, 2019). Optimising the spacing between surface bound probes is essential to minimizing steric hindrance of target DNA binding while ensuring the maximum number of binding sites. This optimisation was achieved by testing different molar ratios of surface bound probe ssDNA and MCH molecules against maximum $\Delta R_{ct}/R_{ct.0}$ and reproducibility. Three different ratios were chosen based on the previous optimisation of DNA immobilisation on gold electrodes carried out by Keighley *et al*. for label-free EIS-based detection (Keighley *et al.*, 2008b). Figure 3.3e shows the percentage increase in observed R_{ct} after 1-hour binding of 100 nM and 1 µM target ssDNA at ratios of 1:5, 1:10, and 1:20. The maximum change in R_{ct} with hybridisation for both 100 nM and 1 µM occurred at a molar ratio of 1:10. Decrease in the observed R_{ct} and reduced reproducibility at a molar ratio of 1:5 can be attributed to the decrease in hybridisation efficiency caused by inhibited recognition of target sequences through steric hindrance (Jolly *et al.*, 2019). While the significant decrease in R_{ct} for a molar ratio of 1:20 was attributed to the reduced number of potential molecular binding sites at lower probe densities (Keighley *et al.*, 2008b). Additionally, the formation of a diffuse layer by higher densities of MCH has been proven to assist with the diffusion of redox-active ions to the electrode surface (Arinaga *et al.*, 2006; Sayikli Şimşek, Nur Sonuç Karaboɨa and Sezgintürk, 2015). A molar ratio of 1:10 provided the highest change in R_{ct} with good reproducibility so was selected for further assay characterisation.

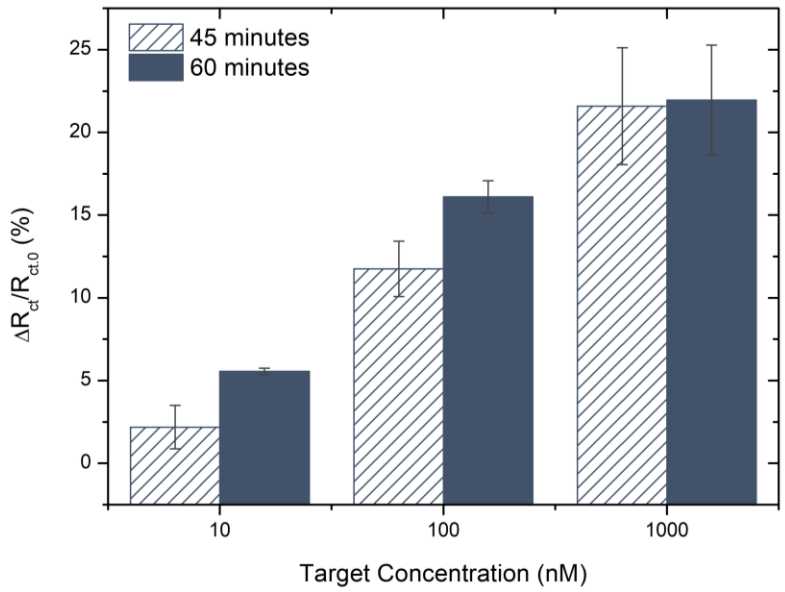

Figure 3.4. Comparison of difference in charge transfer resistance ($\Delta R_{ct}/R_{ct.0}$) due to target DNA binding upon incubation of either 45 or 60 minutes for 10, 100 and 1000 nM concentrations. Error bars represent standard deviation determined from three repeats (n ≥ 3).

The DNA biosensor assay was then further characterised to optimise the hybridisation time. Affinity-based nucleic acid hybridisation assays typically require longer incubation times for molecular binding due to target diffusion to the surface for sequence recognition (Wong and Gooding, 2006; Benvidi *et al.*, 2015). Two target incubation times were tested, 60 minutes being the standard for affinity-based DNA hybridisation and 45 minutes to attempt reduced assay length. Three concentrations of target DNA were used to assess whether there would be any effect of incubation time on observable signal at various concentrations. Figure 3.4 shows the obtained percentage changes in R_{ct} upon hybridisation of 10, 100 and 1000 nM target DNA for both 45 and 60 minutes. For each concentration of target DNA, a higher percentage change in R_{ct} was observed for 60 minutes of hybridisation time. The increase in signal change upon target hybridisation was significantly larger for lower concentrations, with a saturation effect observed towards the higher concentrations at 1 µM. This would suggest that increasing the hybridisation time may lower the LOD and as such potentially increase the linear range for detection. By increasing the time of hybridisation from 45 to 60 minutes, a signal increase of 154.23% was observed

for 10 nM, 36.98% for 100 nM and 1.73% for 1 µM, suggesting diminishing returns with higher concentrations due to probe saturation.

3.3.3. Dose response curve for *E. coli* complementary target DNA

Electrodes were immobilised with a co-immobilised SAM of ssDNA probes and MCH at a ratio of 1:10 and incubated with complementary target DNA ranging from 100 pM to 1 µM for 1 hour per concentration (see Figure 3.5). The electrochemical impedance spectra were then recorded in 50 mM PB + 100 mM K_2SO_4 containing 2 mM of the redox couple $[Fe(CN)_6]^{3-/4-}$. The Nyquist plots for each concentration were fitted with the Randles equivalent circuit and percentage change in charge transfer resistance ($\Delta R_{ct}/R_{ct.0}$) was plotted against a $\log_{10}$ scale of the target concentrations. For each concentration, a consecutive increase in $\Delta R_{ct}/R_{ct.0}$ was observed.

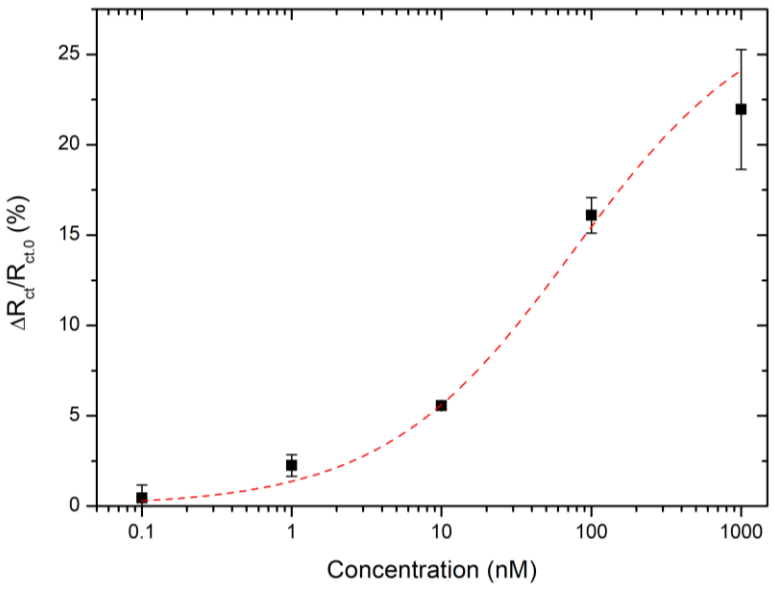

Figure 3.5. Charge transfer resistance $\Delta R_{ct}/R_{ct.0}$ calibration curve versus DNA target oligonucleotide concentration for detection of Escherichia coli O157:H7. Error bars represent standard deviation determined from three repeats (n ≥ 3).

The LOD for the detection of target oligonucleotides was calculated using the following equation:

$$LOD = \frac{3\sigma}{h}$$

Where, σ was the standard deviation of the control and h is the Hill slope. Using this equation, the LOD was found to be 2.71 nM. This higher limit is expected when employing EIS-based detection with thiolated DNA probe molecules for the detection of target oligonucleotides without any nanoparticles to increase surface area, pre-amplification, or post-signal enhancing steps. The dose-response curve was fitted with the standard hill slope for specific binding following the equation:

$$Y = B_{max} * X^h/(K_d^h + X^h)$$

Where, B_{max} is the maximum binding obtained, X is the concentration of target, K_d is the dissociation coefficient and h is Hill slope pertaining to cooperativity. Using this fitting, the dose response curve was fit, and an R squared value of 0.97 was achieved suggesting a strong correlation. The K_d value was observed to be 75.6 nM which is slightly higher than the dissociation constants seen in the literature and may be due to limited charge screening during target hybridisation (Park *et al.*, 2006; Li *et al.*, 2007). The Hill slope, which is useful for determining the degree of cooperativity of the probe/target interaction (Dahlquist, 1978), of 0.69 was observed which is usual for a negatively cooperative binding relationship. Negatively cooperative binding being the relationship whereby affinity of the probe molecule to another target molecule decreases once already bound (McGhee and von Hippel, 1974).

3.3.4. Contact angle validation of self-assembled monolayer immobilisation

Figure 3.6 shows the variance in contact angle between a blank cleaned gold SPR chip surface as well as a gold surface which has been surface modified with a co-immobilised SAM containing a 1:10 ratio of thiolated ssDNA and MCH for ∼16 hours at 4°C overnight. Upon dispensing 6 µL of ultrapure (MilliQ) water on the surface of the gold it can be seen clearly that the contact angle of the ssDNA/MCH self-assembled monolayer is larger than that of the cleaned gold surface. From Figure 3.6a, it can be observed that the clean gold surface showed hydrophilic characteristics with a low contact angle of 27.58°. After SAM formation with the, the contact angle shows a distinct increase to 49.32° (see Figure 3.6b). These results clearly demonstrate an increase in hydrophobicity, characteristic of nucleic acid-

based self-assembled monolayers, confirming immobilisation of the DNA/MCH co-SAM layer.

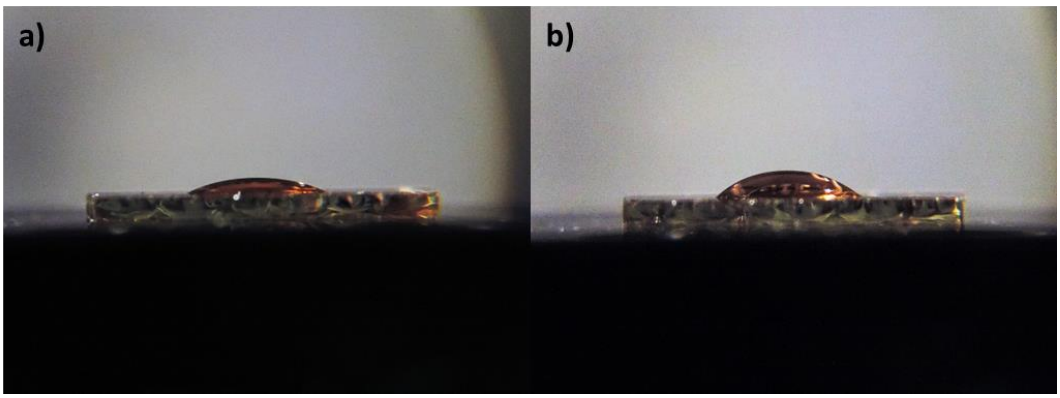

Figure 3.6. Contact angle images for a) a blank cleaned gold thin-film SPR chip and b) a gold thin-film SPR chip immobilised with a self-assembled monolayer comprising a 1:10 ratio of thiolated ssDNA and 6-mercapto-1-hexanol (MCH) with 6 µL of ultrapure (MilliQ) water pipetted.

3.4. Conclusions and Future Work

In this study, a DNA hybridisation-based genosensor has been developed for the detection of *Escherichia coli* bacteria. Polycrystalline gold planar electrodes were used, and surface pre-treatment of these reusable electrodes was characterised to ensure functionalisation of the highest possible molecular density. A surface chemistry utilising thiols for modified probe DNA and spacing molecules was optimised for molar ratio and probe spacing to mitigate steric hindrance during target hybridisation while maintaining the highest number of potential target binding sites. The assay was further optimised by testing target incubation time to ensure maximum signal output without the use of target pre-amplification or post-signal amplification techniques. Finally, SAM functionalisation was further validated by a simple contact angle study to assess changes in surface hydrophobicity due to the nitrogenous bases of the surface-bound DNA.

By following the pre-optimised protocol of Ján Tkáč *et al*. (Tkac and Davis, 2008), it was observed that the commercially advised cleaning of polycrystalline gold electrodes was producing an Au gold oxide monolayer on the surface due to the highly oxidative nature of piranha chemical stripping and electrochemical polishing

in H_2SO_4. Thus, the advised post-cleaning treatments were implemented to remove the oxide monolayer. By doing so a 96.56% increase in surface molecule density was achieved due to the inhibitory effect of the oxide monolayer on thiol-gold bonding. The DNA:MCH molar ratio was then optimised according to the highest change in charge transfer resistance ($\Delta R_{ct}/R_{ct.0}$) to provide optimal spacing between probe ssDNA. After binding of 100 nM and 1 µM target ssDNA this was found to be 1:10. Target incubation time was further optimised with 60 minutes giving the highest $\Delta R_{ct}/R_{ct.0}$ for three target concentrations over 45 minutes (10 nm = 154.23%, 100 nM = 36.98%, and 1 µM = 1/73%) with diminishing return the higher the concentration due to saturation. The dose response of $\Delta R_{ct}/R_{ct.0}$ was carried out with a concentration range of 100 pM to 1 µM revealing a modest limit of detection of 2.71 nM. A linear range of 1 nM to 1 µM was observed, with an R^2 value of 0.97, a dissociation constant (K_d) of 75.6 nM, and Hill slope coefficient of 0.69 which is indicative of a negatively cooperative binding effect as expected. Finally, a simple contact angle study validated the successful binding of the SAM to gold. The data exhibited a 78.82% increase in the contact angle upon successful binding of the SAM due to the hydrophobic nature of the nitrogenous bases of the probe DNA. The optimised genosensor assay developed in this chapter was subsequently implemented in the development of a genosensor for the detection of E. coli. Chapter 4 will further present the integration of a redox-active intercalating species for post-signal amplification to further increase assay sensitivity using this assay.

Future work for the development of this assay could focus on the inclusion of an anti-fouling surface chemistry to prevent non-specific interactions of molecules in clinical biological samples as well as possible contaminants that may exist in water samples from environmental settings. One potential method that has seen significant development in the literature is the use of conductive polymers such as pyrrole and dopamine to improve surface conductivity and assay sensitivity. A further optimisation of this assay on an on-chip platform would also be of interest, such as printed circuit boards (PCBs) or thin-film evaporated gold on glass. Upon successful transfer of this assay to an on-chip platform, the integration of microfluidic sample actuation and pre-treatment such as integrating fluid pumps and sample heat-

inactivation. Through the integration of microfluidics, it would then be feasible to apply the optimised surface chemistry to sequences of other pathogens, including other waterborne bacteria, viruses, and protists to create a multiplexed assay.

References

Arinaga, K. et al. (2006) 'The role of surface charging during the coadsorption of mercaptohexanol to DNA layers on gold: Direct observation of desorption and layer reorientation', Langmuir, 22(13), pp. 5560–5562. Available at: https://doi.org/10.1021/LA060324M/ASSET/IMAGES/LARGE/LA060324MF00002.JPEG.

Benvidi, A. et al. (2015) 'A highly sensitive and selective electrochemical DNA biosensor to diagnose breast cancer', Journal of Electroanalytical Chemistry, 750, pp. 57–64. Available at: https://doi.org/10.1016/J.JELECHEM.2015.05.002.

Bhalla, N. et al. (2016) 'Introduction to biosensors', Essays in Biochemistry. Edited by P. Estrela, 60(1), pp. 1–8. Available at: https://doi.org/10.1042/EBC20150001.

Bonanni, A. and del Valle, M. (2010) 'Use of nanomaterials for impedimetric DNA sensors: A review', Analytica Chimica Acta, 678(1), pp. 7–17. Available at: https://doi.org/10.1016/J.ACA.2010.08.022.

Dahlquist, F.W. (1978) '[13] The meaning of scatchard and hill plots', Methods in Enzymology, 48(C), pp. 270–299. Available at: https://doi.org/10.1016/S0076-6879(78)48015-2.

Gupta, S. et al. (2016) 'Lab-on-Chip Technology: A Review on Design Trends and Future Scope in Biomedical Applications Implantable Micro-systems Design View project Low Power Data Converters View project Lab-on-Chip Technology: A Review on Design Trends and Future Scope in Biomedical Applications', Article in International Journal of Bio-Science and Bio-Technology, 8(5), pp. 311–322. Available at: https://doi.org/10.14257/ijbsbt.2016.8.5.28.

Jolly, P. et al. (2019) 'A PNA-based Lab-on-PCB diagnostic platform for rapid and high sensitivity DNA quantification', Biosensors and Bioelectronics, 123. Available at: https://doi.org/10.1016/j.bios.2018.09.006.

Keighley, S.D. et al. (2008) 'Optimization of DNA immobilization on gold electrodes for label-free detection by electrochemical impedance spectroscopy', Biosensors and

Bioelectronics, 23(8), pp. 1291–1297. Available at: https://doi.org/https://doi.org/10.1016/j.bios.2007.11.012.

Land, K.J. et al. (2019) 'REASSURED diagnostics to inform disease control strategies, strengthen health systems and improve patient outcomes', Nature microbiology. 2018/12/13, 4(1), pp. 46–54. Available at: https://doi.org/10.1038/s41564-018-0295-3.

Lazcka, O., Campo, F.J. del and Muñoz, F.X. (2007) 'Pathogen detection: A perspective of traditional methods and biosensors', Biosensors and Bioelectronics, 22(7), pp. 1205–1217. Available at: https://doi.org/10.1016/J.BIOS.2006.06.036.

Li, D. et al. (2007) 'Kinetic study of DNA/DNA hybridization with electrochemical impedance spectroscopy', Electrochemistry Communications, 9(2), pp. 191–196. Available at: https://doi.org/10.1016/J.ELECOM.2006.08.053.

McGhee, J.D. and von Hippel, P.H. (1974) 'Theoretical aspects of DNA-protein interactions: Co-operative and non-co-operative binding of large ligands to a one-dimensional homogeneous lattice', Journal of Molecular Biology, 86(2), pp. 469–489. Available at: https://doi.org/10.1016/0022-2836(74)90031-X.

Moschou, D. and Tserepi, A. (2017) 'The lab-on-PCB approach: tackling the μTAS commercial upscaling bottleneck', Lab on a Chip, 17(8), pp. 1388–1405. Available at: https://doi.org/10.1039/C7LC00121E.

Park, H. et al. (2006) 'Kinetic and affinity analyses of hybridization reactions between peptide nucleic acid probes and DNA targets using surface plasmon field-enhanced fluorescence spectroscopy', Biointerphases 2006 1:4, 1(4), pp. 113–122. Available at: https://doi.org/10.1116/1.2365386.

Rainbow, J. et al. (2020) 'Integrated Electrochemical Biosensors for Detection of Waterborne Pathogens in Low-Resource Settings', Biosensors. Basel, Switzerland :, p. 36. Available at: https://doi.org/10.3390/bios10040036.

Regan, E.M. et al. (2014) 'A novel cobalt complex for enhancing amperometric and impedimetric DNA detection', Electrochimica Acta, 128, pp. 10–15. Available at: https://doi.org/https://doi.org/10.1016/j.electacta.2013.10.028.

Sayikli Şimşek, Ç., Nur Sonuç Karaboıa, M. and Sezgintürk, M.K. (2015) 'A new immobilization procedure for development of an electrochemical immunosensor for parathyroid hormone detection based on gold electrodes modified with 6-mercaptohexanol and silane', Talanta, 144, pp. 210–218. Available at: https://doi.org/10.1016/J.TALANTA.2015.06.010.

Sekretaryova, A.N. et al. (2019) 'Evaluation of the Electrochemically Active Surface Area of Microelectrodes by Capacitive and Faradaic Currents', ChemElectroChem, 6(17), pp. 4411–4417. Available at: https://doi.org/10.1002/CELC.201900989.

Singh, Simranjeet et al. (2020) 'Biological Biosensors for Monitoring and Diagnosis', pp. 317–335. Available at: https://doi.org/10.1007/978-981-15-2817-0_14.

Sumi, T. and Uosaki, K. (2004) 'Electrochemical Oxidative Formation and Reductive Desorption of a Self-Assembled Monolayer of Decanethiol on a Au(111) Surface in KOH Ethanol Solution'. Available at: https://doi.org/10.1021/JP049558.

Suroviec, A.H. (2012) 'Determining surface coverage of self-assembled monolayers on gold electrodes.', Chem. Educ., 17, pp. 83–85.

Tkac, J. and Davis, J.J. (2008) 'An optimised electrode pre-treatment for SAM formation on polycrystalline gold', Journal of Electroanalytical Chemistry, 621(1), pp. 117–120. Available at: https://doi.org/https://doi.org/10.1016/j.jelechem.2008.04.010.

Trasatti, S. and Petrii, O.A. (1991) 'International Union of Pure and Applied Chemistry Physical Chemistry Division Commission on Electrochemistry: Real Surface Area Measurements in Electrochemistry', Pure and Applied Chemistry, 63(5), pp. 711–734. Available at: https://doi.org/10.1351/PAC199163050711/MACHINEREADABLECITATION/RIS.

Tricase, A. et al. (2022) 'Electrochemical and X-ray Photoelectron Spectroscopy Surface Characterization of Interchain-Driven Self-Assembled Monolayer (SAM) Reorganization', Nanomaterials 2022, Vol. 12, Page 867, 12(5), p. 867. Available at: https://doi.org/10.3390/NANO12050867.

Wong, E.L.S. and Gooding, J.J. (2006) ‘Charge transfer through DNA: A selective electrochemical DNA biosensor’, Analytical Chemistry, 78(7), pp. 2138–2144. Available at: https://doi.org/10.1021/AC0509096/ASSET/IMAGES/MEDIUM/AC0509096E00001.GIF.

Yang, M., McGovern, M.E. and Thompson, M. (1997) ‘Genosensor technology and the detention of interfacial nucleic acid chemistry’, Analytica Chimica Acta, 346(3), pp. 259–275. Available at: https://doi.org/10.1016/S0003-2670(97)90055-6.

4. Signal amplification using a cobalt complex for redox-active intercalation in an electrochemical genosensor

Genosensors detecting the presence of nucleic acids using highly selective nucleic acid probes are an attractive and cost-effective tool for the detection of waterborne pathogens that commonly cause environmental pollution and disease (Kumar *et al.*, 2018b; Vidic and Manzano, 2021). However, due to the relatively low concentrations of relevant biomarkers in fresh and wastewater samples, a method of increasing signal output is often required (Du and Dong, 2017). In this chapter, electrochemical characterisation of a redox-active intercalator compound containing a cobalt redox couple is demonstrated using a DNA biosensor for detection of *E. Coli*. Both the intercalative and redox-active properties were characterised for amperometric and impedimetric detection techniques. The $[Co(GA)_2(aqphen)]Cl$ complex was shown to further increased Faradaic impedance signal upon binding to dsDNA from 21.96% to 28.82%. $[Co(GA)_2(aqphen)]Cl$ also enables measurable Faradaic signal changes without using added redox couple i.e. $[Fe(CN)_6]^{3-/4-}$ as well as DPV. Measurements with CV demonstrate the complexity of the redox mechanism of the $[Co(GA)_2(aqphen)]Cl$ redox reaction and the high electrochemical stability of the generated products. We have also shown for the first time that co-incubation of the target DNA with our intercalating compound can further increase target binding and observable signal outputs through charge screening effects. The minimum concentration of 100 pM target DNA was detected with significant difference from background signal from the negative control, $P<0.001$. Finally, the assay saw a 100-fold increase in sensitivity due to intercalation with $[Co(GA)_2(aqphen)]Cl$ with LOD and LOQ calculated to be 43 pM and 131 pM, respectively.

4.1. Background

Electrochemical biosensors convert molecular binding events into electrical signal outputs that can be easily measured for biomarker quantification (Bhalla *et al.*, 2016). In genosensors, functionalised nucleic acid probes hybridise with and detect target nucleic acids to provide measurable electrical signal changes. These signal changes can be measured by amperometric, potentiometric or impedimetric

techniques. Traditional unlabelled detection methods are typically not used within nucleic acid detection due to reduced assay sensitivity related to relatively small molecule size (Zhou *et al.*, 2022). Various amplification methods often need to be employed with genosensors to boost the observable signal changes from the molecular binding event. Mohammadi et al. split these methods into three strategies that target different components of a genosensor device, including platform amplification, oligonucleotide sequence amplification and detection amplification (Mohammadi, Yammouri and Amine, 2019). Platform amplification methods involve techniques such as use of nanomaterials such as gold nanoparticles (AuNPs) (Vetrone, Huarng and Alocilja, 2012; Liu *et al.*, 2014), carbon nanotubes (CNTs) (Sabaté del Río *et al.*, 2019; Han *et al.*, 2020), and graphene oxide (GOx) (Zupančič, Jolly, *et al.*, 2021a; Najjar, Rainbow, Timilsina, *et al.*, 2022) as well as conductive or electroactive polymers to coat the surface of electrodes (Miodek *et al.*, 2016) (see Figure 4.1a). These techniques aim to increase the sensitivity of genosensor assays by increasing the surface area for probe immobilisation and conductivity of the functionalised surface to aid in signal transduction (Cho, Kim and Park, 2020). Oligonucleotide sequence amplification techniques involve those methods that aim to pre-concentrate nucleic acids contained within the sample by replication through multi-temperature and isothermal methods (see Figure 4.1b). Some amplification methods which are already commonly used in the field of pathogen detection include polymerase chain reaction (PCR), loop-mediated isothermal amplification (LAMP) and rolling circle amplification (RCA) (Yeap *et al.*, 2021). With some modification, these methods can be used at smaller scale and even integrated on-chip in lab-on-a-chip style devices (Fang *et al.*, 2010; Foudeh *et al.*, 2012). By using these sequence amplification techniques, it is possible to take much smaller samples and pre-concentrate targets to levels that are more easily detectable. Both these strategies have been explored further in chapter 6 where it was investigated whether the use of multiple strategies simultaneously can significantly increase sensor performance. The third strategy, which will be explored in this chapter, is detection amplification. Techniques in this strategy include the use of molecules that assist in or further increase the observable signal of a binding event such as the use of intercalators,

redox-active molecules, catalysts, or enzymes etc (see Figure 4.1c). Many of these molecules are considered methods of labelling.

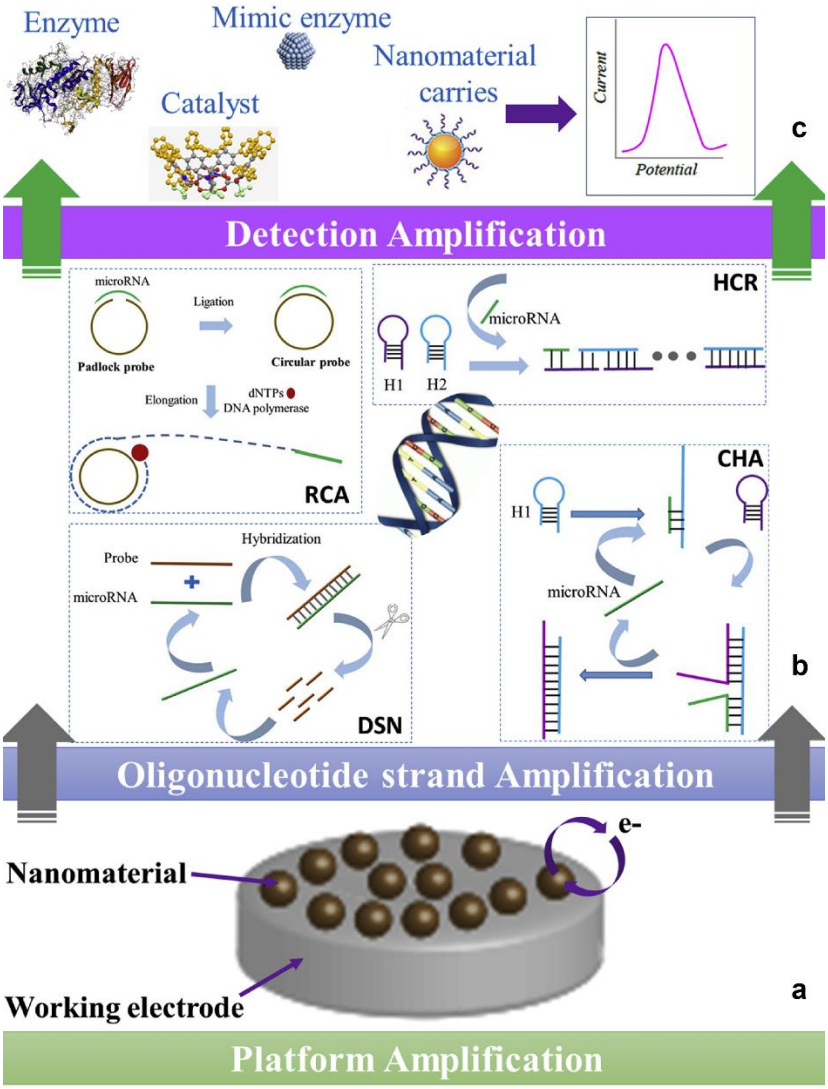

Figure 4.1. Commonly used amplification strategies for genosensors. (a) Platform amplification (gold or carbon nanoparticles). (b) Oligonucleotide strand amplification. (c) Detection amplification using an enzyme, catalyst, and nanomaterials as carriers. HCR, hybridisation chain reaction; CHA, catalytic hairpin assembly; DSN, duplex-specific nuclease (taken from Mohammadi, Yammouri and Amine, 2019).

Two methods of labelling are predominantly used within the literature, these being direct and indirect labelling. Direct labelling consists of modifying either the probe or target with redox-active or nanoparticle molecules whereas indirect labels, such as intercalators, can be utilised for their characteristic electrostatic binding affinities to target nucleic acid molecules (Almaqwashi *et al.*, 2016).

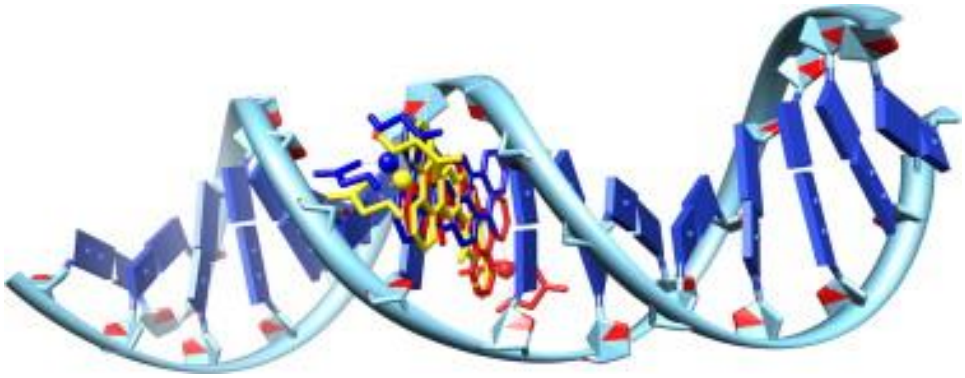

Figure 4.2. Docking of [Co(GA)2(aqphen)]Cl interacting with dsDNA causing unwinding and increase in electrostatic field (taken from Regan *et al*., 2014).

Intercalating molecules work to increase the observable signal by binding to nucleic acids between the base pairs, to the charged phosphate backbone or between the grooves of the double stranded helix (see Figure 4.2) (Sischka *et al.*, 2005; Liu and Sadler, 2011). Since intercalative molecules have such an affinity for disrupting double stranded nucleic acids, they have been commonly explored and developed within the pharmaceutical industry as potential medicines for various diseases caused by genetic mutations e.g., various cancers and neurodegenerative diseases (Jie *et al.*, 2009; Godzieba and Ciesielski, 2019). These include compounds such as Doxorubicin and Daunorubicin which are both frequently used in the treatment of Hodgkin's lymphoma as well as Dactinomycin which is used for treatment of renal tumours and various sarcomas. Cobalt-aqphen is an intercalative compound that inserts itself between the nitrogenous base-pairs of the double-stranded DNA helix structure. This compound is based on a complex used by (H. Bin Lin *et al.*, 2011) containing a mixed-ligand coordination sphere of 1,10-phenanthroline (phen) and glycolic acid (GA). The compound of $[Co(GA)_2(phen)]Cl$ was then modified by (Regan et al., 2014) to contain an extended planar ligand (aqphen = naphtho[2,3-a]dipyrido[3,2-h:2',3'-f]phenazine-5,18-dione) with a conjugated anthraquinone unit to improve binding affinity using a previously mentioned procedure by Rosa López *et al.* (Rosa López *et al.*, 1996) (see Figure 4.3).

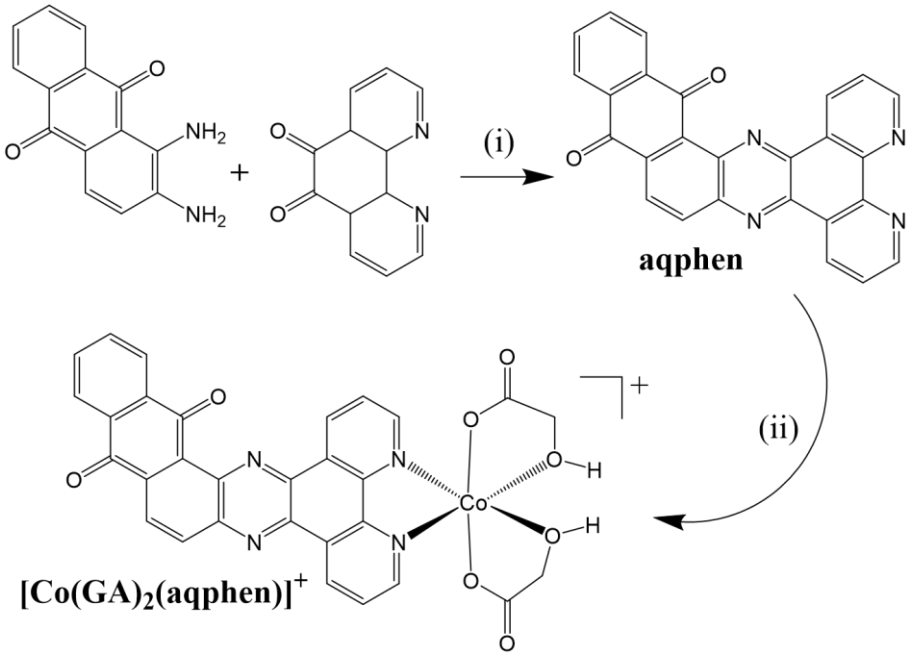

Figure 4.3. Synthesis the cobalt complex. (i) EtOH, heat; (ii) EtOH, 1 eq. CoCl2·6H2O, 2 eq. glycolic acid/NaOH(aq).

This compound has been previously explored by (Regan et al., 2014) to demonstrate its intercalative properties of amplifying both amperometric and Faradaic impedance signals for detection of a 21-base TCT-repeat oligonucleotide sequence. Herein, we have used an environmentally relevant sequence from *E. coli* which could be implemented for the detection of bacteria in fresh and wastewater samples. In the present study, we have focussed on the improvement of compound dissolution using organic solvents for long-term stability of the solution. We also focus on characterising the electrochemical properties of the compound using additional amperometric and non-Faradaic techniques. Finally, we explored the effect of co-incubating the compound with target ssDNA to determine whether primary binding of the compound to ssDNA target molecules may increase overall target binding affinity and reduce assay complexity.

4.2. Methods

4.2.1. Instruments and reagents

Synthetic DNA oligonucleotides, both thiol-modified and unmodified, were purchased HPLC-purified from Sigma-Aldrich (UK). 6-Mercapto-1-Hexanol (97%),

potassium phosphate monobasic solution (1 M), potassium phosphate dibasic solution (1 M), potassium sulphate, potassium hexacyanoferrate (III), potassium hexacyanoferrate (II) trihydrate, magnesium chloride, ethylenediaminetetraacetic acid (EDTA, 0.5 M), dimethyl sulfoxide (≥99.9%, for molecular biology), sulfuric acid (95-98%), hydrogen peroxide solution (30%) and nuclease-free water were all purchased from Sigma-Aldrich (UK). Ethanol (99.8%) was purchased from Fisher Scientific. Polishing pads and alumina slurry (0.05 µm) were purchased from Electron Microscopy Sciences (USA). All aqueous solutions were prepared using 18.2 MΩ cm ultra-pure (Millipore, USA) unless otherwise stated. All data values were analysed using the PSTrace 5.9 software with data graphed using OriginPro 8.5.

4.2.2. Synthesis of $[Co(GA)_2(aqphen)]Cl$

The novel cobalt complex $[Co(GA)_2(aqphen)]Cl$ was synthesised by collaborators at Cardiff University as previously described (Regan et al., 2014). Briefly, $CoCl_2 \cdot 6H_2O$ (0.137 g, 0.576 mmol) was dissolved in ethanol (10 mL) and mixed with naphtho[2,3-a]dipyrido[3,2-h:2’,3’-f]phenazine-5,18-dione (aqphen) (0.237 g, 0.576 mmol) for 30 min under a nitrogen atmosphere. Then, an ethanol/water (95:5) solution (10 mL) of glycolic acid (0.090 g, 1.183 mmol) neutralised by KOH (0.066 g, 1.176 mmol) was added and the mixture stirred for 1 hour. The resulting orange precipitate was filtered and dried in vacuum. Aqueous stock solutions containing 1 mM $[Co(GA)_2(aqphen)]Cl$ were prepared by dissolving the required amount of the complex in DMSO by heating to 70 °C in a sonicating bath for 1-2 hours.

4.2.3. Electrochemical measurements

Electrochemical impedance spectroscopy (EIS), differential pulse voltammetry (DPV) and cyclic voltammetry (CV) used for biosensor detection experiments were performed on a PalmSens4 potentiostat (PalmSens BV, The Netherlands). A three-electrode setup was used with gold disk working electrodes (CH Instruments, USA), a platinum wire counter electrode (ALS Instruments, Japan) and an Ag/AgCl (KCl sat’d) reference electrode (BASi, USA) placed into a salt bridge containing 50 mM PB + 100 mM K_2SO_4, pH 7.0.

For Faradaic measurements the electrochemical impedance spectrum was measured in a solution of 2 mM $K_4[Fe(CN)_6]$ + 2 mM $K_3[Fe(CN)_6]$ in 50 mM PB + 100 mM K_2SO_4, pH 7.0. The impedance spectrum was measured over the frequency range 100 kHz to 100 mHz, with a 10 mV a.c. voltage superimposed on a d.c. bias of 0.2 V, which corresponds to the formal potential of the redox couple vs. an Ag/AgCl reference electrode. For non-Faradaic measurements determining capacitance and open circuit potential (OCP), experiments were carried out in 100 mM PB. The impedance spectrum was measured over a frequency range 100 kHz to 100 mHz, with a 10 mV a.c. voltage superimposed on a d.c. bias of 0 V vs. OCP.

For DPV measurements, electrodes were placed in 100 mM PB and the DPV scans run between −0.257 V and 0.143 V vs. Ag/AgCl with a scan rate of 0.05 V/s, step potential of 0.005 V, pulse potential of 0.05 V and pulse time of 0.05 s). For CV, electrodes were scanned between -0.5 V and 0.5 V in 100 mM PB with a scan rate of 0.2 V/s and step potential of 0.01 V.

4.2.4. Preparation of thiolated DNA self-assembled monolayer

Polycrystalline gold disk working electrodes with a radius of 1.0 mm were cleaned using a previously optimised protocol (Tkac and Davis, 2008). Briefly, working electrodes were stripped of any previously functionalised thiols by pre-treatment of cyclic voltammetry (CV) between -1.5 V and -0.5 V vs. Ag/AgCl at a scan rate of 1.0 V/s and a step potential of 0.01 V for 200 cycles in 0.1 M NaOH. This was followed by mechanical polishing of each WE with an alumina slurry (0.05 µm) on a polishing pad for 3 minutes per electrode. Electrodes were then rinsed with ultrapure water and ultrasonically cleaned (in ultrapure water) for 2 minutes to remove any alumina residue. Electrodes were then chemically cleaned by dipping in hot piranha solution containing hydrogen peroxide solution and sulfuric acid at a respective ratio of 1:3 for 15 minutes. The electrodes were then rinsed and ultrasonicated (in ultrapure water) for a further 1 minute. Electrochemical polishing was performed by cycling working electrodes between -0.2 V and 1.5 V vs. Ag/AgCl at a scan rate of 0.1 V/s and step potential of 0.01 V for 25 cycles in 0.1 M H_2SO_4 aqueous solution. Gold oxides were then immediately electrochemically stripped by running 10 cycles from 0.2 V to 0.8 V vs. Ag/AgCl at the same scan rate and step potential in 0.1 M H_2SO_4. Electrodes

were then placed in absolute ethanol for 20 minutes to chemically reduce any remaining gold oxides formed during the cleaning process.

Each working electrode was then dried under a stream of nitrogen and exposed to 150 µL of a mixed self-assembled monolayer (SAM) containing thiolated DNA and MCH (at a ratio of 1:10) in a humidity chamber for ≥16 hours. Probe ssDNA was modified with a HS-$(CH)_6$ group on the 5' end and had a 22-base sequence of 5'- TTT TTG GTC CGC TTG CTC TCG C -3' from the genome of *E. Coli* O157:H7 serotype. Five thymine bases were added at the 5' end to increase the distance of the probe DNA from the electrode surface. The immobilisation solution contained 0.8 M phosphate buffer (PB) + 1.0 M NaCl + 5 mM $MgCl_2$ + 1 mM ethylene diamine tetraacetic acid (EDTA), pH 7.0. After initial SAM immobilisation, electrodes were rinsed with a wash buffer containing 50 mM PB + 100 mM K_2SO_4 + 10 mM EDTA, pH 7.0, to remove any residual Mg^{2+} ions. To ensure complete coverage of the gold electrode surface and reduce the chance of pinholes, electrodes were backfilled with a solution of 1 mM MCH in ultrapure water for 1 hour. Finally, electrodes were rinsed with ultrapure water and placed in 50 mM PB + 100 mM K_2SO_4, pH 7.0, for 1.5 hours to ensure stability of the SAM.

4.2.5. DNA hybridisation and $[Co(GA)_2(aqphen)]Cl$ incubation

Synthetic complementary ssDNA was incubated on the surface of the optimised biosensor surface with a 17-base sequence of 5'- GCG AGA GCA AGC GGA CC -3'. Target DNA was prepared as aliquots from lyophilised state in nuclease-free water (Sigma-Aldrich, UK) at a stock concentration (100 µM) and serial diluted to working concentrations in 50 mM PB + 100 mM K_2SO_4, pH 7.0. Once the self-assembled monolayer was stable, electrodes were incubated with 100 µL of target ssDNA (100 pM–1 µM) for 1 hour at ambient room temperature (RT). Electrodes were then rinsed with 50 mM PB + 100 mM K_2SO_4, pH 7.0.

Once target DNA had been hybridised onto the electrode surface, electrodes were incubated with 100 µL of $[Co(GA)_2(aqphen)]Cl$ (200 µM) at ambient RT. For separate binding of the cobalt complex after DNA hybridisation, a stock of $[Co(GA)_2(aqphen)]Cl$ was dissolved in DMSO (for molecular biology) to a concentration of 1 mM by

ultrasonication for 3 hours at 70 °C. Stock $[Co(GA)_2(aqphen)]Cl$ was then diluted to 200 µM in 50 mM PB + 100 mM K_2SO_4, pH 7.0 and incubated for 30 minutes. For co-incubation of ssDNA target and $[Co(GA)_2(aqphen)]Cl$, 100 µL of solution containing the concentration of ssDNA and 200 µM of $[Co(GA)_2(aqphen)]Cl$ was prepared in 50 mM PB and 100 mM K_2SO_4, pH 7.0, and incubated on electrodes for 1 hour at ambient RT.

4.3. Results and Discussion

4.3.1. Optimization of $[Co(GA)_2(aqphen)]Cl$ dissolution

Due to the flat structure of the aqphen ligand and the redox-active cobalt being a metal cation, $[Co(GA)_2(aqphen)]Cl$ does not dissolve well in high ionic strength buffers . This causes the compound to form a 'mixture' rather than a fully dissolved solute within these solvents (see Figure 4.4). In Figure 4.4a, it was observed that while the compound mostly dissolved in a low ionic solution e.g., DI or MilliQ, solubility equilibrium was reached before all the particles could be dissolved resulting in a turbid mixture. Upon further dilution in MilliQ to 600 µM (see Figure 4.4b) the compound dissolved well, however, aggregated immediately within a high ionic strength buffer (Figure 4.4c).

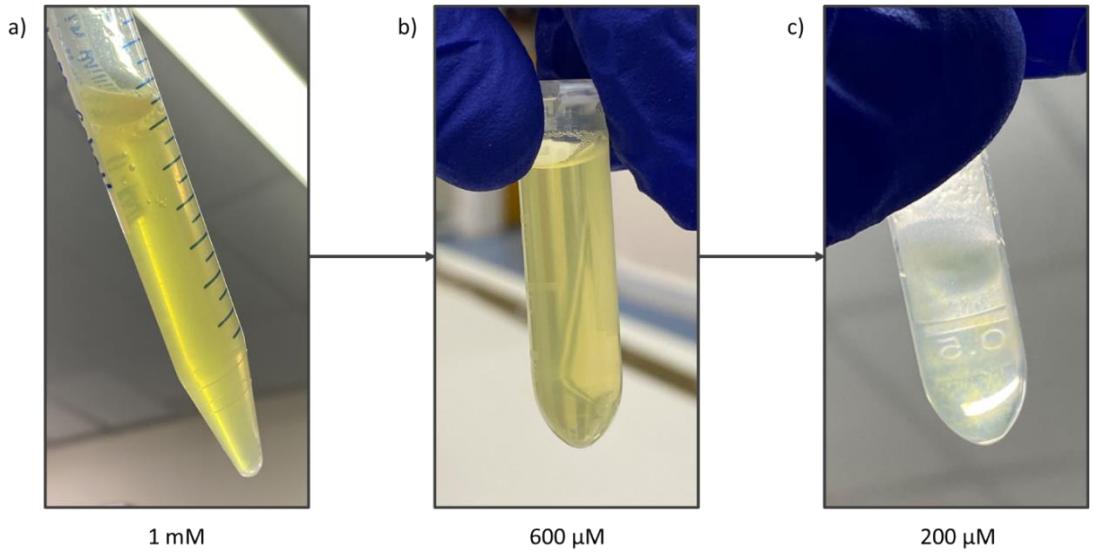

Figure 4.4. Dissolution of $[Co(GA)_2(aqphen)]Cl$ in MilliQ and 50 mM PB + 100 mM K_2SO_4. Dilution involved a) re-suspension of $[Co(GA)_2(aqphen)]Cl$ in ultrapure water at a

concentration of 1 mM, b) dilution in MilliQ to 600 µM and finally c) dilution to 200 µM working concentration.

To increase dissolution, $[Co(GA)_2(aqphen)]Cl$ was dissolved in DMSO (abs.) before diluting in the high ionic strength buffer needed for DNA-based biosensors. DMSO is a highly polar aprotic solvent, unlike water which does act as a hydrogen donor and is a good alternative solvent to use when a compound does not dissolve well in water (Martin, Weise and Niclas, 1967; Brayton, 1986). In this case, $[Co(GA)_2(aqphen)]Cl$ was dissolved to a 1 mM stock concentration in DMSO in which it is highly soluble (see Figure 4.5a). Two dilution pathways were tested, the first being a serial dilution in DMSO and then the high ionic strength buffer 50 mM PB + 100 mM K_2SO_4. In this dilution pathway, $[Co(GA)_2(aqphen)]Cl$ diluted well to 600 µM in DMSO (see Figure 4.5b) but then aggregated at 200 µM when diluted in 50 mM PB + 100 mM K_2SO_4 (see Figure 4.5c). After only 2 minutes the compound had completely aggregated and settled (see Figure 4.5d). It was observed that by diluting the stock solution of 1 mM $[Co(GA)_2(aqphen)]Cl$ directly to 200 µM in a high ionic strength buffer, the compound was more readily dissolved and formed a stable fully dissolved solution for more than 1 hour (see Figure 4.5e). It is also worth mentioning that the stock solution of 1 mM $[Co(GA)_2(aqphen)]Cl$ in DMSO remained stable for more than 6 months at room temperature.

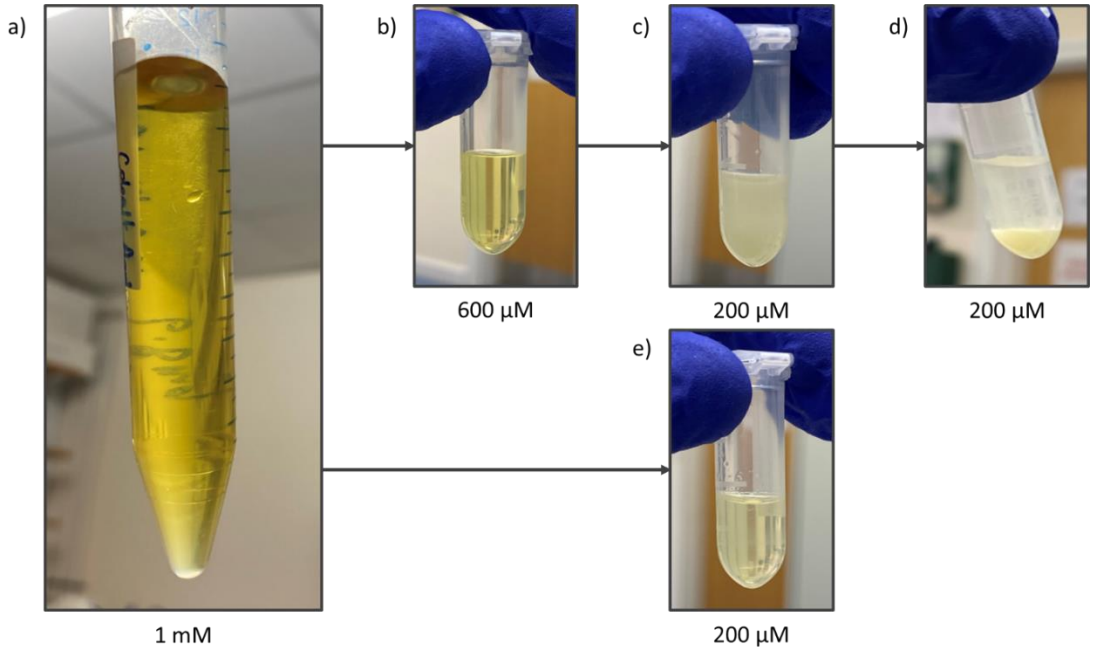

Figure 4.5. Dissolution of [Co(GA)$_2$(aqphen)]Cl in DMSO and 50 mM PB + 100 mM K_2SO_4. Two different dilution methods were tested: first, a) [Co(GA)$_2$(aqphen)]Cl was dissolved in 100% DMSO to 1 mM, b) diluted to 600 µM in 100% DMSO and c) diluted to final working concentration of 200 µM in 50 mM PB + 100 mM K_2SO_4. d) shows aggregation and settling of [Co(GA)$_2$(aqphen)]Cl after 2 minutes. The second dilution method involved a) [Co(GA)$_2$(aqphen)]Cl dissolved in 100% DMSO and e) stock [Co(GA)$_2$(aqphen)]Cl diluted to 200 µM directly in 50 mM PB + 100 mM K_2SO_4.

4.3.2. Impedimetric response to [Co(GA)$_2$(aqphen)]Cl

[Co(GA)$_2$(aqphen)]Cl not only intercalates specifically with dsDNA to increase the electrical field but also contains cobalt which is redox-active and involves Co^{2+} and Co^{3+} being reversibly oxidised and reduced. This metal group can be detected using capacitance changes and influences open circuit potential (OCP). To measure the effect upon both electrical field and redox-capability, electrochemical impedance spectroscopy (EIS) was used with and without the redox couple $[Fe(CN)_6]^{3-/4-}$.

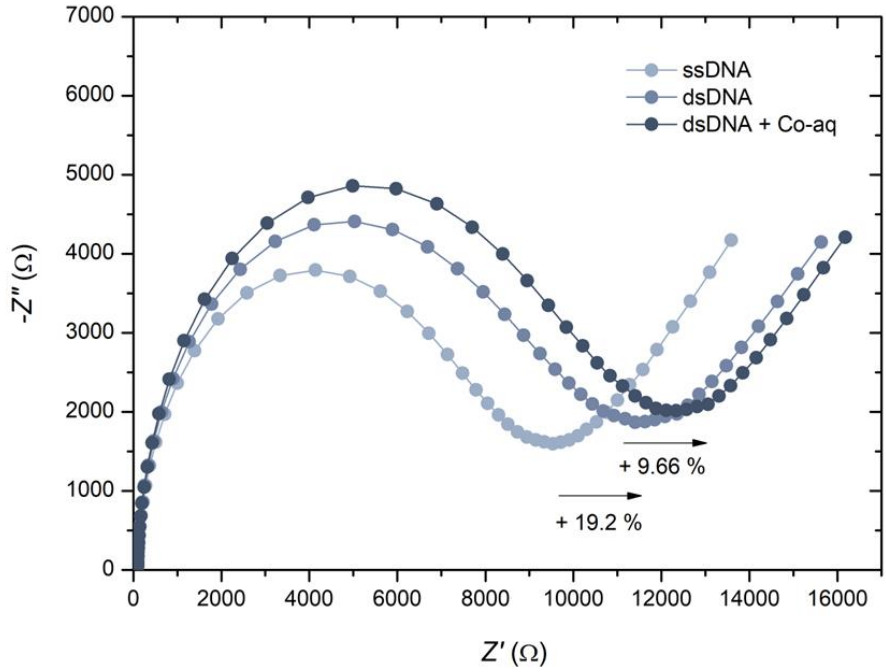

Figure 4.6. A typical Nyquist plot showing responses to DNA hybridisation and $[Co(GA)_2(aqphen)]Cl$ intercalation in 50 mM PB + 100 mM K_2SO_4 + 2 mM $[Fe(CN)_6]^{3-/4-}$. Percentage change in R_{ct} is shown below each curve.

To determine the limit of detection (LOD) of the developed sensor without the assistance of the cobalt compound, electrodes were immobilised with probe DNA and the electrochemical impedance spectra measured upon binding of five concentrations of fully complementary target DNA from 100 pM to 1 µM (See chapter 3, Figure 3.5). The LOD for the detection of target oligonucleotides was calculated to be 2.71 nM. A typical Nyquist plot is shown in Figure 4.6 demonstrating the percentage change in charge transfer resistance (R_{ct}) observed from hybridization of the probe and 1 µM target DNA as well as the change observed for intercalation by 200 µM of the $[Co(GA)_2(aqphen)]Cl$ complex. The change observed after hybridisation of the target DNA is associated with the electrostatic barrier increasing due to the additional negative charge of the phosphate groups on the backbone of the target DNA molecules. An average increase of 21.96% (SD: ±3.31%) was observed upon binding of 1 µM complementary target DNA. The increase in R_{ct} observed after incubation with the cobalt-aqphen intercalator is thought to be a result of structural changes in the DNA double helix whereby the helix unfolds resulting in an increase in

electrostatic field. An average increase of 6.86% (SD: ±2.45%) was seen upon binding of 200 µM $[Co(GA)_2(aqphen)]Cl$ after DNA hybridisation.

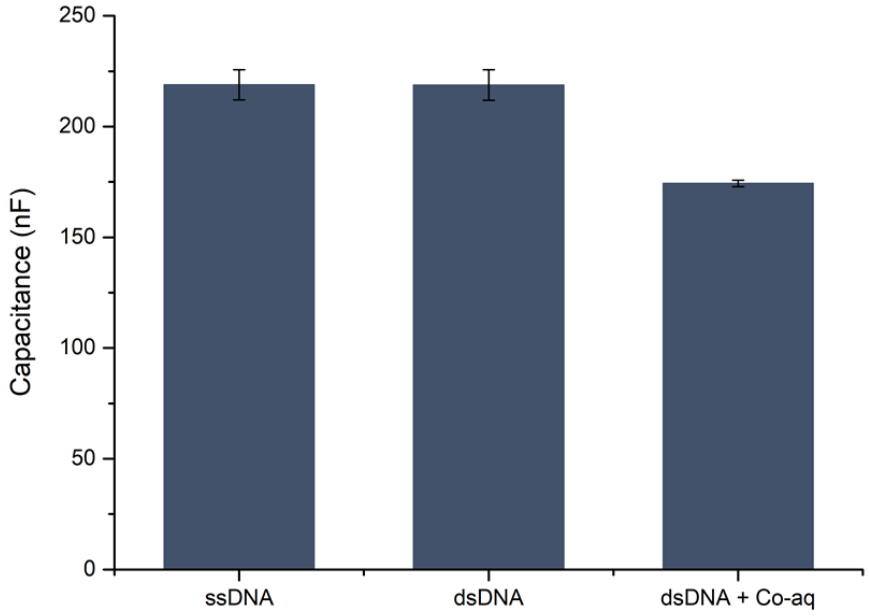

Figure 4.7. The response of DNA hybridisation and $[Co(GA)_2(aqphen)]Cl$ intercalation on capacitance using non-Faradaic EIS in 100 mM PB. Data are shown for (1) ssDNA, (2) dsDNA (1 μM target), and (3) dsDNA + $[Co(GA)_2(aqphen)]Cl$ (200 μM). Error bars represent standard deviations determined from three repeats (n = 3).

To measure the redox-active properties of $[Co(GA)_2(aqphen)]Cl$, measurements using EIS were carried out in 100 mM phosphate buffer electrolyte without $[Fe(CN)_6]^{3-/4-}$. Due to the absence of $[Fe(CN)_6]^{3-/4-}$, the 0.2 V DC bias potential associated with $[Fe(CN)_6]^{3-/4-}$ was removed and instead measurements were carried out using a DC bias of 0 V versus the open circuit potential (OCP). This was done so that effects on both the capacitance of the electrode double-layer (C_{dl}) and OCP could be assessed. Using the same surface chemistry method with probe ssDNA and MCH, measurements were taken after incubating with 1 µM complementary target DNA for 1 hour and again after 30 minutes of $[Co(GA)_2(aqphen)]Cl$ binding. After incubation of the target DNA, a non-significant increase in C_{dl} of 0.06 nF (SD: ±6.87 nF) was observed, compared with binding of $[Co(GA)_2(aqphen)]Cl$ resulting in an

increase of 44.53 nF (SD: ±1.48 nF) (see Figure 4.7). In Figure 4.8, the effect of $[Co(GA)_2(aqphen)]Cl$ binding to dsDNA on the OCP is shown. After binding of target ssDNA, a decrease of 14.66 mV (SD: ±41.85 mV) occurred, it is worth mentioning that the OCP fluctuated significantly due to the lack of redox-active electrolyte in solution and no DC bias being applied to the circuit. After incubating the redox-active $[Co(GA)_2(aqphen)]Cl$, a large decrease of 154.14 mV (SD: ±8.31 mV) was observed which corresponded to the binding of the intercalator. The large decrease in standard deviation value suggests that the redox-active properties of $[Co(GA)_2(aqphen)]Cl$ increased stability of the potential in the circuit.

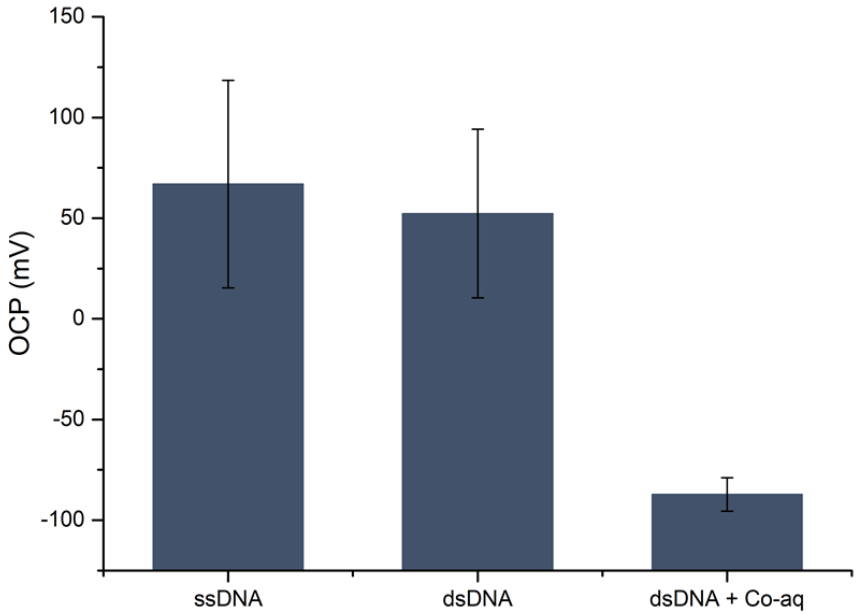

Figure 4.8. The response of DNA hybridisation and $[Co(GA)_2(aqphen)]Cl$ intercalation on OCP using non-Faradaic EIS in 100 mM PB. Data are shown for (1) ssDNA, (2) dsDNA (1 µM target), and (3) dsDNA + $[Co(GA)_2(aqphen)]Cl$ (200 µM). Error bars represent standard deviations determined from three repeats (n = 3).

4.3.3. Amperometric response to $[Co(GA)_2(aqphen)]Cl$

Due to the redox-active properties possessed by the cobalt ligand of the $[Co(GA)_2(aqphen)]Cl$ complex, it was possible to electrochemically assess the redox kinetics and stability of the compound using amperometric techniques. Here we have

utilised cyclic voltammetry (CV) to assess the reversibility and stability of the redox reaction and differential pulse voltammetry (DPV) to measure the binding response to the double-stranded helix. Figure 4.9 shows a typical cyclic voltammogram of probe ssDNA functionalised to the electrode surface with 1 μM target DNA hybridised and 200 μM $[Co(GA)_2(aqphen)]Cl$ bound to the dsDNA helix. Cyclic voltammetry of the surface bound $[Co(GA)_2(aqphen)]Cl$ complex at a scan rate of 0.2 V/s gave peak values of 0.04 V and -0.16 V for the peak anodic potential (E_{pa}) and peak cathodic potential (E_{pc}) respectively. Using these values, peak-to-peak separation (ΔE_p) was calculated to be 200 mV using the calculation below:

$$\Delta E_p = E_{pc} - E_{pa}$$

An ΔE_p value of 200 mV suggests that the redox reaction of $[Co(GA)_2(aqphen)]Cl$ is likely to be a quasi-reversible reaction with a complex mechanism that may involve steps such as proton transfer (Elgrishi *et al.*, 2018b; Guziejewski *et al.*, 2022). The half-wave potential (E½) was then calculated using the peak potentials using the following equation:

$$E^{\frac{1}{2}} = \frac{E_{pa} + E_{pc}}{2}$$

This gave a value of -0.06 V (vs. Ag/AgCl), this value is unique to each compound within a certain electrolyte solution and its various chemical forms. This half-wave potential was then used as the formal potential ($E^{0'}$) in further impedimetric experiments.

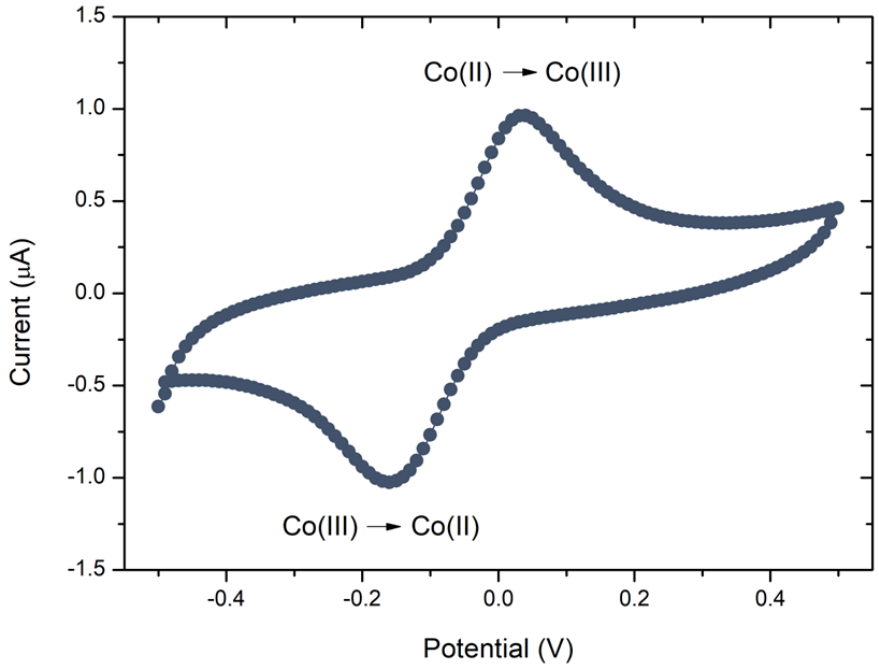

Figure 4.9. Cyclic voltammogram of surface bound [Co(GA)$_2$(aqphen)]Cl in 100 mM PB at a scan rate of 0.2 V/s.

To assess the stability of the electrochemically generated products for the redox reaction of [Co(GA)$_2$(aqphen)]Cl, current ratio was calculated using the current peak values for both oxidation (0.96 µA) and reduction (-1.02 µA) of the compound. This was calculated using the below theoretical equation:

$$\frac{i_{pc}}{i_{pa}} = 1.0$$

The ideal value of 1.0 denotes an electrochemically generated product that is highly stable within the time scale of the experiment and results in an oxidation current peak that is equal to that of the reduction (Elgrishi et al., 2018). The observed value calculated for dsDNA bound [Co(GA)$_2$(aqphen)]Cl of 1.06 suggests a highly stable electrochemical reaction with reversible electron transfer for both the oxidation and reduction of the compound.

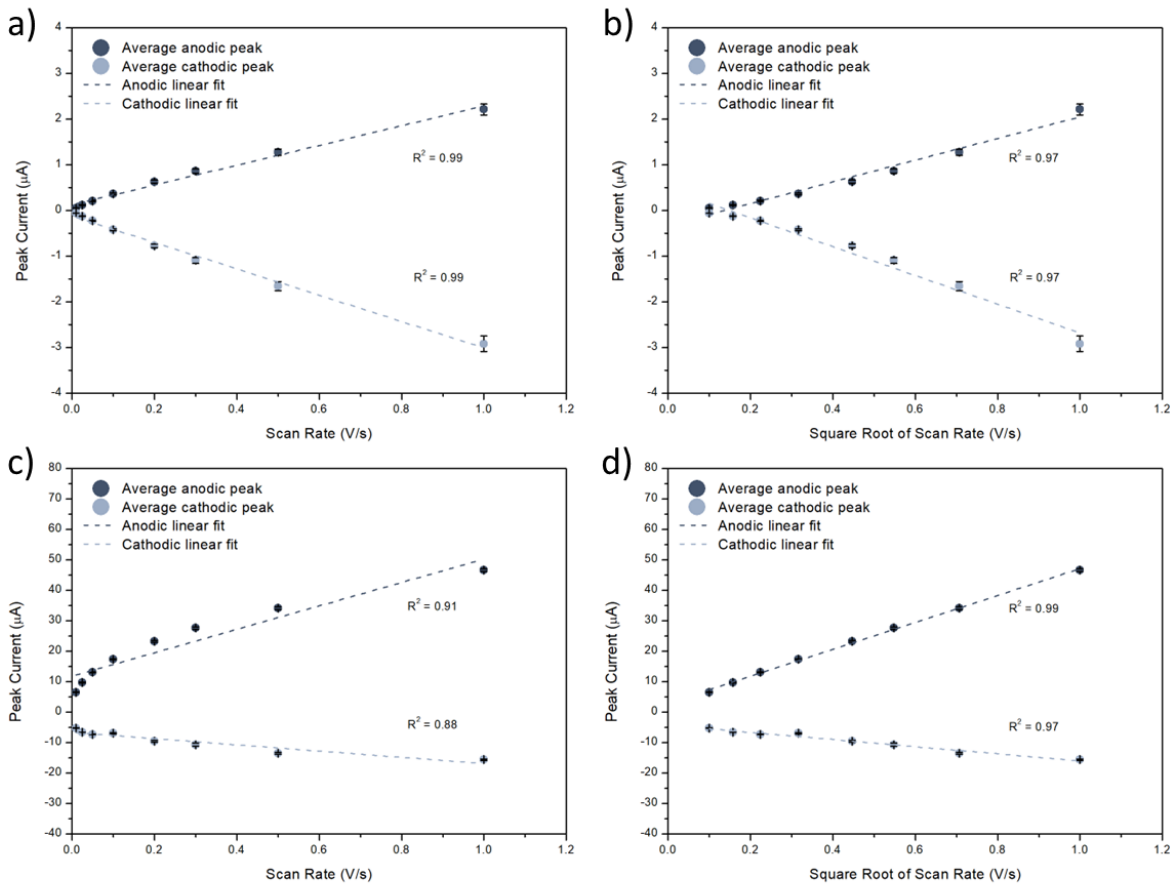

Figure 4.10. Cyclic voltammetry data showing the relationship between peak current and scan rate for the redox process of both the redox-active intercalator (a,b) and the redox couple $[Fe(CN)_6]^{3-/4-}$ (c,d). Error bars represent standard deviations (n=3).

Figure 4.10 shows anodic and cathodic peak current data for cyclic voltammetry measurements at varying scan rates (10 mV/s to 1 V/s) in the absence or presence of the redox couple $[Fe(CN)_6]^{3-/4-}$. By comparing the peak current data to scan rate and the square root of the scan rate, it is possible to determine the type of redox process occurring at the electrode surface. When the peak current fitting is linearly proportional to scan rate the redox process is due to a surface-controlled process. However, if the peak current fitting is linearly proportional to the square root of scan rate, then the redox process is due to a diffusion-based process. Figure 4.10a and Figure 4.10b show cyclic voltametric data where cobalt-aqphen has intercalated with surface-bound dsDNA. The peak current for surface-bound cobalt-aqphen favours a linear relationship with scan rate (R^2 = 0.99 (anodic), 0.99 (cathodic)) over the square root of scan rate (R^2 = 0.97 (anodic), 0.97 (cathodic)). While Figure 4.10c and Figure

4.10d show cyclic voltametric data in the presence of $[Fe(CN)_6]^{3-/4-}$. The peak current for solution-based $[Fe(CN)_6]^{3-/4-}$ favours a linear relationship with the square root of scan rate (R^2 = 0.99 (anodic), 0.97 (cathodic)) over the scan rate (R^2 = 0.91 (anodic), 0.88 (cathodic)). These results suggest that the redox process associated with the surface-bound cobalt-aqphen follows a surface controlled process as expected, while the solution-based $[Fe(CN)_6]^{3-/4-}$ redox process follows a diffusion-based process.

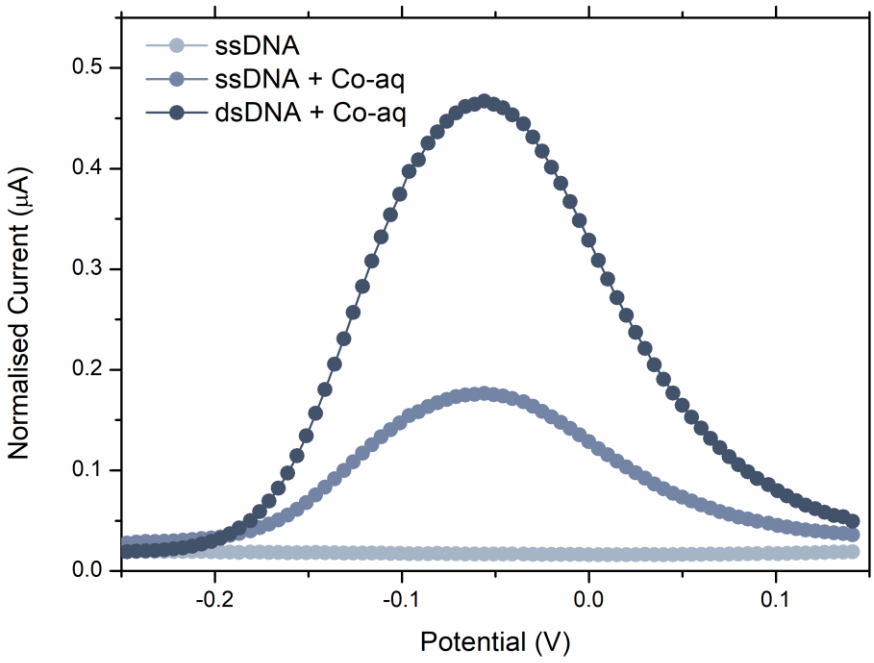

Figure 4.11. Differential pulse voltammograms of DNA hybridisation and $[Co(GA)_2(aqphen)]Cl$ intercalation in 100 mM PB at a scan rate of 50 mV/s. Data are shown for (1) probe ssDNA, (2) ssDNA + 200 μM $[Co(GA)_2(aqphen)]Cl$, and (3) probe ssDNA + 1 μM target DNA + 200 μM $[Co(GA)_2(aqphen)]Cl$.

When $[Co(GA)_2(aqphen)]Cl$ was incubated with dsDNA, a clear peak was observed at -0.066 V versus an Ag/AgCl reference electrode (see Figure 4.11). The current values observed at -0.066 V were 0.017 μA for ssDNA, 0.175 μA for ssDNA + 200 μM $[Co(GA)_2(aqphen)]Cl$ and 0.462 μA for 1 μM target DNA + 200 μM $[Co(GA)_2(aqphen)]Cl$. The current value increase of 2618% for target DNA + $[Co(GA)_2(aqphen)]Cl$ was significantly larger than the addition of $[Co(GA)_2(aqphen)]Cl$

to ssDNA of 929%. However, no peak was observed within the potential range of −0.257 V and 0.143 V (vs. Ag/AgCl) when no $[Co(GA)_2(aqphen)]Cl$ was incubated.

4.3.4. Co-immobilisation of target DNA and $[Co(GA)_2(aqphen)]Cl$

In the previous study by (Regan et al., 2014), it was hypothesised that $[Co(GA)_2(aqphen)]Cl$ may create a positive charge effect that masks the negative charges of the phosphates from the DNA backbone. If this is true, then the effect of masking the negative charges may help facilitate increased binding affinity of the target DNA to the surface-functionalised probe DNA by reducing steric hindrance effect caused by crowding of surface-bound molecules (Keighley et al., 2008). To test this hypothesis we used the same surface chemistry method with ssDNA and MCH, however instead of incubating the target ssDNA and intercalator separately, measurements were taken after co-incubation with 1 µM complementary target DNA and 200 µM of $[Co(GA)_2(aqphen)]Cl$ 100 mM PB for 1 hour. This had the added benefit of reducing the assay time by 30 minutes and reducing the assay complexity for future microfluidic and automated experiments.

After co-incubation, a significant increase in C_{dl} of 53.83 nF (SD: ±8.20 nF) was observed, a 20.88% increase in signal change compared with incubating the target DNA and $[Co(GA)_2(aqphen)]Cl$ separately (see Figure 4.12a). In Figure 4.12b, the effect of co-incubating of target DNA and $[Co(GA)_2(aqphen)]Cl$ to ssDNA on the OCP is shown. After binding a decrease of 152.69 mV (SD: ±2.88 mV) occurred (see Figure 4.12c), this was comparable with the value observed when incubating separately as OCP is not affected by concentration of the redox molecule binding. The current values observed for the DPV measurements were 0.12 µA (SD: ±0.030) for ssDNA and 0.56 µA (SD: ±0.042) for dsDNA + $[Co(GA)_2(aqphen)]Cl$. The current value increase of 366.67% was 109.67% larger than the incubation of target complementary DNA and $[Co(GA)_2(aqphen)]Cl$ separately.

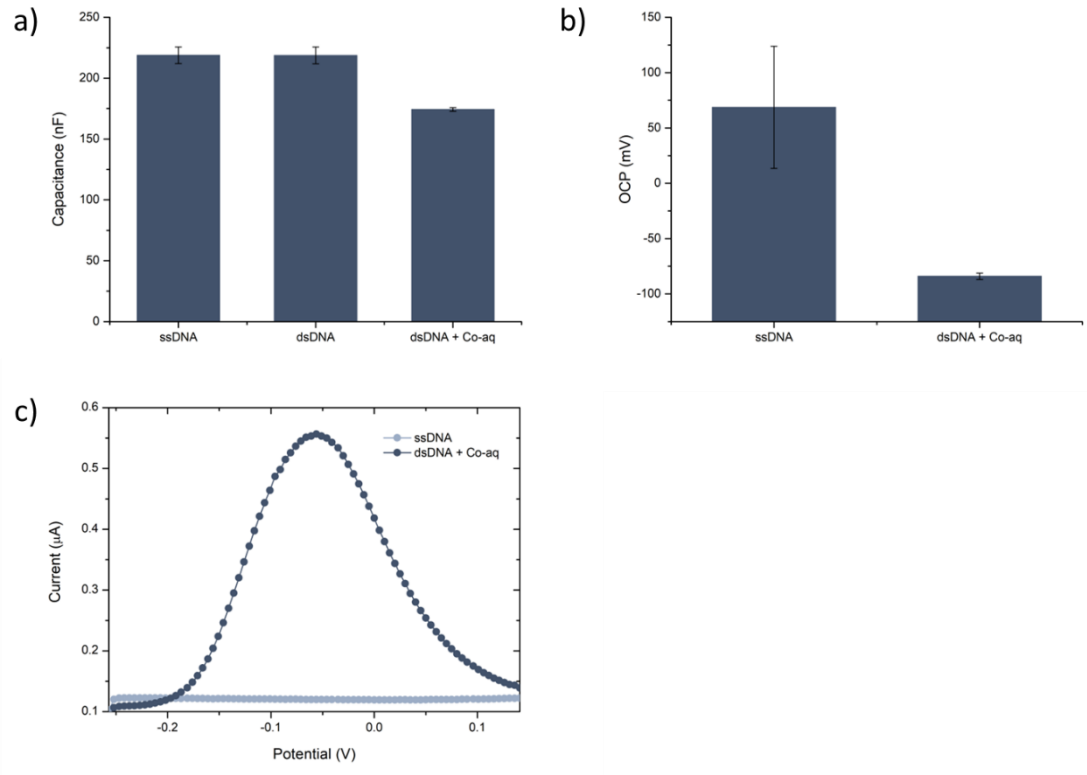

Figure 4.12. Combined data showing co-incubation of target DNA oligonucleotide and [Co(GA)$_2$(aqphen)]Cl intercalator showing the response of simultaneous hybridisation and intercalation on (a) capacitance, (b) OCP and, (c) DPV in 100 mM PB. Error bars represent standard deviations determined from three repeats (n = 3).

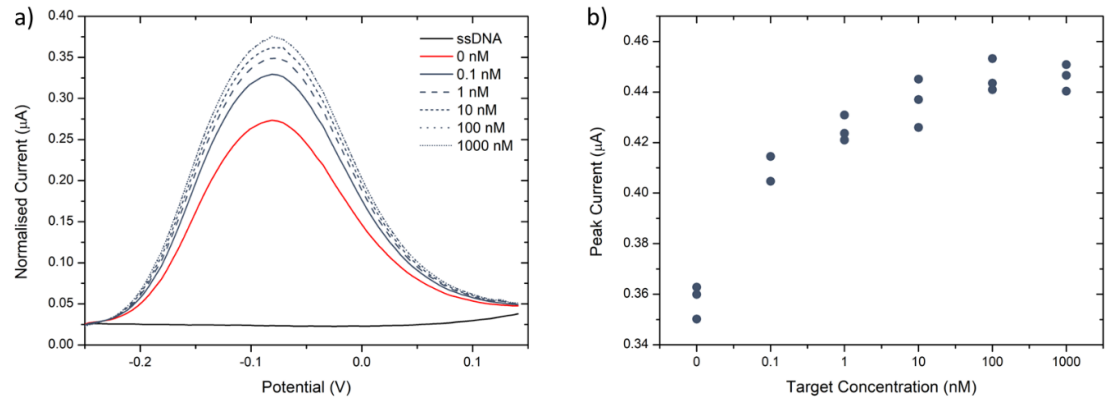

Figure 4.13. Differential pulse voltametric dose response for co-incubated target DNA oligonucleotide and [Co(GA)$_2$(aqphen)]Cl intercalator. a) displays the normalised average peak current voltammograms for each increasing concentration of target DNA with [Co(GA)$_2$(aqphen)]Cl, while b) shows the raw peak current data for each repeat of target concentration in a scatter plot (n=3).

With the dual-immobilisation of target DNA and $[Co(GA)_2(aqphen)]Cl$ optimised, target DNA was serially diluted (0.1-1000 nM) with 200 µM of intercalator. Each concentration was incubated for 1 hour and measured using DPV and Faradaic EIS in 100 mM PB (see Figure 4.13). Results from DPV showed that the minimum concentration of 100 pM gave a significantly higher signal than the negative control of 0 nM + $[Co(GA)_2(aqphen)]Cl$. However, the assay displayed a saturation effect at around 10 nM. An unpaired Student's *t*-test for differences in raw peak current (µA) between 0 nM and 0.1 nM of *E. coli* target DNA with $[Co(GA)_2(aqphen)]Cl$ gave a *P*-value that was significant at the <0.001 level. Due to the signal saturation at relatively low concentration of target DNA with $[Co(GA)_2(aqphen)]Cl$, the LOD was calculated from using a linear slope value from the low concentrations (0-0.1 nM) assuming a linear relationship between 0 and 0.1 nM. Therefore, the limit of detection (LOD) was calculated using the equation below:

$$LOD = 3.3\sigma/S$$

Whereby, σ is the standard deviation of the control response and S was the slope of the concentration curve calculated between 0 nM and 0.1 nM. By doing so, an LOD of 43 pM was achieved by implementing $[Co(GA)_2(aqphen)]Cl$ as a DNA intercalator to amplify signal, which is roughly a 100-fold increase in sensitivity from thiol-based assay without intercalation in chapter 3. The limit of quantitation (LOQ) was calculated to be 131 pM using the equation below:

$$LOQ = 10\sigma/S$$

The results showed a similar trend with capacitive EIS and OCP responses (see Figure 4.14).

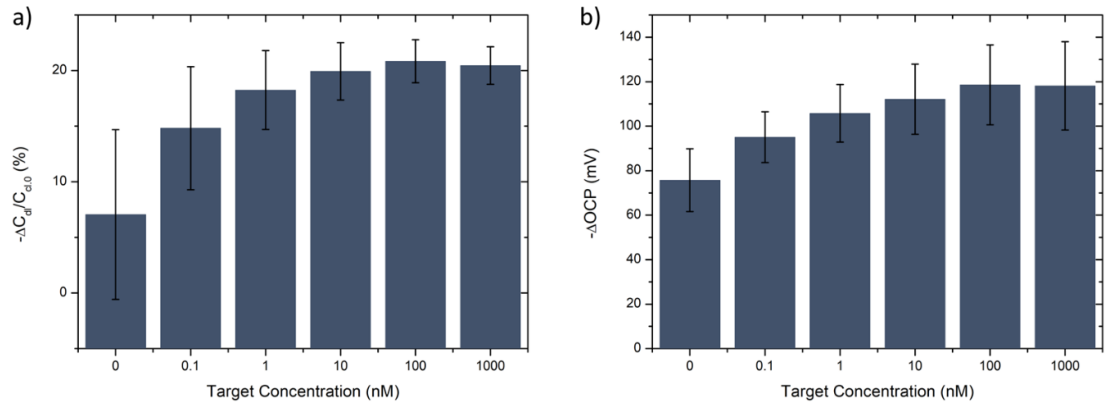

Figure 4.14. Combined data showing the dose response for co-incubation of target DNA oligonucleotide and [Co(GA)$_2$(aqphen)]Cl intercalator with the response of (a) capacitance and (b) OCP in 100 mM PB. Error bars represent standard deviations determined from three repeats (n = 3).

4.4. Conclusions and Future Work

In this study the improvement of compound dissolution has been explored for a previously developed cobalt compound with intercalative and redox-active properties. It was observed that by dissolving the compound in water, a low capacity for dissolution was achieved. However, upon dissolving the compound primarily in the organic solvent DMSO a higher rate of dissolution was achieved, and a stable solution was attained in the high ionic strength buffer required for surface *in-vitro* DNA hybridisation.

To test the efficacy of the [Co(GA)$_2$(aqphen)]Cl a DNA biosensor was fabricated using thiol surface chemistry in chapter 3 of this thesis. Using an optimised concentration ratio of 1:10 of thiolated DNA probes and MCH bound to gold, a sensor with a working range of 1 nM to 1 uM and an LOD of 2.71 nM was developed. Using Faradaic EIS with the redox couple $[Fe(CN)_6]^{3-/4-}$, an average increase of 6.68% was achieved after intercalation of [Co(GA)$_2$(aqphen)]Cl on top of a 21.96% increase with 1 µM target complementary DNA. To measure the redox active properties of [Co(GA)$_2$(aqphen)]Cl, the $[Fe(CN)_6]^{3-/4-}$ redox couple was removed and non-Faradaic EIS was used to observe changes upon capacitance and open circuit potential. Upon binding of [Co(GA)$_2$(aqphen)]Cl, an increase of 44.53 nF was achieved with only +0.06

nF after binding of 1 µM of DNA. Additionally, a decrease of 14.66 mV was observed compared with 154.14 mV after binding of the intercalator. The standard deviation values suggest in both cases that upon binding of the redox-active intercalator, stability in both capacitance and OCP values were increased due to the high redox capability of the compound.

To characterise the redox kinetics and stability as well as the intercalative properties of $[Co(GA)_2(aqphen)]Cl$, CV and DPV were utilised to determine the electrochemical stability and binding capability to the surface-bound DNA duplex. The characteristics of the cyclic voltammogram for the surface bound DNA duplex with intercalated $[Co(GA)_2(aqphen)]Cl$ gave an ΔE_p value of 200 mV suggesting that the redox reaction is quasi-reversible, likely due to the complexity of the redox mechanism (Elgrishi *et al.*, 2018b; Guziejewski *et al.*, 2022). A current ratio of 1.06 was achieved, being very close to the theoretical value of 1.0, suggesting a highly stable electrochemically generated product with highly reversible electron transfer (Elgrishi *et al.*, 2018b). DPV measurements demonstrated a significant 257% increase in the current peak upon binding of $[Co(GA)_2(aqphen)]Cl$, compared with only 7.69% increase after target DNA hybridisation.

Further to this, we have shown that by incubating the target DNA simultaneously with $[Co(GA)_2(aqphen)]Cl$, signal changes are significantly larger with capacitance and DPV. The observable increase in capacitance was 20.88% larger than with individual incubation steps and 109.67% larger for the DPV measurements. Our present theory is that through weak binding of $[Co(GA)_2(aqphen)]Cl$ to the target and probe DNA molecules, a screening effect of the negatively charged phosphate groups on the DNA backbone may occur reducing steric hindrance during DNA hybridisation, resulting in higher DNA binding efficiency. A minimum concentration of 100 pM target DNA was detected with a significant difference, $P<0.001$, from 0 nM background signal causes by $[Co(GA)_2(aqphen)]Cl$. Finally, the sensitivity of the assay with $[Co(GA)_2(aqphen)]Cl$ as an intercalating step was calculated with a LOD of 43 pM and a LOQ of 131 pM. This gave a 100-fold increase in the sensitivity above the developed assay without intercalation observed in chapter 3. However, further

optimisation of the assay is required to limit the signal-to-noise ratio caused by intercalation of the cobalt-aqphen molecule.

In future work, we aim to explore this screening effect further as well as to explore the use of this compound in post-signal amplification within a microfluidic device for integrated DNA sensing. Future experiments would also focus on the optimisation of the cobalt-aqphen concentration and incubation time to lower the background signal caused by non-specific binding of the intercalator to probe ssDNA through weak ionic bonding. Additionally, a wash buffer stage could be added with a chelating agent such as EDTA or minor detergent such as Tween to remove loosely bound molecules from the surface.

References

Almaqwashi, A.A. et al. (2016) ‘Mechanisms of small molecule–DNA interactions probed by single-molecule force spectroscopy’, Nucleic Acids Research, 44(9), pp. 3971–3988. Available at: https://doi.org/10.1093/nar/gkw237.

Bhalla, N. et al. (2016) ‘Introduction to biosensors’, Essays in Biochemistry. Edited by P. Estrela, 60(1), pp. 1–8. Available at: https://doi.org/10.1042/EBC20150001.

Brayton, C.F. (1986) ‘Dimethyl sulfoxide (DMSO): a review’, The Cornell veterinarian, 76(1), pp. 61–90. Available at: http://europepmc.org/abstract/MED/3510103.

Cho, I.-H., Kim, D.H. and Park, S. (2020) ‘Electrochemical biosensors: perspective on functional nanomaterials for on-site analysis’, Biomaterials Research, 24(1), p. 6. Available at: https://doi.org/10.1186/s40824-019-0181-y.

Du, Y. and Dong, S. (2017) ‘Nucleic Acid Biosensors: Recent Advances and Perspectives’, Analytical Chemistry, 89(1), pp. 189–215. Available at: https://doi.org/10.1021/acs.analchem.6b04190.

Elgrishi, N. et al. (2018) ‘A Practical Beginner’s Guide to Cyclic Voltammetry’, Journal of Chemical Education, 95(2), pp. 197–206. Available at: https://doi.org/10.1021/acs.jchemed.7b00361.

Fang, X. et al. (2010) ‘Loop-Mediated Isothermal Amplification Integrated on Microfluidic Chips for Point-of-Care Quantitative Detection of Pathogens’, Analytical Chemistry, 82(7), pp. 3002–3006. Available at: https://doi.org/10.1021/ac1000652.

Foudeh, A.M. et al. (2012) ‘Microfluidic designs and techniques using lab-on-a-chip devices for pathogen detection for point-of-care diagnostics’, Lab on a Chip, 12(18), pp. 3249–3266. Available at: https://doi.org/10.1039/C2LC40630F.

Godzieba, M. and Ciesielski, S. (2019) ‘Natural DNA Intercalators as Promising Therapeutics for Cancer and Infectious Diseases’, Current Cancer Drug Targets, 20(1), pp. 19–32. Available at: https://doi.org/10.2174/1568009619666191007112516.

Guziejewski, D. et al. (2022) ‘Reversible and Quasireversible Electron Transfer under Conditions of Differential Square-Wave Voltammetry’, The Journal of Physical

Chemistry C, 126(12), pp. 5584–5591. Available at: https://doi.org/10.1021/acs.jpcc.2c01188.

Han, S. et al. (2020) 'Label-Free and Ultrasensitive Electrochemical DNA Biosensor Based on Urchinlike Carbon Nanotube-Gold Nanoparticle Nanoclusters', Analytical Chemistry, 92(7), pp. 4780–4787. Available at: https://doi.org/10.1021/acs.analchem.9b03520.

Jie, L. et al. (2009) 'Inhibition of serine/threonine phosphatase PP2A enhances cancer chemotherapy by blocking DNA damage induced defense mechanisms', Proceedings of the National Academy of Sciences, 106(28), pp. 11697–11702. Available at: https://doi.org/10.1073/pnas.0905930106.

Keighley, S.D. et al. (2008) 'Optimization of DNA immobilization on gold electrodes for label-free detection by electrochemical impedance spectroscopy', Biosensors and Bioelectronics, 23(8), pp. 1291–1297. Available at: https://doi.org/https://doi.org/10.1016/j.bios.2007.11.012.

Kumar, N. et al. (2018) 'Emerging biosensor platforms for the assessment of water-borne pathogens', Analyst, 143(2), pp. 359–373. Available at: https://doi.org/10.1039/C7AN00983F.

Lin, H. Bin et al. (2011) 'Crystal structure and DNA binding studies of a cobalt(II) complex containing mixed-ligands of 1, 10-phenathroline and glycollic acid', Chinese Chemical Letters, 22(8), pp. 969–972. Available at: https://doi.org/https://doi.org/10.1016/j.cclet.2011.03.003.

Liu, C. et al. (2014) 'An electrochemical DNA biosensor for the detection of Mycobacterium tuberculosis, based on signal amplification of graphene and a gold nanoparticle–polyaniline nanocomposite', Analyst, 139(21), pp. 5460–5465. Available at: https://doi.org/10.1039/C4AN00976B.

Liu, H.-K. and Sadler, P.J. (2011) 'Metal Complexes as DNA Intercalators', Accounts of Chemical Research, 44(5), pp. 349–359. Available at: https://doi.org/10.1021/ar100140e.

Martin, D., Weise, A. and Niclas, H.-J. (1967) 'The Solvent Dimethyl Sulfoxide', Angewandte Chemie International Edition in English, 6(4), pp. 318–334. Available at: https://doi.org/https://doi.org/10.1002/anie.196703181.

Miodek, A. et al. (2016) 'Electrochemical functionalization of polypyrrole through amine oxidation of poly(amidoamine) dendrimers: Application to DNA biosensor', Talanta, 154, pp. 446–454. Available at: https://doi.org/https://doi.org/10.1016/j.talanta.2016.03.076.

Mohammadi, H., Yammouri, G. and Amine, A. (2019) 'Current advances in electrochemical genosensors for detecting microRNA cancer markers', Current Opinion in Electrochemistry, 16, pp. 96–105. Available at: https://doi.org/https://doi.org/10.1016/j.coelec.2019.04.030.

Najjar, D. et al. (2022) 'Lab-on-a-chip multiplexed electrochemical sensor enables simultaneous detection of SARS-CoV-2 RNA and host antibodies', medRxiv, p. 2021.09.01.21262387. Available at: https://doi.org/10.1101/2021.09.01.21262387.

Regan, E.M. et al. (2014) 'A novel cobalt complex for enhancing amperometric and impedimetric DNA detection', Electrochimica Acta, 128, pp. 10–15. Available at: https://doi.org/https://doi.org/10.1016/j.electacta.2013.10.028.

Rosa López, B. et al. (1996) 'Synthesis of a new phenanthroline derived ligand with acceptor properties', Tetrahedron Letters, 37(31), pp. 5437–5440. Available at: https://doi.org/https://doi.org/10.1016/0040-4039(96)01141-0.

Sabaté del Río, J. et al. (2019) 'An antifouling coating that enables affinity-based electrochemical biosensing in complex biological fluids', Nature Nanotechnology, 14(12), pp. 1143–1149. Available at: https://doi.org/10.1038/s41565-019-0566-z.

Sischka, A. et al. (2005) 'Molecular Mechanisms and Kinetics between DNA and DNA Binding Ligands', Biophysical Journal, 88(1), pp. 404–411. Available at: https://doi.org/https://doi.org/10.1529/biophysj.103.036293.

Tkac, J. and Davis, J.J. (2008) 'An optimised electrode pre-treatment for SAM formation on polycrystalline gold', Journal of Electroanalytical Chemistry, 621(1), pp.

117–120. Available at: https://doi.org/https://doi.org/10.1016/j.jelechem.2008.04.010.

Vetrone, S.A., Huarng, M.C. and Alocilja, E.C. (2012) ‘Detection of Non-PCR Amplified S. enteritidis Genomic DNA from Food Matrices Using a Gold-Nanoparticle DNA Biosensor: A Proof-of-Concept Study’, Sensors 2012, Vol. 12, Pages 10487-10499, 12(8), pp. 10487–10499. Available at: https://doi.org/10.3390/S120810487.

Vidic, J. and Manzano, M. (2021) ‘Electrochemical biosensors for rapid pathogen detection’, Current Opinion in Electrochemistry, 29, p. 100750. Available at: https://doi.org/https://doi.org/10.1016/j.coelec.2021.100750.

Yeap, C.S.Y. et al. (2021) ‘Ultrasensitive pathogen detection with a rolling circle amplification-empowered multiplex electrochemical DNA sensor’, Chemical Communications, 57(91), pp. 12155–12158. Available at: https://doi.org/10.1039/D1CC05181D.

Zhou, X. et al. (2022) ‘Recent Advances in Signal Amplification to Improve Electrochemical Biosensing for Infectious Diseases’, Frontiers in Chemistry, 10. Available at: https://www.frontiersin.org/article/10.3389/fchem.2022.911678.

Zupančič, U. et al. (2021) ‘Graphene Enabled Low-Noise Surface Chemistry for Multiplexed Sepsis Biomarker Detection in Whole Blood’, Advanced Functional Materials, 31(16), p. 2010638. Available at: https://doi.org/https://doi.org/10.1002/adfm.202010638.

5. CRISPR/Cas12a-based electrochemical detection of pathogens utilising a highly conductive anti-fouling nanocomposite coating

This chapter focuses on the development of an electrochemical platform that integrates several aspects of surface chemistry, biotechnology and electrochemical biosensing. Namely, the study focuses on the development of an assay that utilises a novel CRISPR-based diagnostic technique called SHERLOCK (Specific High-sensitivity Enzymatic Reporter unLOCKing). SHERLOCK exploits the Cas12a collateral cleavage ability of DNA for a reductive signal effect. Alongside this, a highly effective surface chemistry was developed by using thin-film gold electrode chips coated with a highly conductive polymer coating containing graphene and bovine serum albumin (BSA) crosslinked with glutaraldehyde. This coating also provides a significant antifouling characteristic for the prevention of non-specific binding by interfering molecules as well as increasing sensitivity. Finally, peptide nucleic acid (PNA) molecules were employed for their stronger affinity to target nucleic acids as well as their resistance to the collateral cleavage of Cas12a. These techniques have been integrated into a single biosensing assay to provide rapid, selective, and ultrasensitive detection of target RNA and DNA nucleic acids that can be easily applied to any potential pathogenic bacterial or viral species. In this chapter, the developed biosensor has been used for the detection of both a viral and bacterial pathogen, namely SARS-CoV-2 (severe acute respiratory syndrome Coronavirus 2) and *Escherichia coli* respectively, which have been responsible for major health impacts in both high as well as low/middle-income countries (LMICs). Herein, an assay has been developed to achieve sensitive, selective ($P<0.001$) and rapid (approx. 1 hour) assay detection of viral RNA and bacterial DNA molecular biomarkers. Using the developed assay, it was possible to detect nucleic acid concentrations in unamplified and amplified samples of 0.21-1.26 pM for Stx-1 and Stx-2 of *E. Coli* and 1.33 aM for SARS-CoV-2 (0.8 cp/µl). The experimental content in this chapter was carried out by the thesis author and has been published in Najjar *et al.* (Najjar *et al*., 2022).

5.1. Background

The COVID-19 pandemic has highlighted the need for more cost-effective molecular diagnostics for SARS-CoV-2 RNA as well as devices for rapid and sensitive detection of a plethora of other pathogenic species in other outbreaks. Specifically, the clinical timeline of SARS-CoV-2 infections consists of an acute phase, when viral RNA is directly detectable in clinical samples, such as saliva or nasal samples, followed by a recuperative phase when serological biomarkers, such as IgM, IgA and IgG antibodies, are present in saliva and serum samples (see Figure 5.1a) (Isho *et al.*, 2020a; Wölfel *et al.*, 2020). From Figure 5.1b, it can be observed that to detect the presence of SARS-CoV-2 in patients at the earliest possible stage, rapid and sensitive molecular (nucleic acid) diagnostics must be used.

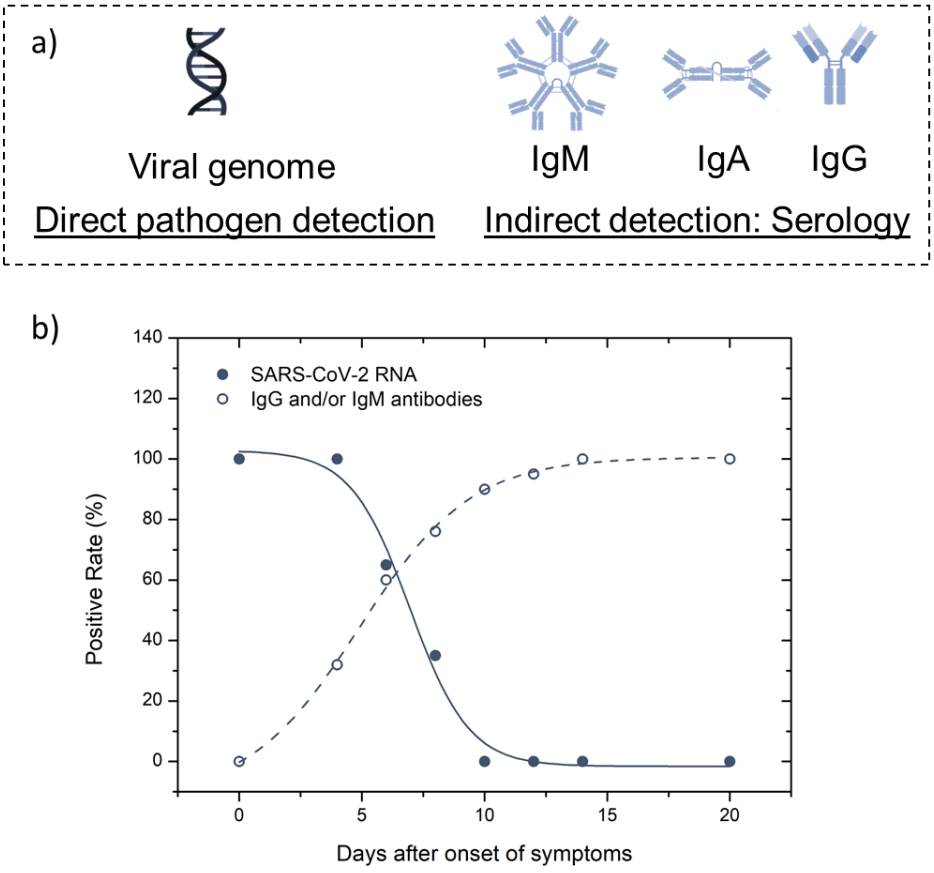

Figure 5.1. Detection approaches for pathogenic species. a) Direct pathogen detection approaches detect the virus, its genome, or viral antigens. These assays are useful during the primary phase of disease, typically 0-7 days after onset of symptoms. Serological assays measure the adaptive immune response (antibodies: IgG/IgM/IgA) that the patient generates

after the infection, known as seroconversion. b) Positive rate for isolation of viral RNA (filled circle) and serological markers (IgG and/or IgM – empty circle) are shown versus days after symptom onset. The fitted sloped are dose-response analysis curves. This data was replotted (Isho et al., 2020b; Wölfel et al., 2020).

Molecular diagnostic platforms are key to detecting infections for not only early-stage monitoring but also for key pandemic-related contact tracing to prevent further spread. Traditional methods of molecular monitoring involving methods such as quantitative polymerase chain reaction (qPCR) are inadequate for effective real-time monitoring and on-site testing of pathogens. This is due to their inherent reliance on bulky expensive equipment, cold sample and reagent storage, long sample-in-answer-out times, and operational complexity requiring trained professionals (Rainbow *et al.*, 2020b). While rapid testing for at-home use do exist, they often rely primarily on sample self-collection and mailing, or are based on lateral flow assay antigen testing, which have been shown to be less accurate than molecular techniques (Mak *et al.*, 2020). One potential path towards the development of diagnostics for simple, rapid at-home or on-site testing are integrated electrochemical biosensing platforms. Through integration of several techniques into one platform, it is possible to develop a simple diagnostic tool with high sensitivity and selectivity and rapid sample-in-answer-out time that is capable of being easily reprogrammed for the detection of any potential pathogen of interest.

In this study, we have developed for the first time an integrated electrochemical detection assay that implements sample isothermal amplification, CRISPR-based diagnostics, an antifouling conductive nanocomposite, and high-specificity peptide nucleic acid surface probes (PNAs). CRISPR-based detection is a relatively novel area of diagnostics, taking advantage of the enzyme family of endonucleases, i.e., Cas12a, which has a cleavage activity specific to dsDNA targets matching its guide RNA (gRNA). CRISPR-based diagnostics exemplify high specificity, ease of flexible programming and physiological compatibility and has been used to develop several diagnostic tools (Gootenberg *et al.*, 2017; Kaminski *et al.*, 2020; Lee *et al.*, 2020). Recently, CRISPR-based diagnostics have also been integrated with electrochemical biosensing platforms with limits of detection (LOD) as low as picomolar to

femtomolar levels (Xu *et al.*, 2020; Li *et al.*, 2021; Zamani *et al.*, 2021). However, this is not sensitive enough for the detection of SARS-CoV-2 or other pathogens in fresh and wastewater samples which can be as low as attomolar levels. By integrating nucleic acid amplification, it is possible to further decrease these detection limits significantly. Furthermore, by using isothermal methods of amplification it is possible to easily integrate these techniques into a point-of-care (PoC) or on-site diagnostic device due to their relative simplicity and single temperature requirement. Finally, electrochemical platforms offer the opportunity for electronic interfacing with cloud-based data banks and telemedicine. The simplicity of this device would make it user-friendly, and its potential for integration would make it ideal for enabling use in POC situations such as hospitals and pandemic testing sites, in LMICs, as well as on-site monitoring for environmental applications.

5.2. Methods and Materials

The methods in this study are a simplified version of a more comprehensive assay that has been further published (Najjar *et al*., 2022). The published study further involves optimisation of a serology-based detection assay multiplexed with the CRISPR viral RNA detection developed in this chapter, utilising a 3D-printed microfluidic lab-on-a-chip platform. However, this work was completed after the experimental work conducted in this thesis by the collaborators at the Wyss Institute after the conclusion of this internship and is not included in the work presented in this thesis. For more information, please refer to the study published (Najjar *et al*., 2022).

5.2.1. Reagents and instrumentation

Gold thin-film chips were custom manufactured by Telic Company, USA. 1-ethyl-3-(3-dimethylaminopropyl) carbodiimide hydrochloride (EDC) was purchased from ThermoFisher, USA). SARS-CoV-2 full length genomic viral RNA samples were purchased from Twist Bioscience, USA. Synthetic probe PNA was purchased lyophilized from PNABio Inc, USA. All other reagents were purchased from Sigma-Aldrich, USA, unless otherwise specified. All other nucleic acid samples were

purchase from Integrated DNA Technologies, USA. All samples were diluted in ultrapure water at 18.2 MΩ.cm at 25 °C unless otherwise specified.

5.2.2. Thin-film chip preparation

Thin-film gold chips were custom manufactured using a standard photolithography process with deposition of 15 nm of chromium and 100 nm of gold on a glass wafer. The area of electrodes was controlled by depositing a layer of 2 µm of insulating layer (SU-8). Before use, gold chips were cleaned by 5 minutes of sonication in acetone followed by isopropanol for a further 5 minutes. To ensure a clean surface, the chips were then treated with oxygen plasma using a Zepto Diener plasma cleaner (Diener Electronics, Germany) at 0.5 mbar and 50% power for 2 minutes.

5.2.3. Nanocomposite coating preparation and binding-site activation

The nanocomposite coating was prepared on gold chips using a previously described method (Zupančič *et al*., 2021; Najjar *et al*., 2022). Briefly, amine-terminated reduced graphene oxide (rGOx) was dissolved in a solution of 5 mg/ml bovine serum albumin (BSA) in 10 mM PBS solution (pH 7.4) and ultrasonicated using an ultrasonicating probe for 1 hour using a 1 s on/off cycle at 50% power. The solution was then heat denatured for 5 minutes at 105 °C and then centrifuged at 16.1 relative centrifugal force (RCF) for 15 minutes to pellet excess aggregate. The solution was then removed, being careful to avoid uptake of the centrifugated pellet and added to a separate Eppendorf tube. The amine-terminated rGOx and denatured BSA was then crosslinked using 70% glutaraldehyde (GA) at a ratio of 69:1 to form the nanocomposite. The nanocomposite solution was then drop cast to cover the gold electrodes and incubated in a humid environment at 4 °C for approximately 20-24 hours to fully adhere the conductive nanocomposite (Sabaté del Río *et al.*, 2019). The chips were then washed by agitation in PBS in a petri dish at 500 RPM for 10 minutes and dried under purified air. To activate the binding sites of the nanocomposite, 1-ethyl-3-(3-dimethylaminopropyl) carbodiimide hydrochloride (EDC) and N-Hydroxysuccinimide (NHS) were dissolved in 50 mM MES buffer (pH 6.2) at 400 mM and 200 mM, respectively, and deposited on the prepared gold chips for 30 minutes. After binding site activation, the chips were rinsed with ultrapure water and dried

with purified air. The nanocomposite was then ready for functionalisation with capture probe PNA.

5.2.4. Chip functionalisation with PNA probe

To functionalise the working electrode (WE) with a capture probe, custom-synthesized amine-terminated peptide nucleic acid (NH_2-AEEA-ACAACAACAACAACA) was used. Peptide nucleic acid (PNA) is a synthetic analogue of DNA with a backbone consisting of repeating units of N-(2-aminoethyl) glycine linked through amide bonds. PNA contains the same four nucleotide bases as DNA (adenine, cytosine, guanine, and thymine) but are connected through methylene bridges and a carbonyl group to the central amine of a peptide backbone (Jolly *et al.*, 2019). The replacement of the sugar-phosphate backbone provides a neutrally charged nucleic acid analogue that offer strong binding affinities and reduced steric hindrance upon target binding (Ray and Nordén, 2000). Stock PNA was diluted to 20 µM in 50 mM MES buffer (pH 6.2) and spotted on the WE. One electrode was spotted with 1 mg/mL BSA as a negative control. The spotted chips were incubated overnight in a humid environment at 4 °C. After capture probe functionalisation, chips were washed by agitation of chips in PBS at 500 RPM for 10 minutes and spun to remove excess solution. Gold electrodes were then blocked with 1 M ethanolamine dissolved in 10 mM PBS at pH 7.4 for 30 minutes and further blocked with 1% BSA in 10 mM PBS containing 0.05% Tween 20 (see Figure 5.2).

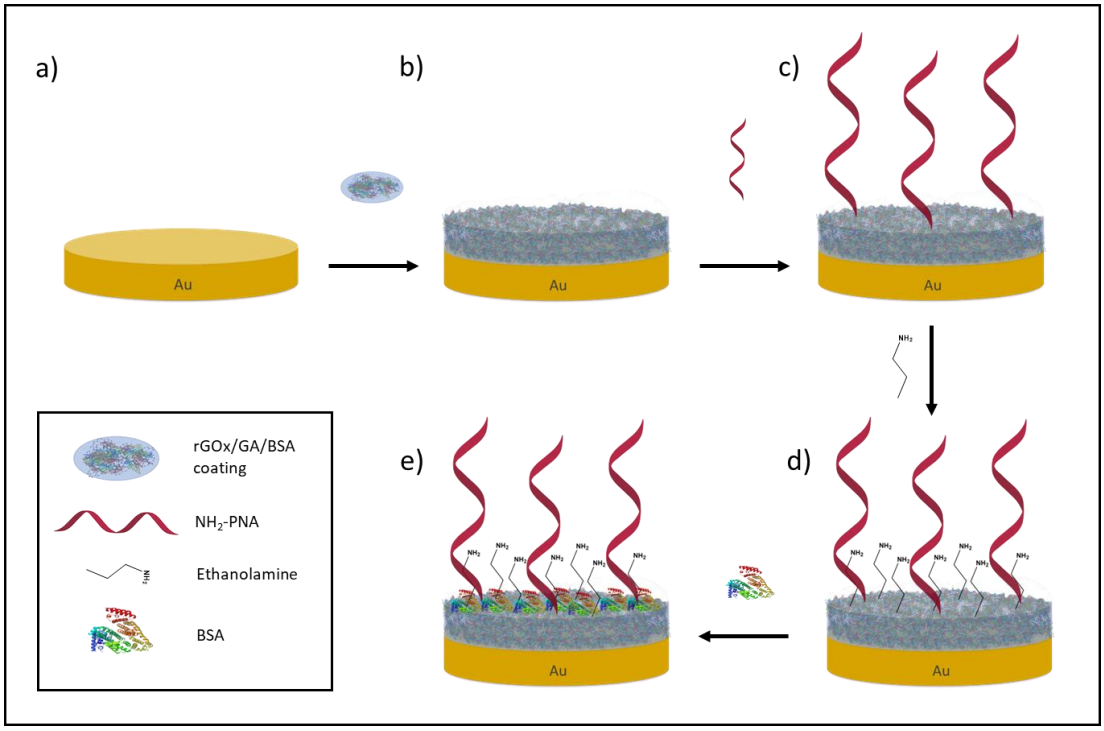

Figure 5.2. Schematic representation of the surface chemistry formed for the CRISPR-based detection assay. a) bare thin-film gold working electrode, b) rGOx/GA/BSA nanocomposite coating was incubated on the gold chips overnight at RT, c) amine-terminated PNA probe molecules were then spotted on working electrode and incubated overnight at 4 °C, d) the surface was then blocked with ethanolamine for 30 minutes at RT, e) and finally further blocked with 1% BSA at RT for 30 minutes.

5.2.5. Detection of RT-LAMP amplified SARS-CoV-2 viral RNA using the CRISPR-Cas12a/gRNA assay with electrochemically active TMB reporter

The reporter (RP) sequence used for the CRISPR electrochemical assay was a partially complementary 30-mer ssDNA (/5Biosg/ATTATTATTATTATTTGTTGTTGTTGTTGT) conjugated to a biotin which binds to polystreptavidin-horse radish peroxidase (HRP). Upon Cas12a activation by target RNA, the ssDNA-biotin RP was cleaved in solution, preventing complete binding to the complementary PNA sequence on the surface. Polystreptavidin-HRP was then added and able to bind to the ssDNA biotin moiety. The concentration of HRP bound to the surface was ascertained by HRP-dependent oxidation of precipitating 3,3',5,5'-Tetramethylbenzidine (TMB). TMB precipitation then forms an insulating, non-soluble layer on the electrode surface, significantly increasing observed current. Full-length genomic RNA (MT106054.1) was serially

diluted and amplified with 2X LAMP master mix (NEB) for 30 minutes at 65 °C. Viral RNA was extracted from saliva via purification with the QiAmp viral RNA extraction kit. As with the protocol explained above, 5 µl of the viral RNA was added to 2.5 µl of the 10X primer mix (see Table 5.1), 12.5 µl of the LAMP master mix (NEB) and 5 µl water. LAMP mixtures were incubated for 30 minutes at 65 °C. After LAMP amplification, 4 µl of the amplified LAMP product was mixed with 10 µl nuclease-free water and 5 µL CRISPR mix, which contained 4 nM RP, 100 nM Cas12a and 200 nM gRNA in 10X NEB 2.1 buffer. Mixtures were incubated for 20 minutes at 37 °C, during which time the ssDNA biotinylated reporter was cleaved. After that, 15 µl of the LAMP/RP/Cas12a mixture was deposited on the chips for 5 minutes. Thereafter, the chips were washed and incubated with polystreptavidin-HRP and then TMB for 5 minutes and 1 minute, respectively. Final measurement was then performed in PBST using a potentiostat (Autolab PGSTAT128N, Metrohm; VSP, Bio-Logic) by CV scan with 1 V/s scan rate between −0.5 and 0.5 V vs. an on-chip integrated gold quasi reference electrode. Peak oxidation current was calculated using Nova 1.11 software.

Table 5.1. Best performing LAMP primer sequences and their final concentrations in LAMP assays.

Primer	**Concentration (µM)**	**Sequence**
FIP	1.6	TCAGCACACAAAGCCAAAAATTTATTTTTCTGTGCAAAGGAAATTAAGGAG
BIP	1.6	TATTGGTGGAGCTAAACTTAAAGCCTTTTCTGTACAATCCCTTTGAGTG
F3	0.2	CGGTGGACAAATTGTCAC
B3	0.2	CTTCTCTGGATTTAACACACTT
Loop F	0.4	TTACAAGCTTAAAGAATGTCTGAACACT
Loop B	0.4	TTGAATTTAGGTGAAACATTTGTCACG

5.2.6. Detection of unamplified *E. coli* Shiga toxins (Stx-1 and Stx-2)

The same assay was employed for the detection of Shiga toxin-related DNA from *E. coli* using the biotinylated RP DNA alongside polystreptavidin-HRP and reduce TMB that was carried out for SARS-CoV-2 detection. For the detection of Shiga-toxin DNA samples were not amplified and target DNA was spiked into the CRISPR reaction mixture. 4 µl of the unamplified Shiga-toxin DNA was mixed with 10 µl nuclease-free water and 5 µL CRISPR mix, which contained 4 nM RP DNA, 100 nM Cas12a and 200 nM of the respective gRNA in 10X NEB 2.1 buffer (see Table 5.2).

Table 5.2. Guide RNA and target DNA sequences for E. Coli Stx-1 and Stx-2 biomarkers.

gRNA name	**gRNA sequence**	**Target DNA sequence**
gRNA *Stx*-1	GGGUAAUUUCUACUAAGUGUAGAU UCUGCAUCCCCGUACGACUG	CAGTCGTACGGGGATGCAGATAAA
gRNA *Stx-2*	GGGUAAUUUCUACUAAGUGUAGAU AUCAUAUCUGGCGUUAAUGG	CCATTAACGCCAGATATGATGAAA

Mixtures were incubated for 20 minutes at 37 °C, during which time the ssDNA biotinylated reporter was cleaved. After that, 15 µl of the RP/Cas12a mixture was deposited on the chips for 15 minutes. Thereafter, the chips were washed and incubated with polystreptavidin-HRP and then TMB for 5 minutes and 1 minute, respectively. Final measurement was then performed in PBST using a potentiostat (Autolab PGSTAT128N, Metrohm; VSP, Bio-Logic) by CV scan with 1 V/s scan rate between −0.5 and 0.5 V vs. an on-chip integrated gold quasi reference electrode. Peak oxidation current was calculated using Nova 1.11 software. The conserved regions of dsDNA gene block (gBlock) sequences for *Stx*-1 and *Stx*-2 are shown in Table 5.3.

Table 5.3. dsDNA gBlock sequences representative of Stx-1 and Stx-2 coding regions from E. Coli plasmid. Cas12a/gRNA targeting regions used as assay target DNA are highlighted.

Shiga gBlock DNA	**DNA gBlock sequence**
gBlock *Stx*-1	TTTTTCACATGTTACCTTTCCAGGTACAACAGCGGTTACATTGTCTGGTGACAG TAGCTATACCACGTTACAGCGTGTTGCAGGGATCAGTCGTACGGGGATGCAG ATAAATCGCCATTCGTTGACTACTTCTTATCTGGATTTAATGTCGCATAGAGGA ACCTCCCTCCCGCAGTCTGGGGCAAGAGCGATGTTACGGT
gBlock *Stx*-2	TTTTACACATATATCAGTGCCCGGTGTGACAACGGTTTCCATGACAACGGACA GCAGTTATACCACTCTGCAACGTGTCGCAGCGCTGGAACGTTCCGGAATGCAA ATCAGTCGTCACTCACTGGTTTCATCATATCTGGCGTTAATGGAGTTCAGTGGT AATACAATGACCAGAGATGCATCCAGAGCAGTTCTGCGTT

5.3. Results and Discussion

5.3.1. Development of the SHERLOCK CRISPR-Cas12a electrochemical diagnostic assay

The assay developed within this study capitalises on the Cas12a enzyme taken from the bacteria species *Lachnospiraceae*, serotype ND2006. This specific Cas enzyme has been shown to have cleavage affinity towards dsDNA oligonucleotides matching the guide RNA (gRNA) sequence it is conjugated with. Upon contact with nearby complementary target dsDNA sequences, conjugated Cas12a/gRNA cleaves the dsDNA and becomes activated, continuing to collaterally cleave any ssDNA in proximity (English *et al.*, 2019; Gayet *et al.*, 2020). To take advantage of this characteristic of Cas12a, an electrochemical assay was developed utilising a biotinylated reporter probe (RP) ssDNA sequence. In the absence of target dsDNA, Cas12a/gRNA is not activated and the RP binds to a partially complementary surface-bound highly specific ssPNA sequence on the antifouling nanocomposite covered gold electrode (Jolly *et al*., 2019; Zupančič *et al*., 2021). Polystreptavidin-HRP was then conjugated to the biotin group of the RP, which catalyses the precipitation of 3,3',5,5'-Tetramethylbenzidine (TMB) onto the surface of the electrode. When all

these reactions occur, reduced precipitated TMB on the electrode surface results in a significant peak current increase observed by using cyclic voltammetry (CV) between -0.5 and 0.5 V (see Figure 5.3b). However, in the presence of target dsDNA, the RP sequence is collaterally cleaved, and the biotinylated portion of the sequence is not bound to the surface, preventing downstream binding of polystreptavidin-HRP and precipitation of TMB, leading to low or no current signal (see Figure 5.3c). To further increase the sensitivity of this assay, isothermal LAMP amplification was used to amplify the dsDNA target of SARS-CoV-2 (see Figure 5.3a). The Cas12a/gRNAs and primers (see Table 5.1) used in the LAMP reaction (Lu *et al.*, 2020; Rabe and Cepko, 2020; Rohaim *et al.*, 2020; Yan *et al.*, 2020; Nawattanapaiboon *et al.*, 2021) were previously evaluated from the conserved regions of the SARS-CoV-2 genome to determine the most sensitive sequences (Najjar *et al*., 2022).

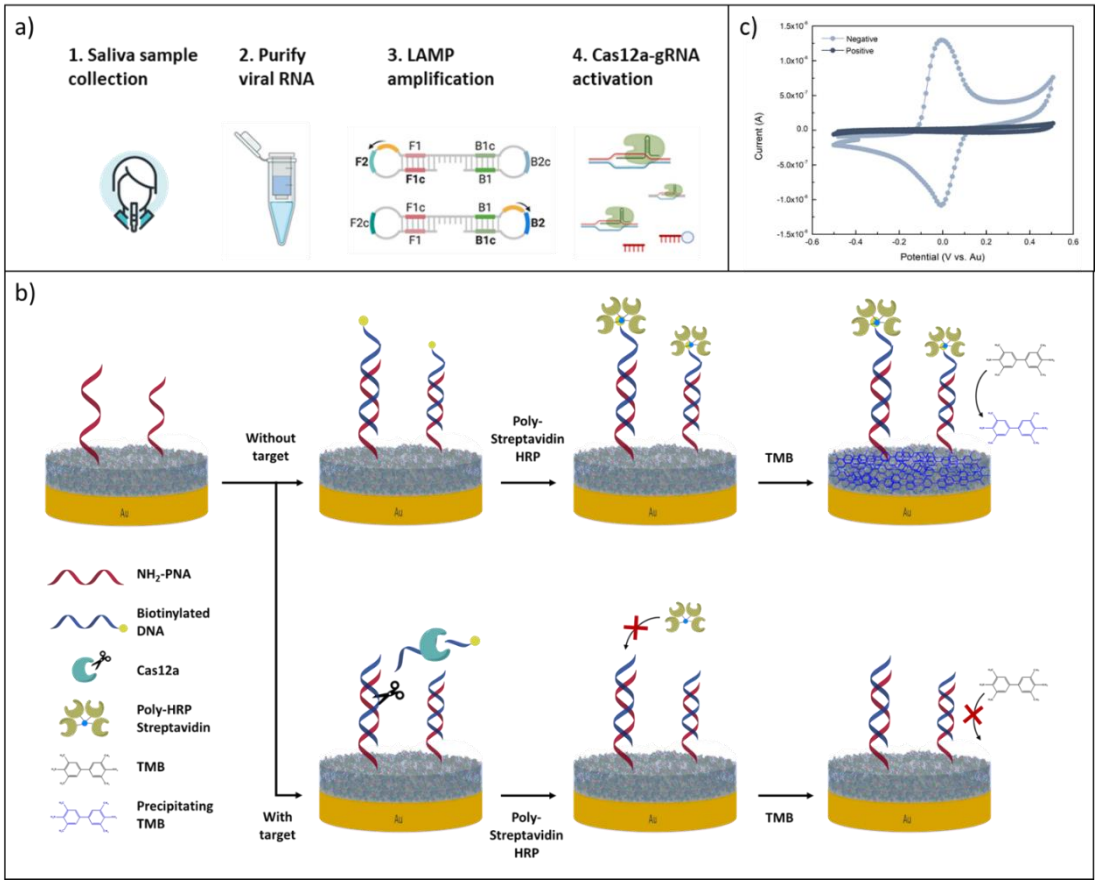

Figure 5.3. a) Example of potential process of sample collection, pre-treatment, amplification with LAMP and CRISPR-based Cas12a-gRNA complex activation. b) Schematic representation of the surface chemistry of the electrochemical assay. Without viral RNA (top row), the biotinylated ssDNA RP probe is not cleaved; leading to the binding of polystreptavidin-HRP to

the PNA/biotin-DNA duplex when added to the sensor electrodes and consequently precipitating TMB, resulting in an increase in current. In contrast, the biotinylated RP ssDNA is hydrolysed in the presence of viral target RNA-activated Cas12a/gRNA complex (bottom row), cleaving the biotin group. Thus, polystreptavidin-HRP does not bind to the surface of the electrodes, resulting in no TMB precipitation and no increase in current. c) Cyclic voltammogram showing the typical expected oxidation peak signal of precipitated TMB achieved after incubation containing SARS-CoV-2 negative (light blue) and positive (dark blue) samples.

5.3.2. Optimisation of the reporter probe (RP) signal-to-noise ratio for SARS-CoV-2

The electrochemical assay was optimised to maximise the observed peak current signal output by adjusting the binding efficiency of the RP through concentration and incubation time. By doing so, we were able to develop a rapid assay with high signal-to-noise ratio (see Figure 5.4 and Figure 5.5). A wide range of RP concentrations (1-50 nM) were first tested to determine the highest possible peak current signal. In the absence of Cas12a/gRNA and dsDNA target, each concentration was incubated on the electrode surface for 30 minutes before adding the polystreptavidin-HRP and TMB. Peak current values showed that all concentrations of RP produced similar peak current values, however, 10-50 nM showed significant background signal on electrode immobilised with BSA as a negative control suggesting non-specific binding of the RP at high concentrations. The lower concentrations of RP showed no background signal however, and so concentrations 0.5, 1 and 5 nM were further tested (see Figure 5.5) with varied incubation times.

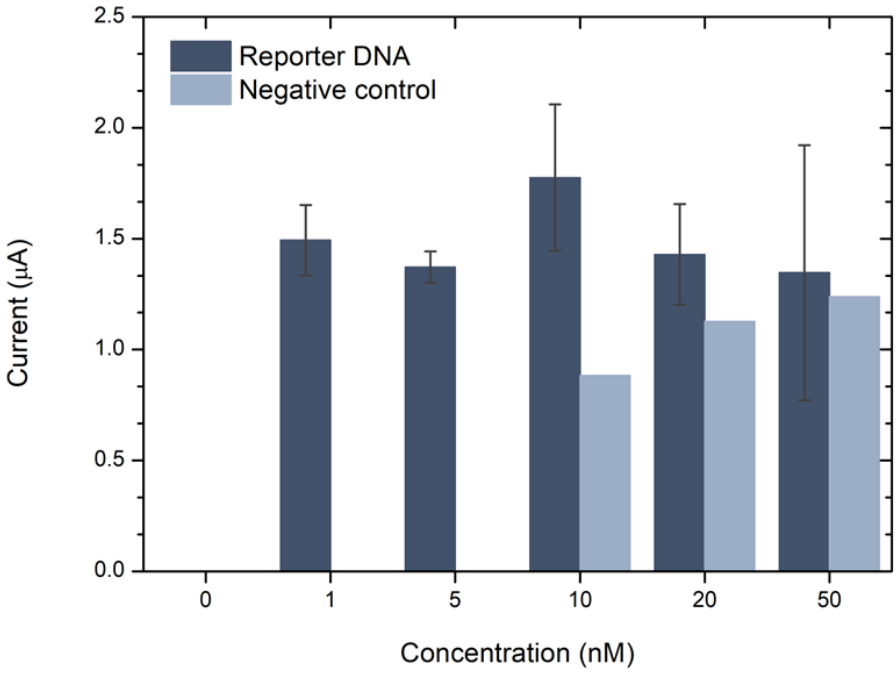

Figure 5.4. Optimization of the reporter DNA concentration used in the CRISPR-based electrochemical assay (n=3).

Lower incubation timings were tested with low RP concentrations of 0.5, 1 and 5 nM to both minimise the assay time and use of reagents. Each RP concentration was tested as before, however, with incubation times of 5, 10 and 15 minutes. Data showed that at the longer incubation time of 15 minutes, some background signal was observed for all concentrations. Overall, of all the concentrations of RP tested, 1 nM and 5 minutes of incubation produced a high enough signal-to-noise ratio with no background and a rapid response time.

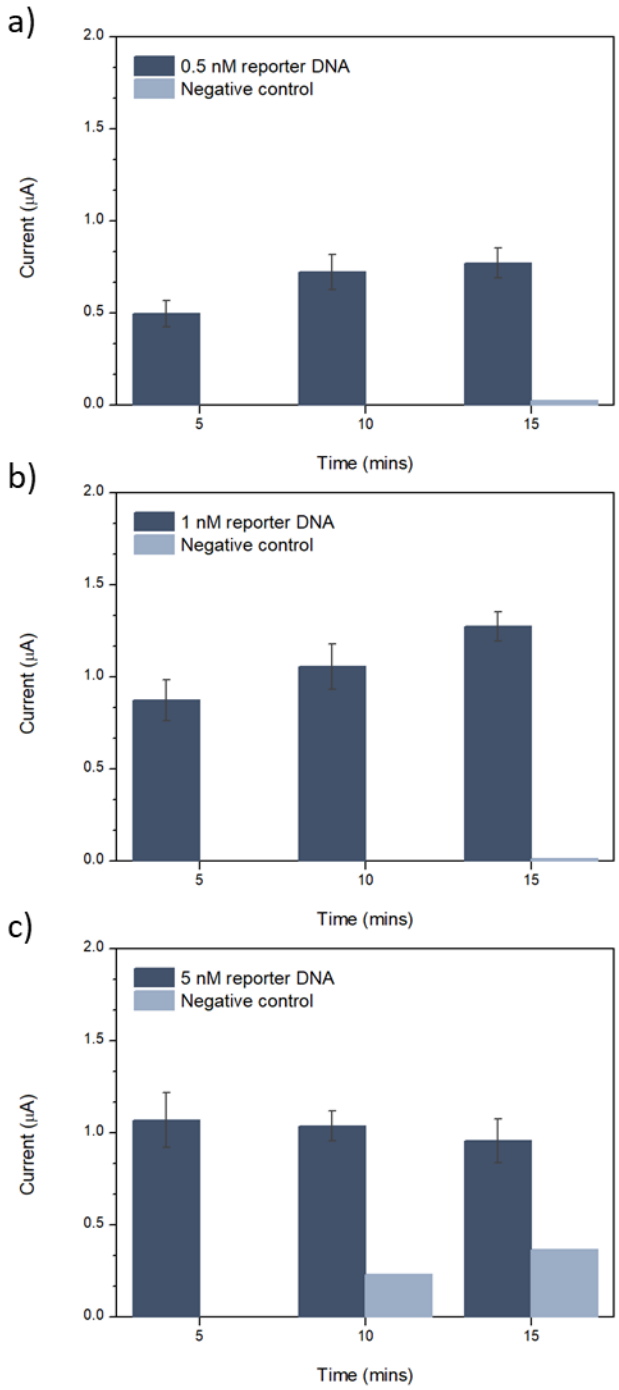

Figure 5.5. Optimization of the incubation time of the reporter probe (RP) for the CRISPR-based electrochemical assay with reporter probe concentrations 0.5 nM, 1 nM, and 5 nM over 5, 10 and 15 minutes. Negative control consisted of surface bound BSA in the place of PNA sequence. Error bars represent standard deviation of three repeats (n≥3).

Using the fully optimised protocol for the electrochemical sensing assay, 9 samples spiked with SARS-CoV-2 viral RNA and 9 samples negative for the viral RNA were

tested with the CRISPR-Cas12a/gRNA reaction and were showed to be clearly distinguishable (see Figure 5.6). All SARS-CoV-2 positive samples gave a low peak current signal output, while samples negative for SARS-CoV-2 gave high signals comparable to those from the optimisation of the RP concentrations and incubation timings. Additionally, SARS-CoV-2 positive and negative samples were further significantly different according to a student's *t*-test which produce a *P*-value below 0.001.

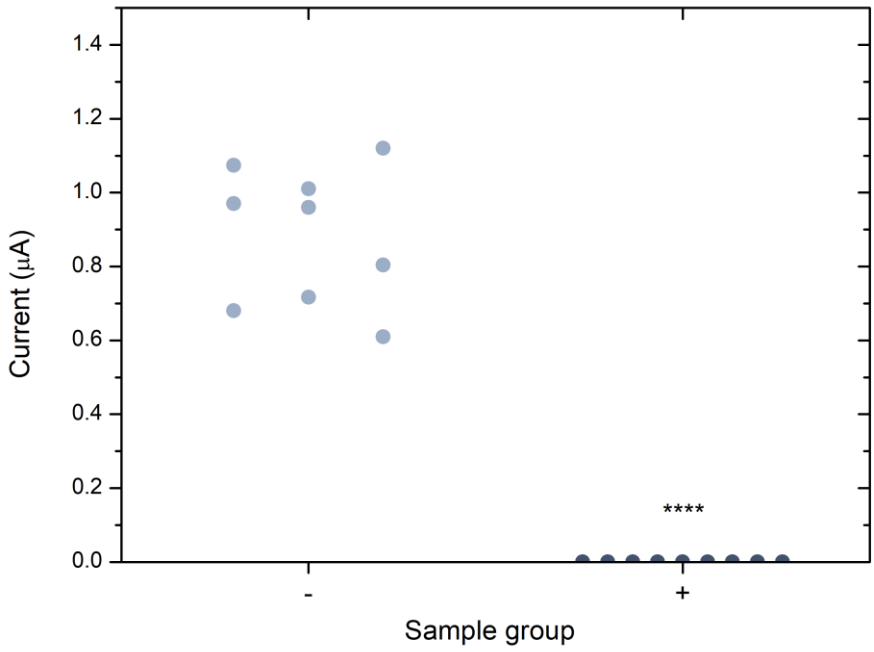

*Figure 5.6. Comparison of samples containing SARS-CoV-2 viral RNA (dark blue, +ve, n=9) had low/zero current signal with the TMB assay, showing a significant difference from sample containing no SARS-CoV-2 viral RNA (light blue, -ve, n=9). **** = student's t-test P < 0.001.*

5.3.3. Determination of assay sensitivity and limit of detection (LOD) using unamplified, and RT-LAMP amplified SARS-CoV-2 genomic viral RNA samples

Various concentrations of full-length viral RNA from SARS-CoV-2 (12.8-8000 cp/µL) were then assessed using the developed assay by serially diluting in water and amplifying using the RT-LAMP protocol (see Figure 5.7). The data showed that viral RNA serially diluted down to 12.8 cp/µL in water and amplified using RT-LAMP gave clear zero peak current signal suggesting positive signal using the electrochemical

assay, indicative of no precipitating TMB due to cleavage of the RP by activated Cas12a. Negative control samples containing 0 cp/µL of viral RNA in water gave positive signal, however, indicating precipitation of TMB on the electrode surface. An unpaired student's *t*-test suggested a significant difference in the peak current between 12.8 cp/µL of SARS-CoV-2 genomic viral RNA and the negative control with a *P*-value of <0.0001.

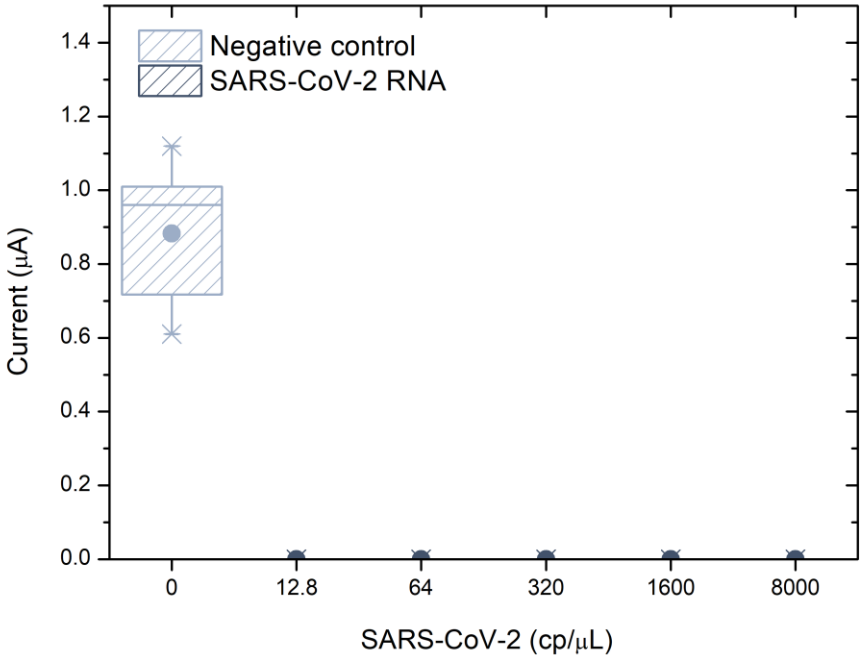

Figure 5.7. Limit of detection of the electrochemical CRISPR-based assay Error bars represent standard deviation of biological replicates (n≥6). Raw data: negative control (0 cp/µL) number of replicates = 9, mean = 0.83, standard deviation = 0.184; 12.8-8000 cp/µL number of replicates = 6, mean = 0.00, standard deviation = 0.00.

Sensitivity of the assay was then determined using the data obtained in Figure 5.7 using a logistic regression analysis with the regression curve shown in Figure 5.8. The results of the logistic regression analysis determined that serial dilutions of the SARS-CoV-2 genomic viral RNA down to a concentration of 0.8 cp/µL (1.33 aM) had a 95% probability of producing a clear positive signal using the electrochemical assay developed in this study. Table 5.4 contains the raw data used to fit the logistic regression curve. Each concentration was assessed with 5 independent biological

replicates (n=5). This LOD of 0.8 cp/µL (1.33 aM) was more sensitive than the fluorescent output determined alongside the current study of 2.3 cp/µL (Najjar *et al*., 2022) and comparable to, if not lower than, high-performing gold standard RT-qPCR assays used traditionally in laboratories produced in half the assay time (FDA, 2021).

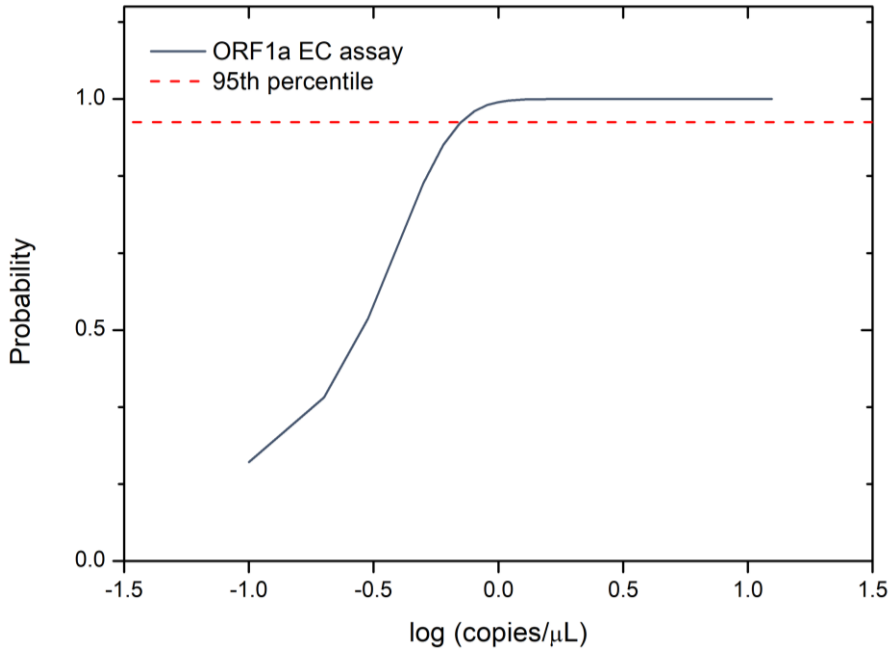

Figure 5.8. Sensitivity of the viral RNA electrochemical assay was assessed according to a 95% probability of leading to a clear positive signal using a logistic regression curve analysis (each concentration was probed with 5 independent biological repeats).

Table 5.4. Raw data used in the logit regression curve analysis to determine the LOD of the electrochemical CRISPR-based SARS-CoV-2 RNA assay.

								LOD
Electrochemical assay	**RNA (cp/µL)**	12.5	6.25	1	0.30	0.15	0	0.8 cp/µl 1.33 aM
	Replicates (+ve/total)	5/5	5/5	5/5	3/5	2/5	0/5	

5.3.4. Detection of unamplified *E. coli* genomic DNA using the SHERLOCK CRISPR-Cas12a/gRNA assay

During this study, the CRISPR-Cas12a-based detection assay was also implemented in the detection of unamplified *E. coli* genomic DNA from two genes that produce different Shiga toxins, namely, Shiga toxin-1 (Stx-1) and Shiga toxin-2 (Stx-2). These toxins readily cause mucosal and submucosal oedemas, haemorrhages, bloody diarrhoea, and haemolytic uraemic syndrome (HUS) through endothelial cell necrosis and apoptosis (Bauwens *et al.*, 2011; Chan and Ng, 2016). Often leading to higher cases of infection, disease, and mortality in LMIC countries from water and foodborne outbreaks with children under five and immunocompromised individuals being more susceptible to severe complications and mortality (Conrad *et al.*, 2016).

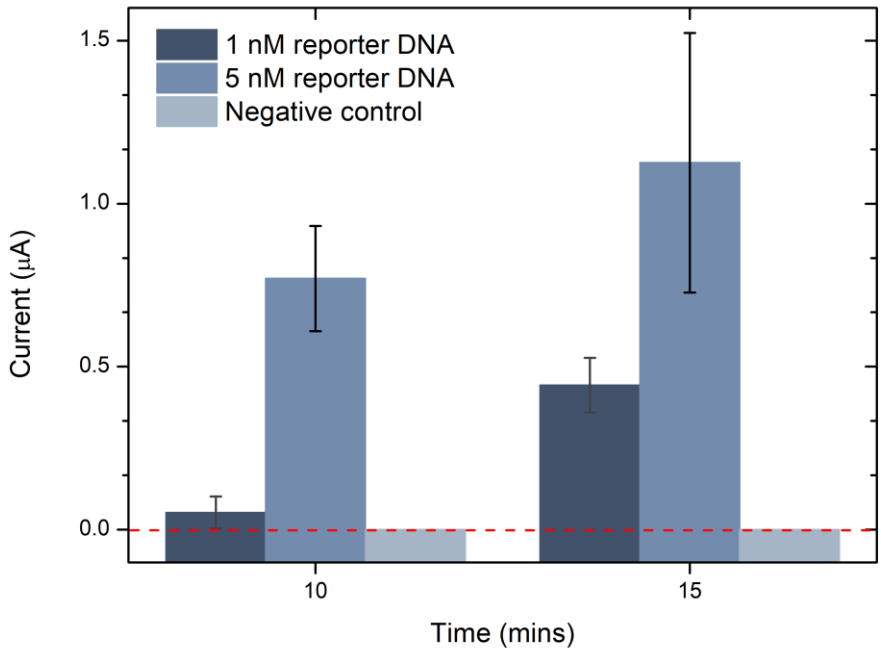

Figure 5.9. Re-optimisation of the reporter DNA concentration and incubation time with Cas12a/Stx-1 gRNA for use in the E. coli Stx-1 and Stx-2 detection assays. Error bars represent standard deviation determined from at least three repeats (n≥3).

The concentration and incubation time of the reporter DNA within the CRISPR/Cas12a mixture was further optimised for this assay to maximise signal-to-noise ratio for the *E. coli* guide RNA and target DNA reaction. Reporter DNA

concentrations of 1 and 5 nM were each tested for incubation of 10 and 15 minutes (see Figure 5.9). The results suggest that incubating 5 nM of the reporter DNA for 15 minutes gives the highest mean current output of 1.13 µA, a 46.75% increase from the second highest current observed with 5 nM reporter DNA incubated for 10 minutes.

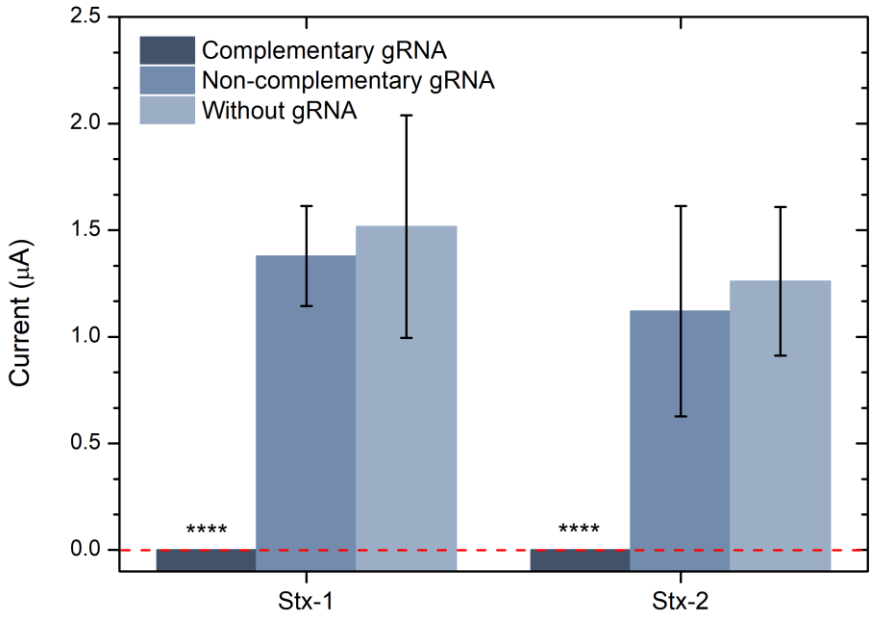

*Figure 5.10. Graph shows the mean average current values for specific guide RNA (dark blue), non-specific guide RNA sequences (mid-blue) and no guide RNA (light blue). Error bars represent standard deviation determined from at least three repeats (n≥3). **** = unpaired student's t-test P < 0.001.*

The *E. coli* assay was then tested with negative controls to ensure specificity of the signal. For both Stx-1 and Stx-2 target DNA two negative controls were tested, complementary gRNA with each target DNA (i.e., no Stx-1 gRNA with Stx-1 target DNA) and non-complementary gRNA with each target DNA (i.e., Stx-2 gRNA with Stx-1 target DNA), and no gRNA added to the Cas12a to further assess background activity (see Figure 5.10). In the presence of complementary gRNA with both Stx-1 and Stx-2 target DNA, Cas12a was guided to the target DNA, activating the enzyme, and leading to cleavage of the biotinylated reporter DNA which inhibited

downstream binding of polystreptavidin-HRP and prevented precipitation of TMB leading to an absence of current signal. However, in both cases of non-complementary gRNA being added to Cas12a and a lack of gRNA being added, maximum current was observed, suggesting binding of polystreptavidin-HRP and precipitation of TMB on the electrode surface as expected. According to an unpaired student's *t*-test between the complementary and non-complementary gRNA for both Stx-1 and Stx-2 a significant difference was observed with a *P*-value below <0.001. Suggesting overall that the activity of the Cas12a collateral cleavage was specifically initiated by addition of complementary gRNA to the respective Shiga toxin target DNA.

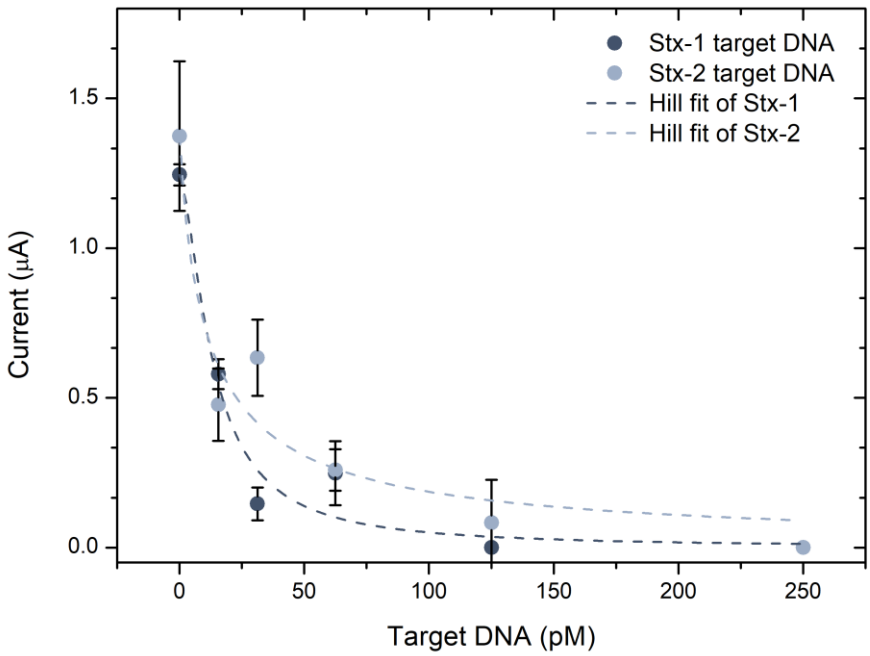

Figure 5.11. Dose response curves for observed current relating to CRISPR/Cas12a-based detection of E. coli Shiga toxin 1 (Stx-1) and Shiga toxin 2 (Stx-2) DNA. Error bars represent standard deviation determined from at least three repeats (n≥3).

The dose response curves were fitted using the Hill fit for the binding of ligands (see Figure 5.11) to macromolecules following the formula below:

$$y = Start + (End - Start)\frac{x^n}{k^n + x^n}$$

Where, *x* is the concentration of the target, *k* is the Michaelis' constant, and *n* is the number of cooperative sites. The LOD for both Shiga toxin 1 and 2 target sequences were determined using the following equation:

$$LOD = \frac{3\sigma}{h}$$

Where, σ is the standard deviation of the control and *h* is the Hill slope. Using this equation, the LOD for Stx-1 and Stx-2 were calculated to be 210 fM and 1.26 pM, respectively (Table 5.5). The limit of quantitation (LOQ) was then calculated for both target sequences using the following equation:

$$LOQ = \frac{10\sigma}{h}$$

Limit of detection (LOD) is the lowest concentration of analyte in the sample that is easily determined against the control value, while the limit of quantitation (LOQ) is the lowest concentration of analyte in the sample that is determined with a reasonable accuracy and repeatability. The LOQ for the Stx-1 and Stx-2 sequences were determined to be 703 fM and 4.55 pM, respectively (Table 5.5). Additionally, these limits were achieved without the use of target sequence amplification and could be easily increased with the use of a sample isothermal amplification technique e.g., LAMP or recombinase polymerase amplification (RPA).

Table 5.5. Raw data for the dose responses of Stx-1 and Stx-2 with mean average current and limits of detection and limits of quantitation calculated. Error bars represent standard deviation determined from at least three repeats (n≥3).

Target concentration (pM)		**0**	**15.6**	**31.25**	**62.5**	**125**	**250**	**LOD**	**LOQ**
Stx-1	**Current (µA)**	1.245	0.579	0.146	0.248	0	0	210 fM	703 fM
Stx-2		1.374	0.478	0.634	0.259	0.082	0	1.26 pM	4.55 pM

5.4. Conclusions and Future Work

In this study, a novel electrochemical assay has been developed for the ultrasensitive sample-in-answer-out detection of SARS-CoV-2 viral RNA and *E. coli* genomic DNA. This assay has integrated multiple techniques to achieve this including: 1) development of a high-sensitivity and specificity electrochemical sensor chip utilising a previously developed graphene-based antifouling conductive nanocomposite (Zupančič *et al*., 2021), peptide nucleic acid sensing probes, and a chip-based polystreptavidin-HRP/TMB-based precipitation chemistry to achieve limits of detection at the pico-/femtomolar level with *E.coli* genomic DNA; 2) implementation of a CRISPR-based detection technique utilising Cas12a's cleavage ability of dsDNA targets and collateral cleavage of ssDNA sequences to produce a flexibly programmable tool for detection of multiple pathogenic nucleic acid biomarkers; and 3) integration of target nucleic acid isothermal amplification by LAMP assay to achieve ultrasensitive single-molecule level detection of SARS-CoV-2 viral RNA samples.

While other electrochemical CRISPR-based platforms have been developed, the achieved LODs have not been sensitive enough for the detection of various viral loads in clinical samples or pathogens presents in contaminated fresh and wastewater (Xu *et al.*, 2020; Li *et al.*, 2021; Zamani *et al.*, 2021). By integrating LAMP amplification with our assay, it was possible to achieve ultrasensitive single-molecule LOD of 1.33 aM (0.8 cp/µl) for SARS-CoV-2 viral RNA. By combining all these techniques, we have developed a platform capable of ultrasensitive detection of nucleic acids through enzyme-based detection with CRISPR/Cas12a that can easily be reprogrammed for detection of a plethora of potential pathogen targets. Using the antifouling conductive nanocomposite, the assay can also be used for the detection of nucleic acids directly in clinical and environmental samples without the need for reagent- and time-demanding sample pre-treatments and may also enable detection in the on-site monitoring of waterborne pathogens. Through the optimisation of the electrochemical assay reaction conditions, we have enabled significantly low background for both SARS-CoV-2 detection and detection of unamplified *E. coli* DNA, improved sensitivity, and rapid sample detection time of approximately 1 hour (see

Table 5.6). The selectivity of our assay was also significantly high, a student's *t*-test between the lowest concentration of SARS-CoV-2 (12.8 cp/µl) and negative control producing a *P*-value of <0.001. While an unpaired student's *t*-test between Cas12a guided with complementary and non-complementary gRNA also achieved a *P*-value of <0.001.

Table 5.6. Comparison table showing the difference in limit of detection (LOD) with targets detected either with or without target pre-amplification steps.

Target	**Limit of Detection (Mol)**	**Target pre-amplification?**
SARS-CoV-2 RNA	1.33 aM	Yes - with 2X LAMP master mix for 30 minutes at 65 °C
E. coli Stx-1 DNA	703 fM	None
E. coli Stx-2 DNA	4.55 pM	None

Future areas of work aim to focus on the detection of clinical sample from both clinical samples such as saliva and serum (outside the scope of this thesis) as well as environmental samples such as contaminated freshwater and wastewater for monitoring of infections at the community level. The anti-fouling nanocomposite utilised in this study would provide a suitable surface for detection in these matrices. It would also be beneficial to further develop the assay to allow for acquisition of quantitative data for the purposes of disease state monitoring and environmental contamination level assessment. Further development of a fully integrated biosensing platform would also be of interest. Specifically, the development of sample and reagent flow using microfluidics, micro-scaling of the electronics and potentiostat for electrochemical readout, and development of a cartridge for single-use user-friendly sample loading would allow for PoC and on-site use by a more general user base. Finally, research into reagent long-term storage would also be key

for the storage of potential assay kits that could further enable the commercial use of a future device.

The SHERLOCK diagnostic platform, with the aid of target pre-amplification, allows for the development of diagnostic devices that can enter the commercial sphere. By leveraging the ability to produce large quantities of target amplicons alongside ultra-selective CRISPR-Cas aided detection with both optical and electrochemical readout techniques at the micro-scale it is possible to ensure rapid and ultrasensitive detection of target nucleic acid biomarkers. By using these techniques, affordable diagnostic tools can be produced for accessible use by clinicians and consumers for both on-site and point-of-care (PoC) diagnostics and monitoring purposes. Due to the engineerability of both the amplification and CRISPR cleavage protocols, it is also possible to create a highly flexible platform for the detection of a plethora of targets. This could range from medical biomarkers for both diseases and disorders to environmental biomarkers to monitor and mitigate outbreaks while meeting the REASSURED criteria for PoC diagnostic devices.

References

Bauwens, A. et al. (2011) 'Differential cytotoxic actions of Shiga toxin 1 and Shiga toxin 2 on microvascular and macrovascular endothelial cells', Thrombosis and Haemostasis, 105(3), pp. 515–528. Available at: https://doi.org/10.1160/TH10-02-0140/ID/JR25454-1.

Bloom, D.E., Black, S. and Rappuoli, R. (2017) 'Emerging infectious diseases: A proactive approach', Proceedings of the National Academy of Sciences of the United States of America, 114(16), pp. 4055–4059. Available at: https://doi.org/10.1073/PNAS.1701410114/ASSET/9605D5BA-3DAC-4F84-B8F0-40284C4D0E5F/ASSETS/GRAPHIC/PNAS.1701410114FIG03.JPEG.

Chan, Y.S. and Ng, T.B. (2016) 'Shiga toxins: from structure and mechanism to applications', Applied Microbiology and Biotechnology, 100(4), pp. 1597–1610. Available at: https://doi.org/10.1007/S00253-015-7236-3/TABLES/1.

Conrad, C. et al. (2016) 'Shiga toxin-producing Escherichia coli and current trends in diagnostics', Animal Frontiers, 6(2), pp. 37–43. Available at: https://doi.org/10.2527/AF.2016-0021.

English, M.A. et al. (2019) 'Programmable CRISPR-responsive smart materials', Science, 365(6455), pp. 780–785. Available at: https://doi.org/10.1126/SCIENCE.AAW5122/SUPPL_FILE/AAW5122_ENGLISH_SM.PDF.

European Food Safety Authority (2011) 'Shiga toxin-producing E. coli (STEC) O104:H4 2011 outbreaks in Europe: Taking Stock', EFSA Journal, 9(10). Available at: https://doi.org/10.2903/J.EFSA.2011.2390.

FDA (2021) CDC 2019-Novel Coronavirus (2019-nCoV) Real-Time RT-PCR Diagnostic Panel. Available at: https://www.fda.gov/media/134922/download (Accessed: 14 January 2021).

Federspiel, F. and Ali, M. (2018) 'The cholera outbreak in Yemen: Lessons learned and way forward', BMC Public Health, 18(1), pp. 1–8. Available at: https://doi.org/10.1186/S12889-018-6227-6/TABLES/1.

Gayet, R. v. et al. (2020) ‘Creating CRISPR-responsive smart materials for diagnostics and programmable cargo release’, Nature Protocols 2020 15:9, 15(9), pp. 3030–3063. Available at: https://doi.org/10.1038/s41596-020-0367-8.

Gootenberg, J.S. et al. (2017) ‘Nucleic acid detection with CRISPR-Cas13a/C2c2’, Science, 356(6336), pp. 438–442. Available at: https://doi.org/10.1126/SCIENCE.AAM9321/SUPPL_FILE/PAPV2.PDF.

Huremović, D. (2019) ‘Brief History of Pandemics (Pandemics Throughout History)’, Psychiatry of Pandemics, p. 7. Available at: https://doi.org/10.1007/978-3-030-15346-5_2.

Isho, B. et al. (2020a) ‘Persistence of serum and saliva antibody responses to SARS-CoV-2 spike antigens in COVID-19 patients’, Science Immunology, 5(52). Available at: https://doi.org/10.1126/SCIIMMUNOL.ABE5511/SUPPL_FILE/ABE5511_TABLE_S4.XLSX.

Jolly, P. et al. (2019) ‘A PNA-based Lab-on-PCB diagnostic platform for rapid and high sensitivity DNA quantification’, Biosensors and Bioelectronics, 123. Available at: https://doi.org/10.1016/j.bios.2018.09.006.

Kaminski, M.M. et al. (2020) ‘A CRISPR-based assay for the detection of opportunistic infections post-transplantation and for the monitoring of transplant rejection’, Nature Biomedical Engineering 2020 4:6, 4(6), pp. 601–609. Available at: https://doi.org/10.1038/s41551-020-0546-5.

King, L.A. et al. (2012) ‘Outbreak of Shiga Toxin–Producing Escherichia coli O104:H4 Associated With Organic Fenugreek Sprouts, France, June 2011’, Clinical Infectious Diseases, 54(11), pp. 1588–1594. Available at: https://doi.org/10.1093/CID/CIS255.

Lee, R.A. et al. (2020) ‘Ultrasensitive CRISPR-based diagnostic for field-applicable detection of Plasmodium species in symptomatic and asymptomatic malaria’, Proceedings of the National Academy of Sciences of the United States of America, 117(41), pp. 25722–25731. Available at: https://doi.org/10.1073/PNAS.2010196117/SUPPL_FILE/PNAS.2010196117.SAPP.PDF.

Li, F. et al. (2021) ‘An ultrasensitive CRISPR/Cas12a based electrochemical biosensor for Listeria monocytogenes detection’, Biosensors and Bioelectronics, 179, p. 113073. Available at: https://doi.org/10.1016/J.BIOS.2021.113073.

Lu, R. et al. (2020) ‘Development of a Novel Reverse Transcription Loop-Mediated Isothermal Amplification Method for Rapid Detection of SARS-CoV-2’, Virologica Sinica, 35(3), pp. 344–347. Available at: https://doi.org/10.1007/S12250-020-00218-1/FIGURES/1.

Mak, G.C. et al. (2020) ‘Evaluation of rapid antigen test for detection of SARS-CoV-2 virus’, Journal of Clinical Virology, 129, p. 104500. Available at: https://doi.org/10.1016/J.JCV.2020.104500.

Michaud, C.M. (2009) ‘Global Burden of Infectious Diseases’, Encyclopedia of Microbiology, p. 444. Available at: https://doi.org/10.1016/B978-012373944-5.00185-1.

Najjar, D. et al. (2022) ‘A lab-on-a-chip for the concurrent electrochemical detection of SARS-CoV-2 RNA and anti-SARS-CoV-2 antibodies in saliva and plasma’, Nature Biomedical Engineering 2022, pp. 1–11. Available at: https://doi.org/10.1038/s41551-022-00919-w.

Nawattanapaiboon, K. et al. (2021) ‘Colorimetric reverse transcription loop-mediated isothermal amplification (RT-LAMP) as a visual diagnostic platform for the detection of the emerging coronavirus SARS-CoV-2’, Analyst, 146(2), pp. 471–477. Available at: https://doi.org/10.1039/D0AN01775B.

Paneth, N. et al. (1998) ‘A rivalry of foulness: official and unofficial investigations of the London cholera epidemic of 1854.’, American Journal of Public Health, 88(10), p. 1545. Available at: https://doi.org/10.2105/AJPH.88.10.1545.

Rabe, B.A. and Cepko, C. (2020) ‘SARS-CoV-2 detection using isothermal amplification and a rapid, inexpensive protocol for sample inactivation and purification’, Proceedings of the National Academy of Sciences of the United States of America, 117(39), pp. 24450–24458. Available at:

https://doi.org/10.1073/PNAS.2011221117/SUPPL_FILE/PNAS.2011221117.SAPP.PDF.

Rainbow, J. et al. (2020) 'Integrated Electrochemical Biosensors for Detection of Waterborne Pathogens in Low-Resource Settings', Biosensors. Basel, Switzerland :, p. 36. Available at: https://doi.org/10.3390/bios10040036.

Ray, A. and Nordén, B. (2000) 'Peptide nucleic acid (PNA): its medical and biotechnical applications and promise for the future', The FASEB Journal, 14(9), pp. 1041–1060. Available at: https://doi.org/10.1096/FASEBJ.14.9.1041.

Ritchie, H. et al. (2020) 'Coronavirus Pandemic (COVID-19)', Our World in Data [Preprint]. Available at: https://ourworldindata.org/coronavirus (Accessed: 19 September 2022).

Rohaim, M.A. et al. (2020) 'Artificial Intelligence-Assisted Loop Mediated Isothermal Amplification (AI-LAMP) for Rapid Detection of SARS-CoV-2', Viruses 2020, Vol. 12, Page 972, 12(9), p. 972. Available at: https://doi.org/10.3390/V12090972.

Sabaté del Río, J. et al. (2019) 'An antifouling coating that enables affinity-based electrochemical biosensing in complex biological fluids', Nature Nanotechnology, 14(12), pp. 1143–1149. Available at: https://doi.org/10.1038/s41565-019-0566-z.

Wölfel, R. et al. (2020) 'Virological assessment of hospitalized patients with COVID-2019', Nature 2020 581:7809, 581(7809), pp. 465–469. Available at: https://doi.org/10.1038/s41586-020-2196-x.

Xu, W. et al. (2020) 'Surpassing the detection limit and accuracy of the electrochemical DNA sensor through the application of CRISPR Cas systems', Biosensors and Bioelectronics, 155, p. 112100. Available at: https://doi.org/10.1016/J.BIOS.2020.112100.

Yan, C. et al. (2020) 'Rapid and visual detection of 2019 novel coronavirus (SARS-CoV-2) by a reverse transcription loop-mediated isothermal amplification assay', Clinical Microbiology and Infection, 26(6), pp. 773–779. Available at: https://doi.org/10.1016/J.CMI.2020.04.001.

Zamani, M. et al. (2021) ‘Electrochemical Strategy for Low-Cost Viral Detection’, ACS Central Science, 7(6), pp. 963–972. Available at: https://doi.org/10.1021/ACSCENTSCI.1C00186/ASSET/IMAGES/LARGE/OC1C00186_0005.JPEG.

Zupančič, U. et al. (2021) ‘Graphene Enabled Low-Noise Surface Chemistry for Multiplexed Sepsis Biomarker Detection in Whole Blood’, Advanced Functional Materials, 31(16), p. 2010638. Available at: https://doi.org/https://doi.org/10.1002/adfm.202010638.

6. Conclusions and Future Work

This thesis aimed to improve the diagnostic capability of DNA-targeting biosensors through the integration of various techniques for the sensitive and selective detection of waterborne pathogens in freshwater. With that in mind, this thesis has provided a step towards the development of potential biosensing devices. The work in this thesis has explored the implementation of simple and cost-effective surface chemistries, electrochemical signal amplification through the intercalation of a novel redox-active molecule with dsDNA, and the development of an integrated diagnostic assay with sample isothermal amplification, highly selective target detection using CRISPR/Cas, antifouling conductive nanocomposite coating and simple labelled amperometric detection to achieve ultrasensitive detection of both bacterial and viral nucleic acids.

Electrochemical biosensors implementing naturally occurring and synthetic nucleic acids as probe molecules are an increasingly popular area of research within the literature. It can be observed from a large portion of published literature that the approaches towards achieving ultra-sensitive detection of nucleic acid targets are becoming increasingly complex. From the standpoint of developing biosensing devices for commercial diagnostic and monitoring purposes, complexity in sensor development and use is not advantageous when considering commercial fabrication capabilities as well as storage and distribution requirements. Additionally, developed diagnostic and monitoring tools need to be rapid and relatively simple to use so that they can be accessible to those that need them in rural and developing areas for point-of-care (PoC) and *in-situ* situations. However, for the detection of nucleic acid targets in fresh- and wastewater samples, biosensor devices that integrate various sample processing techniques alongside sensing are imperative for detecting particularly low target concentrations in the highly complex and fouling-capable matrix of water. By combining synthetic nucleic acid probes with simple-but-effective surface chemistries, electrochemical techniques, and signal amplification methods, it is possible to develop an integrated approach that can achieve the goals mentioned above.

To develop an integrated diagnostic biodevice for the detection of waterborne pathogens, this thesis has explored several areas within an interdisciplinary theme (see Figure 6.1). Areas explored within this thesis include the detection of waterborne pathogens including bacteria such as *E. Coli* as well as viruses including the recent SARS-CoV-2 virus. Electrochemical techniques have been employed within this thesis include impedimetric techniques such as electrochemical impedance spectroscopy, capacitance and OCP measurements. Amperometric techniques have also been explored, making use of CV and DPV for the detection and characterisation of various redox processes. This thesis has taken advantage of several surface chemistry techniques including passive adsorption of thiol-modified molecules to gold, amine functionalisation using EDC/NHS chemistry as well as the use of an anti-fouling nanocomposite coating containing conductive amine-terminated reduced graphene oxide (rGOx). Further to the use of the various surface chemistries, the assays used herein were all further developed and optimised to ensure a low signal-to-noise ratio, and high binding capability by modifying probes distance using spacing molecules such as MCH and reducing non-specific binding with backfilling and blocking steps. Due to the low concentration of target nucleic acids found in water samples, various methods of signal amplification were also investigated such as DNA intercalation with redox-active molecules, pre-treatment of samples through isothermal amplification, labelling techniques catalysed by enzyme precipitation and the doping of surface chemistries with conductive nanomaterials. Finally, various forms of integrating these techniques into single assays have been explored to reduce assay time, including multi-electrode platforms etc.

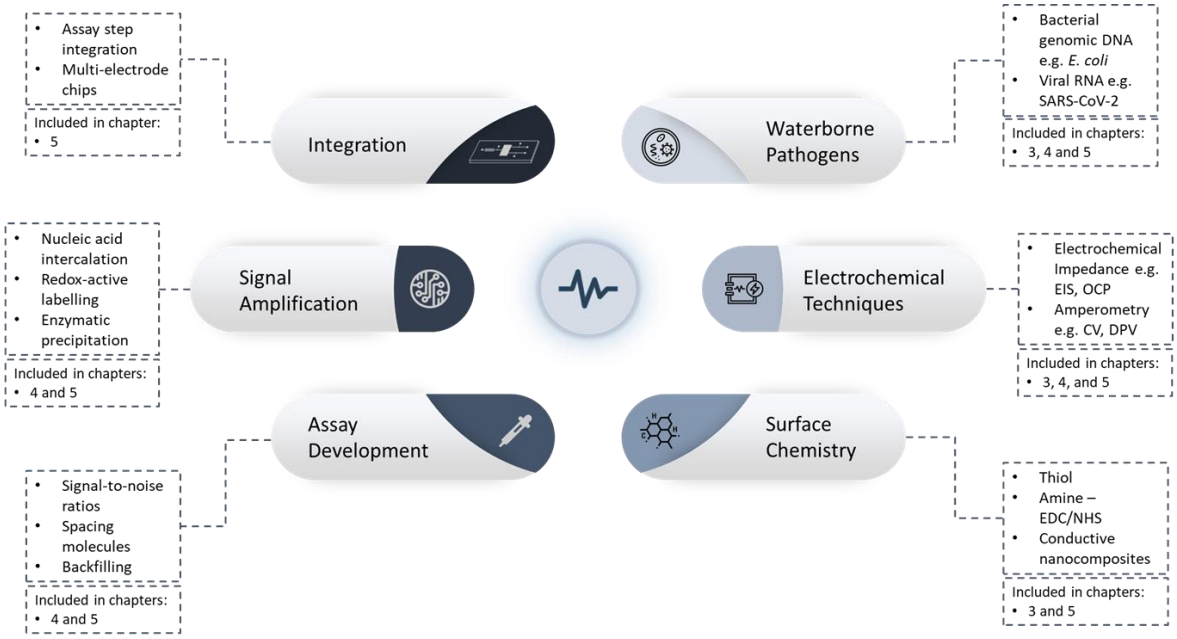

Figure 6.1. Research themes and disciplines included in this thesis throughout the various experimental projects, the chapters involved in each research area are displayed.

6.1. Summary

The primary focus of this thesis has been the development of an electrochemical biosensing assay for the detection of nucleic acids associated with waterborne bacteria and viruses. Biosensors are these days ubiquitous within everyday life, from lateral flow pregnancy and disease antigen tests to implantable electrochemical glucose sensors. However, electrochemical biosensors still have a way to go in research and development before they can be truly realised for their potential in diagnostics and monitoring of a plethora of clinical diseases and environmental contaminants. Specifically, some of the challenges that face electrochemical genosensors for commercial viability include biofouling by clinical samples at PoC and for *in-situ* monitoring applications. These sensors also need to be able to detect low concentrations while maintaining the use of commercially feasible simple surface chemistries and a minimum of assay steps. Finally, it is important to develop with miniaturisation in mind to ensure that commercial devices are easily deliverable to the PoC and areas where they are needed while maintaining low cost and simplicity.

In chapter 3 of this thesis, a simple co-immobilised SAM using thiol-based surface chemistry was developed for the cost-effective detection of genomic DNA for *E. Coli*

detection. The experimental work and results of this thesis explored the importance of gold surface preparation and the effects of surface oxide monolayers on the effectiveness of thiol functionalisation. Two gold surface preparation methods were tested with the key difference being the removal of previously bound thiols and generated gold oxide monolayers in a previously optimised cleaning protocol (Tkac and Davis, 2008). By introducing these steps, a 96.56% increase in surface-bound molecules was observed, increasing the potential binding sites for surface hybridisation with target DNA. Probe DNA surface density was also optimised due to the negative charge present in surface-bound DNA-DNA interactions to minimise steric hindrance and maximise potential binding sites. Optimised spacing of DNA molecules was achieved using the spacer molecule MCH, which when mixed at specific molar ratios can be used to produce highly controlled surface-bound ratios. MCH was also used as a surface-blocking agent to reduce the incidence of non-specific binding. From the results of surface DNA:MCH ratio optimisation it was found that the ratio of 1:10 provided the highest change in R_{ct} of 21.96 ± 3.31% upon hybridisation with the highest tested target DNA concentration. Optimisation of this molar ratio was slightly different to previous literature with a similar experimental setup (Keighley *et al.*, 2008; Regan *et al.*, 2014). This is likely due to the difference in probe oligonucleotide length from the probes used in these studies. Suggesting that this optimisation step is necessary with each co-immobilised thiol-based SAM for any assay using varied lengths of probe oligonucleotides. A final limit of detection of 2.71 nM was achieved using the simple thiol-based surface chemistry assay which was comparable to other genosensing assays that do not incorporate any signal enhancement method. However, for the detection of pathogens in water, a highly sensitive assay is required to detect concentrations as low as femtomolar to attomolar level, or sample amplification is required.

The second experimental study in this thesis, chapter 4, therefore focussed on the integration of a signal amplification method to increase the sensitivity of electrochemical DNA biosensing. This study focussed specifically on the use of redox-active intercalation of dsDNA bound to the electrode surface to increase impedance signals and to enable sensitive amperometric detection of surface-based DNA

hybridisation. A previously developed novel intercalating compound was synthesised and tested in collaboration with the Physical Organic Chemistry group at Cardiff University called cobalt aqphen, or $[Co(GA)_2(aqphen)]Cl$ (Regan *et al.*, 2014). This compound is a redox-active intercalating compound that binds between the bases of nucleotide pairs through the aqphen ligand. In doing so, this intercalation causes a structural change in the helix that causes an increase in electrical field by increasing the length of the dsDNA helix which could be measured through impedimetric detection methods. Additionally, due to the redox-active cobalt moiety, it was possible to measure the amplified amperometric signal of target DNA binding as well as the effects on capacitance and OCP. Upon intercalation of the cobalt aqphen to dsDNA, a significant decrease in both capacitance and OCP was observed. Additionally, a 257% increase in peak current was observed with amperometric DPV measurements. It was also observed that by incubating cobalt aqphen with target DNA simultaneously, an increase in target DNA binding efficiency was observed. Our current theory is that the cobalt aqphen screens the negative charge of the DNA molecules, mitigating steric hindrance effects and increasing potential binding signal by 20.88% and 109.67% for capacitive and amperometric detection, respectively. The minimum tested concentration of 100 pM target ssDNA gave a significantly larger peak current change than the 0 nM control ($[Co(GA)_2(aqphen)]Cl$ + probe ssDNA, $P<0.001$). A calculated LOD of 43 pM demonstrated an almost 100-fold increase in assay sensitivity by employing $[Co(GA)_2(aqphen)]Cl$ intercalation of the assay developed in chapter 3. However, due to the opposing charges of positively charged cobalt aqphen and the negative charge of the DNA backbone, non-specific binding of the intercalator was observed in the presence of surface-functionalised ssDNA probes. It is our current assumption that the passive binding of cobalt aqphen to ssDNA may be reduced significantly by further optimisation of cobalt aqphen concentration and incubation time.

Chapter 5 of this thesis demonstrates a complex but highly sensitive and selective integrated assay that allowed attomolar level detection of RNA from the SARS-CoV-2 virus and femtomolar level detection of *E. Coli* genomic DNA. These assays were developed in collaboration with the Wyss Institute for Biologically Inspired

Engineering at Harvard University during a visiting graduate internship during the beginning of the COVID-19 pandemic. In this study, a novel electrochemical assay was developed for the flexible detection of both SARS-CoV-2 RNA and *E. Coli* DNA. In both assays, the CRISPR-Cas12a enzyme was exploited for its highly specific interaction with target DNA and collateral cleavage of surrounding DNA to conduct cleavage of a biotinylated reporter DNA sequence causing downstream precipitation of TMB which could be measured using CV. In the case of the SARS-CoV-2 assay, isothermal amplification through the integration of an RT-LAMP assay was employed to amplify viral RNA further to enable highly sensitive attomole level detection. After being reverse transcribed and amplified in the case of SARS-CoV-2 RNA, the Cas12a enzyme was conjugated with guide RNA complementary to the target DNA sequence, allowing for selective primary cleavage of the target. Once the target DNA was cleaved, Cas12a became 'activated' for collateral cleavage of nearby DNA sequences. Using this characteristic collateral cleavage, we designed a reporter probe functionalised with biotin on the 5' end which was cleaved by Cas12a upon detection of the target viral sequence. If the reporter probe was cleaved, the biotin group from the reporter sequence would not bind to the PNA probes on the electrode surface and downstream binding of polystreptavidin-HRP and TMB precipitation would not occur, leading to a low/zero current signal for a positive result. Using the developed assay, a single molecule (0.8 cp/uL) limit of detection (equivalent to 1.33 aM) was achieved for the detection of RT-LAMP amplified SARS-CoV-2 viral RNA. This assay was also utilised to detect unamplified *E. Coli* DNA sequences related to the Stx-1 and Stx-2 toxin proteins. Target DNA sequences were detected using the same method described above with the only difference being the guide RNA sequences conjugated with the Cas12a enzyme. Limits of detection for Stx-1 and Stx-2 were obtained at 210 fM and 1.26 pM, respectively. Additionally, several controls were carried out whereby the guide RNA complementary to each target DNA was swapped demonstrating that the activity of the conjugated Cas12a was highly specific towards only fully complementary target DNA. Further to this, the detection of both SARS-CoV-2 viral RNA and *E. Coli* genomic DNA using this assay displays how easily modifiable it is for the detection of any target bacterial and viral pathogens. By simply

swapping out the guide RNA and RT-LAMP primers it would be possible to quickly implement this detection assay for any pathogen of concern.

While this thesis was not able to demonstrate the full integration of an electrochemical DNA biosensor for waterborne pathogens, due to various time and resource constraints, it has demonstrated the advantages and effectiveness of incorporating various electrochemical and biochemical techniques. By integrating multiple techniques such as electrochemical detection, various surface chemistries and signal amplification methods it is possible to achieve highly selective and ultrasensitive detection of pathogen-related nucleic acids. Developments in integrated biosensing platforms and chip-based devices such as printed circuit boards (PCB), silicon-based chips and 3D printed cartridges are rapidly expanding the possibilities of highly integrated devices and ease of miniaturisation. Some of the suggestions in the future work section below look at opportunities that could be further investigated for integrating the techniques explored throughout this thesis.

6.2. Future work

The work presented in this thesis has raised several potential areas of future experimental work that could be explored as well as further possibilities for collaborations. Some of this work has been explored in pilot studies and others have been planned for future projects. Additionally, the work presented on CRISPR-based detection of SARS-CoV-2 was further developed to produce a multiplexed molecular and serological biosensing platform for viral RNA and host antibodies with integrated microfluidics and sample pre-treatment and amplification in a 3D printed cartridge device (Najjar *et al.*, 2022). Several future experimental project concepts are detailed below.

6.2.1. Rapid anti-fouling surface chemistry for electrochemical genosensors with pyrrole

An important area of research for devices being developed for on-site, point-of-care (PoC) and monitoring purposes is the issue of device biofouling by non-specific molecules in both clinical and environmental samples. Anti-fouling techniques are therefore an important concept to focus on to develop devices that can either

prevent or mitigate the effects of biofouling such as reduced target binding efficiency, potential signal loss and reduced conductivity. Additionally, any anti-fouling strategy implemented must ensure that there is no loss in electrochemical properties. One such technique explored in this thesis was the doping of a nanocomposite coating with highly conductive rGOx nanoparticles to provide anti-fouling using bovine serum albumin (BSA) to prevent non-specific molecule binding and complete coverage of the gold electrode surface. However, this strategy was time-consuming in its fabrication and required expensive reagents. One method that has been extensively explored in the literature is the electrical deposition and polymerisation of the conductive redox-active molecule pyrrole (Singh, Kathuroju and Jampana, 2009; Jain, Jadon and Pawaiya, 2017; Cete *et al.*, 2020). However, most strategies implementing the use of pyrrole as a conductive anti-fouling technique do so by creating complex structures on the surface to attach functional groups such as using amine-terminated linkers with EDC/NHS conjugation chemistries (Jolly *et al.*, 2016; Miodek *et al.*, 2016). These complex structures and layering methods are not conducive to commercialisation processes and so a simpler technique is required.

One possible method to reduce the complexity of implementing pyrrole as a conductive anti-fouling technique would be to directly functionalise polypyrrole with DNA probe oligonucleotides that are modified with amine groups. This has been shown previously by Jolly *et al*. whereby they demonstrated the covalent functionalisation of polypyrrole films with PEG through electro-oxidation of present amine groups (Jolly *et al.*, 2016). The same principle can be applied to amine-modified DNA oligonucleotide probes. Some preliminary work has been carried out to show that quick and simple modification is possible with these DNA oligonucleotides (see Figure 6.2). The entire fabrication process takes no longer than 5 minutes to complete from a clean electrode surface to a functional sensor that can be incubated with target sequences. However, to achieve maximum target binding and sensitivity the probe surface density would need to be improved by experimentally optimising the probe DNA sample concentration and the number of DNA electro-deposition cycles.

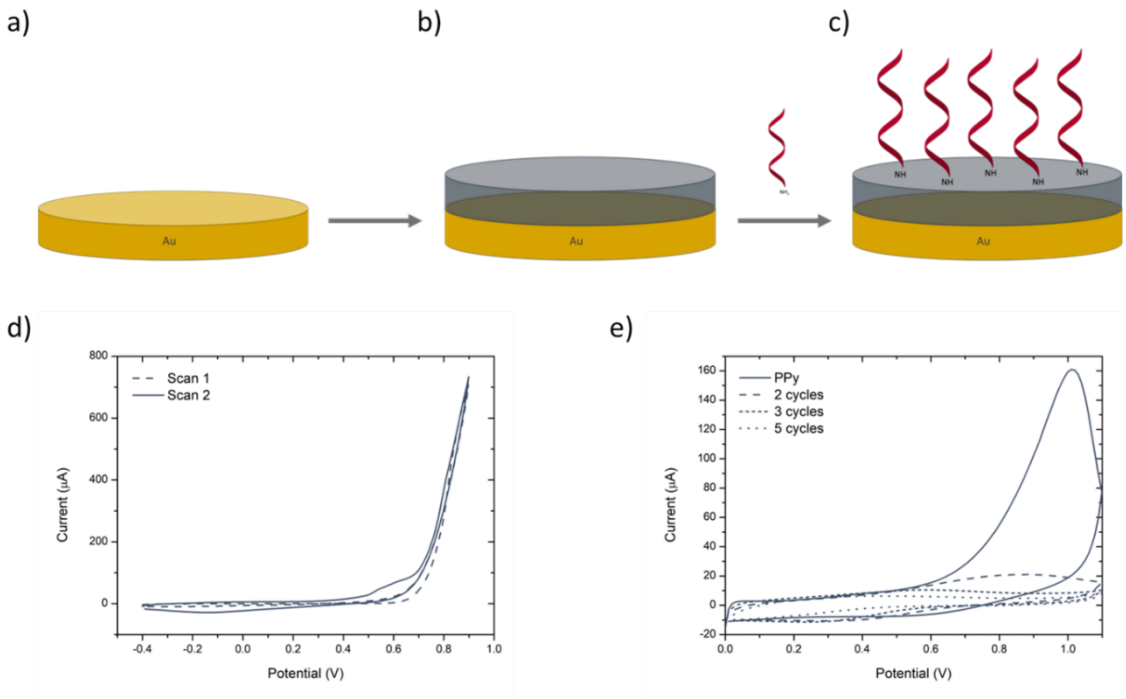

Figure 6.2. Schematic representation of potential PPy/amine-ssDNA sensor fabrication. a) bare gold electrode. b) formation of poly(pyrrole) thin film via electro-polymerisation. c) electrodeposition of amine-terminated oligonucleotide probes by electro-oxidation of pyrrole to attach amine groups. d) cyclic voltammetric graph showing electro-polymerisation of poly(pyrrole) thin films. e) cyclic voltammetric graph displaying the effect of varying the number of electrodeposition cycles with amine-terminated oligonucleotide probes on peak oxidation current.

Another way to achieve an optimised probe surface density using this technique could be to electro-deposit amine-terminated oligonucleotides that are already hybridised to the target sequence. By doing so, the optimal probe density upon electro-deposition could be achieved and then the target DNA sequence could be removed using various techniques such as mild molecular detergents, ultrapure water or ultrasonication (see Figure 6.3).

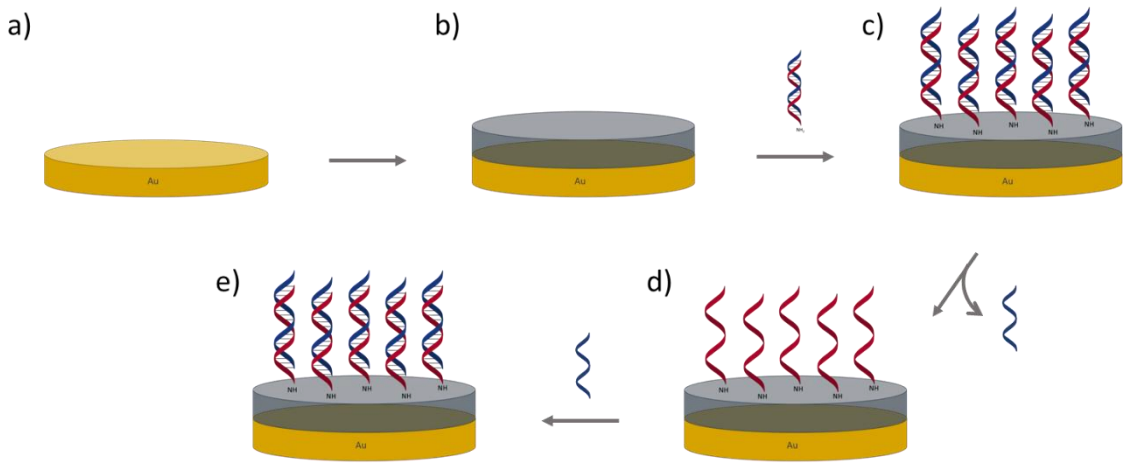

Figure 6.3. Schematic representation of PPy/amine-ssDNA sensor fabrication whereby optimum probe density is achieved by electro-depositing amine-terminated dsDNA. a) bare gold electrode. b) formation of poly(pyrrole) thin film via electro-polymerisation. c) electrodeposition of amine-terminated dsDNA by electro-oxidation of pyrrole to attach amine groups. d) removal of target DNA sequence by mild agitation or molecular detergents etc. e) incubation of target DNA sequence from the experimental sample.

6.2.2. Sample pre-treatment and reducing sample and reagent volumes with a 3D gel-electrophoresis chip device

Electrochemical diagnostic devices that integrate multi-functionality and chip-based miniaturisation are attractive platforms for the detection of biomarker molecules related to disease and environmental pollution. Current techniques for disease and environmental biomarker assessment, while sensitive and selective, often suffer from large sample and reagent requirements and lack ease of integration. Microfluidic electrochemical devices promise sensitivity, selectivity and rapid results within a portable miniaturised device that is simple to use (Rainbow *et al.*, 2020). Microchip electrophoresis (MCE) devices are diagnostic platforms that integrate electrophoretic sample transport with target molecule detection. In collaboration with the Wyss Institute for Biologically Inspired Engineering at Harvard University, we demonstrated the first steps towards the development of an integrated MCE platform for the electrochemical detection of target biomarkers. This work describes the development of an electrochemical impedance spectroscopy (EIS)-based microchip electrophoresis (MCE) device with separated detection electrodes and integrated electrophoretic sample injection. By developing a capture-probe

functionalised gel channel that can be increased in cross-sectional size and length both sensitivity and dynamic range can be decoupled and further increased. Additionally, the capture gel can be functionalized with multiple capture probe molecules including nucleic acids and proteins for the detection of various target biomarkers.

In this preliminary work, a printed circuit board (PCB) with integrated sensing and electrophoresis electrodes were designed using Altium software and ordered from a commercial vendor (see Figure 6.4). A three-layered microfluidic chip can be fabricated by laminating double-sided tape with laser-cut microfluidic channels onto a PCB by lamination. A PMMA layer with laser-cut inlets/outlets can then be bonded through lamination to the double-sided tape layer. Amine-terminated probe molecules with a Cy3 fluorescent tag were incubated with N-hydroxysuccinimide acrylate to introduce a vinyl group to a probe molecule with amine groups. The modified probe can then be co-polymerised into a standard polyacrylamide gel. An unmodified linear polyacrylamide gel is first injected into the microfluidic channels, before injecting the Cy3-tagged probe functionalised capture gel into the capture region using fluorescence imaging. Electrophoretic injection of Alexa Fluor 488-tagged BSA was tested using a LabSmith HVS448 programmable voltage source to control the voltage in each inlet/outlet. The injection of controlled volumes of a sample was viewed using a fluorescence microscope.

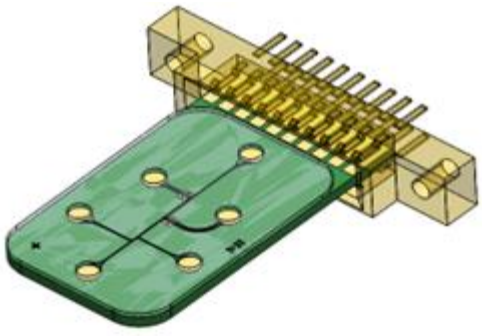

Figure 6.4. Three-layer MCE device with electrode-integrated PCB sensing layer and dsTape/PMMA microfluidic layers.

In the preliminary work, a low-cost MCE device with integrated electrodes for electrochemical sensing and electrophoretic sample injection was developed. We

have demonstrated the fabrication of a device containing both transport and probe-functionalised polyacrylamide gels as well as electrophoretic sample injection. Fluorescence microscopy images validated the positioning of the 3D matrix capture gel (see Figure 6.5a) as well as electrophoretic sample injection of bovine serum albumin (BSA) samples (see Figure 6.5b-f). However, bubble formation was observed from the integrated electrodes during electrophoretic injection due to bipolarity under a high-voltage electrical field.

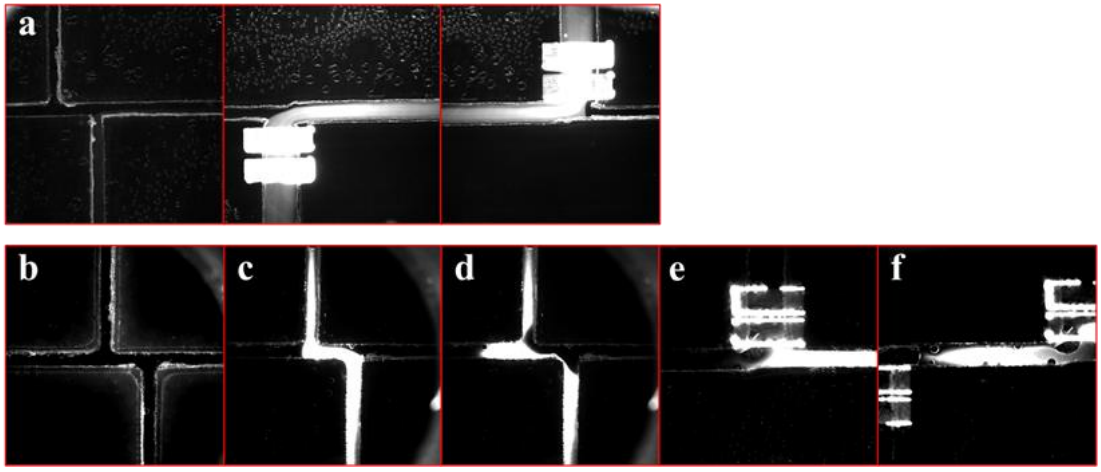

Figure 6.5. a) Fluorescence microscopy images of Cy3-tagged probe-functionalised capture gel positioning, b) double-T junction for sample loading and volume control before sample injection, c) after sample injection into the loading junction, d) movement of sample to away from loading junction, e) movement of sample into capture region, f) sample in the capture gel region channel.

This work demonstrates the aspects involved in the integration of an MCE device utilizing multiple techniques and technologies. It also demonstrates the first steps toward a working MCE device implementing a DNA-functionalized capture gel for biomarker capture and detection as well as electrophoretic injection of BSA protein samples via integrated on-chip electrodes. However, further work is required to improve the design and functionality of the MCE device. Firstly, the orientation and design of the electrophoresis electrodes required further testing and refinement to improve the sample flow of target molecules into the T-junction as well as through the capture gel. Additionally, a new capture region can be designed to avoid the bipolarity under such a high-voltage electric field causing hydrolysis of the polyacrylamide gels. To test the electrochemical detection capability of the device, a

capture gel containing an application-relevant probe molecule such as capture nucleic acids or antibodies would be developed to enable the detection of disease and environmental biomarkers.

6.2.3. Further optimisation of cobalt-aqphen intercalation to reduce non-specific interactions with ssDNA

While the use of cobalt aqphen as an intercalator to increase signal output for electrochemical DNA hybridisation was successfully applied for the detection of *E. Coli* DNA, non-specific binding of the compound to ssDNA was observed. Further optimisation of this assay protocol is required to prevent non-specific signal associated with the intercalating compound with ssDNA. One way in which the protocol can be further optimised is by testing various concentrations of the cobalt aqphen intercalator as well as varying the incubation time to achieve a low signal-to-noise ratio. This would be comparable to the optimisation that was carried out within the CRISPR-based detection study details in chapter 5 for the reporter probe. Another way of potentially decreasing the signal observed with non-specific binding of cobalt aqphen with ssDNA probes would be to introduce a washing step after incubation. Some potential wash buffers include ethylenediaminetetraacetic acid (EDTA) which can remove metal ions through a chelating reaction. However, the effect of EDTA on the compound stability of $[Co(GA)_2(aqphen)]Cl$ would need to be assessed. Another wash buffer commonly seen in the literature is phosphate buffer saline containing 0.1 or 0.05% Tween 20 (PBST). Tween acts as a mild surfactant which prevents non-specific background binding. Finally, another potential way to decrease the passive binding of cobalt aqphen to the probe part of the SAM would be to replace DNA with PNA molecules. It is our current hypothesis that the cobalt aqphen binds to the probe ssDNA through weak electrostatic interactions due to the negative charge of DNA. By replacing DNA with neutrally charged PNA the passive electrostatic attraction might be avoided.

6.2.4. Simplification of CRISPR-based assay using a redox-active reporter probe (RP)

One of the disadvantages of the CRISPR-based electrochemical detection assay developed in chapter 5 of this thesis was the multi-step surface chemistry used to produce a measurable amperometric signal. In the developed assay, biotinylated reporter probes were partially hybridised with surface bound PNA. To allow for amperometric detection of the reporter probe binding, polystreptavidin-HRP was conjugated to the biotin group of the reporter probe to facilitate reduced TMB precipitation. Multi-step surface chemistry protocols are not ideal due to the potential for increased error that they introduce with each additional conjugation step. In the proposed experiment, the reporter probe would be modified with a redox-active label instead of the biotin group (see Figure 6.6). Common redox-active labels include ferrocene, methylene blue, and ruthenium which have been frequently used in the literature with electrochemical biosensor assays (Kang *et al.*, 2009; Pheeney and Barton, 2012; Flamme *et al.*, 2018). By integrating the redox-active label with the reporter probe, we could mitigate signal variation from electrode-to-electrode by removing the need for downstream surface chemistry steps. This proposed change would produce a more refined and reproducible assay that also provides the benefit of simplifying assay complexity for the end-user and for final microfluidic device design.

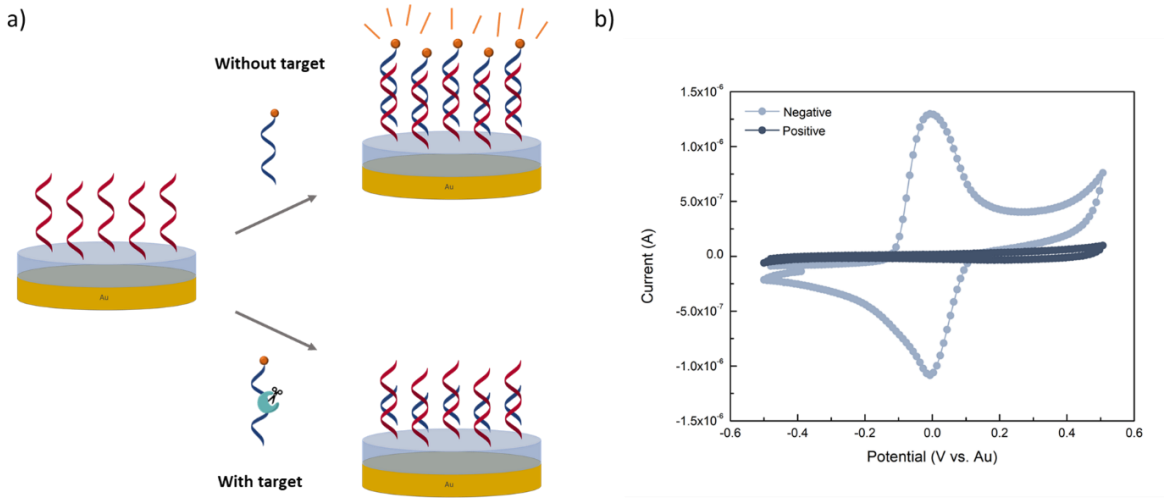

Figure 6.6. Schematic representation of a simplified surface chemistry assay for CRISPR-based detection using reporter probe with redox-active modification. a) in the presence of target DNA Cas12a with becomes activated, collateral cleavage of the reporter probe occurs and the redox-active label is lost leading to decreasing current signal with increasing target concentration. b) cyclic voltammetry shows an example of the current signals obtained with a positive and negative target sample.

6.2.5. CRISPR-based biosensing assay using recombinase polymerase amplification (RPA) to enable ease-of-integration

With the further simplification of the CRISPR-based assay by using redox labels conjugated directly to the reporter probe, another way to further simplify this assay would be to use recombinase polymerase amplification (RPA) instead of LAMP. Similar to LAMP, RPA is a single-tube isothermal amplification method that was developed as an alternative to the traditional polymerase chain reaction (PCR) method. However, unlike LAMP which is carried out at 60-62 °C, RPA has an ideal working temperature range of 37-42 °C while also being effective at room temperature (Lobato and O'Sullivan, 2018; Wu *et al.*, 2020). This makes RPA an ideal one-pot method for amplifying target nucleic acids in low-cost and rapid diagnostic devices for on-site and PoC testing and can easily be increased in efficiency by being held in hand (Li, Macdonald and von Stetten, 2018). By implementing RPA in the CRISPR-based protocol developed in chapter 5 it is possible to reduce the need for external heating elements in the development of a microfluidic device. Additionally, because the CRISPR reaction can be carried out in room temperature the whole assay

prior to incubation with the electrode can be done in a one-pot setup to increase protocol simplicity for the user. A microfluidics cartridge has been developed as part of the published work by Najjar *et al*. which uses RT-LAMP for target RNA amplification (see Figure 6.7) (Najjar *et al.*, 2022). By using RPA instead of LAMP, it would be possible to remove the additional reservoir for CRISPR reagent input and the heating power resistor element for the LAMP reaction to further simplify the cartridge design. Through the integration of the different components within this thesis and the further work discussed herein the ability to develop a sample-in-answer-out biodevice system for diagnosis and monitoring of pathogens in freshwater systems is closer to being realised.

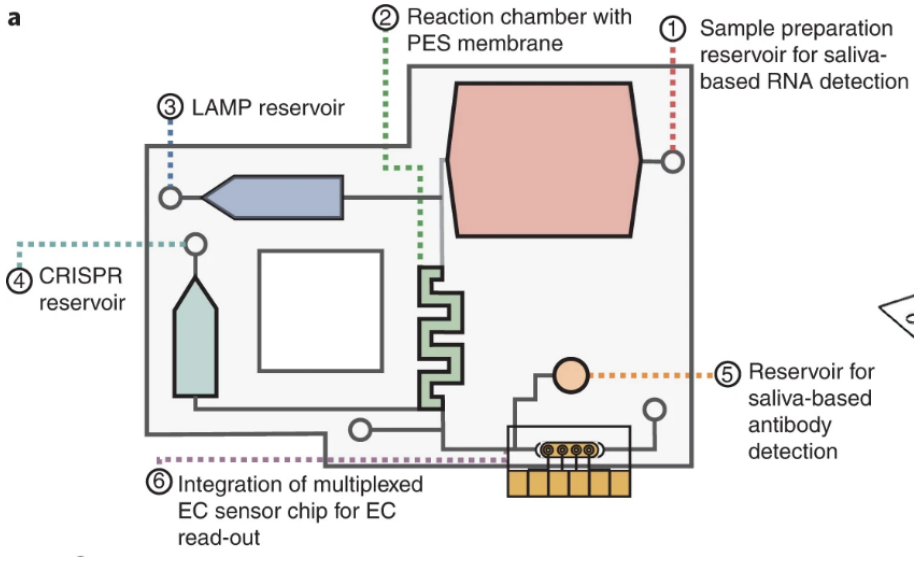

Figure 6.7. a) Microfluidic cartridge design for multiplexed CRISPR-based and serology detection of SARS-CoV-2 RNA and antibodies in saliva samples. (1) Sample and proteinase K mixture input into the sample preparation reservoir, where it incubates. (2) The sample is pumped over the PES membrane inside the reaction chamber for RNA capture and heated to denature potential reaction inhibitors. (3) The LAMP solution is then pumped from the reservoir into the reaction chamber and incubated. (4) The CRISPR mixture is pumped into the reaction chamber, incubated, and then flowed over the EC sensor chip. (5) The saliva for antibody detection is pumped over the EC sensor chip. (6) After the addition of polystreptavidin-HRP and TMB, results from the EC sensor chip are read with a potentiostat (taken from Najjar et al., 2022).

References

Cete, S. et al. (2020) 'A novel biosensor with the use of polypyrrole–poly(sodium-4-styrenesulphonate) as a dopant in the determination of glucose', Chemical Papers, 74(3), pp. 799–808. Available at: https://doi.org/10.1007/S11696-019-00907-6/TABLES/3.

Flamme, M. et al. (2018) 'Applications of Ruthenium Complexes Covalently Linked to Nucleic Acid Derivatives', Molecules : A Journal of Synthetic Chemistry and Natural Product Chemistry, 23(7). Available at: https://doi.org/10.3390/MOLECULES23071515.

Jain, R., Jadon, N. and Pawaiya, A. (2017) 'Polypyrrole based next generation electrochemical sensors and biosensors: A review', TrAC Trends in Analytical Chemistry, 97, pp. 363–373. Available at: https://doi.org/10.1016/J.TRAC.2017.10.009.

Jolly, P. et al. (2016) 'Electro-Engineered Polymeric Films for the Development of Sensitive Aptasensors for Prostate Cancer Marker Detection', ACS Sensors, 1(11), pp. 1308–1314. Available at: https://doi.org/10.1021/acssensors.6b00443.

Kang, D. et al. (2009) 'Comparing the Properties of Electrochemical-Based DNA Sensors Employing Different Redox Tags', Analytical chemistry, 81(21), p. 9109. Available at: https://doi.org/10.1021/AC901811N.

Keighley, S.D. et al. (2008) 'Optimization of DNA immobilization on gold electrodes for label-free detection by electrochemical impedance spectroscopy', Biosensors and Bioelectronics, 23(8), pp. 1291–1297. Available at: https://doi.org/https://doi.org/10.1016/j.bios.2007.11.012.

Li, J., Macdonald, J. and von Stetten, F. (2018) 'Review: a comprehensive summary of a decade development of the recombinase polymerase amplification', Analyst, 144(1), pp. 31–67. Available at: https://doi.org/10.1039/C8AN01621F.

Lobato, I.M. and O'Sullivan, C.K. (2018) 'Recombinase polymerase amplification: Basics, applications and recent advances', TrAC Trends in Analytical Chemistry, 98, pp. 19–35. Available at: https://doi.org/10.1016/J.TRAC.2017.10.015.

Miodek, A. et al. (2016) 'Electrochemical functionalization of polypyrrole through amine oxidation of poly(amidoamine) dendrimers: Application to DNA biosensor', Talanta, 154, pp. 446–454. Available at: https://doi.org/https://doi.org/10.1016/j.talanta.2016.03.076.

Najjar, D. et al. (2022) 'A lab-on-a-chip for the concurrent electrochemical detection of SARS-CoV-2 RNA and anti-SARS-CoV-2 antibodies in saliva and plasma', Nature Biomedical Engineering 2022, pp. 1–11. Available at: https://doi.org/10.1038/s41551-022-00919-w.

Pheeney, C.G. and Barton, J.K. (2012) 'DNA electrochemistry with tethered methylene blue', Langmuir, 28(17), pp. 7063–7070. Available at: https://doi.org/10.1021/LA300566X/ASSET/IMAGES/MEDIUM/LA-2012-00566X_0009.GIF.

Rainbow, J. et al. (2020) 'Integrated Electrochemical Biosensors for Detection of Waterborne Pathogens in Low-Resource Settings', Biosensors. Basel, Switzerland :, p. 36. Available at: https://doi.org/10.3390/bios10040036.

Regan, E.M. et al. (2014) 'A novel cobalt complex for enhancing amperometric and impedimetric DNA detection', Electrochimica Acta, 128, pp. 10–15. Available at: https://doi.org/https://doi.org/10.1016/j.electacta.2013.10.028.

Singh, M., Kathuroju, P.K. and Jampana, N. (2009) 'Polypyrrole based amperometric glucose biosensors', Sensors and Actuators B: Chemical, 143(1), pp. 430–443. Available at: https://doi.org/10.1016/J.SNB.2009.09.005.

Tkac, J. and Davis, J.J. (2008) 'An optimised electrode pre-treatment for SAM formation on polycrystalline gold', Journal of Electroanalytical Chemistry, 621(1), pp. 117–120. Available at: https://doi.org/https://doi.org/10.1016/j.jelechem.2008.04.010.

Wu, H. et al. (2020) ‘A Recombinase Polymerase Amplification and Lateral Flow Strip Combined Method That Detects Salmonella enterica Serotype Typhimurium With No Worry of Primer-Dependent Artifacts’, Frontiers in Microbiology, 11, p. 1015. Available at: https://doi.org/10.3389/FMICB.2020.01015/BIBTEX.